ADVANCED THERMOSETS BASED ON THIOL-ISOCYANATE CHEMISTRY

Francesco Gamardella

UNIVERSITAT ROVIRA i VIRGILI

Advanced thermosets based on thiol-isocyanate chemistry

FRANCESCO GAMARDELLA

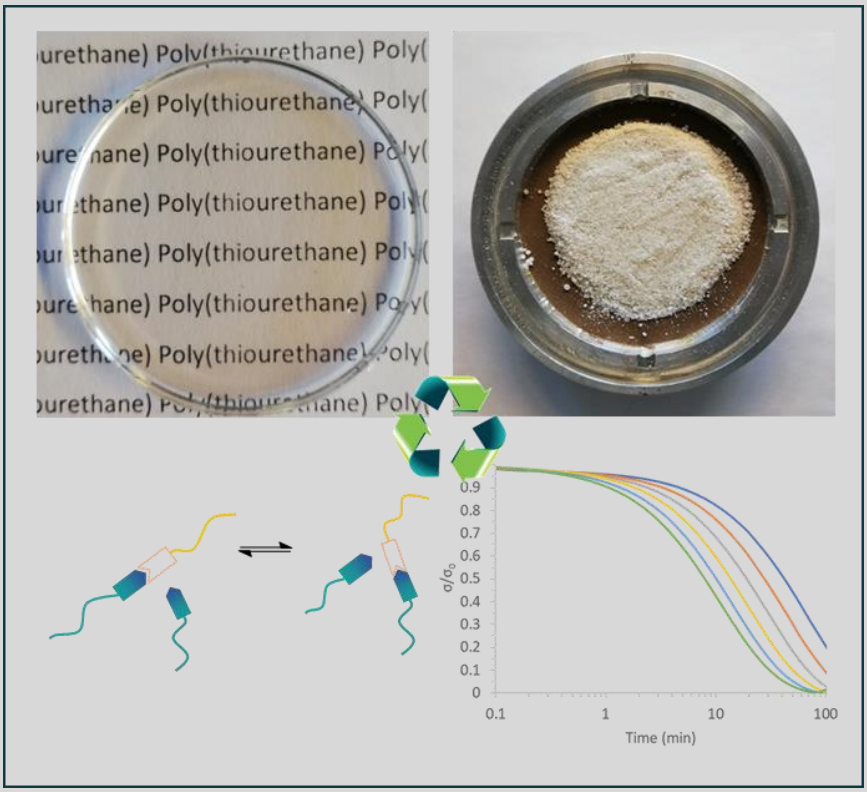

DOCTORAL THESIS
2021

Advanced thermosets based on thiol-isocyanate chemistry

by

Francesco Gamardella

Doctoral Thesis

Supervisors:

Angles Serra i Albet

Xavier Ramis i Juan

Universitat Rovira i Virgili

Tarragona

2021

UNIVERSITAT ROVIRA I VIRGILI

Departament Química Analítica i Química Orgànica
Campus Sescelades, Edifici N4
Carrer Marcel·lí Domingo s/n
43007 Tarragona

Professor Àngels Serra i Albet of the Department of Analytical and Organic Chemistry at the Universitat Rovira i Virgili and Professor Xavier Ramis i Juan of the Department of Heat Engines at ETSEIB, Universitat Politècnica de Catalunya.

Certify:

that the Doctoral Thesis, entitled "Advanced thermosets based on thiol-isocyanate chemistry" presented by Francesco Gamardella to obtain the title of Doctor, has been carried out under our direction and that it fulfils all the requirements to be eligible for the Doctor International Mention.

Tarragona, April 2021

Doctoral Thesis Supervisors

Prof. Àngels Serra i Albet

Prof. Xavier Ramis i Juan

Acknowledgments

In this part of the thesis, I would like to thank all the people who helped and supported me during this period.

Firstly, I would like to express my sincere gratitude to my promotor Angels Serra for supervising my thesis. I greatly appreciate her constant support and guidance, teaching me the art of the research and of the science. Thank you for leaving always open your door for your constant interest in my work, and for have trusted me and have always been encouraging.

I would wish to express my sincere gratitude to my co-promotor Xavier Ramis for his help and precious contribution during this period, you have been an invaluable help. Thank you very much for your guidance, advice and for always being kind every time that I came to your laboratory in Barcelona.

I would like to extend my special thanks to Silvia de La Flor for co-authoring a large number of articles and for guiding me with her knowledge in the mechanics of polymer.

I also want to thank Filip Du Prez, for giving me the opportunity to join his group during my stay in Ghent, despite the difficult circumstances and all the restriction due to the pandemic. It has been an honour for me to work with you.

Thanks to Toni and Marta as they were extremely welcoming from the very beginning, like you would in a family.

Thank you to my other co-authoring, Valentina a lovely person and talented girl with whom I had great pleasure working with, Sara for her help in the mechanical tests and Federico to whom I leave the legacy of poly(thiourethane).

Thanks to all the colleagues/friends from the laboratory in Tarragona: Isaac for being my mentor from the Erasmus; Xavi for always bringing joy and news to the laboratory; Dailyn for her patient and help during all these years; David for his help with the DMA; Adrià to always be available for any help. Thanks to all the guys that are passed from the laboratory, even if for a shorter time Alberto, Ruben, Ali, Nuria, Aina and Jordi; all of you has been awesome colleagues and friends. Thanks to Osman and Xavi Fernandez the other part of the group in Barcelona.

I would like also to thank my colleagues in the University of Ghent, especially Christian was a pleasure collaborate with you.

Thanks to my Tarragona/Italian family Mario, Mimmo, Gianmarco and especially Claudio, with whom I have shared beautiful and difficult moments in the laboratory and house during the last three years.

I would like to thank my love Rita for accompanying me during this adventure. Thank for all your support, encouragement, and pressure, which helped me to reflect on the right choices and never give up. I am blessed to have you on my side.

Thanks to my family, that has always supported me. My brother, firstly thank to take care of the family and to be always present when I need some help. To my mother who has always left me free in my choices and has supported me in all those I have done, thank you for being always strong even in difficult times, you are my example. Thank a lot at my extended family: Nonna, zio Lino, zia Anna, Zio Cosimo, Corrado, Cinzia, Armida, zia Milli, Marilena, Erminio, Filomena and all the others. Thank you to the family of Rita in which I am so well welcomed, thank you for all!

I know I leave a few people, so I want to thank all of them which I have not mentioned above but have contributed during this part of my life.

Ringraziamenti

In questa parte della tesi, vorrei ringraziare tutte le persone che mi hanno aiutato e sostenuto durante questo periodo.

In primo luogo, vorrei esprimere la mia sincera gratitudine al mio promotore Angels Serra, per la supervisione della mia tesi. Apprezzo molto il suo costante supporto e la sua guida, insegnandomi l'arte della ricerca e della scienza. Grazie per aver lasciato sempre aperta la tua porta e per il tuo costante interesse per il mio lavoro, per esserti fidata di me e per essere sempre stata incoraggiante.

Vorrei esprimere la mia sincera gratitudine al mio co-promotore Xavier Ramis per il suo aiuto e prezioso contributo durante questo periodo, sei stato un aiuto inestimabile. Grazie mille per la tua guida, i consigli e per essere sempre gentile ogni volta che sono venuto nel tuo laboratorio a Barcellona.

Vorrei estendere i miei ringraziamenti speciali a Silvia de La Flor coautrice di un gran numero di articoli e per avermi guidato con le sue conoscenze nella meccanica dei polimeri.

Voglio anche ringraziare Filip Du Prez, per avermi dato l'opportunità di unirmi al suo gruppo durante la mia permanenza a Gand, nonostante le difficili circostanze e tutte le restrizioni dovute alla pandemia. È stato un onore per me lavorare con te.

Grazie a Toni e Marta che sono stati fin dall'inizio estremamente accoglienti, come faresti in una famiglia.

Grazie agli altri co-autori, Valentina una persona adorabile e ragazza di talento con cui ho avuto un grande piacere di lavorare, Sara per il suo aiuto nelle prove meccaniche e Federico a cui lascio l'eredità dei politiouretani.

Grazie a tutti i collegh /amici del laboratorio di Tarragona: Isaac per essere stato il mio mentore dall'Erasmus; Xavi per aver portato sempre gioia e news al laboratorio; Dailyn per la sua paziente e aiuto durante tutti questi anni; David per il suo aiuto con la DMA; Adrià per essere sempre disponibile per qualsiasi aiuto. Grazie a tutti i ragazzi che sono passati dal laboratorio, anche se per un periodo più breve Alberto, Ruben, Ali, Nuria, Aina e Jordi; siete stati tutti colleghi e amici fantastici. Grazie a Osman e Xavi Fernandez l'altra parte del gruppo a Barcellona.

Vorrei anche ringraziare i miei colleghi dell'Università di Ghent, in particolare Christian è stato un piacere lavorare con te.

Grazie alla mia famiglia tarragonese/italiana Mario, Mimmo, Gianmarco e soprattutto Claudio, con cui ho condiviso momenti belli e difficili in laboratorio e casa negli ultimi tre anni.

Ringrazio il mio amore Rita per avermi accompagnato in questa avventura. Grazie per tutto il tuo supporto, incoraggiamento e pressione, che mi hanno aiutato a riflettere sulle scelte giuste e non mollare mai. Sono fortunato ad averti nella mia vita.

Grazie alla mia famiglia, che mi ha sempre sostenuto. A mio fratello, innanzitutto grazie per esserti preso cura della famiglia e per essere sempre presente quando ho bisogno di aiuto. A mia mamma che mi lascia sempre libero nelle mie scelte e mi sostiene in tutte quelle che faccio, grazie per essere sempre forte anche nei momenti difficili, tu sei il mio esempio. Grazie mille alla mia famiglia allargata: Nonna, zio Lino, zia Anna, zio Cosimo, Corrado, Cinzia, Armida, zia Milli, Marilena, Erminio, Filomena e tutti gli altri. Grazie alla famiglia di Rita nella quale sono stao sempre ben accolto, grazie di tutto.

So che dimentico alcune persone, quindi voglio ringraziare tutte loro che non ho menzionato sopra ma che hanno contribuito durante questa parte della mia vita.

To my dad

Table of contents

Abstract

Thermosetting polymers, thanks to their permanent crosslinked nature, show outstanding mechanical and thermal properties, which allow them to be widely used in industrial applications where high mechanical performances and dimensional stability are required. Unfortunately, the reprocessing and recycling of thermosets is a really difficult task due to their permanent three-dimensional structures, which prevent these materials from melting or dissolving in any solvent. Because of the growing amount of plastic generated at industrial level, the correct reuse or disposal of these polymers is extremely important to prevent their accumulation in landfills and pollute the environment.

In this context, covalent adaptable networks (CANs), covalently crosslinked polymers which are able to change their topology via exchange of the covalent bonds are attracting growing interest. These materials with the ability to be reshaped, to flow and to self-repair, represents a promising approach to improve the lifetime and recyclability of the thermosetting polymers, partially relieving the environmental pressure. They behave as thermosets at service temperature but become malleable at high temperature when the exchange reaction occurs.

To date, crosslinked poly(urethane)s (PU)s have been recognized to show network reconfiguration enabled by dynamic exchange of the covalent bonds. Poly(urethane)s prepared from multifunctional isocyanates and polyols, thanks to their structural versatility, are one of the most used materials in different applications such as elastomers, coatings, rigid foams and adhesives.

Poly(thiourethane)s (PTUs) are related to PU oxygen counterparts, showing comparable properties due to the presence of similar hydrogen bonding but, in addition, they present several advantages. One example is that the formation of PTUs from isocyanates and thiols is not accompanied by any side-reactions contrary to what occurs in the PU synthesis. However, poly(thiourethane) chemistry did not receive broad interests until the thiol-isocyanate reaction was recognized as a click-reaction, with the formation of highly homogeneous network structures.

In this work we exploited the potentiality of this class of materials, starting from the study of the viability of the “thiol-isocyanate” reaction in acid and basic conditions to reach an optimization of the curing process. When a base catalyst is used, the thiol-isocyanate reaction is very fast, and the system is difficult to process. Thus, we proposed the use of a thermally activated latent base, to obtain temporal and kinetic control of the curing processes.

In addition, we explored the potential of this type of thermosets to be used as smart materials, thanks to their narrow thermal transitions, which allows quick movements and a rapid change in their properties. In this context we suggested a possible application of poly(thiourethane) as smart mechanisms for autonomous control, simulating an open-valve application.

Furthermore, we implemented a novel dual-curing procedure based on the combination of thiol-isocyanate and thiol-epoxy click reactions, where both reactions are sequentially activated by temperature. The intermediate/final materials shown different properties depending on the selected ratio between the isocyanate and epoxy groups.

This work was mainly focused on the study and the development of simple and new dynamic crosslinked networks, which can be efficiently remolded and recycled. First, we demonstrated the suitability of thiourethane dynamic chemistries to prepare materials with the targeted properties by the so called model compounds. Once demonstrated that the thiourethane chemistry can be considered as a new type of CANs, the poly(thiourethane)s materials were prepared using a tin-catalyst. The effect of the proportion of dibutyl tin-dilaurate (DBTDL) on the relaxation behaviour as well as the influence of the macromolecular architecture on viscoelastic properties, was studied by changing the structure of the diisocyanate monomers. The PTU materials were successfully recycled by grinding and hot-pressing, and the recycled materials were fully characterized by mechanical, thermomechanical and Fourier Transform Infrared Spectroscopy analyses, confirming their recyclability without appreciable changes in the network structure.

To develop more environmentally friendly PTUs covalent adaptable networks the metal-based catalyst, DBTDL, was substituted by less toxic latent organocatalysts. The use of thermally generated base catalysts represents, at the same time, an interesting opportunity to reach a temporal control of the curing reaction and to increase the amount of catalyst which could help to improve the rate of the exchange process.

Lastly, the viscoelastic properties of materials prepared with a 10 % of molar stoichiometric imbalance, in isocyanate or thiol groups were evaluated at elevated temperatures.

List of abbreviations

A	Area/Pre-exponential factor
ATR	Attenuated total reflection
BG	Base generator
CAN	Covalent adaptable network
CFRP	Carbon fibre reinforced plastics
CTE	Coefficient of thermal expansion
Cp	Heat capacity
DBN	1,5-diazabicyclo[4.3.0]non-5-ene
DBTDL	dibutyltin dilaurate
DBU	1,8-diazabicyclo[5.4.0]undec-7-ene
DGEBA	Diglycidyl ether of bisphenol A
DMA	Dynamical mechanical analysis
DMAP	4-(N,N-dimethylamino)pyridine
DSC	Differential scanning calorimetry
DTGA	Derivative of thermogravimetric curve
E	Elastic modulus/ Young modulus/ Tensile modulus
$\mathbf{E_a}$	Activation energy
E'	Storage modulus/ Relaxed modulus
E''	Loss modulus
$\mathbf{E'_g}$	Storage modulus at glassy region
$\mathbf{E'_r}$	Storage modulus at rubbery region
F	Force
$\mathbf{F_{SR}}$	Recovery force
FTIR	Fourier transform infrared spectroscopy
FWHM	Full width at half maximum
G	Shear modulus
G'	Elastic shear modulus
HDI	Hexamethylene diisocyanate
HMDI	4,4'-Methylene bis(cyclohexyl isocyanate)
HV	Vickers hardness

IPDI	Isophorone diisocyanate
J	Heat flux per unit area/Joule
K	Kelvin degree
L	Length
m	Gradient of the slope/Meters
min	Minutes
Mt	Million metric tons
M_w	Molecular weight
phr	Parts per hundred of resin
PDMS	Poly(dimethylsiloxane)
PETMP	Pentaerythritol tetrakis (3-mercaptopropionate)
PTIL	Poly(1,2,3-triazolium)
PTSA	p-toluenesulfonic acid
PTU	Poly(thiourethane)
PU	Poly(urethane)
R	Gas constant
R_f	Shape fixity ratio
R_r	Shape recovery ratio
s	Seconds
S3	Trimethylolpropane tris(3-mercaptopropionate)
SM	Shape-memory
SME	Shape-memory effect
SMP	Shape-memory polymer
SRE	Stress-relaxation experiment
t	Time
T	Temperature
$T_{2\%}$	Temperature of decomposition for a 2% weight loss
T_g	Glass transition temperature
$T_g^{E'}$	Onset Temperature
T_m	Melting temperature
T_{max}	Maximum temperature
T_{tans}	Transition temperature

$T_{tan\delta}$	Temperature of maximum of the tan δ peak
T_v	Topology freezing temperature
TBD	Triazabicyclodecene
TEA	Triethylamine
TDI	Toluene 2,4-diisocyanate
TGA	Thermogravimetric analysis
V_r	Shape-recovery velocity
W_{rel}	Relative work output
WLF	William-Landel-Ferry
x	Conversion
°C	Celsius degree
1-MI	1-Methyl imidazole
3D	Three dimensional
σ	Stress
σ_0	Initial stress
σ_b	Stress at break
η	Viscosity
τ	Relaxation time
τ*	Characteristic relaxation time
ΔH	Enthalpy of the curing process

Chapter I

Introduction and Objectives

I-1 Polymers

Polymers, commonly known with the generic term “plastics”, are nowadays key materials in many industrial sectors and in our daily life. The word "polymer" is derived from the Greek words “polis” (many) and “meros” (part). Therefore, polymers are materials which consist of large molecules whose structure is made up of several smaller repeating units, called monomers. They are used in a great number of applications and fields such as packaging, textile, automotive, building, aerospace or pharmacy. The broad applicability of these materials is due to their low cost and high performances, which arise from the combination of several properties, among others: easy processing, versatility, durability and high strength to weight ratio.

The production of plastics has continuously increased over the last 60 years from the 1.7 million metric tons (Mt) produced in 1950 to 348 Mt in 2017.[1] However, the mismatch between the increasing of the production rate and an adequate result in waste management has led to a serious environmental problems.[2,3] For this reason, in 2018, the European Commission communicated the “European Strategy for Plastics in a Circular Economy”, emphasizing the need of improved design and production of plastics to facilitate reuse, repair, and recycling.[4,5] From the data provided by Geyer *et al.*[6] , from 1950 to date about 6000 Mt of plastic waste has been generated and around 5000 Mt of them has been discarded in landfills or in the natural environment, as it is shown in the following graph (Fig. I-1).

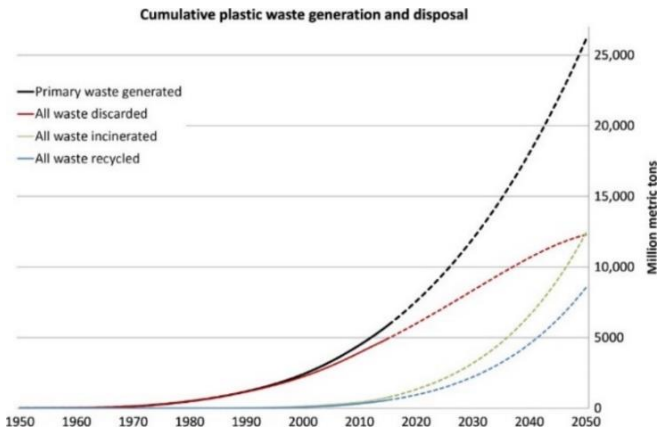

***Figure I-1**. Cumulative plastic waste generation and disposal, in Mt. Solid lines show historical data from 1950 to 2015; dashed lines show projections of historical trends to 2050, by Geyer et al.[6].*

Polymeric materials can be classified following different criteria. To give few examples, polymers can be classified according to their chain architectures as linear, branched or crosslinked, among others. They can further be divided according to their polymerization mechanism as polyaddition, polycondensation or ring-opening, or according to their origin source as natural, semi-synthetic and synthetic polymers.[7]

Since in the present work we are mainly interested in the behaviour of polymeric materials with the temperature, in order to study their reprocessability, recyclability and their ability to respond to a stimulus, we will use as the classification criterium, their response to the temperature. Depending on their thermal behaviour, polymers are divided into two main classes: thermoplastics and thermosets.

I-1.1 Thermoplastic and thermosetting polymers

Thanks to their easy preparation and high capability to flow under the action of heat and pressure, thermoplastics represent roughly 80% of the total plastic consumption and of polymeric materials used nowadays.[8] This polymer class consists of macromolecular chains of very large molar mass, not covalently linked together but entangled, leading to topological restrictions of molecular motion produced by other chains, Figure I-2A. When heated, the chains are able to diffuse by a phenomenon called reptation, leading to an increase in their fluidity. Upon cooling, the polymer hardens and assumes the shape of the mould. Thermoplastics can withstand multiple heating and cooling cycles without serious damage, allowing for reprocessing and recycling.

Depending on the degree of crystallinity of thermoplastic polymers, they can exhibit, during cooling, hardening by glass transition or crystallization. Semi-crystalline and amorphous thermoplastics at low temperatures, below glass transition, exist as hard and rigid glasses. As the temperature increases, the polymer chains are free to diffuse, and the polymer starts to flow. Semicrystalline polymers present a sharp melting point after which they can flow, while, in the case of amorphous thermoplastics, the state of the polymer changes from glass to a rubbery elastomer first, and then to a viscous melt that can flow.[9-11] The classic evolution of the elastic modulus of amorphous thermoplastic polymers is presented in Figure I-2B.

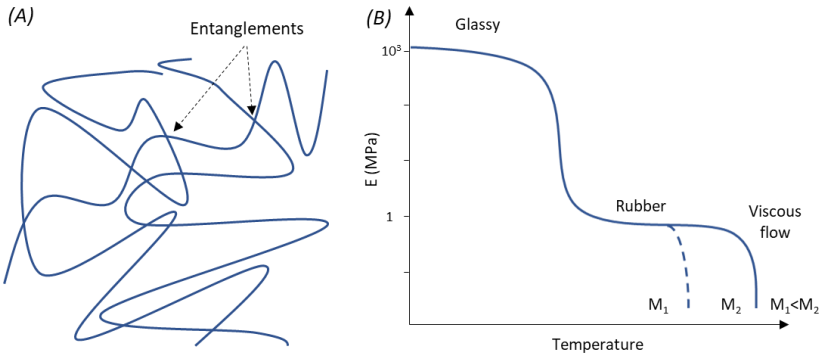

Figure I-2. *(A) Schematic image of a thermoplastic molecular structure. (B) Typical evolution of elastic modulus against temperature of amorphous thermoplastic polymers of different molecular weight.*

The ability to flow allows to process them via industrial techniques such as extrusion and injection moulding and to recycle them in a relatively easy way. As drawback, thermoplastic polymers are relatively weak, and they can suffer degradation by heat, solvents and environmental attack and their mechanical properties are reduced on increasing temperature.

Thermosets, on the other hand, are crosslinked polymers that have a three-dimensional network, as a result of an irreversible polymerization process, known as curing. The curing process usually occurs in a mould, designed to obtain the final desired shape because, once the reaction is complete, thermosets cannot be reshaped or reprocessed. In this case, the molecular weight of the structure is infinite at the molecular level and the chains become covalently linked one to the other in the curing process, resulting in a rigid and densely crosslinked structure as depicted in Figure I-3A. The resulting polymer networks are characterized by being hard, infusible, and insoluble in any organic solvent. Only a small fraction of the material (the sol fraction, if any) can eventually dissolve, whereas the linked structure (the gel fraction) can only swell in the presence of a proper solvent.[12]

Thermosets, due to their crosslinking points, become softer when heated above their glass transition temperature (T_g), but they never flow. Thermosets present a T_g higher than room temperature, and elevated T_gs usually correspond to high mechanical and thermal properties. Below T_g, the materials have excellent mechanical properties as high elastic modulus and hardness. Above T_g, the polymer networks present a theoretically infinite rubber plateau, up to thermal degradation as represented in Figure I-3B.

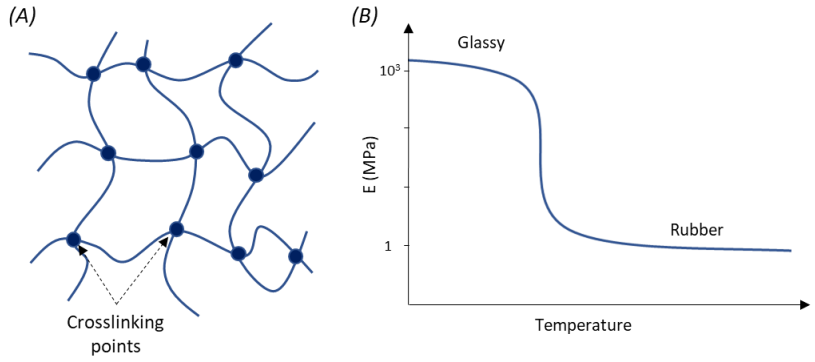

Figure I-3. *(A) Schematic image of a thermosetting molecular structure. (B) Typical evolution of elastic modulus against temperature of a thermosetting material.*

The superior mechanical and thermal properties of these polymers allow them to be extensively used in industrial applications where high mechanical performances and dimensional stability are required, especially at elevated temperatures. Thermosets currently account for 15-20 % of global plastic production.[13] However, their permanent three-dimensional structure hinders reshaping, reprocessing, or recycling once they are cured, resulting in a serious environmental issue. For these reasons, they are considered among the most difficult materials to be recycled.[14]

I-2 Recycling of polymers

In view of the increasing amount of polymer waste generated, the recycling of plastics at the end of their service life is extremely important to prevent these materials from being disposed in landfills and to preserve the environment. Usually, polymers need hundreds of years to degrade under normal environment conditions.

To improve waste management, the European Union[15,16] emanated guidelines to optimize the use and management of plastics. The following hierarchy has been established in waste management, which will be applied in order of priority to reduce the amount of waste described.[17,18]

1. Prevention (measures taken before a material gets disposed, to reduce the overall amount of waste)

2. Preparing for reuse (checking, cleaning, or repairing materials that can be re-used without any other pre-processing)

3. Recycling (any recovery operation by which products or materials are reprocessed into products, materials, or substances whether for the original or other purposes)

4. Other recovery (i.e., energy recovery)

5. Disposal (any operation which is not recovery)

There are mainly four types of recycling processes: reuse of the polymer, mechanical, thermal and chemical recycling (Figure I-4). Thermoplastics can be remelted and reprocessed into new structures using heat and pressure, which lend themselves to relatively easy recycling technology, while thermosets are not appropriate for various types of recycling processes due to their permanent network structure.[19] The following sections will provide a description of the various recycling methods for both types of polymers.

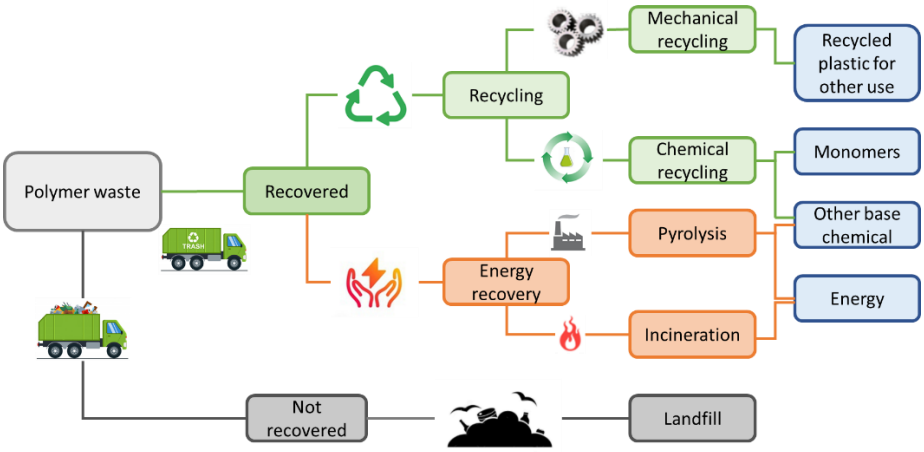

***Figure I-4**. Roadmap of the polymer waste treatment, from waste to obtain new resource.*

I-2.1 Recycling of thermoplastic

The first option to recycle thermoplastic polymers (primary recycling) consists of a minimization of the waste generated reusing in-plant scrap plastics for the same application or for another application where lower mechanical performances are required, without any special treatment. This process remains the most popular, as it ensures simplicity and low cost, uncontaminated wastes are reintroduced to the extrusion cycle in order to produce similar products.[17]

Secondary recycling is mechanical, that is a post-consumer recycling. In this case, the material to be recycled may have been contaminated during its use, as a result additional steps are needed before to reintroduce thermoplastics in the manufacturing line. Commercial thermoplastic polymers are first classified, cleaned, washed and reduced in suitable size to be later melted and processed by industrial techniques.[20]

Chemical recycling (tertiary recycling) is defined as the process leading to total or partial depolymerization of polymers to the monomers, oligomers or other chemical substances. The word “chemical” is employed as a change in the chemical structure of the polymer occurs during this procedure, the plastic materials are transformed

into smaller molecules using solvents, temperature, pressure, catalyst, or a combination of them.[21]

Chemical recycling is usually solvent assisted to facilitate depolymerization and break down the polymer matrix into lower molecular weight compounds, the chemical nature of which can be correlated to the original material. An interesting approach that is classified as tertiary recycling is the pyrolysis, which consist of a thermal degradation of the organic materials in inert atmospheres.[22,23] Pyrolysis needs high temperatures and long decomposition times requiring a high deal of energy to decompose the polymer matrix, making it less economically competitive compared to other existing processes.[24,25]

The last option, to prevent plastic waste from being deposited in landfills, is the incineration or quaternary recycling. This process leads to volume reduction of waste through incineration, recovering its energy content, since polymers have a good calorific value about 30-40 MJ/kg. The disadvantage of incineration is the emission of numerous toxic substances, most of which are released into the atmosphere as dioxins.[26]

I-2.2 Recycling of thermosets

All current recycling technologies focused on thermoplastics take advantage of their melt processability or of their solubility in an appropriate solvent. Thermosetting polymers compared to thermoplastics are much more difficult to be recycled due to their irreversible covalent networks, which is unfavorable for their sustainable use.[27]

Mechanical recycling processes (primary or secondary) are not applicable to traditional thermosetting wastes, due to their permanent network structures and lack of processability. Nevertheless, they can be pulverized into particles or powders via shredding, grinding, or milling and used as filler or reinforcement for new applications.[28] The use of recycled thermosets as fillers is not economically competitive with conventional fillers such as calcium carbonate and silicates which are indeed cheaper.[14]

Chemical recycling technologies can also be applied to thermosets and composites, pyrolysis and solvolysis are the most studied techniques to recycle thermosets and especially thermosetting composites. Pyrolysis is an interesting technology for thermosetting waste treatment, as they are difficult to depolymerize in a reactive solvent. By this technique most thermosets can effectively be thermally degraded, but these processes are typically very energy intensive and costly, often requiring temperatures over 400°C.[29] Solvolysis is the preferred recovery procedure, because it is less expensive as lower temperatures are generally necessary to depolymerize the thermoset compared to pyrolysis. Solvolysis of crosslinked polymers consist of use an appropriate reactive solvent to depolymerize the material by cleavage of covalent

bonds in the three-dimensional network, often in presence of catalyst to facilitate the process.[30] Industrially, it is mainly applied with polymer composites, allowing in some cases to recover the fibres breaking down the polymeric matrix.[31] Solvolysis can play an important role in developing a circular economy for thermoset, but it is still difficult to apply since thermoset present high resistance to many solvents. To expand the use of this technique new degradable thermosets stable during their useful lifetimes are needed. For example, polymers with ester, carbonate or acetal groups have been proposed. These materials can be degraded in alkaline or acid conditions, respectively.[19] Many chemical recycling technologies still need to be improved to reach their full potential, since recycling of thermosets may involve strong chemicals and relatively high temperature for a long-time frame. These issues limit the large-scale applications of the chemical recycling of thermosets and their composites.[32]

Considering these difficulties in recycling thermosetting materials, most of them are landfilled or incinerated after their useful life. Incineration for energy recovery does not involve material recovery, and it is not classified as a suitable recycling technology.[33] Therefore, developing strategies to recycle crosslinked polymers effectively and conveniently remains a remarkable challenge.

An alternative pathway to reduce the thermosetting waste generated is to extend the lifetime of the materials, repairing them during their service life, adopting self-healing systems. Self-healing polymers are materials capable of healing internal cracks or damage automatically without any external intervention.[34] To do that usually microspheres containing healing agents are dispersed in the thermosetting polymer. By this method, when a crack occurs the microspheres break and the healing agent is released, fixing the crack in the material.[35,36] This method is effective only for a limited time because once the microspheres are exhausted, no further healing process can occur.

A more interesting approach to obtain self-healing polymers is the use of dynamic chemistry, designing polymers capable of repairing molecular and macroscale damages via a temporary local increase in the mobility of polymeric chains.[37,38]

I-3 Dynamic covalent chemistry

In recent years, significant advances have been made to repair, recycle and reprocess crosslinked polymers, and to break the barrier that separates thermoplastics from thermosets on recycling issues. As we have seen, the recycling of thermosets remains a harsh task, very complex and energy-intensive and often the original polymer architecture is damaged after the recycling process.[39] To solve these problems, dynamic covalent chemistry has attracted great attention and reversible interconnections have been incorporated into the network structure.[40-44] The dynamic covalent chemistry includes a group of chemical processes that allow the molecular

constitution of a chemical system to undergo changes over time or in response to stimuli.

***Figure I-5**. Representation of the concept of covalent adaptable network.*

The incorporation of appropriate dynamic covalent bonds in polymer networks is a good strategy to obtain easily recyclable and re-usable thermosetting materials without losing the original polymer structure.[45] These bonds provide dynamic features such as adaptability, malleability or self-healing properties. Covalent adaptable networks (CANs) contain enough reversible covalent bonds to enable the crosslinked structure to respond chemically to an applied stimulus. The dynamic covalent bonds can be broken and reformed under the appropriate conditions without irreversible side reactions.[46]

Dynamic covalent chemistry is not a new concept in the polymeric field, already in 1956 a pioneering work of Tobolsky *et al*.[47] showed how poly(urethane)s could experiment chemical stress relaxation at high temperature, anticipating the current concept of CANs. The recent rediscovery of this concept is due to the extraordinary work of Leibler and co-workers[48,49] that reported the possibility to obtain malleable epoxy networks. These materials can be reshaped, self-welded and recycled, opening new frontiers to recycle and reprocess thermosetting polymers. After Leibler's discovery, more and more materials and chemistries in this field have been investigated and reported in the literature.[50-52]

CANs can be classified into two main categories, according to their exchange mechanism: dissociative and associative, and further divided according to the consecutive or simultaneous mechanism of the interchange reaction.[53]

I-3.1 Dissociative CANs

Dissociative CANs are crosslinked networks with reversible covalent bonds, in which linkages first dissociate and then reform in the same place or in another (Figure I-6) autonomously or under a stimulus such as light or heat. During the exchange mechanism, there is a decrease of the network connectivity and crosslinking density, with an important change in the macromolecular structure, which can enable the polymer to flow without complete depolymerization of the network.

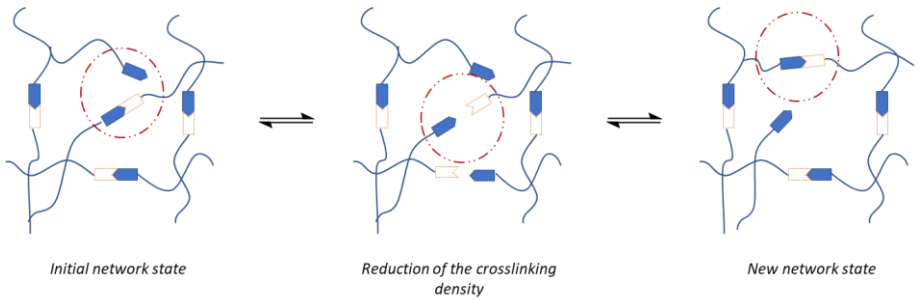

Figure I-6. *Schematic representation of dissociative reversible covalent chemistry. Inspired by the graph published by Winne et al.*[52].

CANs that follow a dissociative exchange mechanism, via application of a stimulus, can tune the reaction equilibrium in both directions: from highly to lowly crosslinking state and vice-versa.

Increasing the temperature, the chemical reaction equilibria can shift to the initial reactive moieties, converting the rigid thermoset into a low-viscosity material with a reduction in the crosslinking density. This change in the network structure results in a change of viscoelastic properties, and in some cases with a sudden drop in viscosity, and the material could become soluble in the presence of an appropriate solvent, as is typically observed in thermoplastic materials. Upon cooling, the reaction moves to the formation of covalent linkages, and the network is formed again, whereby the polymer recovers the superior properties of thermosetting materials such as stiffness and insolubility. This reversion allows the network to be reprocessed and repaired extending the utility life of the polymer.

Different dissociative chemical processes have been reported in the literature such as: thiol-Michael addition[54] or disulfide exchange,[55-57] among others, but the most extensively explored dissociative reversible exchange mechanisms is the Diels-Alder (DA) reaction. The DA reaction, discovered by Otto Paul Hermann Diels and Kurt Alder in 1928,[58] is a concerted [4+2] cycloaddition reaction between a diene and dienophile to form a cyclohexene adduct. The reaction can be reversed at elevated temperatures via a dissociative retro-Diels-Alder (rDA) reaction.

The first work reported in self-healing of thermosets based on DA reaction was published by Chen *et al.*[59] introducing the concept and starting the new trend in self-healing materials.[60] The activation temperatures of the DA and retro-DA reactions depend largely on the choice of the diene and dienophile structures, the furan-maleimide system is the most often selected due to its suitable temperature profile for reversible binding.[61,62] A schematic representation of the reaction is shown in Figure I-7.

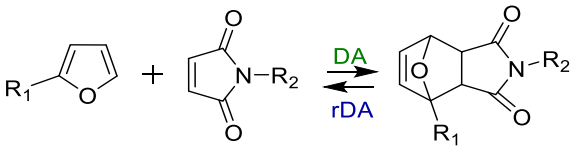

***Figure I-7**. Reversible Diels-Alder reaction implying furan and maleimide starting compounds.*

Although these strategies offer broad possibilities to combine reprocessability, self-healing and excellent welding performance of thermosetting polymers, their large application is limited because of the abrupt viscosity drop of the material during the exchange process.[63,64]

I-3.2 Associative CANs

The other class of crosslinked dynamic polymers is the associative CANs. These polymers show a fixed crosslinking density during the exchange of covalent bonds, a bond dissociates while a new one is formed, and the number of bonds remains theoretically constant without any drastic drop in the viscosity profiles. The final network shows identical chemical functionality with different connectivity.

The associative exchange mechanism can occur by following two different pathways: stepwise (Figure I-8A) or concerted (Figure I-8B).[52] In Figure I-8, the exchange mechanisms are presented in absence of catalyst, but the different reactions can also occur in presence of a catalyst, which is sometimes essential to facilitate the exchange reaction and to reach the thermodynamic equilibrium in a practical time.

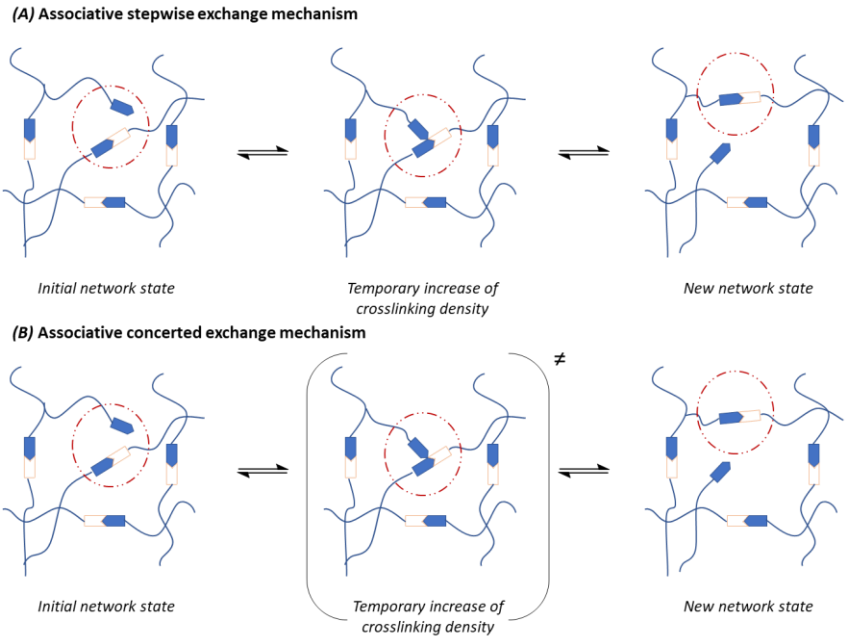

***Figure I-8.** Schematic representation of (A) stepwise and (B) concerted associative reversible covalent chemistry. Inspired by the graph published by Winne et al.[52].*

In the first scenario the exchange reaction proceeds through the formation of short-lived intermediate states, where firstly occurs an addition reaction followed by an elimination reaction. This gives an overall substitution effect leading to a change in the network topology without altering crosslinking density.

In a concerted exchange mechanism, the bond breaking and bond making occur in a single step, without involving any intermediate state, only going through a transition state always keeping constant the crosslinking density. At the associative CANs belong the new class of materials that have been called as "vitrimers" by Leibler and co-workers in 2011.[49]

I-3.3 Vitrimers

Leibler and co-workers, in their seminal study,[49] developed associative covalent-adaptable networks that can flow once heated, exhibiting a viscosity-temperature relationship comparable to vitreous silica, which inspired Leibler to call them "vitrimers".

Vitrimers are covalently linked networks with dynamic bonds that allow the network to change its topology via exchange reactions keeping constant the number of chemical bonds. Upon heating, vitrimers behave like a viscoelastic liquid, but at the same time they do not dissolve in good solvents, even at elevated temperature, showing only a limited soluble fraction.

The constant network functionality allows the material to remain insoluble and show a gradual Arrhenius-type viscosity change with temperature, as it is represented in Figure I-9, and observed in typical inorganic silica materials.

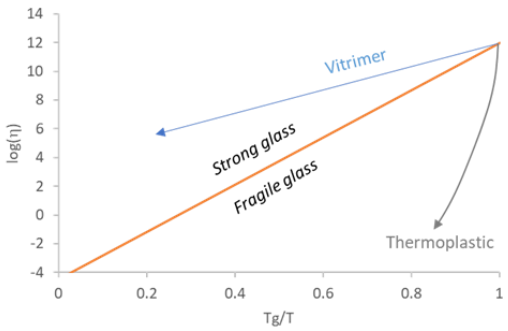

***Figure I-9**. Angell fragility plot of the logarithm of the viscosity as a function of the inverse temperature, scaled to Tg, for thermoplastics and vitrimers. Inspired by the graph published by Denissen et al.[53].*

Figure I-9 shows the Angell fragility plot[65] where thermoplastics, below the silica reference, are characterized by a very fast decrease in viscosity close to their T_g, while vitrimers that are above the silica reference show an Arrhenius-like dependence of the viscosity, which results in a gradual viscosity decrease similar to vitreous silica.

This gradual decrease in the viscosity allows them to be processed in a wide range of temperature without a precise control of temperature. These properties open up new possibilities for thermosetting materials to be used in industrial processes with their easy shaping without the need for a specific mould to prevent loss of structural integrity.[66] In particular, this ability to flow without losing their network integrity allows vitrimers to be recycled easily by hot pressing. In general, vitrimeric materials can be ground into small pieces and then reformed under heat and pressure. The recycled material shows the same or comparable thermal and mechanical properties of the original one.

I-3.4 Transition temperatures in vitrimeric materials

As shown in the previous section the gradual decrease in viscosity distinguishes vitrimers from thermoplastic and some dissociative CANs.

To describe the viscoelastic behaviour of vitrimers, in addition to the glass transition temperature (T_g), a new ideal transition temperature has been defined: the topology freezing transition temperature (T_v). The T_v describes the characteristic transition from a viscoelastic solid to a viscoelastic liquid and it is defined as the temperature at which the melt viscosity reaches 10^{12} Pa·s. In Figure I-10, the logarithm of the viscosity as a function of the temperature is represented for vitrimers and depending on the position of the T_v, above or below the T_g, it is possible to observe two different scenarios.

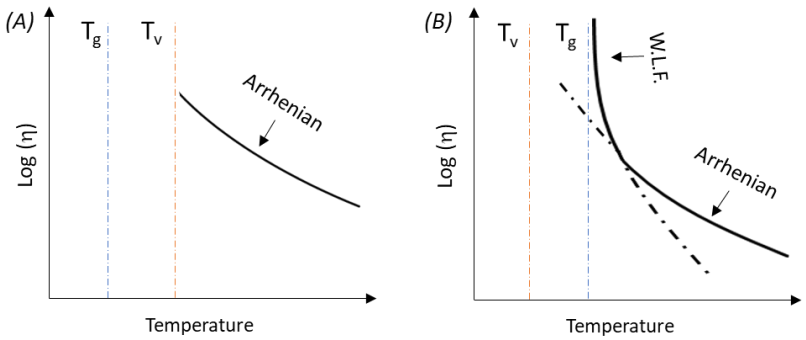

Figure I-10. *Representation of the logarithm of the viscosity as a function of the temperature for vitrimers with (a) $T_v>T_g$ (b) $T_v<T_g$. Inspired by the graph of Denissen et al.*[53]

In both scenarios, the covalent exchange takes place after T_g, since in the glassy state all the segmental movements are hindered. In the first case, Figure I-10A, the T_v is located above the T_g and the vitrimer behaves like a classic thermoset until T_g, changing its state from the glassy to the rubbery. Then, exceeded the T_v, the exchange reactions are fast enough to change the network topology and the polymer flows like a viscoelastic liquid with a viscosity decrease that follows an Arrhenius temperature dependence.

In the second case, Figure I-10B, the T_v is located below the T_g. Exceeding the T_g, the bond exchange is already fast, the vitrimer evolves rapidly from a glassy solid to a viscoelastic liquid and the bond exchange may occurs for a period of time via William-Landel-Ferry (WLF) behaviour, and then it follows an Arrhenius kinetics.[67,68] Importantly, T_v cannot be considered as a specific threshold of the material, but as a reference temperature which is characteristic of the specific dynamic exchange mechanism within the molecular design.[69] In fact, the position of the T_v gives a reference of how fast occurs the relaxation process, always above T_g, since the exchange reactions below T_v occur slowly, depending on the observation time, while above T_v we can process the vitrimer in shorter time.

I-3.5 Vitrimer-like polymers

Recently, it has been noted that dissociative CANs also can exhibit an Arrhenius viscosity relationship during stress relaxation experiments without any sudden drop in viscosity during the covalent bond exchange. In addition, this category of polymer shows a stable rubbery plateau at elevated temperature after the glass transition temperature. These considerations make these materials difficult to distinguish from vitrimers, thus it was introduced another class of CANs the "vitrimer-like polymers".[70,71]

In these networks, during the exchange mechanism, the reassociation of the bonds remains favoured in reference to the dissociation due to the high rate of bond reformation or the large equilibrium constant in favor of the associated state at high temperatures.[72] In such conditions, the stress-relaxation is governed by the bond exchange and these materials show rheological behavior indistinguishable from vitrimers. Moreover, the network integrity is well maintained after grinding and hot-pressing the polymer, similar to what happens with vitrimers.[73]

The main characteristic that could distinguish polymers that exhibit vitrimer-like properties from vitrimers is the possibility to partially o complete dissolve the network in an appropriate solvent.[52] These materials are difficult to dissolve in most solvents and a precise selection of the solvent and temperature is required to completely dissolve the sample. The possibility of achieving a complete dissolution of the CANs could constitute an alternative chemical recycling route in reference to the mechanical recycling of the vitrimers, which would make vitrimer-like polymers more sustainable than vitrimers.

I-4 Bond exchange mechanisms

In the last decades the concept of covalent adaptable networks has attracted more and more attention to relieve the environmental pressure on thermosetting materials. To date, several reversible covalent-chemistries have been explored and used to synthesized reprocessable crosslinked polymers, very often starting from the

rediscovery of "old" chemical reactions. In this section, an overview will be given of the most used chemical exchange processes to obtain materials that exhibit vitrimeric properties, based on different reviews.[13,52,53,60,67,74-76]

I-4.1 Transesterification

The first vitrimers reported by Leibler and co-workers[49] in 2011 were based on the well-known transesterification reaction. The authors synthesized elastomeric and hard epoxy resins, by reacting diglycidylether of bisphenol A (DGEBA) with a carboxylic acid or anhydride, in the presence of zinc acetate as the catalyst.[49] The resulting thermosets, upon heating, were able to rearrange the network topology via transesterification reaction as it is depicted in Figure I-11. Importantly, for activating the transesterification of an ester, the presence of free hydroxyl groups was described as essential.

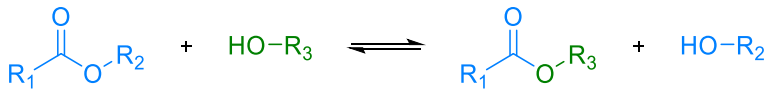

Figure I-11. *Transesterification reaction between esters and hydroxyl moieties.*

Successively, the Leibler's group demonstrated the possibility to control, in an effective way, the kinetics of the exchange reaction in epoxy vitrimers by changing the amount and structure of the external catalyst. It was observed that on changing the catalyst, the rate of relaxation and the activation energy of the relaxation process were clearly affected. Nevertheless, on increasing the catalyst loading, only the relaxation rates were increased while the activation energies remained almost constant.[48,77]

After these discoveries, the transesterification reaction gained a lot of interest in the scientific field, also for the extensive use of epoxy-based materials in a great number of industrial applications.

In 2013, Williams and co-workers[78] synthesized an environmentally friendly epoxy resin from renewable chemical feedstock able to relax the stress without the use of any catalyst. Also, Han *et al.*[79] prepared a catalyst-free epoxy vitrimer, reacting a hyperbranched epoxy with succinic anhydride, demonstrating that catalyst-free transesterification is possible by increasing the concentration of hydroxyl moieties.

In addition, the possible use of epoxy vitrimers in composite materials was demonstrated by Tournilhac and co-workers[80] who synthesized an epoxy vitrimer that is compliant with continuous fibre composite technology. Also, Legrand *et al.*[81] demonstrated the possibility to incorporate silica nanoparticles in the epoxy matrix without loss of vitrimeric properties.

To date, the transesterification is the most studied exchange mechanism to obtain vitrimers, thanks to the wide availability of monomers like alcohols, acids, epoxides

and ester containing compounds. In this way, the concept of transesterification has been extended to other polyesters which intrinsically provide abundant ester groups.[82-86]

I-4.2 Transcarbamoylation

Polyurethanes (PU)s are one of the most common polymers used to obtain thermosets and elastomers, therefore the investigation performed on the dynamic nature of carbamate bonds has been very important to reduce their environment impact.

The vitrimeric characteristics of PUs were demonstrated for the first time in 2015 by Dichtel and co.,[87] that investigated the reprocessability of polyhydroxyurethane (PHU) networks, taking inspiration from the "old" works of the Tobolsky's group on the stress relaxation in crosslinked polyurethanes.[47,88]

Dichtel's group synthesized PUs by the reaction of polyfunctional cyclic carbonates with amines providing one hydroxyl group per carbamate linkage, without the use of any catalyst. This methodology is more environmentally friendly and safer because of the elimination of isocyanates as starting monomers. These materials underwent topological exchange at elevated temperatures, via hydroxyl mediated transcarbamoylation (Figure I-12), within a large reprocessing time between 4-8 h at 160 °C. However, the mechanical properties of PUs after reprocessing were only recovered in a proportion of around 75%.[87,89]

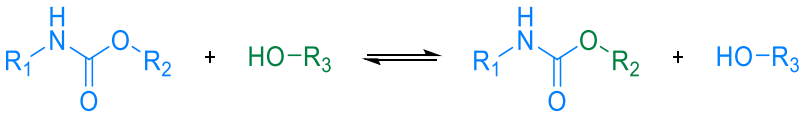

***Figure I-12**. Hydroxyl mediated transcarbamoylation reaction between urethanes and hydroxyl groups.*

In 2016, Xie and co-workers[90] discovered a more direct and practical approach to reprocessing PUs. They demonstrated that PUs without an excess of hydroxyl groups could relax stress via transcarbamoylation reaction in the presence of a catalytic amount of dibutyltin dilaurate (DBTDL), as represented in Figure I-13. This explanation was supported by a stress-relaxation study on different PUs varying the concentration of the residual hydroxyl groups. They observed a relaxation rate, which was independent on the amount of free hydroxyl groups in the network structure. The carbamate exchange reaction was also proved through chemical studies performed on model compounds.[90]

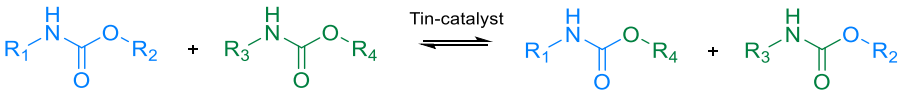

***Figure I-13.** Tin-mediated transcarbamoylation reaction between urethane moieties.*

Based on the transcarbamoylation interchange, Peiyao *et al.*[91] , demonstrated the ability of the PUs to be recycled, in the presence of DBTDL, recovering around 85-90% of the original stress at break.

Trying to clarify the mechanism of the dynamic urethane bonds, Dichtel's group[92] performed a mechanistic study of the exchange mechanism in polyurethane networks in the presence of another Lewis acid, tin (II) octoate. The urethane reversion to isocyanate and alcohol was demonstrated to be the main responsible of the exchange mechanism. For these materials, a dissociative mechanism was proposed, in absence of free hydroxyl group in the network, although the relaxation studies showed a vitrimer-like behaviour without any sudden decrease in viscosity, fitting an Arrhenius model.

In addition, Sardon and co-workers[93] demonstrated that the dynamic nature of polyurethane networks is dependent on different factors: isocyanate type, NCO/OH ratio, and type of catalyst. They proposed two different exchange mechanisms: associative in the presence of free alcohol groups and dissociative by means of urethane linkages dissociation. They found that DBTDL was able to accelerate both types of exchange mechanisms, while p-toluenesulfonic acid (PTSA) effectively catalyzed only the associative exchange and 1,5,7-triazabicyclodec-5-ene (TBD) was inefficient in both cases.

Very recently, Dichtel's group demonstrated that commercial PU thermosets, without any excess of hydroxyl groups, can be reprocessed via post-synthetic introduction of DBTDL, a scheme of the experimental procedure is proposed in Figure I-14. This process imparts malleability in crosslinked polyurethane via direct carbamate exchange, in agreement with the previous discoveries.[94]

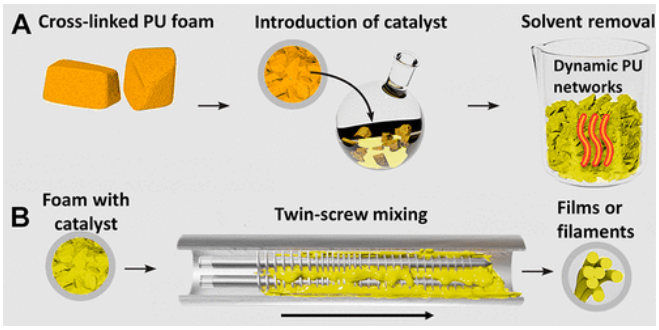

Figure I-14. *(A) Method of introduction of catalyst into static PU foams (B) Scheme of microcompounding catalyst-loaded PU foam into filaments, by Dichtel et al.*[94]

I-4.3 Imine-amine exchange

Imines, referred as Schiff bases, are formed by the reversible condensation reaction of primary amines with aldehydes (Figure 1.15a).[95] Their dynamic nature has been known for a long time,[96,97] in particular imine can show dynamic behaviour via associative or dissociative pathways.[53]

The associative dynamic character is based on either metathesis (imine-imine interchange) (Figure I-15b), or transamination (imines react with amines) as depicted in Figure I-15c. To follow an associative mechanism, it is essential to previously remove the water produced in the preparation of the imine network, since imines react reversibly with water (Figure I-15a); or alternatively to start from functional monomers with imine groups in their structure. This last strategy is the easiest, when synthesizing thermosets with imine structures.

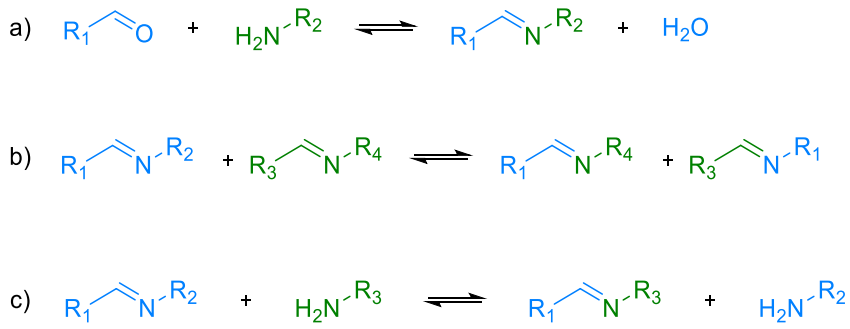

Figure I-15. *Reversible reaction of imine: (a) condensation reaction, (b) imine metathesis and (c) transamination.*

The potentiality of polyimines as vitrimeric materials was extensively studied by Zhang and co-workers.[98-100] They synthesized recyclable crosslinked polyimines via condensation of polyfunctional amines and aldehydes. These materials exhibited Arrhenius type malleability through imine exchange or imine metathesis at high temperature. Additionally, these materials were reprocessed at a lower temperature by adding water through imine condensation/hydrolysis, leading to a green chemical recycling process.[98] In 2016 they found that the imine bond exchange is mainly catalyzed by residual dangling primary amine chain ends, present in the network, via transamination reaction. In accordance with the previous results, Caccia *et al.* showed that even a small amount of primary amines can produce a transamination exchange reaction.[101] In addition, imine chemistry is also interesting since polyimine vitrimers could be synthesized from biobased compound, as vanillin.[102-105] For example, Avérous and co-workers[104] synthesized a family of biobased polyimine vitrimers without an excess of amine. The malleability was achieved via exchange of imine linkages. Moreover, they accelerated the relaxation rate of the materials by reducing

the crosslinking density, pointing out that the relaxation properties can be tuned by only changing the physical properties of the networks.

I-4.4 Transamination of vinylogous urethanes

Du Prez's group exploited the transamination reaction in vinylogous urethane networks.[106] Vinylogous urethane vitrimers were synthesized via condensation reaction of polyfunctional amines and acetoacetate esters in the presence of an excess of amine, which is required to participate in an associative exchange mechanism. The exchange reaction occurred at temperatures above 100 °C, also in absence of catalyst, via rapid addition/elimination reactions between chain-end amines of vinylogous urethane and primary amine, as it is represented in Figure I-16.

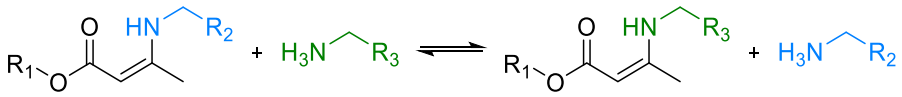

Figure I-16. *Transamination reaction between vinylogous urethanes and amines.*

The vinylogous urethane exchange reaction could be accelerated by addition of acid and base additives.[66] Depending on the acidic or basic catalyst selected and the amount of free amines, two different chemical exchange mechanisms could be observed. In the protic pathway, the mechanism occurred via an iminium intermediate, while in aprotic conditions it passed through a direct Michael addition mechanism.[107]

Taplan *et al.* obtained a vinylogous urethane elastomer that relaxed in only 0.3 s at 160 °C by adding proton donor species (i.e. p-toluenesulfonic acid).[108] This allowed reprocessing for the first time a vitrimer by means of an industrial procedure via extrusion techniques.

Vinylogous urethane or imine based materials are quite promising as malleable crosslinked materials, notably for their fast relaxation rate compared to other types of covalent adaptable networks.

I-4.5 Olefin metathesis

In 2012, Lu *et al.*[109] reported the use of olefin metathesis to generate adaptative and malleable polymer networks. In this study, polybutadiene was radically crosslinked using second-generation Grubbs ruthenium alkylidene catalyst. The malleability of the network is derived from the olefin metathesis reaction, which covalently shuffles C-C double bonds in the bulk of the network, as it is depicted in Figure I-17a. Moreover, Guan and co-workers also demonstrated the effect of the catalyst concentration on the relaxation behaviour of the materials.[110] As expected, the higher the catalyst load, the higher self-healing properties were reached.

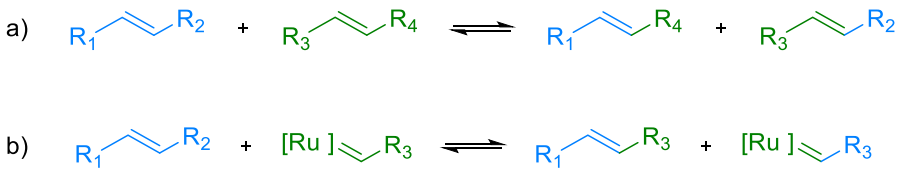

Figure I-17. *Olefin metathesis: a) between two olefinic compounds and b) by using a second generation Grubbs catalyst.*

These materials rapidly relax stress and can be reprocessed even at room temperature, due to the high activity of Grubbs catalyst, leading to a self-healing behaviour under ambient conditions (Fig. I-17b). However, since this exchange reaction is already active at room temperature the materials could display undesirable creep phenomena at service temperature. To solve this problem, the Guan's group significantly improved durability and mechanical properties of polyolefins containing Grubbs catalyst including hydrogen-bonding moieties in the network.[111]

Further developments on this chemistry were made using latent ruthenium catalysts. In this way, the reaction had to be activated by thermal or photo stimuli, resulting in a more robust polymeric material.[112,113]

I-4.6 Disulfide interchange

Recently, dynamic sulphur-based chemistries have been deeply implemented in the preparation of crosslinked networks to obtain degradable, reprocessable and self-healable materials. Tobolsky *et al.*[114,115] initially investigated sulphur containing materials in the 1960's, using the disulfide exchange to achieve stress relaxation in vulcanized rubbers.

In the last decades, several research groups incorporated disulfide moieties in epoxy thermosetting networks. In 1990 Tesoro *et al*. synthesized reprocessable and degradable thermosetting epoxy resins thanks to the ability of the disulfide bonds to cleave, reform, and exchange under certain conditions.[116,117]

Klumperman and co-workers investigated the self-healing ability of disulfide exchange, reporting that two different mechanisms can occur as represented in Figure I-18.[56,118]

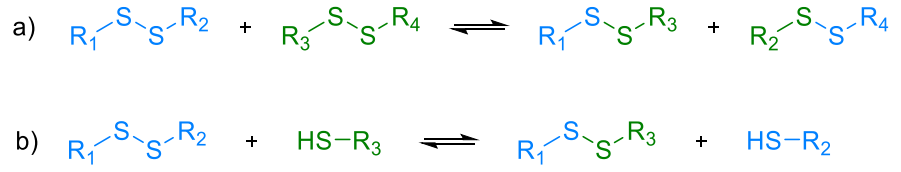

Figure I-18*. a) Exchange reaction between disulfides; b) Exchange reaction between thiol and disulfide.*

In a first work, they used the disulfide-disulfide exchange chemistry to introduce a self-healing ability in a covalently crosslinked rubber, Figure I-18a. Also, an associative exchange mechanism via an addition/elimination substitution with free thiols was also proposed, as it can be seen in Figure I-18b. However, as the free thiols can easily oxidate in oxygen atmosphere, these materials showed deterioration of the dynamic properties over time.[118]

The disulfide metathesis can be also photo activated, as demonstrated by the Rowan's group,[119] that obtained a photohealable polydisulfide network, in which cracks could be rapidly healed via ultraviolet light (UV) irradiation.

Odriozola and co-workers increased the bond exchange rate, in disulfide based thermosets, incorporating aromatic disulfides bridges in the network structure instead of aliphatic disulfides.[55,120,121]

In their first work,[120] poly(urea-urethane)s elastomers were reprocessed through aromatic disulfide metathesis at room temperature in absence of catalyst. They also incorporated aromatic disulfide moieties in epoxy matrices, obtaining 'dynamic'' epoxy resins that had mechanical properties equivalent to the reference epoxy counterparts, while displaying new features such as (re)processability, reparability and recyclability.[122]

I-4.7 Siloxane and silyl ether exchange

The equilibrium exchange of siloxane dynamic bonds was already explored in 1954 by Osthoff *et al.*,[123] which discovered that stress relaxation of crosslinked poly(dimethylsiloxane) (PDMS) elastomers can be triggered via acid or base catalyst at elevated temperature.[124]

Similar to other dynamic reversible reactions, McCarthy and co-workers[125] in 2012 rediscovered this "old" chemistry, synthesizing self-healing PDMS rubbers trough siloxane anionic equilibration, which is represented in Figure I-19. In this work, McCarthy qualitatively demonstrated the healing properties of the PDMS in presence of base catalyst.

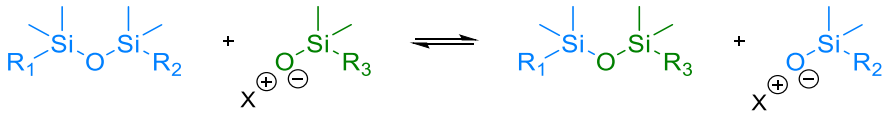

Figure I-19. *Siloxane silanol exchange reaction in basic medium.*

In 2017, Guan and co-workers[68] implemented Si-O based materials reporting the first example of a silyl ether exchange-based vitrimer, introducing a silyl ether linkage in a polystyrene network. The exchange occurred via an addition/elimination reaction in presence of free hydroxyl groups (Fig. I-20a) and the resulting vitrimer exhibited a fast relaxation in combination with a high T_g.

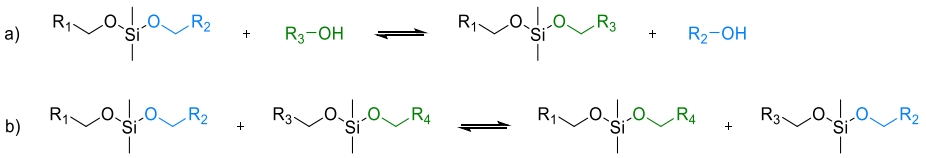

Figure I-20. *Exchange reaction between silyl ethers and alcohols; b) silyl ether-silyl ether exchange reaction.*

Two years later, Guan and co-workers[126] reported that silyl ether groups can directly exchange without the need of free hydroxyl groups, via metathesis reaction of silyl ether catalyzed by a Brønsted or Lewis acid catalyst, Figure I-20b. The resulting malleable thermosets showed exceptional thermal and oxidative stability, thanks to the absence of free alcohol moieties in the network, which can lead to possible side-reactions and to oxidation phenomena, especially at elevated temperature.

I-4.8 Boronic ester and dioxaborolane metathesis

Boronic esters are cyclic esters formed through the condensation reaction between boronic acids and alcohols, usually 1,2- or 1,3-diols.[127]

The dynamic exchange with hydroxyls and diols has been used in boronic ester transesterification vitrimers by Guan's group,[128] that synthesized two crosslinked polymers that show malleability and self-healing properties, based on the chemical process shown in Figure I-21a.

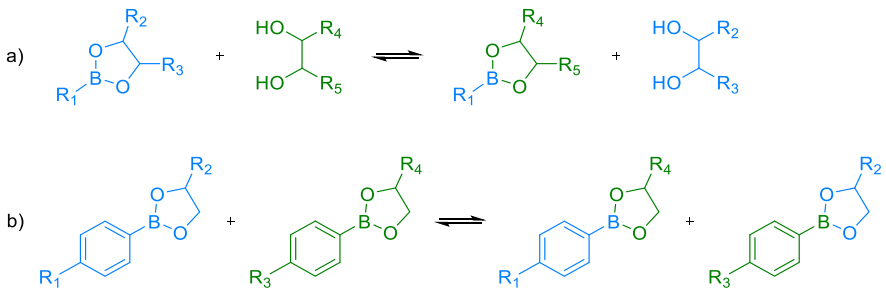

Figure I-21. *a) Exchange reaction between boronic esters and diols; b) Metathesis reaction between two dioxaborolanes.*

Similar to the silyl ethers exchange described in the previous section, in 2017, Nicolaÿ and Leibler[129] discovered that dioxaborolanes could also be exchanged through the metathesis reaction, without the need of free hydroxyl moieties in the polymer network, as it is represented in Figure I-21b. In this way, the reaction could start at moderate temperatures, from 60 °C, also in absence of catalyst. Moreover, these dioxaborolanes were thermally and chemically resistant, also thanks to the absence of free diols, avoiding side reactions at elevated temperature. Leibler and co-workers[130] incorporated dioxaborolanes as crosslinking groups in commercial thermoplastic polymers, such as polystyrene, high-density polyethylene and

poly(methyl methacrylate) via functionalized monomers or post-polymerization modification, converting for the first time thermoplastics in vitrimers. In additional studies, they demonstrated the possibility to process polyethylene vitrimers via injection moulding and reaction extrusion. Despite all these improvements the hydrolytic stability of the boronic ester moieties remains a trouble that could limit the industrial application of this chemistry.

I.4.9 Transalkylation of triazolium salts

Transalkylation exchange reactions were reported for the first time by Drockenmuller and co-workers as a new vitrimer chemistry.[131] The poly(1,2,3-triazolium) (PTIL) materials were synthesized via one-pot process without addition of any catalyst or solvent, by the reaction of alkyl halides and poly(1,2,3-triazoles). The bond exchange between triazolium and extra alkyl halide dangling chains in the network was studied first by using model compounds and later in bulk materials. This exchange reaction is presented in Figure I-22. The model studies seemed to indicate an associative mechanism and it was confirmed by stress relaxation experiments on the poly(1,2,3-triazolium) based materials which also showed an Arrhenius temperature dependence. The prepared polymers were also insoluble in a series of solvents at elevated temperature, fulfilling all the standards to be a vitrimer. In this way Drockenmuller and co-workers reported the first example of ionic-conductive vitrimers.[131]

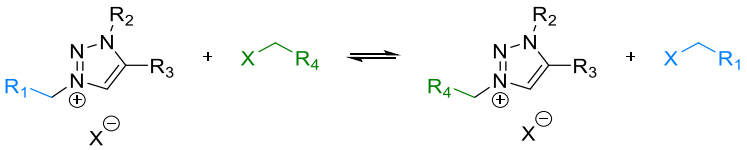

***Figure I-22**. Transalkylation exchange reaction of triazolium salts.*

In a further study of the same research group[132] they tuned the viscoelastic properties of PTIL materials varying the monomer/crosslinker ratio. The materials were tested by X-ray photoelectron spectroscopy and rheometry experiments to correlate variations in the chemical composition of the networks with variations of the viscosity profiles. Based on the combination of these techniques, they discovered that the exchange mechanism was non-concerted and dissociative, and it occurred via two-step dealkylation and realkylation mechanisms. These results contradicted for the first time the definition of vitrimers, showing that a dissociative exchange mechanism can also display the viscoelastic characteristics of vitrimers.[132]

In conclusion, they demonstrated the possibility for dissociative CANs to show vitrimer-like properties and reported a valuable example of how to tune material properties by changing monomers structure, stoichiometry or catalyst.[73]

I.4.10 Transesterification of phthalate monoesters

In 2019 Du Prez and co-workers,[133] trying to obtain an example of free-catalyst transesterification, developed the phthalate monoester transesterification as a new dynamic chemistry for CANs. The reaction is presented in Figure I-23.

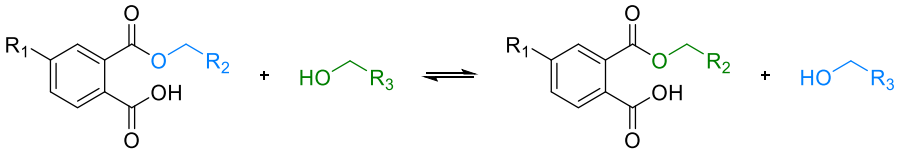

***Figure I-23**. Transesterification exchange reaction of phthalate monoesters by alcohols.*

Since this reaction was the first example of this chemistry in the field of CANs, they first conducted a study based on model compounds to assess the effect of the neighbouring groups on the transesterification kinetics and to determine whether the mechanism was associative or dissociative. Surprisingly, the model study showed that the monoesters undergo fast transesterification via a dissociative mechanism, due to the free carboxylic acid as internal catalysts, which reversibly forms an activated phthalic anhydride intermediate. Moreover, a series of polymeric materials were synthesized by the reaction of diols and triols with bifunctional phthalic anhydrides. The viscoelastic properties of the materials, determined via stress relaxation experiments, showed a linear evolution of the viscosity with temperature, despite the dissociative mechanism, indicating that the degree of depolymerization was not dominant within the range of temperature analyzed. The dissociative nature the polymer was demonstrated by dissolution experiments in a hot solvent, which resulted in the full dissolution of the polymeric network.[133]

I-5 Applications of vitrimers and advanced thermosets

As described in previous sections, different interesting chemistries are suitable for synthesizing malleable materials and other chemistries will surely be described in the future. In fact, the reprocessable and recyclable properties of these materials have attracted the interest of the scientific community, especially due to the increasing attention paid to the accumulation of plastic waste in the environment. Moreover, the unique viscoelastic properties of CANs can be relevant in many industrial fields. In the next sections we will discuss some applications of the vitrimers and advanced thermosets materials.

I-5.1 Malleable thermosets

Vitrimers, as “malleable thermosets”, can address various problems inherent to the thermoset nature such as healing, reprocessing and recycling ability, but at the same time preserve the dimensional stability, chemical and creep resistance of their nature.[67,76] These improvements can be achieved thanks to the characteristic gradual

decrease of viscosity with temperature. By applying appropriate stimuli as temperature and pressure, it is possible to extend the lifetime of the material, repairing the possible cracks that could be formed during its use. In this way, the thermosetting waste can be reduced by enabling remolding and reuse of materials without increasing costs for consumers.[74,45] The processability of the vitrimers allows these materials to be reshaped in another form, once they are cured, without the need of a specific mould or to be reused in other applications changing their shape.

Moreover, the vitrimeric characteristics can convert thermosets into recyclable materials. In a typical recycling process, the material is ground in small pieces and then reformed into a new specimen through a hot-pressing procedure. The resulting materials, after this procedure, maintain their properties almost unaltered even for several cycles.

Furthermore, if they are "vitrimer-like polymers" they can be subjected to a chemical recycling process that allows the starting monomer or another useful compound to be recovered, using an appropriate solvent.[70] A roadmap of the possible CAN waste treatment is proposed in Figure I-24.

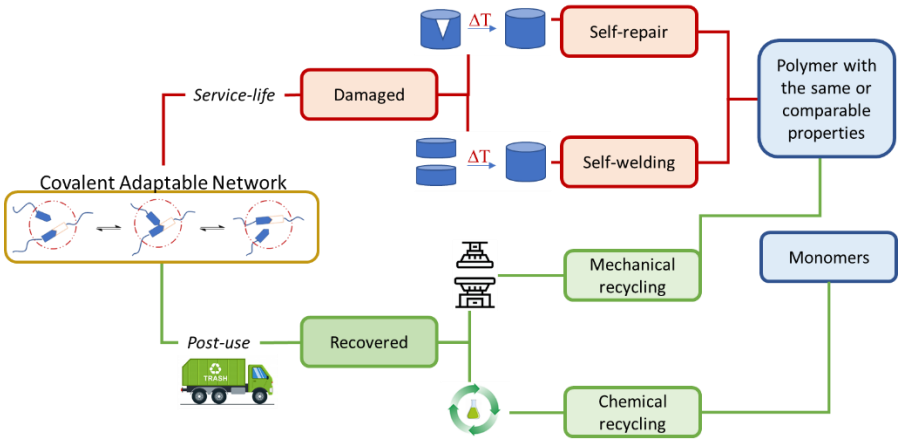

***Figure I-24**. Roadmap of the possible CAN waste treatment, from waste to obtain new resource.*

I-5.2 Industrial applications

Vitrimers thank to their unique properties will be able to find numerous applications in different industrial fields, although to date most of the applications are still limited to academic studies.

Due to the ability of vitrimers to self-weld, with the formation of interfacial crosslinks between the polymer interfaces, they can be used in the future in adhesive industrial applications. In fact, different examples of welding of vitrimers have been reported in the literature, [82,134-138] but their industrial use is still in its early stages.

An industrial field, where vitrimer can provide an added value is the preparation of polymer composites. Using vitrimeric matrices as binding agents for the fibres can allow to process, recycle, repair, and even recover the expensive fibres in composite materials.

Until now different dynamic covalent chemistries have been used to produce composite vitrimers such as: transesterification,[80,139] transamination,[140-142] imine exchange[143,144] and disulfide exchange.[122,145,146]

At industrial level an interesting start-up company, Mallinda, focused their research and production on malleable fibre reinforced polymer composites using a polyimine-based polymer. Taynton *et al.*[100,144] prepared carbon fibre reinforced plastics (CFRPs), in absence of catalyst, that exhibit malleable behaviour only when heated above the glass transition temperature. Moreover, those materials could also be recycled by dissolution in ethanol solution, as shown in Figure I-25.

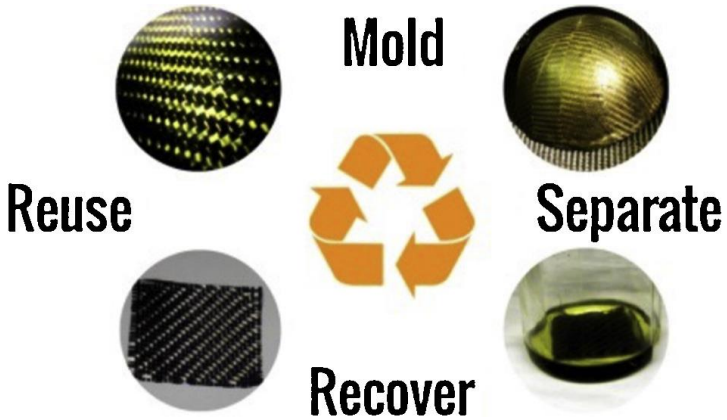

***Figure I-25**. New recycling paradigm of the polyimine-based composites, by Taynton et al.[144].*

I-5.3 Shape-memory polymers

Today, there is an increasing demand for polymers for advanced applications. Advanced polymeric materials that exhibit special functions in response to external conditions are defined as smart polymers, also called stimuli-responsive polymers.[147] Vitrimers, are opening new possibilities in this field with their ability to undergo permanently macroscopic changes in their shape in response to a stimulus.[148,149]

Shape-memory polymers (SMP)s are a class of stimuli-responsive materials that are capable to adopt a temporary shape and then recover to their original shape upon the application of an external stimulus, known as shape memory effect (SME).[150,151] An example of SME is presented in Figure I-26.

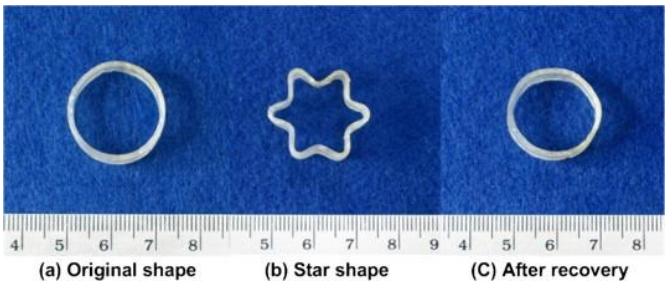

***Figure I-26**. Qualitatively illustration of the shape-memory effect in polymers, by Sun et al.[152].*

The SME is the ability of a SMP to store and release large energy contributions as a form of shape transformation, generating motion. The SME is not an intrinsic property of the polymer, since an external programming is necessary to reconfigure and adapt the network structure.

This effect usually consists of a thermomechanical process during which the material is heated up to a temperature close to or higher than a structural transition of the network (T_{trans}) and deformed to a second temporary shape by application of an external force.

The T_{trans} of a SMP is a temperature which coincides with the polymer glass transition temperature (T_g) or melting temperature (T_m). In the rubbery state the polymer can be easily deformed, and the chains are aligned in the direction of the applied external force.

From an energy point of view, the polymer goes from an equilibrium high entropy random coil state to a non-equilibrium low entropy aligned state, stabilized by cooling down the polymer, and maintaining applied the external force.[153]

This non-equilibrium state will remain stable until an appropriated external stimulus is applied, and the strain energy stored during cooling is released driven by the entropic change during the shape-recovery. SMPs are divided in different categories depending on their network structure, on the triggering stimulus and many others.

In this thesis, we focused our attention on the shape memory thermosets activated by temperature, one of the main subjects of our research group.[154-158]

I-5.3.1 Shape-memory thermosets

Thermoset-based SMPs are increasingly studied for their mechanical performance, durability and a high degree of shape recovery due to an excellent rubber elasticity at the rubbery region.[159,160]

SM thermosets, after the curing process, take their permanent shape, once they are heated above T_g. The flexibility and segmental mobility of the chains increase allowing a large deformation of the material in a second and temporary shape. During this deformation process, the chains move away from the equilibrium state, and by cooling

down the SMP below the T_g, the network stabilized because of the reduction of the chain mobility due to the vitrification process, fixing the temporary shape under a non-equilibrium state. Once the temperature increases above T_g, the network can move towards the equilibrium state producing the recovery of the original shape. In Figure I-27 a scheme of the SME for thermosetting shape-memory polymers is presented.

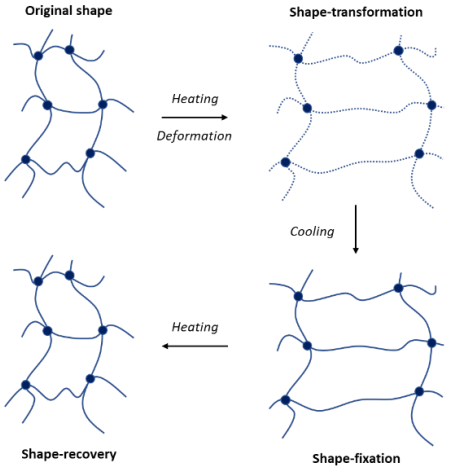

***Figure I-27**. Representation of the SME in thermosetting polymers activated by temperature.*

Currently, thermosetting SMPs are studied and applied in many research areas such as robotics,[161,162] aerospace,[163] textile application,[164,165] biomedical devices[166,167] and many others.

SMPs usually can retain only two shapes, the permanent and the programming shape, but recent technological advances have allowed the introduction of multi-shape-memory materials, which are able to adopt different temporary shapes and then recover to its permanent shape incorporating several discrete thermal transitions or molecular switches into SMPs.[168-170]

As a drawback, SMPs usually take permanent shape of simple geometry that is impossible to change due to the permanent covalent bond nature of the network structure.

I.5.4 Thermadapt shape memory polymers

The concept of vitrimers has addressed limitations in many polymer fields and opened new possibilities and applications previously unthinkable. For instance, the design of a shape memory material with an appropriate vitrimer chemistry could overcome the above mentioned classical limitations of the shape memory thermosets, offering the possibility to manipulate the permanent shape of the materials, changing their topology by covalent bond exchange.[74] This ability can be used in shape-memory

thermosets to generate unlimited permanent shapes and to simplify the preparation of SMPs with complex geometry without the need of a complex mould.

Using vitrimeric materials, it is possible to combine the permanent shape changing, when the material is heated above the T_v, with the conventional shape memory effect governed by the entropic change, an example of this effect is proposed in Figure I-28.

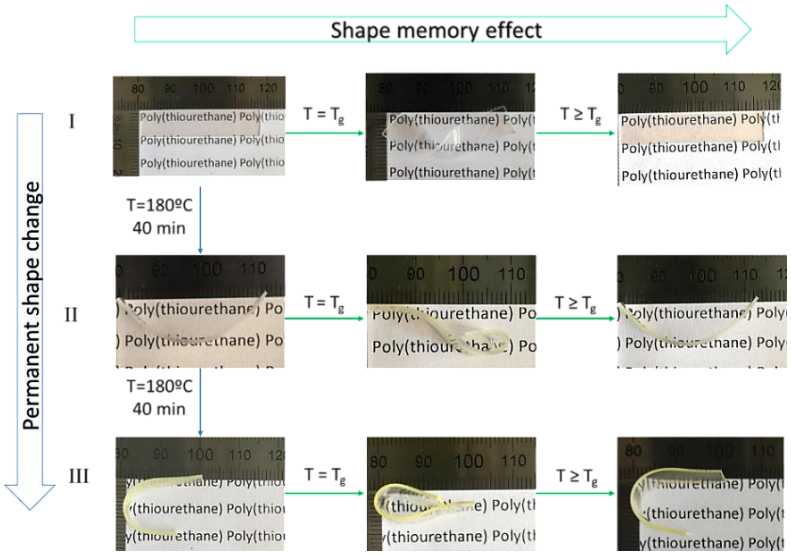

Figure I-28. *Representation of shape memory behaviour and permanent/plastic shape change for vitrimer.*

To distinguish the behaviour of vitrimeric SMPs from the commonly SM behaviour of thermosets and thermoplastic a new term was coined by Xie and co-workers, who called this phenomenum thermadapt shape memory.[60,90]

This characteristic behaviour has attracted significant attention and epoxy resins,[171-173] and polyurethanes[90,174-178] have been the most explored shape memory CANs, simplifying the preparation of different and complex permanent shapes.

I.5.5 Dual curing

An interesting technique to obtain advanced thermosets is the dual curing procedure, which combines the possibility to develop custom-tailored materials, with a large set of properties, with flexible processing ability.[179]

Dual curing is a novel methodology to develop dual network thermosets. This procedure combines two different polymerization processes which can take place simultaneously or sequentially during the curing process, triggered by similar or different stimulus such as heat or UV light.[180]

Simultaneous dual-curing is not particularly interesting for advanced applications since it only affects the properties of the final materials. Therefore, the interest of the scientific community is focused on sequential dual-curing systems.[181-183]

Sequential dual-curing processing is a highly attractive strategy that provides stable and well-defined intermediate materials after completion of the first curing stage, displaying high deformability and malleability as long as the intermediate material is stable.[184]

The structure of the intermediate and final network and properties of the dual-cured materials can be tuned by changing the monomer structures, functionality, and stoichiometric ratio of the monomers involved in the reaction.[185,186] A scheme of the sequential dual-curing procedure is presented in Figure I-29.

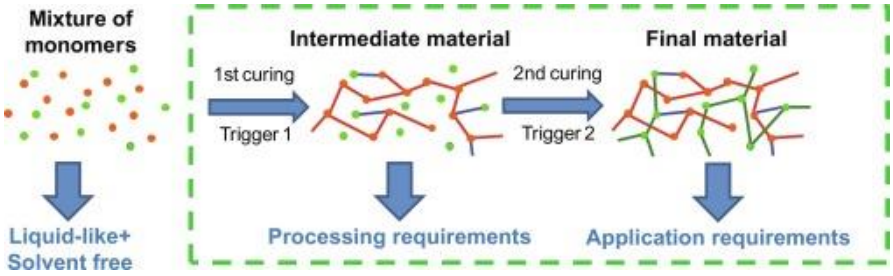

***Figure I-29**. General representation of dual-curing processing by Ramis et al.[180]*

Different polymerization reactions are suitable to be employed in the dual-curing of thermosetting formulations, nevertheless "click" reactions (which will be presented in the following section) are of especial interest for their specificity. Because of the control of the intermediate material characteristics is mainly performed by selecting the convenient stoichiometry of the reactants participating in the first polymerization stage, click reactions are usually selected to carry out this step, since using this chemistry the stoichiometry is assured. As an example, two click reactions, the photoinitiated "thiol-ene" followed by the thermal "thiol-epoxy", were combined by Guzman *et al*.[187] to obtain dual networks with customized properties.

I.6 Click-chemistry

The term "click-reaction" was coined by Sharpless *et al.*[188] to describe a variety of chemical reactions characterized by their orthogonality, selectivity, and high efficiency.

Click reactions have the following characteristics: modularity, high yielding or even quantitative, stereospecific, insensitive to oxygen, humidity or water, solvent-free, and they are performed using readily available starting materials and reagents in mild conditions.[188,189] Thus, these reactions can be considered as environmentally friendly

from the point of view of the low residues generated, atom economy and energy saving.

A large number of chemical reactions fit the click-criteria, among them "thiol-click" reactions are interesting since they proceed rapidly in reference to other click reactions and under mild and solvent-free conditions and therefore can be performed in an environmentally friendly manner.[190] Thiol chemistry according to the reaction mechanism can be divided in base-catalysed nucleophilic reactions like thiol-epoxy, thiol Michael and thiol-isocyanate, and radical-mediated reactions as thiol-ene and thiol-yne.[191]

At the same time, the thiol-click reactions show some disadvantages such as the unpleasant thiol smell or short shelf stability for many formulations due to the high reactivity of the monomers involved in the reaction.[192] The last issue can be controlled with the use of latent catalysts. These types of catalysts are passive until an external stimulus activate them and the reaction is triggered. In this way, the pot-life of the formulation can be increased and the kinetics of the reaction can be controlled.

I.6.1 Thiol-isocyanate reaction

Thiols (R-SH) are the sulphur analogous of alcohols (R-OH), where the oxygen atom is substituted by the sulphur, but their functions and reactivities are quite different.

The lower electronegativity of the sulphur atom in reference to the oxygen makes the S-H bond longer and weaker than the O-H. Thus, the thiol bond is less polarized than the hydroxyl, which leads to weaker hydrogen bonding and lower boiling points of thiol compounds. Thiols are also more acidic than alcohols, due to the weakness of the S-H bond and the distribution of the negative charge within 3d sulphur orbitals. Furthermore, thiols are more nucleophilic than alcohols, which means that in the presence of a base catalyst that generate thiolate anions, the reaction will proceed rapidly in reference to their oxygen-based counterparts.[193]

Thiol-isocyanate reaction, in the presence of a base, has been a well-known reaction for many years,[194] but only recently it has been included in the family of the click reactions and is increasingly attracting attention of the scientific community.[195] In fact, the thiol-isocyanate nucleophilic coupling reaction leads to a fast, efficient and high-yielding process without the formation of by-products.[196]

The reaction mechanism of the thiol and isocyanate in presence of base catalyst is presented in Figure I-30a. The reaction starts by the rapid abstraction of a proton by the base from a thiol, due to its relatively low pK_a value, with the formation of thiolate anion, which are the species that attack the partially positive charged isocyanate carbonyl carbon. This leads to the formation of a negative charge on the nitrogen in the thiourethane, which extracts a proton from a neighbouring thiol to stabilize the thiourethane moieties with the subsequent generation of a new thiolate anion.

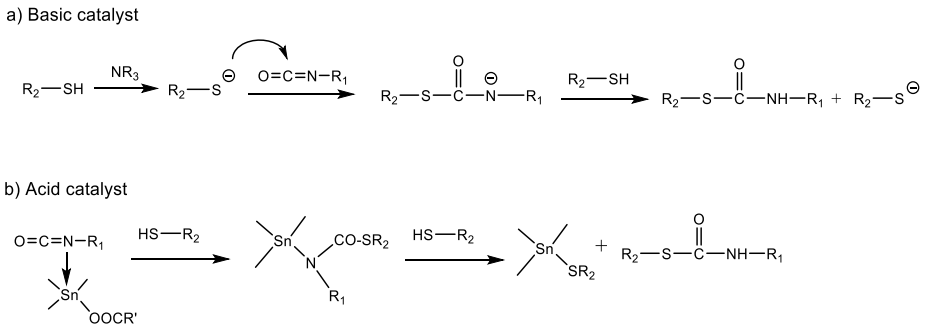

Figure I-30. *Proposed mechanisms of poly(thiouretane) formation in both basic and acidic conditions.*

The most common basic catalysts involved in the thiol-isocyanate reaction are tertiary amines such as triethylamine (TEA)[197] or amidine compounds such as 1,5-diazabicyclo[4.3.0]non-5-ene (DBN) or 1,8-diazabicyclo[5.4.0]undec-7-ene (DBU),[198] leading to a very rapid reaction. The reaction times are frequently of the order of seconds, that can limit their use in polymer synthesis.[199] To overcome this issue, the use of a latent amine initiators has been proposed by Salmi *et al*.[200] and Shin *et al*.,[201] and in both works the reaction was triggered by UV irradiation.

Alternatively, this reaction can be catalyzed by Lewis acids,[202] usually by Tin catalyst like dibutyltin dilaurate (DBTDL),[203] and the mechanism of the poly(thiourethane) formation is shown in Figure I-30b. The reaction proceeds via the coordination of the tin-catalyst with the oxygen or nitrogen lone pairs of the isocyanate (electrophilic activation) which can be attacked by the low nucleophilic thiols, with a slower reaction rate.

The main application where crosslinked poly(thiourethane)s (PTUs) have been used is the preparation of optical materials, thanks to their high refractive indexes. In the preparation of optical PTUs usually tin catalysts have been selected to obtain excellent homogeneity, optical characteristics and good mechanical performance.[204,205]

I.7 Objectives

I.7.1 Problem statement

As already stated in the previous sections of this work, the design and preparation of polymeric materials that combine the reprocessing properties of thermoplastics and the advantages of thermosets is crucial to relieve the environmental pressure. Different reversible covalent networks have been explored and used to form reprocessable materials, among them the polyurethane crosslinked materials are one of the most widely studied.

Poly(thiourethane)s (PTUs), compared to their oxygen counterparts (PU), can present similar properties due to the presence of hydrogen bonding in both materials, but they

present several advantages. They are obtained by click-type reactions from isocyanates and thiols. Thus, their formation it is not accompanied by side-reactions contrary to what occurs in the poly(urethane) synthesis and therefore, a homogeneous material with tailored properties can be easily obtained.

Since the vitrimeric behaviour in poly(urethanes) was attributed to a transcarbamoylation or carbamate exchange reaction, it was hypothesized that analogue mechanisms can occur with poly(thiourethane) thermosets. Furthermore, since thiols are more acidic than alcohols and sulfide anions are more nucleophilic than alkoxides and at the same time better leaving groups, the exchange process in poly(thiourethane)s could be faster than the one observed in poly(urethane)s.

It is important to notice, that at the beginning of this project, no examples of poly(thiourethane) bond exchange chemistry to obtain covalent adaptable networks had been described yet. Parallel to our work, Torkelson and co-workers[206] used poly(thiourethane)s to develop a new type of adaptative covalent networks, illustrating the strong interest of the scientific community in these materials.

I.7.2 Goals of the thesis

The main objective of this doctoral thesis is to design, synthesize and characterize advanced poly(thiourethane)s thermosets (PTUs) with the ability to be reprocessed and recycled thanks to the introduction of novel covalent exchange chemistries.

The study on the poly(thiourethane) materials has been divided in five main sections:

I) Preparation and characterization of "thiol-isocyanate" based materials triggered by a tin catalyst or latent amines. More in detail, the main objectives identified in this section are:

- Understanding the viability of the "thiol-isocyanate" reaction in acid and basic conditions catalysed by DBTDL and two latent catalysts that release 1-methylimidazole.
- Investigate the influence of different aliphatic isocyanates on the kinetics of the reaction and on the final thermal and mechanical properties of the synthesized materials.

II) Development of a new dual-curing procedure, exploiting the approach of the click chemistry to obtain a sequential dual-curing processing combining "thiol-isocyanate" and "thiol-epoxy" reactions. The specific objective of the section II is the following:

- Design of a new dual-curing system based on the thiol-isocyanate/thiol-epoxy reactions and further characterization of the physical and thermomechanical properties of the dual-cured materials.

III) Development and characterization of PTU based shape-memory polymers using latent-amines. The specific objective of this part is the following:

- Design and development of a series of poly(thiourethane) thermosets for shape-memory applications with different activation temperature, but similar performance.

IV) Development and characterization of covalent adaptable networks based on PTU chemistry, to demonstrate their ability to undergo a topological change and to study the effect of the proportion of DBTDL on the transcarbamoylation process. The specific objectives of the section IV are:

- Demonstrate the viability of transthiocarbamoylation process by using model compounds.
- Evaluate the effect of the proportion of the tin-catalyst on the relaxation behaviour.
- Investigate the recyclability of the materials prepared with different isocyanates.

V) Development of more environmentally friendly PTUs covalent adaptable networks catalyzed by latent organic catalysts, with the objectives of:

- Replace the metal-based catalyst with a less toxic latent organocatalyst for the additional purpose of accelerating the transthiocarbamoylation process.
- Investigate the effect of the isocyanate/thiol ratio on the relaxation behavior and on the recyclability of the final PTU materials.
- Optimize the recycling conditions of the poly(urethanes) obtained by latent organocatalysts

Observations for the reader

This thesis work is presented as a compilation of scientific papers, which were published during the PhD period. The reader should thus, consider the presented articles as subsequent insights and learnings on the topic of poly(thiourethane)s and their vitrimeric behaviour. Given the novelty of the subject treated, some of the initial conclusions reported were revised in light of new scientific papers, published in parallel to this work by other research groups. These new learnings have led us to tune our conclusions in the last published paper and has driven the general conclusions reported in this thesis work. This learning process has shaded light on the degradation mechanism of poly(thiourethane)s and their vitrimeric behaviour.

References

1 The New Plastics Economy, https://www.ellenmacarthurfoundation.org/publications/the-new-plastics-economy-rethinking-the-future-of-plastics-catalysing-action, (accessed Sept. 29, 2020).

2 E. Foschi and A. Bonoli, *Adm. Sci.*, 2019, **9**, 18.

3 H. Sardon and A. P. Dove, *Science*, 2018, **360**, 380–381.

4 R. Hatti-Kaul, L. J. Nilsson, B. Zhang, N. Rehnberg and S. Lundmark, *Trends Biotechnol.*, 2020, **38**, 50–67.

5 P. Schröder, M. Anantharaman, K. Anggraeni and T. J. Foxon, *The Circular Economy and the Global South: Sustainable Lifestyles and Green Industrial Development*, Routledge, New York, NY, 2019.

6 R. Geyer, J. R. Jambeck and K. L. Law, *Sci. Adv.*, 2017, **3**, e1700782.

7 J. R. Fried, *Polymer Science and Technology, 3rd Edition*, Prentice Hall., London, United Kingdom, 3rd edn., 2014.

8 M. Biron, *Material Selection for Thermoplastic Parts: Practical and Advanced Information*, William Andrew, Oxford, United Kingdom, 2015.

9 R. O. Ebewele, *Polymer Science and Technology*, CRC Press, Boca Raton, Florida, 2000.

10 E. L. Thomas, *Structure and properties of polymers*, VCH, Weinheim, Germany, 1993.

11 M. Biron, *Thermoplastics and Thermoplastic Composites*, William Andrew, Oxford, United Kingdom, 2018.

12 J.-P. Pascault, H. Sautereau, J. Verdu and R. J. J. Williams, *Thermosetting Polymers*, CRC Press, New York, NY, 2002.

13 D. J. Fortman, J. P. Brutman, G. X. De Hoe, R. L. Snyder, W. R. Dichtel and M. A. Hillmyer, *ACS Sustain. Chem. Eng.*, 2018, **6**, 11145–11159.

14 W. Post, A. Susa, R. Blaauw, K. Molenveld and R. J. I. Knoop, *Polym. Rev.*, 2020, **60**, 359–388.

15 Waste and recycling, https://ec.europa.eu/environment/topics/waste-and-recycling_en, (accessed March 3, 2021).

16 *Directive 2008/98/EC of the European Parliament and of the Council of 19 November 2008 on waste and repealing certain Directives (Text with EEA relevance)*, 2008, vol. OJ L.

17 J. Datta and P. Kopczyńska, *Crit. Rev. Environ. Sci. Technol.*, 2016, **46**, 905–946.

18 A. Jacob, *Reinf. Plast.*, 2011, **55**, 45–46.

19 S. Ma and D. C. Webster, *Prog. Polym. Sci.*, 2018, **76**, 65–110.

20 R. Francis, *Recycling of Polymers: Methods, Characterization and Applications*, John Wiley & Sons, Weinheim, Germany, 2016.

21 N. Singh, D. Hui, R. Singh, I. P. S. Ahuja, L. Feo and F. Fraternali, *Compos. Part B Eng.*, 2017, **115**, 409–422.

22 S. M. Al-Salem, A. Antelava, A. Constantinou, G. Manos and A. Dutta, *J. Environ. Manage.*, 2017, **197**, 177–198.

23 S. D. Anuar Sharuddin, F. Abnisa, W. M. A. Wan Daud and M. K. Aroua, *Energy Convers. Manag.*, 2016, **115**, 308–326.

24 F. Meng, J. McKechnie, T. A. Turner and S. J. Pickering, *Compos. Part Appl. Sci. Manuf.*, 2017, **100**, 206–214.

25 L. O. Meyer, K. Schulte and E. Grove-Nielsen, *J. Compos. Mater.*, 2009, **43**, 1121–1132.

26 S. M. Al-Salem, P. Lettieri and J. Baeyens, *Prog. Energy Combust. Sci.*, 2010, **36**, 103–129.

27 T. Gutierrez, Ed., *Reactive and Functional Polymers Volume Four: Surface, Interface, Biodegradability, Compostability and Recycling*, Springer International Publishing, Cham, Switzerland, 2020.

28 J. M. Garcia and M. L. Robertson, *Science*, 2017, **358**, 870–872.

29 M. Shen, H. Cao and M. L. Robertson, *Annu. Rev. Chem. Biomol. Eng.*, 2020, **11**, 183–201.

30 C. Morin, A. Loppinet-Serani, F. Cansell and C. Aymonier, *J. Supercrit. Fluids*, 2012, **66**, 232–240.

31 Q. Guo, Ed., *Thermosets: Structure, Properties, and Applications*, Elsevier, Amsterdam, Netherlands, 2017.

32 X. Kuang, Y. Zhou, Q. Shi, T. Wang and H. J. Qi, *ACS Sustain. Chem. Eng.*, 2018, **6**, 9189–9197.

33 Y. Yang, R. Boom, B. Irion, D.-J. van Heerden, P. Kuiper and H. de Wit, *Chem. Eng. Process. Process Intensif.*, 2012, **51**, 53–68.

34 N. I. Khan, S. Halder, S. B. Gunjan and T. Prasad, *IOP Conf. Ser. Mater. Sci. Eng.*, 2018, **377**, 012007.

35 S. Billiet, X. K. D. Hillewaere, R. F. A. Teixeira and F. E. D. Prez, *Macromol. Rapid Commun.*, 2013, **34**, 290–309.

36 X. K. D. Hillewaere, R. F. A. Teixeira, L.-T. T. Nguyen, J. A. Ramos, H. Rahier and F. E. D. Prez, *Adv. Funct. Mater.*, 2014, **24**, 5575–5583.

37 S. J. Garcia, *Eur. Polym. J.*, 2014, **53**, 118–125.

38 M. M. Perera and N. Ayres, *Polym. Chem.*, 2020, **11**, 1410–1423.

39 L. Imbernon and S. Norvez, *Eur. Polym. J.*, 2016, **82**, 347–376.

40 S. J. Rowan, S. J. Cantrill, G. R. L. Cousins, J. K. M. Sanders and J. F. Stoddart, *Angew. Chem. Int. Ed.*, 2002, **41**, 898–952.

41 C. J. Kloxin and C. N. Bowman, *Chem. Soc. Rev.*, 2013, **42**, 7161–7173.

42 Y. Jin, C. Yu, R. J. Denman and W. Zhang, *Chem. Soc. Rev.*, 2013, **42**, 6634–6654.

43 T. Maeda, H. Otsuka and A. Takahara, *Prog. Polym. Sci.*, 2009, **34**, 581–604.

44 Y. Jin, Q. Wang, P. Taynton and W. Zhang, *Acc. Chem. Res.*, 2014, **47**, 1575–1586.

45 A. Khan, N. Ahmed and M. Rabnawaz, *Polymers*, 2020, **12**, 2027.

46 R. J. Wojtecki, M. A. Meador and S. J. Rowan, *Nat. Mater.*, 2011, **10**, 14–27.

47 J. A. Offenbach and A. V. Tobolsky, *J. Colloid Sci.*, 1956, **11**, 39–47.

48 M. Capelot, D. Montarnal, F. Tournilhac and L. Leibler, *J. Am. Chem. Soc.*, 2012, **134**, 7664–7667.

49 D. Montarnal, M. Capelot, F. Tournilhac and L. Leibler, *Science*, 2011, **334**, 965–968.

50 P. R. Christensen, A. M. Scheuermann, K. E. Loeffler and B. A. Helms, *Nat. Chem.*, 2019, **11**, 442–448.

51 C. Jehanno and H. Sardon, *Nature*, 2019, **568**, 467–468.

52 J. M. Winne, L. Leibler and F. E. D. Prez, *Polym. Chem.*, 2019, **10**, 6091–6108.

53 W. Denissen, J. M. Winne and F. E. D. Prez, *Chem. Sci.*, 2016, **7**, 30–38.

54 B. Zhang, Z. A. Digby, J. A. Flum, P. Chakma, J. M. Saul, J. L. Sparks and D. Konkolewicz, *Macromolecules*, 2016, **49**, 6871–6878.

55 A. Rekondo, R. Martin, A. R. de Luzuriaga, G. Cabañero, H. J. Grande and I. Odriozola, *Mater. Horiz.*, 2014, **1**, 237–240.

56 J. Canadell, H. Goossens and B. Klumperman, *Macromolecules*, 2011, **44**, 2536–2541.

57 Y. Amamoto, H. Otsuka, A. Takahara and K. Matyjaszewski, *Adv. Mater.*, 2012, **24**, 3975–3980.

58 O. Diels and K. Alder, *Justus Liebigs Ann. Chem.*, 1928, **460**, 98–122.

59 X. Chen, M. A. Dam, K. Ono, A. Mal, H. Shen, S. R. Nutt, K. Sheran and F. Wudl, *Science*, 2002, **295**, 1698–1702.

60 W. Zou, J. Dong, Y. Luo, Q. Zhao and T. Xie, *Adv. Mater.*, 2017, **29**, 1606100.

61 P. A. Pratama, M. Sharifi, A. M. Peterson and G. R. Palmese, *ACS Appl. Mater. Interfaces*, 2013, **5**, 12425–12431.

62 F. García and M. M. J. Smulders, *J. Polym. Sci. Part Polym. Chem.*, 2016, **54**, 3551–3577.

63 K. Yu, P. Taynton, W. Zhang, M. L. Dunn and H. Jerry Qi, *RSC Adv.*, 2014, **4**, 10108–10117.

64 B. J. Adzima, H. A. Aguirre, C. J. Kloxin, T. F. Scott and C. N. Bowman, *Macromolecules*, 2008, **41**, 9112–9117.

65 C. A. Angell, *Science*, 1995, **267**, 1924–1935.

66 W. Denissen, M. Droesbeke, R. Nicolaÿ, L. Leibler, J. M. Winne and F. E. Du Prez, *Nat. Commun.*, 2017, **8**, 1–7.

67 B. Krishnakumar, R. V. S. P. Sanka, W. H. Binder, V. Parthasarthy, S. Rana and N. Karak, *Chem. Eng. J.*, 2020, **385**, 123820.

68 Y. Nishimura, J. Chung, H. Muradyan and Z. Guan, *J. Am. Chem. Soc.*, 2017, **139**, 14881–14884.

69 M. Guerre, C. Taplan, J. M. Winne and F. E. D. Prez, *Chem. Sci.*, 2020, **11**, 4855–4870.

70 B. R. Elling and W. R. Dichtel, *ACS Cent. Sci.*, 2020, **6**, 1488–1496.

71 P. Chakma, C. N. Morley, J. L. Sparks and D. Konkolewicz, *Macromolecules*, 2020, **53**, 1233–1244.

72 M. Hayashi, *Polymers*, 2020, **12**, 1322.

73 A. Jourdain, R. Asbai, O. Anaya, M. M. Chehimi, E. Drockenmuller and D. Montarnal, *Macromolecules*, 2020, **53**, 1884–1900.

74 N. J. Van Zee and R. Nicolaÿ, *Prog. Polym. Sci.*, 2020, **104**, 101233.

75 G. M. Scheutz, J. J. Lessard, M. B. Sims and B. S. Sumerlin, *J. Am. Chem. Soc.*, 2019, **141**, 16181–16196.

76 Y. Jin, Z. Lei, P. Taynton, S. Huang and W. Zhang, *Matter*, 2019, **1**, 1456–1493.

77 M. Capelot, M. M. Unterlass, F. Tournilhac and L. Leibler, *ACS Macro Lett.*, 2012, **1**, 789–792.

78 F. I. Altuna, V. Pettarin and R. J. J. Williams, *Green Chem.*, 2013, **15**, 3360–3366.

79 J. Han, T. Liu, C. Hao, S. Zhang, B. Guo and J. Zhang, *Macromolecules*, 2018, **51**, 6789–6799.

80 E. Chabert, J. Vial, J.-P. Cauchois, M. Mihaluta and F. Tournilhac, *Soft Matter*, 2016, **12**, 4838–4845.

81 A. Legrand and C. Soulié-Ziakovic, *Macromolecules*, 2016, **49**, 5893–5902.

82 J. P. Brutman, P. A. Delgado and M. A. Hillmyer, *ACS Macro Lett.*, 2014, **3**, 607–610.

83 M. Hayashi, R. Yano and A. Takasu, *Polym. Chem.*, 2019, **10**, 2047–2056.

84 F. I. Altuna, C. E. Hoppe and R. J. J. Williams, *Polymers*, 2018, **10**, 43.

85 T. Liu, B. Zhao and J. Zhang, *Polymer*, 2020, **194**, 122392.

86 H. Zhang and X. Xu, *Compos. Part Appl. Sci. Manuf.*, 2017, **99**, 15–22.

87 D. J. Fortman, J. P. Brutman, C. J. Cramer, M. A. Hillmyer and W. R. Dichtel, *J. Am. Chem. Soc.*, 2015, **137**, 14019–14022.

88 P. C. Colodny and A. V. Tobolsky, *J. Am. Chem. Soc.*, 1957, **79**, 4320–4323.

89 D. J. Fortman, J. P. Brutman, M. A. Hillmyer and W. R. Dichtel, *J. Appl. Polym. Sci.*, 2017, **134**, 44984.

90 Q. Zhao, W. Zou, Y. Luo and T. Xie, *Sci. Adv.*, 2016, **2**, e1501297.

91 Y. Peiyao, W. Zhao, X. Fu, Z. Liu, W. Kong, C. Zhou and J. Lei, *RSC Adv.*, 2017, **7**, 26858–26866.

92 J. P. Brutman, D. J. Fortman, G. X. De Hoe, W. R. Dichtel and M. A. Hillmyer, *J. Phys. Chem. B*, 2019, **123**, 1432–1441.

93 F. Elizalde, R. H. Aguirresarobe, A. Gonzalez and H. Sardon, *Polym. Chem.*, 2020, **11**, 5386–5396.

94 D. T. Sheppard, K. Jin, L. S. Hamachi, W. Dean, D. J. Fortman, C. J. Ellison and W. R. Dichtel, *ACS Cent. Sci.*, 2020, **6**, 921–927.

95 M. Ciaccia and S. D. Stefano, *Org. Biomol. Chem.*, 2015, **13**, 646–654.

96 M. E. Belowich and J. F. Stoddart, *Chem. Soc. Rev.*, 2012, **41**, 2003–2024.

97 P. Kovaříček and J.-M. Lehn, *J. Am. Chem. Soc.*, 2012, **134**, 9446–9455.

98 P. Taynton, K. Yu, R. K. Shoemaker, Y. Jin, H. J. Qi and W. Zhang, *Adv. Mater.*, 2014, **26**, 3938–3942.

99 H. Zheng, Q. Liu, X. Lei, Y. Chen, B. Zhang and Q. Zhang, *J. Polym. Sci. Part Polym. Chem.*, 2018, **56**, 2531–2538.

100 P. Taynton, H. Ni, C. Zhu, K. Yu, S. Loob, Y. Jin, H. J. Qi and W. Zhang, *Adv. Mater.*, 2016, **28**, 2904–2909.

101 M. Ciaccia, R. Cacciapaglia, P. Mencarelli, L. Mandolini and S. D. Stefano, *Chem. Sci.*, 2013, **4**, 2253–2261.

102 S. Dhers, G. Vantomme and L. Avérous, *Green Chem.*, 2019, **21**, 1596–1601.

103 S. Wang, S. Ma, Q. Li, W. Yuan, B. Wang and J. Zhu, *Macromolecules*, 2018, **51**, 8001–8012.

104 R. Hajj, A. Duval, S. Dhers and L. Avérous, *Macromolecules*, 2020, **53**, 3796–3805.

105 Y. Xu, K. Odelius and M. Hakkarainen, *ACS Sustain. Chem. Eng.*, 2020, **8**, 17272–17279.

106 W. Denissen, G. Rivero, R. Nicolaÿ, L. Leibler, J. M. Winne and F. E. D. Prez, *Adv. Funct. Mater.*, 2015, **25**, 2451–2457.

107 M. Guerre, C. Taplan, R. Nicolaÿ, J. M. Winne and F. E. Du Prez, *J. Am. Chem. Soc.*, 2018, **140**, 13272–13284.

108 C. Taplan, M. Guerre, J. M. Winne and F. E. D. Prez, *Mater. Horiz.*, 2020, **7**, 104–110.
109 Y.-X. Lu, F. Tournilhac, L. Leibler and Z. Guan, *J. Am. Chem. Soc.*, 2012, **134**, 8424–8427.
110 Y.-X. Lu and Z. Guan, *J. Am. Chem. Soc.*, 2012, **134**, 14226–14231.
111 J. A. Neal, D. Mozhdehi and Z. Guan, *J. Am. Chem. Soc.*, 2015, **137**, 4846–4850.
112 A. Ben-Asuly, A. Aharoni, C. E. Diesendruck, Y. Vidavsky, I. Goldberg, B. F. Straub and N. G. Lemcoff, *Organometallics*, 2009, **28**, 4652–4655.
113 A. Ben-Asuly, E. Tzur, C. E. Diesendruck, M. Sigalov, I. Goldberg and N. G. Lemcoff, *Organometallics*, 2008, **27**, 811–813.
114 A. V. Tobolsky, W. J. MacKnight and M. Takahashi, *J. Phys. Chem.*, 1964, **68**, 787–790.
115 Y. Takahashi and A. V. Tobolsky, *Polym. J.*, 1971, **2**, 457–467.
116 G. C. Tesoro and V. Sastri, *J. Appl. Polym. Sci.*, 1990, **39**, 1425–1437.
117 V. R. Sastri and G. C. Tesoro, *J. Appl. Polym. Sci.*, 1990, **39**, 1439–1457.
118 M. Pepels, I. Filot, B. Klumperman and H. Goossens, *Polym. Chem.*, 2013, **4**, 4955–4965.
119 B. T. Michal, C. A. Jaye, E. J. Spencer and S. J. Rowan, *ACS Macro Lett.*, 2013, **2**, 694–699.
120 R. Martin, A. Rekondo, A. R. de Luzuriaga, G. Cabañero, H. J. Grande and I. Odriozola, *J. Mater. Chem. A*, 2014, **2**, 5710–5715.
121 I. Azcune and I. Odriozola, *Eur. Polym. J.*, 2016, **84**, 147–160.
122 A. R. de Luzuriaga, R. Martin, N. Markaide, A. Rekondo, G. Cabañero, J. Rodríguez and I. Odriozola, *Mater. Horiz.*, 2016, **3**, 241–247.
123 R. C. Osthoff, A. M. Bueche and W. T. Grubb, *J. Am. Chem. Soc.*, 1954, **76**, 4659–4663.
124 S. W. Kantor, W. T. Grubb and R. C. Osthoff, *J. Am. Chem. Soc.*, 1954, **76**, 5190–5197.
125 P. Zheng and T. J. McCarthy, *J. Am. Chem. Soc.*, 2012, **134**, 2024–2027.
126 C. A. Tretbar, J. A. Neal and Z. Guan, *J. Am. Chem. Soc.*, 2019, **141**, 16595–16599.
127 Y. Guan and Y. Zhang, *Chem. Soc. Rev.*, 2013, **42**, 8106–8121.
128 O. R. Cromwell, J. Chung and Z. Guan, *J. Am. Chem. Soc.*, 2015, **137**, 6492–6495.
129 M. Röttger, T. Domenech, R. van der Weegen, A. Breuillac, R. Nicolaÿ and L. Leibler, *Science*, 2017, **356**, 62–65.
130 R. G. Ricarte, F. Tournilhac, M. Cloître and L. Leibler, *Macromolecules*, 2020, **53**, 1852–1866.
131 M. M. Obadia, B. P. Mudraboyina, A. Serghei, D. Montarnal and E. Drockenmuller, *J. Am. Chem. Soc.*, 2015, **137**, 6078–6083.
132 M. M. Obadia, A. Jourdain, P. Cassagnau, D. Montarnal and E. Drockenmuller, *Adv. Funct. Mater.*, 2017, **27**, 1703258.
133 M. Delahaye, J. M. Winne and F. E. Du Prez, *J. Am. Chem. Soc.*, 2019, **141**, 15277–15287.
134 S. Zhang, T. Liu, C. Hao, L. Wang, J. Han, H. Liu and J. Zhang, *Green Chem.*, 2018, **20**, 2995–3000.
135 J. Tang, L. Wan, Y. Zhou, H. Pan and F. Huang, *J. Mater. Chem. A*, 2017, **5**, 21169–21177.
136 A. Trejo-Machin, L. Puchot and P. Verge, *Polym. Chem.*, 2020, **11**, 7026–7034.
137 Z. Zhou, X. Su, J. Liu and R. Liu, *ACS Appl. Polym. Mater.*, 2020, **2**, 5716–5725.
138 A. Breuillac, A. Kassalias and R. Nicolaÿ, *Macromolecules*, 2019, **52**, 7102–7113.
139 K. Yu, Q. Shi, M. L. Dunn, T. Wang and H. J. Qi, *Adv. Funct. Mater.*, 2016, **26**, 6098–6106.

140 W. Denissen, I. De Baere, W. Van Paepegem, L. Leibler, J. Winne and F. E. Du Prez, *Macromolecules*, 2018, **51**, 2054–2064.

141 L. Bai and J. Zheng, *Compos. Sci. Technol.*, 2020, **190**, 108062.

142 Y. Spiesschaert, M. Guerre, L. Imbernon, J. M. Winne and F. Du Prez, *Polymer*, 2019, **172**, 239–246.

143 H. Memon, Y. Wei, L. Zhang, Q. Jiang and W. Liu, *Compos. Sci. Technol.*, 2020, **199**, 108314.

144 D. A. Kissounko, P. Taynton and C. Kaffer, *Reinf. Plast.*, 2018, **62**, 162–166.

145 F. Zhou, Z. Guo, W. Wang, X. Lei, B. Zhang, H. Zhang and Q. Zhang, *Compos. Sci. Technol.*, 2018, **167**, 79–85.

146 F. Ji, X. Liu, D. Sheng and Y. Yang, *Polymer*, 2020, **197**, 122514.

147 M. Wei, Y. Gao, X. Li and M. J. Serpe, *Polym. Chem.*, 2017, **8**, 127–143.

148 M. D. Hager, S. Bode, C. Weber and U. S. Schubert, *Prog. Polym. Sci.*, 2015, **49–50**, 3–33.

149 A. Lendlein and O. E. C. Gould, *Nat. Rev. Mater.*, 2019, **4**, 116–133.

150 A. Lendlein and T. Sauter, *Macromol. Chem. Phys.*, 2013, **214**, 1175–1177.

151 M. Heuchel, T. Sauter, K. Kratz and A. Lendlein, *J. Polym. Sci. Part B Polym. Phys.*, 2013, **51**, 621–637.

152 L. Sun, W. M. Huang, Z. Ding, Y. Zhao, C. C. Wang, H. Purnawali and C. Tang, *Mater. Des.*, 2012, **33**, 577–640.

153 W. M. Huang, Y. Zhao, C. C. Wang, Z. Ding, H. Purnawali, C. Tang and J. L. Zhang, *J. Polym. Res.*, 2012, **19**, 9952.

154 A. Belmonte, D. Guzmán, X. Fernández-Francos and S. De la Flor, *Polymers*, 2015, **7**, 2146–2164.

155 A. Belmonte, C. Russo, V. Ambrogi, X. Fernández-Francos and S. De la Flor, *Polymers*, 2017, **9**, 113.

156 A. Belmonte, G. C. Lama, G. Gentile, P. Cerruti, V. Ambrogi, X. Fernández-Francos and S. De la Flor, *Eur. Polym. J.*, 2017, **97**, 241–252.

157 D. Santiago, X. Fernández-Francos, F. Ferrando and S. D. la Flor, *J. Polym. Sci. Part B Polym. Phys.*, 2015, **53**, 924–933.

158 D. Santiago, A. Fabregat-Sanjuan, F. Ferrando and S. D. la Flor, *J. Polym. Sci. Part B Polym. Phys.*, 2016, **54**, 1002–1013.

159 J. Hu, W. Chen, P. Fan, J. Gao, G. Fang, Z. Cao and F. Peng, *Polym. Test.*, 2017, **62**, 335–341.

160 F. Xie, L. Huang, J. Leng and Y. Liu, *J. Intell. Mater. Syst. Struct.*, 2016, **27**, 2433–2455.

161 J. D. Carrico, T. Tyler and K. K. Leang, *Int. J. Smart Nano Mater.*, 2017, **8**, 144–213.

162 Y. Bar-Cohen, V. F. Cardoso, C. Ribeiro and S. Lanceros-Méndez, in *Advanced Piezoelectric Materials (Second Edition)*, ed. K. Uchino, Woodhead Publishing, Cambridge, Massachusetts, 2017, pp. 319–352.

163 Y. Liu, H. Du, L. Liu and J. Leng, *Smart Mater. Struct.*, 2014, **23**, 023001.

164 J. Hu and S. Chen, *J. Mater. Chem.*, 2010, **20**, 3346–3355.

165 J. Hu and J. Lu, in *Smart Polymers and their Applications*, eds. M. R. Aguilar and J. San Román, Woodhead Publishing, Cambridge, Massachusetts, 2014, pp. 437–475.

166 H.-M. Chen, L. Wang and S.-B. Zhou, *Chin. J. Polym. Sci.*, 2018, **36**, 905–917.

167 W. Zhao, L. Liu, F. Zhang, J. Leng and Y. Liu, *Mater. Sci. Eng. C*, 2019, **97**, 864–883.

168 I. Bellin, S. Kelch, R. Langer and A. Lendlein, *Proc. Natl. Acad. Sci. U. S. A.*, 2006, **103**, 18043–18047.

169 H. Du, L. Liu, F. Zhang, J. Leng and Y. Liu, *Compos. Part B Eng.*, 2019, **173**, 106905.

170 Q. Zhao, H. J. Qi and T. Xie, *Prog. Polym. Sci.*, 2015, **49–50**, 79–120.

171 F. I. Altuna, C. E. Hoppe and R. J. J. Williams, *RSC Adv.*, 2016, **6**, 88647–88655.

172 Z. Pei, Y. Yang, Q. Chen, Y. Wei and Y. Ji, *Adv. Mater.*, 2016, **28**, 156–160.

173 Z. Yang, Q. Wang and T. Wang, *ACS Appl. Mater. Interfaces*, 2016, **8**, 21691–21699.

174 Z. Wen, M. K. McBride, X. Zhang, X. Han, A. M. Martinez, R. Shao, C. Zhu, R. Visvanathan, N. A. Clark, Y. Wang, K. Yang and C. N. Bowman, *Macromolecules*, 2018, **51**, 5812–5819.

175 P. Yan, W. Zhao, L. Jiang, B. Wu, K. Hu, Y. Yuan and J. Lei, *J. Appl. Polym. Sci.*, 2018, **135**, 45784.

176 H. Zhuo, H. Wen, G. Liu, H. Chen and S. Chen, *Polymer*, 2018, **158**, 25–31.

177 N. Zheng, J. Hou, Y. Xu, Z. Fang, W. Zou, Q. Zhao and T. Xie, *ACS Macro Lett.*, 2017, **6**, 326–330.

178 Z. Fang, N. Zheng, Q. Zhao and T. Xie, *ACS Appl. Mater. Interfaces*, 2017, **9**, 22077–22082.

179 O. Konuray, X. Fernández-Francos, X. Ramis and À. Serra, *Polymers*, 2018, **10**, 178.

180 X. Ramis, X. Fernández-Francos, S. De la Flor, F. Ferrando and À. Serra, in *Thermosets (Second Edition)*, ed. Q. Guo, Elsevier, Amsterdam, Netherlands, 2018, pp. 511–541.

181 X. Fernández-Francos, O. Konuray, X. Ramis, À. Serra and S. De la Flor, *Materials*, 2021, **14**, 107.

182 H. Kim, S. Han and Y. Seo, *Langmuir*, 2020, **36**, 9250–9258.

183 Y. Cui, J. Yang, D. Lei and J. Su, *Ind. Eng. Chem. Res.*, 2020, **59**, 11381–11388.

184 A. Belmonte, X. Fernández-Francos, À. Serra and S. De la Flor, *Mater. Des.*, 2017, **113**, 116–127.

185 S. Chatani, D. P. Nair and C. N. Bowman, *Polym. Chem.*, 2013, **4**, 1048–1055.

186 X. Fernández-Francos, A.-O. Konuray, A. Belmonte, S. De la Flor, À. Serra and X. Ramis, *Polym. Chem.*, 2016, **7**, 2280–2290.

187 D. Guzmán, X. Ramis, X. Fernández-Francos and A. Serra, *RSC Adv.*, 2015, **5**, 101623–101633.

188 H. C. Kolb, M. G. Finn and K. B. Sharpless, *Angew. Chem. Int. Ed.*, 2001, **40**, 2004–2021.

189 J. E. Moses and A. D. Moorhouse, *Chem. Soc. Rev.*, 2007, **36**, 1249–1262.

190 C. E. Hoyle and C. N. Bowman, *Angew. Chem. Int. Ed.*, 2010, **49**, 1540–1573.

191 O. Konuray, X. Fernández-Francos, S. De la Flor, X. Ramis and À. Serra, *Polymers*, 2020, **12**, 1084.

192 C. E. Hoyle, A. B. Lowe and C. N. Bowman, *Chem. Soc. Rev.*, 2010, **39**, 1355–1387.

193 I. V. Koval', *Russ. J. Org. Chem.*, 2005, **41**, 631–648.

194 E. Dyer and D. W. Osborne, *J. Polym. Sci.*, 1960, **47**, 361–371.

195 A. B. Lowe and C. N. Bowman, *Thiol-X Chemistries in Polymer and Materials Science*, Royal Society of Chemistry, Croydon, United Kingdom, 2013.

196 H. Li, B. Yu, H. Matsushima, C. E. Hoyle and A. B. Lowe, *Macromolecules*, 2009, **42**, 6537–6542.

197 J. Shin, H. Matsushima, J. W. Chan and C. E. Hoyle, *Macromolecules*, 2009, **42**, 3294–3301.

198 S. Kuypers, S. Kumar Pramanik, L. D'Olieslaeger, G. Reekmans, M. Peters, J. D'Haen, D. Vanderzande, T. Junkers, P. Adriaensens and A. Ethirajan, *Chem. Commun.*, 2015, **51**, 15858–15861.

199 S. Chatani, R. J. Sheridan, M. Podgórski, D. P. Nair and C. N. Bowman, *Chem. Mater.*, 2013, **25**, 3897–3901.

200 H. Salmi, X. Allonas and C. Ley, *Prog. Org. Coat.*, 2016, **100**, 81–85.

201 J. Shin, J. Lee and H. M. Jeong, *J. Appl. Polym. Sci.*, 2018, **135**, 46070.

202 Y. Jia, B. Shi, J. Jin and J. Li, *Polymer*, 2019, **180**, 121746.

203 A. Kultys, M. Rogulska and S. Pikus, *J. Polym. Sci. Part Polym. Chem.*, 2008, **46**, 1770–1782.

204 C. Lü, Z. Cui, Z. Li, B. Yang and J. Shen, *J. Mater. Chem.*, 2003, **13**, 526–530.

205 N. G. Ireni, R. Narayan, P. Basak and K. V. S. N. Raju, *Polymer*, 2016, **97**, 370–379.

206 L. Li, X. Chen and J. M. Torkelson, *Macromolecules*, 2019, **52**, 8207–8216.

Chapter II

Experimental Methods

II-1 Differential scanning calorimetry (DSC)

Differential scanning calorimetry (DSC) provides quantitative and qualitative information about physical and chemical changes that involve endothermic or exothermic processes, or changes in the heat capacity. The DSC device measures the amount of heat that flow into or out of samples subject to dynamic or isothermal heating procedures. The technique is based on detect the difference in the amount of heat required to increase the temperature of a sample and reference as a function of temperature.[1] DSC is the most widely used analytical technique to characterize thermoset thanks to the possibility to quickly measure the glass transition temperature. During crosslinking reaction, the formation of new chemical and physical bonds is accompanied by a release of heat (a typical exotherm curve of a curing process is shown in Figure II-1a).

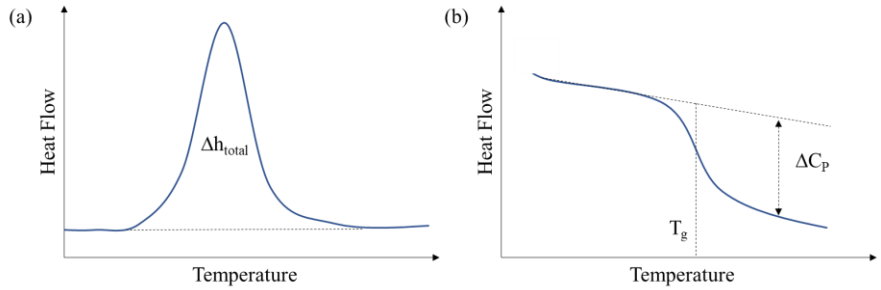

Figure II-1. *DSC analysis of polymeric materials: (a) heat released as a function of the temperature during the curing process and (b) variation of the heat capacity as a function of the temperature during a glass transition in a thermosetting polymer.*

In a kinetic study by DSC the heat released is directly related to the extent of the reaction, as follows:

$$\frac{dx}{dt} = \frac{dh\ /\ dt}{\Delta h_t} \qquad (1)$$

$$x = \frac{\Delta h_t}{\Delta h_{total}} \qquad (2)$$

Where *dx/dt* is the curing rate, *x* is the degree of curing, *dh/*d*t* is the heat flow, Δh_t is the heat released from the beginning to the time *t* and Δh_{total} is the total heat released during the curing process.

On the other hand, second order transitions, such as the glass transition, are measured through step variation of the heat capacity associated to the structural reorganization of the network (see the heat capacity jump and the determination method during the glass transition in Figure II-1b).

In this thesis, DSC experiments were carried out using a Mettler DSC-3+, Figure II-2. Samples of ~ 5-10 mg of weight were placed in covered aluminium pans with pierced lids and analysed in nitrogen atmosphere with a gas flow of 50 cm^3/min.

Figure II-2. *DSC-3+ device from Mettler Toledo (left) and detail of its furnace (right).*

II-2 Thermogravimetric analysis (TGA)

Thermogravimetric analysis (TGA) is a technique where the mass of a polymer is constantly measured as a function of temperature or time while the sample is subjected to a controlled temperature program in a controlled atmosphere.

The TGA is used for different scopes such as: material characterization, degradation studies, determination of organic, inorganic or moisture content. The instrument consists of a precision balance, located in a furnace, which can measure the weight as a function of temperature and time while a purge gas flowing through the furnace creates an inert, oxidizing or reducing atmosphere.[2]

A thermobalance Mettler Toledo TGA 2 (Figure II.3) was used to analyze the thermal degradation of cured samples. The most important parameters extracted from the analysis of such curves are the initial degradation temperature, the temperature of the maximum degradation rate and the char yield.

Figure II-3. *Thermobalance Mettler TGA 2 (left) and a detailed image of the oven of the TGA (right).*

II-3 Fourier-transformed infrared spectroscopy (FT-IR)

Infrared (IR) spectroscopy is one of the most common and widely used spectroscopic techniques employed to determine specific structures of organic compounds. In this technique infrared light interacts with a sample which can be solid or liquid. A certain amount of incident light goes through the sample and a certain amount gets absorbed by the molecules of the sample, obtaining the absorption and transmission spectrum.[3] The signal is transferred to a computer in which Fourier transform (FT) is carried out. The term FTIR comes from the fact that a Fourier transform is required to convert the raw data into the actual spectrum.[4] The principle which allows following the curing reaction using FTIR measurements is the Lambert-Beer law, which is as follows:

$$A = \varepsilon \cdot C \cdot L \tag{3}$$

where A is the absorbance of a specie at a certain frequency, ε is the absorptivity coefficient, C is the concentration and L is the optical pathway.

The resultant absorbance bands are proportional to the concentration of different functional groups. Therefore, the curing process can be followed by monitoring the signals of the groups involved in the reaction, before, during and after the curing process. Since the absorbance is proportional to the optical pathway, L, it is needed to normalize the analyzed band against a reference band which remains constant during the curing process. Thus, the conversion x can be determined by FT-IR experiments and written as follows:

$$x = 1 - \frac{A'_t}{A'_0} \tag{4}$$

where A'_t is the normalized absorbance at a certain time and A'_0 is the initial.

In this work, the infrared spectroscopy has been used to determine the progress of the “thiol-isocyanate” reaction and to evaluate a possible change in the spectra of the PTU materials occurred after the recycling process.

The FT-IR spectra were recorded with a FT-IR spectrophotometer Bruker Vertex 70 (Figure II-4), with resolution of 4 cm^{-1} in absorbance mode. The spectrophotometer is equipped with an attenuated total reflection (ATR) device which is temperature controlled (heated single-reflection diamond ATR crystal)

Figure II-4. *Photograph of the FT-IR Bruker Vertex 70.*

II-4 Gel-point determination (Rheometer)

The curing of thermosets is a complex process, in which crosslinks between polymer chains are formed during the chemical reactions producing an infusible and insoluble polymer network. During this process two distinct physical phenomena can take place, gelation and vitrification of the material.

The gelation time is defined as the time in which covalent bonds connect across the network and a material of infinite molecular weight is produced. Above the gel point, the material loses its ability to flow and cannot be processed anymore, therefore gelation represents the limit of the work life. The gelation leads to a drastic change in the physical response: the viscosity tends to infinite and the material response becomes more elastic than viscous. The vitrification takes place when the material behaves as a glass and the glass transition temperature becomes equal to the cure temperature.[5]

In this investigation, the gel-point was determined by means of rheological experiments. The experiments were carried out using a Rheometer AR-G2 (Figure II-5a) (TA Instruments, New Castle, DE) equipped with an electrical heated plate (EHP) and parallel plate geometry (Figure II-5b). The network formation and gel point determination of the “thiol-isocyanate” systems are presented and studied in Chapter V.

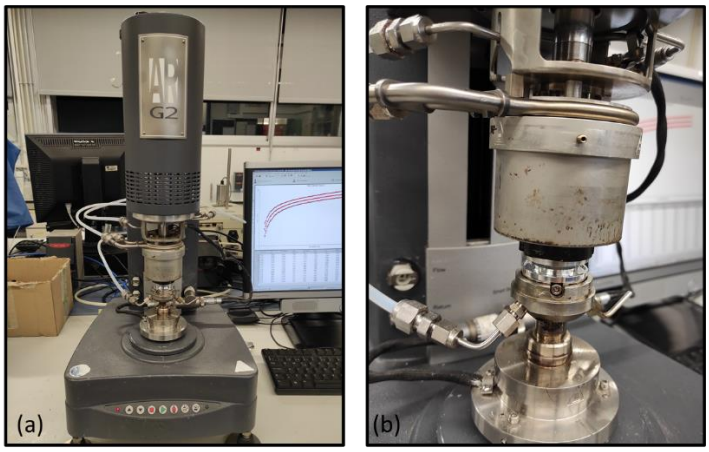

***Figure II-5**. Pictures of the rheometer AR-G2: (a) device and (b) parallel plate geometry.*

II-5 Dynamic-mechanical analysis (DMA)

Viscoelastic materials, like polymers, exhibit both viscous and elastic behaviour when they undergo deformation. DMA is a powerful and commonly used technique to study the viscoelastic behaviour of polymers. There are three fundamental test methods to characterize the viscoelastic behaviour of polymers: creep, stress relaxation and dynamic mechanical analysis.

The most common test is the dynamic mechanical analysis, in which a sinusoidal pulse is applied to the sample and the sample will deform sinusoidally (Figure II-6).[6]

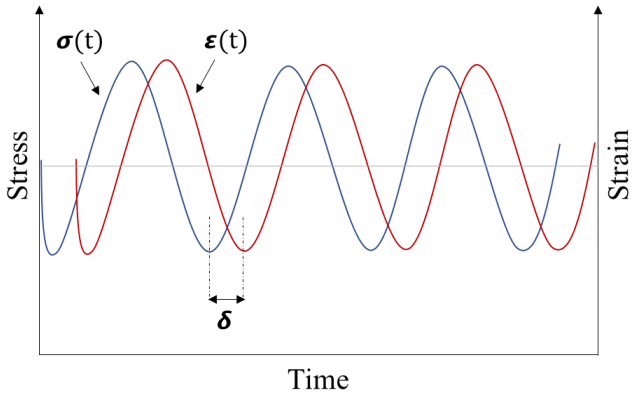

***Figure II-6.** Applied strain and related stress as a function of time in DMA.*

At any given time, the strain applied to the sample, ε(t), follows the expression:

$$\varepsilon = \varepsilon_0 \sin(\omega t) \qquad (5)$$

where ε_o is the strain amplitude, ω is the oscillation frequency and t is the time. The resultant stress, $\sigma(t)$, has the same frequency but a phase lag δ:

$$\sigma = \sigma_0 \sin(\omega t + \delta) \quad (6)$$

Rewriting equation 6 as follow:

$$\sigma = \sigma_0 \sin(\omega t) \cos\delta + \sigma_0 \cos(\omega t) \sin\delta \quad (7)$$

The above equation indicates that the stress has two components: $\sigma_0 \cos\delta$ which is in phase with the strain and $\sigma_0 \sin\delta$ which is 90° out of phase with the strain. For small strain amplitudes and time independent polymers (linear viscoelastic regime) the resulting stress can be written in terms of the dynamic storage modulus (*E'*) and the dynamic loss modulus (*E"*):

$$E' = \frac{\sigma_0}{\varepsilon_0} \cos\delta \quad (8)$$

$$E'' = \frac{\sigma_0}{\varepsilon_0} \sin\delta \quad (9)$$

The storage modulus *E'* represents the elastic response or the ability to store energy of the material, while the loss modulus *E''* represents the viscous response or the ability to lose energy of the material. The relation between both moduli determines the damping capabilities of the polymer:

$$tan\,\delta = \frac{E''}{E'} \quad (10)$$

The tangent of the phase angle (tan *δ*) or damping factor provides a measure of how much energy is lost due to the viscous nature of the material.

Oscillatory tests, at a fixed frequency of 1 Hz and dynamic heating between 2 and 5 °C/min, are usually carried out, to determine the thermomechanical parameters of the polymer. A typical DMA analysis of a crosslinked polymer is showed in Figure II-7.

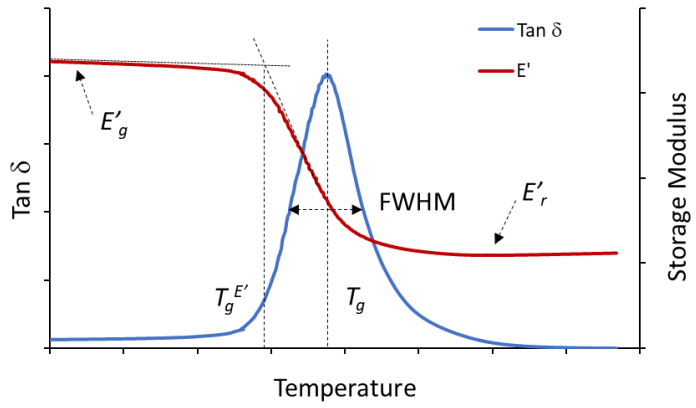

Figure II-7. *Evolution of the storage modulus and tan δ as a function of the temperature at fixed frequency for a thermoset subjected to an oscillatory stress DMA experiment.*

The thermal transition processes can be described by the appearance of a peak in the *tan δ* curve. The shape of the curve is indicative of the homogeneity of the material, as the narrower the *tan δ* peak is, the more homogeneous the network structure. The parameter used to quantify the homogeneity is the "full width at half maximum" (FWHM). The peak of the *tan δ* curve is normally used to evaluate the glass transition temperature (T_g). The other method used to determine the T_g, which tends to be similar to the T_g defined by pure thermal methods, is to consider the onset temperature of the decrease in the storage modulus, named $T_g^{E'}$. The T_g temperatures determined by the two different methods are not identical. It is important to consider that glass transition occurs in a temperature range and the frequency and heating rate affect the transition. Criteria for determining the T_g are selected depending on the study and in this thesis the T_g is generally assumed as the temperature of the maximum of the peak of the *tan* δ curve.

The evolution of *E'* is also important and crosslinked polymers present two plateaux before and after the glass transition. The relatively flat region at lower temperatures corresponds to the glassy state of the polymer and the value of *E'* is comparable to that obtained from static three-point-bending methods, as long as the experiment proceeds under linear elasticity conditions. The rubbery modulus after the glass transition is related to the crosslinking density of the network. The relation, according to the rubber elasticity theory,[7,8] follows the following expression:

$$\nu_F = \frac{E_R}{3RT} \tag{11}$$

where *R* is the universal constant for gases, *T* is the temperature at which the E_R is determined and ν_F is the density of crosslinks.

II-5.1 Creep and Relaxation experiments

Creep is defined as the tendency of a polymer to distort under a fix external load. A creep test involves loading a sample with a continuous stress and recording the resulting strain over an extended period of time. The test can be paired with a recovery test, which assesses how the material relaxes once the stress is removed.[9]

The inverse of creep experiment is a stress-relaxation experiment. In this test a sample is studied by applying a constant deformation to the specimen and measuring the stress required to maintain that strain as a function of time. The sample is quickly distorted to a set length and the stress needed to hold the strain decreases over time.

Creep and stress-relaxation data can be treated as mainly reciprocal, and the deformation mechanisms associated with these experiments are both related to the molecular segmental motions of the polymer. In a creep experiment, the continuous loading gradually induces strain accumulation as the polymer molecules tend to rotate and unwind to accommodate the load. Similarly, in relaxation test, after the sudden

initial strain, over time the molecules will again rotate and unwind so that less stress is needed to maintain the same strain level.[10] The viscoelastic flow properties of a thermoplastic are due to the lack of primary bonds between molecular chains that allow molecular movement. In thermosets due to the presence of crosslinking sites between molecular chains the segmental motion is further limited.

A typical creep test for thermoplastic and thermosets is presented in Figure II-8a. For a thermoset the strain will tend to a constant value after a long time because the crosslinks do not allow flow, even if some creep does occur in thermosets at high temperature if the crosslink density is low enough, in highly crosslinked materials no creep is usually observed. For a thermoplastic the strain can increase untethered as the molecular chains start to rotate and unwind allowing viscous flow. Once the stress is removed also the resulting strain variation depends on the nature of the polymer, Figure II-8b. For an ideal thermoset material, the strain will decay to zero after a sufficient interval of time, since they retain a remarkable memory of their original structure. For an ideal thermoplastic material, a residual deformation will remain even after a very long (or infinite) time.

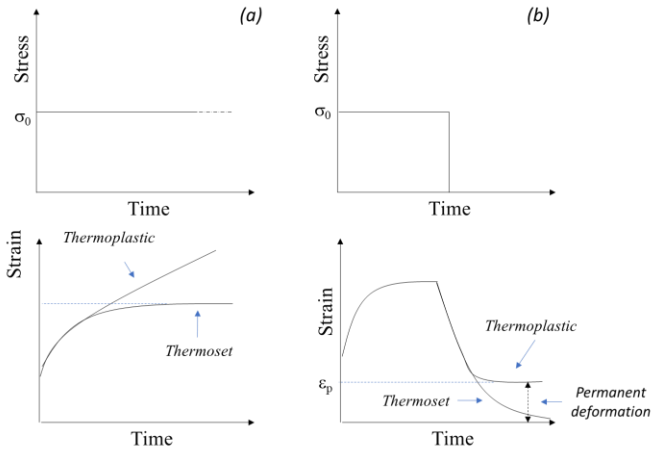

Figure II-8. *(a) Creep and (b) creep recovery tests: stress input above and qualitative stress response for thermoplastic and thermosetting polymers below.*

A typical strain input and stress output for thermosetting and thermoplastic polymers in a relaxation test are shown Fig. II-9. For an ideal thermoplastic polymer, the stress decay to zero at long enough times. For a crosslinked polymer, the stress can decrease to a finite value, since viscous flow cannot occur as the crosslinking points hinder chain movements.[11]

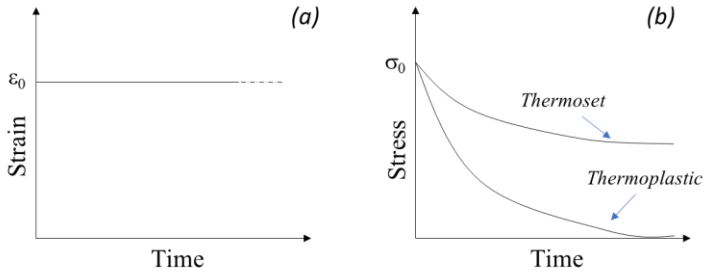

Figure II-9. *Relaxation test: (a) strain input; and (b) qualitative stress response for thermoplastic and thermosetting polymers.*

DMA measurements were carried out with a DMA Q800 (TA Instruments) equipped with 3-point-bending, single cantilever, or tension film clamp depending on the tested sample (Figure II-10).

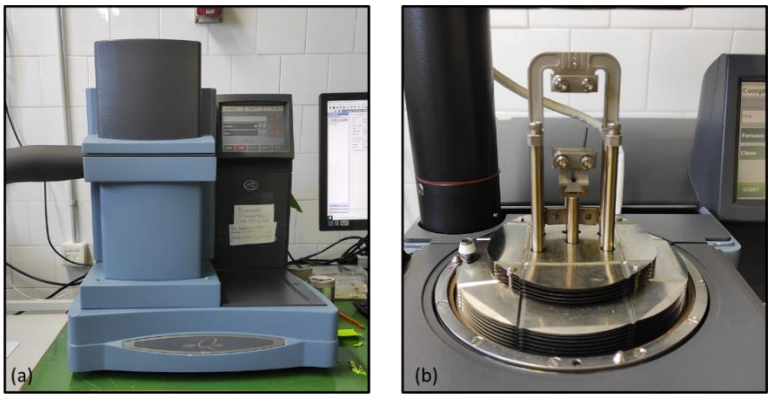

Figure II-10. *Photographs of the TA Instruments DMA Q800 equipment: (a) device and (b) tension film clamp.*

II-6 Tensile tests

Tensile tests consist of applying a controlled uniaxial stress to a sample until failure occurs and the stress/strain response of the material is registered by a computer. The tensile properties of the material depend on the experimental conditions such as: temperature, humidity and testing rate.

A typical stress/strain curve of a thermoset at room temperature is presented in Figure II-11a. The stress at break (σ_b) and deformation at break (ε_b) are determined from the failure point. The elastic modulus *E* is calculated from the slope of the curve in the linear part of the curve.

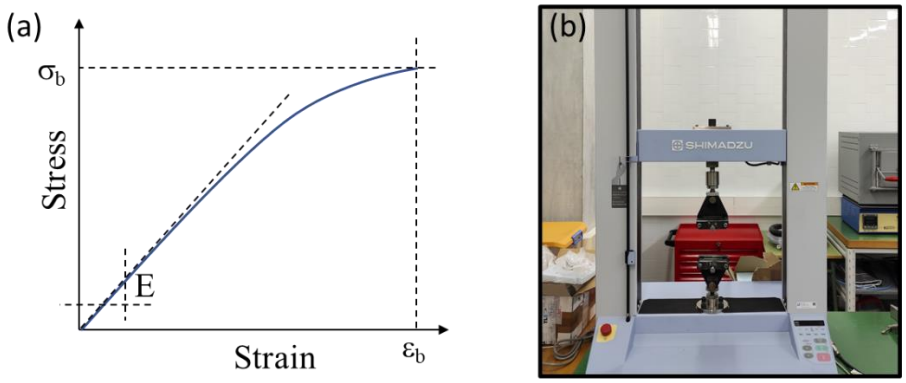

Figure II-11. *(a) Typical stress/strain response of a thermosets at room temperature and (b) photograph of the tensile machine (Shimadzu AGS-X).*

The specimen size was adapted from ASTM D638 requirements, adopting a Type IV dog-bone shape (Figure II-12).

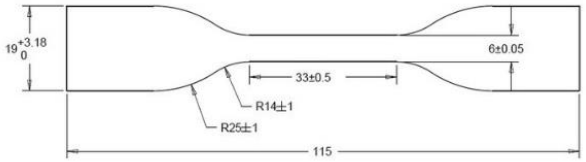

Figure II-12. *ASTMD638 - IV, details of the specimen dimensions (in mm).*

In this investigation, uniaxial tensile experiments at room temperature were carried out using an electromechanical universal testing machine (Shimadzu AGS-X) with a 1000 N load cell at 5 mm/min (Figure II-11b).

II-7 Characterization of covalent adaptable networks

Covalent adaptable networks (CANs) are crosslinked networks with dynamic covalent bonds that allow the network to undergo topological change. Therefore, the characterization of a CAN usually starts from an analysis of the exchange pathway, to confirm the existence of the dynamic interactions.

Once the dynamic nature of the covalent bonds is demonstrated the typical characterization of covalent adaptable networks can be divided in three major parts:

I) *Characterization of the crosslinked network*

First, the thermosetting character of the dynamic crosslinked network has to be determined by:

- *Infrared spectroscopy:* to confirm that the reaction is completed and a fully crosslinked network is formed.

- *Dynamic mechanical analysis:* to ensure that the network exhibits a stable rubbery plateau up to the glass transition temperature, since the flow properties will be calculated at high temperature. In addition, from the DMTA analyses the value of the glass transition temperature and elastic modulus in the rubbery state are determined.
- *Thermogravimetric analysis:* to evaluate the thermal stability of the materials, as the characterization and processing of CANs require numerous heating steps at high temperatures for long periods of time.
- *Dissolution tests:* to demonstrate that the network integrity in an organic solvent is maintained. Samples can swell but do not dissolve in good solvents even after immersion at elevated temperature for a long period of time.

II) *Viscoelastic characterization*

Once the crosslinked nature of network is proved, the second part of the characterization is focused on the analysis of the viscoelastic properties of the CANs at elevated temperatures. To evaluate these characteristics, different experiments can be performed:

Stress-relaxation experiments (SRE)s: to evaluate the viscosity-temperature relationships, SREs are performed at different temperatures until the material reach a complete stress relaxation process. In the case of covalent adaptable networks, the stress relaxation is achieved through interchange of bonds. Two pairs of neighbouring bonds are broken, and new bonds are formed in a new no-load configuration. When all bonds are reshuffled the stress reach the zero value. This is represented in Figure II-13.

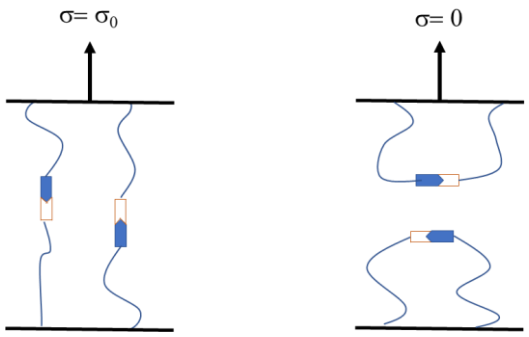

Figure II-13. *Schematic representation of the exchange of covalent bond in a stress-relaxation experiment.*

From the stress-relaxation results the characteristic relaxation time (τ^*) is extrapolated, defined as the time required for the stress relaxation modulus to reach 37% (1/e) of its initial value. The viscosity and the characteristic relaxation time are correlated via the Maxwell equation[12]:

$$\eta = E' \cdot \tau^* \tag{12}$$

where η is the viscosity, E' the storage modulus in the rubbery state and τ^* is the characteristic relaxation time. The relaxation times, τ^*, obtained at each temperature are then plotted in an Arrhenius plot to verify that τ^* and consequentially η follow an Arrhenius relationship, Eq. 13:

$$\tau^* = \tau_0 \cdot e^{\left(\frac{E_a}{RT}\right)} \tag{13}$$

where τ_0 is the characteristic relaxation time at infinite T, E_a is the activation energy of the bond exchange reaction, R is the universal gas constant and T is the temperature. Rewriting Eq. 13 as follows:

$$\ln \tau^* = \ln \tau_0 + \frac{E_a}{RT} \tag{14}$$

the activation energy (E_a) of the exchange mechanism and the topology freezing transition temperature (T_v) can be calculated, referring to Figure II-14.

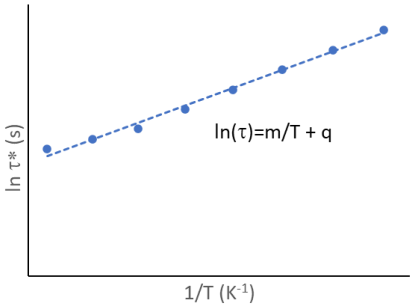

Figure II-14. *Schematic representation of the variation of the relaxation time with the inverse of the temperature.*

The activation energy is calculated directly from the slope of the line, while the T_v can be calculated substituting the value of viscosity of 10^{12} Pa·s (liquid to solid transition) and the elastic modulus in the Maxwell equation obtaining the relaxation time (τ^*). Then the extrapolated value of τ^* is substituted in the Arrhenius relationship to calculate the hypothetical T_v, using Eq. 15:

$$T_v = \frac{m}{\ln(\tau^*) - q} \tag{15}$$

where m and q are the slope and the intercept of the straight line.

Dilatometry experiments: Dilatometry experiments allow to determine the evolution of specific volume with temperature, in the case of CANs these experiments are useful to locate the glass transition temperature and then the topological transition temperature, T_v. This test is convenient and simple to confirm that the network is

capable of topological rearrangement and provides an easy way to understand when the exchange reaction became effective.

Creep experiments: creep-recovery experiments are performed to ensure that the material does not show plastic deformation at the service temperature, behaving like a crosslinked at ambient temperature or slight above the glass transition. In particular, elastomeric CANs are susceptible to this problem under conditions of use, as the molecular chains already present certain mobility at room temperature.

To further validate that CANs behave like a viscoelastic liquid at elevated temperatures, creep experiments are typically performed. From a series of creep experiments at different temperatures it is possible to determine the viscosity and represent the Angell Fragility Plot.[13] The viscosity η (Pa·s) can be calculated from the slope of the linear part of the graph strain-temperature, as showed in Figure II-15.

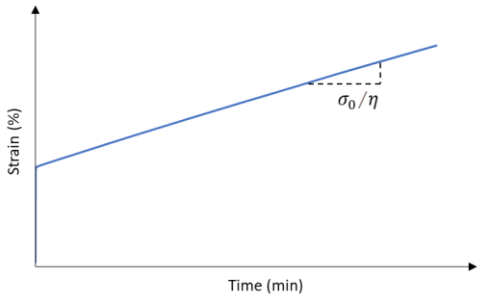

Figure II-15. *Schematic representation of the viscoelastic behavior during a creep experiment performed on a vitrimer at high temperature.*

Then, the logarithm of the extrapolated viscosity at different temperatures is represented as function of the inverse temperature scaled to transition temperature, thus obtaining the Angell Fragility plot.[14] Hypothetical T_v is normally selected as transition temperature in the case of vitrimers.[15] In this work, to elaborate the Angell Fragility Plot we referred to the T_v, if the T_v is located above the T_g, or to the T_g , if the T_v is located below the T_g since no physical transition can happen in the glassy state.

III) *Recyclability*

Once, the ability to flow has been demonstrated, the CANs can be reprocessed and recycled. To investigate the recyclability of CANs, crosslinked materials are grinded into small particles and then reformed into a new specimen by hot pressing, as showed inf Figure II-16.[16,17] The duration and the temperature of the hot-pressing procedure can be extrapolated approximatively from the results of the relaxation experiments. To ensure good contact between the polymer powder, the pressure must be adjusted carefully.

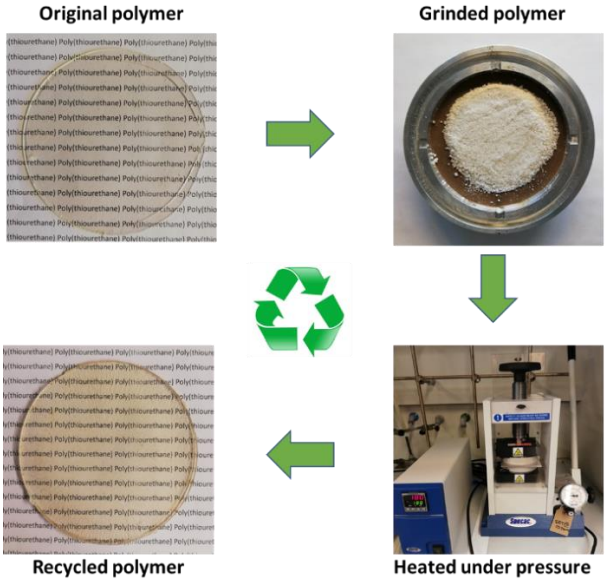

Figure II-16. *Photographs of a typical recycling procedure from the original to the obtained of the recycled sample.*

The properties of the recycled materials are evaluated by comparison with those of the initial material. The properties are assessed performing a new standard characterization of crosslinked network via DMA and FTIR and TGA analysis on the recycled sample. Furthermore, in order to ensure that the mechanical properties of the materials are not compromised during the recycling process, the tensile properties of the original and reprocessed materials are tested by means of a uniaxial tensile test.

References

1 E. A. Turi, Ed., *Thermal Characterization of Polymeric Materials, Two-Volume Set, Volume 1-2, Second Edition*, Academic Press, San Diego, California, 2nd edition., 1997.
2 J. D. Menczel and R. B. Prime, *Thermal Analysis of Polymers: Fundamentals and Applications*, John Wiley & Sons, Hoboken, New Jersey, 2009.
3 P. R. Griffiths, John Wiley & Sons, Ltd, Hoboken, New Jersey, 2009, pp. 1–64.
4 O. Faix, in *Fourier Transform Infrared Spectroscopy*, eds. S. Y. Lin and C. W. Dence, Springer, Berlin, Germany, 1992, pp. 83–109.
5 J.-P. Pascault and R. J. J. Williams, Eds., *Epoxy Polymers: New Materials and Innovations*, Wiley-VCH, Weinheim, Germany, 1st edition., 2010.
6 K. P. Menard and N. R. Menard, *Dynamic Mechanical Analysis, Third Edition*, CRC Press, Boca Raton, Florida, 2020.
7 L. E. Nielsen, *J. Macromol. Sci. Part C*, 1969, **3**, 69–103.
8 J.-P. Pascault, H. Sautereau, J. Verdu and R. J. J. Williams, *Thermosetting Polymers*, CRC Press, New York, NY, 2002.
9 A. B. Strong, *Plastics: Materials and Processing*, Prentice Hall, Saddle River, New Jersey, 2000.
10 H. F. Brinson and L. C. Brinson, *Polymer Engineering Science and Viscoelasticity: An Introduction*, Springer US, New York, NY, 2nd edn., 2015.
11 S. Turner, in *The Physics of Glassy Polymers*, ed. R. N. Haward, Springer, Dordrecht, Netherlands, 1973, pp. 223–278.
12 J. C. Maxwell, *Proc. R. Soc. Lond.*, 1867, **15**, 167–171.
13 D. Montarnal, M. Capelot, F. Tournilhac and L. Leibler, *Science*, 2011, **334**, 965–968.
14 C. A. Angell, *Science*, 1995, **267**, 1924–1935.
15 M. Capelot, M. M. Unterlass, F. Tournilhac and L. Leibler, *ACS Macro Lett.*, 2012, **1**, 789–792.
16 B. Krishnakumar, R. V. S. P. Sanka, W. H. Binder, V. Parthasarthy, S. Rana and N. Karak, *Chem. Eng. J.*, 2020, **385**, 123820.
17 Z. P. Zhang, M. Z. Rong and M. Q. Zhang, *Prog. Polym. Sci.*, 2018, **80**, 39–93.

Chapter III

Preparation of poly(thiourethane) thermosets by controlled thiol-isocyanate click reaction using a latent organocatalyst

Reactive and Functional Polymers 134 (2019) 174–182

Preparation of poly(thiourethane) thermosets by controlled thiol-isocyanate click reaction using a latent organocatalyst

Francesco Gamardella[1], Xavier Ramis[2], Silvia De la Flor[3], Àngels Serra[1]

[1] Dept.of Analytical and Organic Chemistry, Universitat Rovira i Virgili, C/ Marcel·lí Domingo, 43007, Tarragona, Spain

[2] Thermodynamics Laboratory, ETSEIB Universitat Politècnica de Catalunya, Av. Diagonal, 08028, Barcelona, Spain

[3] Department of Mechanical Engineering, Universitat Rovira i Virgili, Av. Països Catalans, 26, 43007 Tarragona, Spain

Abstract

Different poly(thiourethane) thermosets were prepared by means of a thiol-isocyanate click reaction, starting from three diisocyanates with different structure (isophorone diisocyanate, IPDI, 4,4'-methylene bis(cyclohexy isocyanate), HMDI and hexamethylene diisocyanate, HDI and a tetrathiol, pentaerythritol tetrakis(3-mercaptopropionate), PETMP. The curing process was catalyzed by basic and acid catalysts. The use of a thermally activated base generator (1-methylimidazolium tetraphenylborate, BG1MI), which is an organocatalyst, allowed a better control of the onset of the polymerization compared to the dibutyltin dilaurate (DBTDL) or commonly used tertiary amines. The curing evolution was investigated by DSC and FTIR spectroscopy.

The materials were characterized by thermomechanical and mechanical tests. The chemical structure of the network was correlated with the thermal and mechanical data determined. Homogeneous materials were obtained in all cases with glass transition temperature (T_g) values in the range between 75 and 150 °C. The thermal degradation of these materials was investigated and a complex degradation mechanism with three different steps was observed.

The thermosets obtained using the latent organocatalyst have similar thermal and thermomechanical characteristics to the ones obtained by using the common DBTDL.

Keywords:

poly(thiourethanes), click reaction, thermosets, latency, organocatalysts.

1. Introduction

Click-chemistry, introduced for the first time by Kolb *et al.* in 2001 [1], has attracted a broad interest in the field of thermosets due to its efficiency, selectivity, speed and effective reaction mechanism, that leads to the formation of highly homogeneous materials with high crosslinking density and without the formation of unexpected structures and volatile by-products [2]. There are several efficient reactions that can be considered as click reactions, among them the nucleophilic addition of thiols to isocyanate satisfied all the criteria required to be considered as "click reaction" [3-6].

Although the reaction that leads to the formation of poly(thiourethanes) (PTUs) is known for a long time [7], it has been less investigated than the process leading to the formation of their oxygen analogs, poly(urethanes) (PUs), which have a great industrial importance, reflected in a nearly 5% of total polymer production [8]. The formation of poly(thiourethanes) is not accompanied by side-reactions, often observed in the poly(urethanes) synthesis with the formation of urea and allophanates [9].

Poly(thiourethanes), also named poly(thiocarbamates), are very versatile polymeric materials due to their biocompatibility, excellent physical, mechanical and optical properties. In comparison to poly(urethanes), the incorporation of sulfur to the backbone of the polymeric structure increases flexibility, crystallinity and feasibility to incorporate these structures to polymerizable systems [10,11]. Moreover, the enhanced refractive index makes PTUs suitable for optical applications. In fact, Lu *et al.* prepared PbS/PTU and ZnS/PTU polymer nanocomposites as optical materials with high refractive index in the range between 1.5 and 2 [12,13]. Jaffrennou *et al.* studied a poly(thiourethane) thermosetting system based on trithiol/diisocyanate formulations for optical applications [14], and Ireni *et al.* synthesized a poly(thiourethane-urethane-urea) with impressive optical properties, transmittance (>90%) and a refractive index value of 1.5 [15]. Poly(thiourethane)s have also been applied in microfluidics and microparticles preparation [16,17]. Some papers on coatings applications of these materials have also been published [18,19].

In the preparation of poly(urethanes) and poly(thiourethanes), the reaction can be catalyzed by several bases and by different Lewis acids [20]. Depending on the characteristics of the catalyst used, the activation occurs through two different ways. When a basic catalyst is selected, the base activates the alcohol or thiol by forming the corresponding anion (nucleophilic activation) which are the species that attack the isocyanate carbon (see Scheme 1). Alternatively, when a Lewis acid is used, the acid coordinates with the oxygen or nitrogen lone pairs of the isocyanate (electrophilic activation), which can be attacked by less nucleophilic agents like neutral thiols or alcohols [21,22]. Generally speaking, thiols are more acidic than alcohols, and the basic catalyst helps to form thiolate anions, with an accentuated nucleophilic

character, higher than alkoxides. According to that, the reactivity of thiols is higher than the reactivity of alcohols and subsequently, the attack to the isocyanate is much faster in the formation of PTUs.

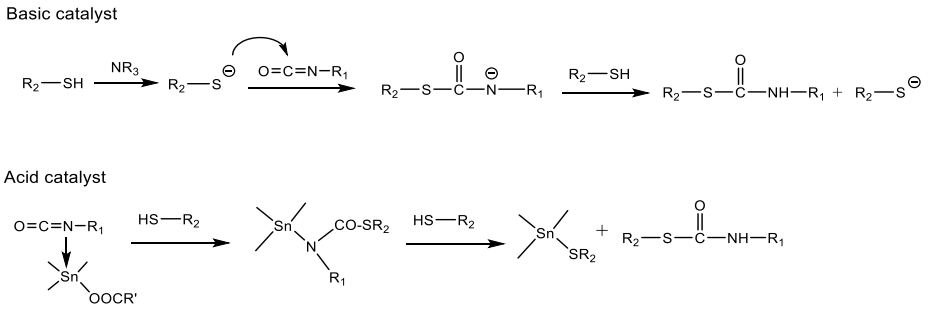

Scheme III-1. *Proposed mechanisms of poly(thiouretane) formation in both basic and acidic conditions.*

The aim of the present work is the preparation and characterization of a series of poly(thiourethane) networks, investigating the most adequate curing schedule and conditions to obtain thermosets with high performance. According to that, the selection of the catalyst and its proportion is the key point to reach a high technical applicability in the desired processing time.

The most common basic catalysts involved in the thiol-isocyanate polycondensation are tertiary amines such as triethylamine (TEA) or amidine compounds such as 1,5-diazabicyclo[4.3.0]non-5-ene (DBN) or 1,8-diazabicyclo[5.4.0]undec-7-ene (DBU) [23,24]. Recently, Shin *et al.* reported the use of amines to perform thiol-isocyanate-ene ternary networks by sequential and simultaneous click reactions [25]. The same research group described the synthesis of elastic segmented poly(thiourethane)s by sequential thiol-ene and thiol-isocyanate reactions in the presence of TEA [26]. In presence of a basic catalyst, once initiated the reaction is too fast and the system is difficult to process due to the high reactivity of the monomers involved in the reaction. The fast reaction can be attributed to the low pK_a of thiol species and their easy deprotonation in presence of a base. Thus, the formation of poly(thiourethane) networks is much faster, and consequently more problematic in terms of processing, than the formation of crosslinked poly(urethanes) [12,13,27,28].

To reduce the speed of the reaction, one of the possibilities is to decrease the amount of catalyst. However, in many studies a low degree of conversion of the monomers involved was obtained, which leads to a reduction of the T_g values. The use of a latent basic catalyst, that releases a base after the application of an external stimulus could be a solution to prepare poly(thiourethanes) in a controlled way.

In addition to the use of bases, the most common acid catalysts used by several authors to prepare PTUs for optical applications are organometallic tin compounds,

especially dibutyltin dilaurate (DBTDL) [12,13,14]. For example, Kultys *et al.* selected DBTDL to synthetize a new copolymeric thermoplastic, poly(thiourethane-urethane)s [29]. The use of DBTDL leads to low reaction rates, resulting in long curing times or high curing temperatures, which can negatively affect the performance of the crosslinked materials. In addition to that, the European Union have restricted the use of organotin-based compounds. Therefore, the use of organocatalyst in the preparation of polymeric materials is one of the improvements to be made to fulfil the EU regulations and to open new possibilities of application in the biomedical field [30,31]. In previous studies of our group, the use of latent bases has been explored to catalyze well-controlled crosslinking procedures. A commercially available encapsulated imidazole, LC-80, and photo-latent bases as tertiary ammonium tetraphenylborates (BG) that liberated amines on reaching a certain temperature, were used in the preparation of thermosets by thiol-epoxy reaction [32,33]. Shin *et al.* described the use of a photo-latent base in the preparation of poly(thiourethane)s triggered by UV-irradiation. However, this system has some limitations such as lower curing degree in shadowed areas, possible vitrification of the material and that the photochemical processes are restricted to the preparation of thin layers [34].

In the present study, we tested the latent bases (LC-80 and 1-methylimidazolium tetraphenylborate (BG1MI)) as efficient catalyst for thiol-isocyanate reaction, their performances were compared with DBTDL by means of calorimetric and FT-IR studies. Three different isocyanates: isophorone diisocyanate (IPDI), 4,4'-methylene bis(cyclohexyl isocyanate) (HMDI) and hexamethylene diisocyanate (HDI); and a pentaerythritol tetrakis(3-mercaptopropionate) (PETMP) (see Scheme 2) were used as starting monomers.

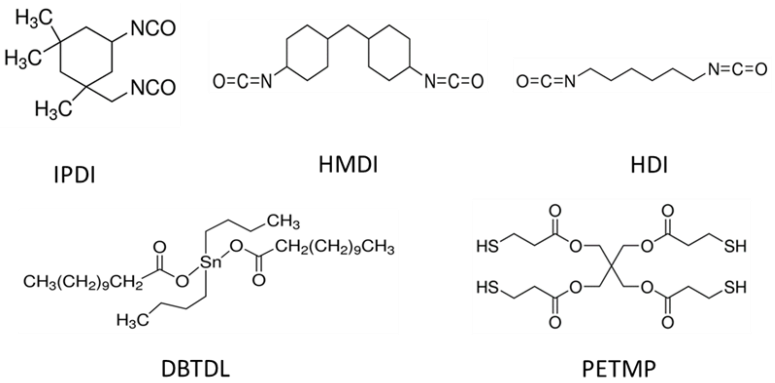

Reactive and Functional Polymers 134 (2019) 174–182

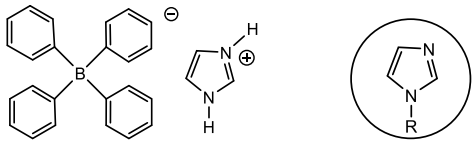

BG1MI LC80

Scheme III-2. *Structure of the starting compounds.*

The mechanical and thermal properties of the resultant poly(thiourethane) thermosets were investigated by thermomechanical and thermogravimetric analysis, and by mechanical tests.

2. Experimental Methods

2.1. Materials

Pentaerythritol tetrakis(3-mercaptopropionate) (PETMP), dibutyltin dilaurate (DBTDL) and hexamethylene diisocyanate (HDI) were purchased from Sigma-Aldrich. Isophorone diisocyanate (IPDI) and 4,4'-methylene bis(cyclohexyl isocyanate) (HMDI) from Acros Organics. Technicure® LC-80 (encapsulated imidazole) were provided by AC Catalysts. The base generator, 1-methylimidazolium tetraphenylborate (BG1MI), was synthesized according to a reported methodology [33,35] and its characterization was performed by FTIR and ^{1}H-NMR spectroscopy (see supporting information).

2.2. Preparation of the formulations

The different formulations were prepared by adding the corresponding amount of diisocyanate, to a solution of the selected amount of LC80 or BG1MI in the thiol. Isocyanate and thiol groups are mixed in stoichiometric proportions. In case of using DBTDL as the catalyst, it was first dissolved in the isocyanate and the corresponding amount of thiol was added. The different catalysts were added in several proportions 0.5, 1 and 2 phr, in reference to the thiol amount (parts of catalysts per hundred parts of thiol).

The thiol-catalyst mixtures were manually stirred until homogeneity at room temperature, with the exception of BG1MI, in which a temperature of 80°C and magnetic stirring was required. This mixture was cooled down and then the diisocyanate was added. The samples were studied freshly prepared.

2.3. Sample preparation

For DMTA analysis, the prepared formulations were poured onto aluminium moulds and cured sequentially at 80, 100, 130 and 160 °C one hour at each temperature.

For tensile test, films were prepared by pouring the formulations between two glasses (protected with an adhesive sheet of Teflon) and using Teflon spacers to ensure a homogeneous thickness of 0.4 mm. The curing schedule applied was as before and a

post-curing of 2 h at 170 °C was done to reach the complete curing. The films were die-cut to obtain Type V specimens adapted for ASTM D638-14 requirements.

2.4. Characterization techniques

A differential scanning calorimeter (DSC) Mettler DSC-3+ calibrated using an indium standard (heat flow calibration) and an indium-lead-zinc standard (temperature calibration) was used to analyze the curing evolution. Samples of approximately 5-10 mg were tested in aluminum pans with a pierced lid in a nitrogen atmosphere with a gas flow of 50 mL/min. The dynamic studies were performed in a temperature range of 30-250 °C with a heating rate of 10 °C/min. The enthalpy (*ΔH*) released during curing of the samples was calculated by integration of the calorimetric signal using a straight baseline, with the help of the STARe software.

^{1}H NMR spectra were registered in a Varian Gemini 400 spectrometer. $CDCl_3$ was used as the solvent. For internal calibration, the solvent signal corresponding to $CDCl_3$ was used. δ (^{1}H) = 7.26 ppm.

The conversion (α) of isocyanate groups as function of the time were determined by monitoring the evolution of the peak at 2250 cm^{-1}. The degree of conversion of isocyanate were calculated as:

$$\alpha = 1 - \frac{A_t}{A_0} \quad (1)$$

where *A* is the normalized area of the isocyanate band, and the subscripts *t* and *0* indicate the curing time and at the beginning of the curing, respectively. The peak at 1680 cm^{-1} (stretch of ester ring of thiol) was used as an internal standard. The band corresponding to the S-H stretch vibration of the thiol group at 2570 cm^{-1} was only analyzed from a qualitative point of view, due to its weak intensity.

Dynamic mechanical thermal analyses (DMTAs) were performed with a TA Instruments DMA Q800 analyzer. Prismatic rectangular samples (15 x 6 x 1.5 mm^3), after isothermal cure, were analyzed by three-point bending at a heating rate of 3°C/min from 35 to 180 °C using a frequency of 1 Hz and oscillation of 0.1% of sample deformation.

The Young's moduli (*E*) were determined under flexural conditions at 30°C, with the same clamp and geometry samples, by using a force ramp at a constant rate of 1 N/min, and ensuring that only the elastic behaviour of the material was evaluated. Three samples of each material were analyzed and the results were averaged. *E* was calculated from the slope of the linear proportional part of the load-deflection curve according to the following equation:

Reactive and Functional Polymers 134 (2019) 174–182

$$E = \frac{L^3 m}{4bt^3} \quad (2)$$

where *E* is the elastic modulus of the sample (MPa), *L* is the support span (mm), *b* and *t* are the width and the thickness, respectively, of the sample tested (mm) and *m* is the gradient of the slope in the linear region (N/mm).

The thermal stability of the cured samples was studied by thermogravimetric analysis (TGA), using a Mettler TGA/SDTA 851e thermobalance. All experiments were performed under inert atmosphere (N_2 at 100 mL/min). Pieces of cured samples of 10-15 mg were degraded between 30 and 600 °C at a heating rate of 10 °C/min.

Tensile tests at room temperature were carried out by using an electromechanical universal testing machine (Shimadzu AGS-X 10 kN) at a crosshead speed of 1 mm/min and using Type V samples according to ASTM D638-14 standard. Three samples of each material were analyzed and the results were averaged.

Vickers microindentation hardness was measured with a Wilson Wolpert (Micro-Vickers 401 MAV) device following ASTM E384-16 standard procedure. For each material at least 20 determinations were made with a confidence level of 95%. The Vickers hardness number (*HV*) was calculated from the following equation:

$$HV = \frac{1.854 * F}{d^2} \quad (3)$$

where *F* is the load applied to the indenter in kgf (0.05 kgf) and *d* is the arithmetic mean of the length of the two diagonals of the surface area of the indentation measured after load removal in mm.

3. Results and Discussion

3.1. Calorimetric study of the curing process

In order to obtain a temporal control of the reaction, we investigated the curing process in the presence of the acid catalyst dibutyltin dilaurate (DBTDL) and two latent basic catalysts, LC80 and BG1MI; which are an encapsulated imidazole and a tetraphenyl borate imidazolium salt, respectively, which on heating release the base [33]. Isophorone diisocyanate (IPDI) and pentaerythritol tetrakis(3-mercaptopropionate) (PETMP) were selected as starting monomers. Stoichiometric formulations of the monomers were used in all cases to reach the highest crosslinking density.

Dynamic calorimetric studies were performed to analyze the curing evolution of thiol-isocyanate formulations with 1 phr of the different catalyst selected. Fig. III-1 shows the calorimetric curves for the formulations studied.

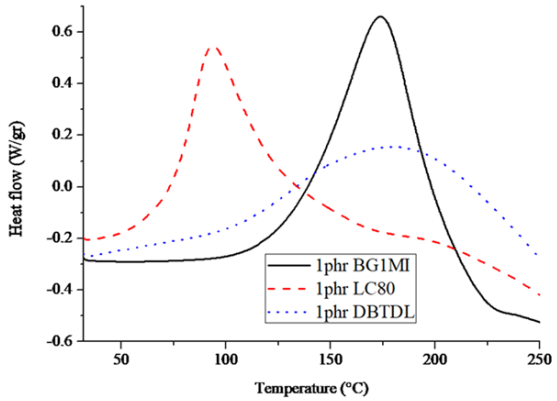

Figure III-1. *DSC curves of formulations of PETMP-IPDI and 1 phr of the different catalysts selected.*

The exotherms in Figure III-1 present different shapes and temperatures at which the curing process starts, depending on the catalyst selected. The use of BG1MI allowed a significant control of the initiation of the reaction, since the curing reaction starts at temperatures higher than 100 °C, in which the imidazolium salt decomposes releasing the base, as represented in Scheme 3 [35]. An approximate enthalpy was evaluated from the DSC curves, and the values are 72 kJ / isocyanate equivalent using BG1MI as a catalyst, 45 kJ / i.e. with LC80 and 64 kJ / i.e. with DBTDL. The lower values obtained by using LC80 and DBTDL as catalysts are due to the fact that polymerization begins immediately with these catalysts and part of the reaction heat is lost in the preparation of the experiment.

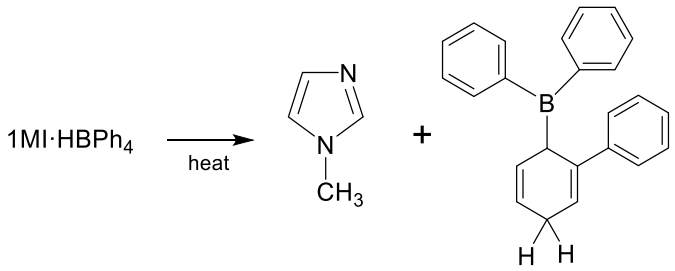

Scheme III-3*. Thermal activation of the base generator BG1MI.*

Surprisingly, the LC80 did not show the expected latent behavior, and the reaction started already at room temperature, evidenced by a slight increase in viscosity during the preparation of the sample at room temperature. This makes the evaluation of the curing enthalpy unreliable for this material. This behavior is contrary to the one observed in thiol-epoxy systems in which the samples could be stored during more than one week at 35°C without any appreciable change in viscosity [32]. The use of DBTDL as the catalyst leads to a broad curve, which starts at room temperature

without recovery the base-line, indicating that the curing is still not finished at 250°C or that some degradation processes occur.

The effect of varying the proportion of catalysts on the curing reaction was also investigated by DSC. The calorimetric curves for the different catalysts are collected in Figure III-2. The shape of the curves did not allow us to determine accurately the enthalpy released by gram of mixture or by isocyanate mol.

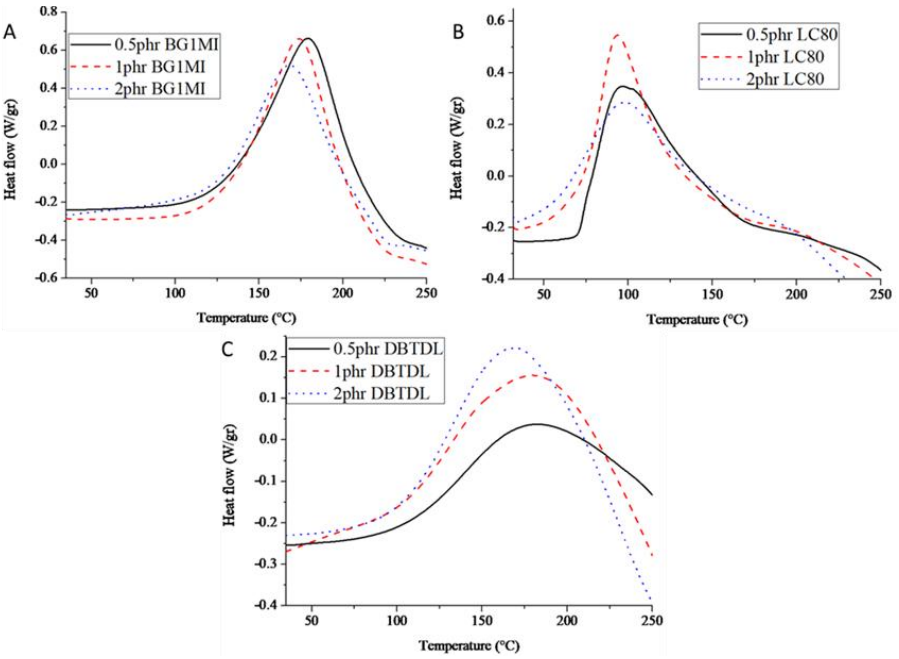

***Figure III-2**. DSC curves of formulations of PETMP-IPDI and the different catalysts in proportions of 0.5, 1 and 2phr.*

In Figure III-2A we cannot see many differences among the curing exotherms on varying the amount of BG1MI and in all cases the latent character was maintained; only a slight decrease of the peak of the maximum of the curve on increasing the amount of the catalyst was observed. In the case of the LC80, decreasing the amount of catalyst to 0.5 phr seems to improve the latency of the system, since the shape of the exotherm changes and the reaction starts at 70°C. However, the mixture with 0.5 phr of LC80 was not stable for long time at room temperature and after half an hour a clearly change in the viscosity of the mixture was observed, probably due to the release of the imidazole by swelling or partial dissolution of the capsules. The formulations based on DBTDL did not show a latent characteristic, but the polymerization speed clearly increased with the DBTDL proportion. The curing seems to be finished at 250°C when 2 phr of catalyst are used in the formulation, although probably thermal degradation takes place in some proportion since the baseline does not recover.

With the results obtained we investigated the kinetic behaviour of three different aliphatic diisocyanates; IPDI, HMDI and HDI. According to the low stability of LC80 formulations, only DBTDL and BG1MI were used as catalysts in a proportion of 0.5 phr. It should be commented that both LC80 and BG1MI follow the same anionic reaction mechanism, since both release imidazole, but in different conditions. Figure III-3 present the calorimetric curves of these formulations.

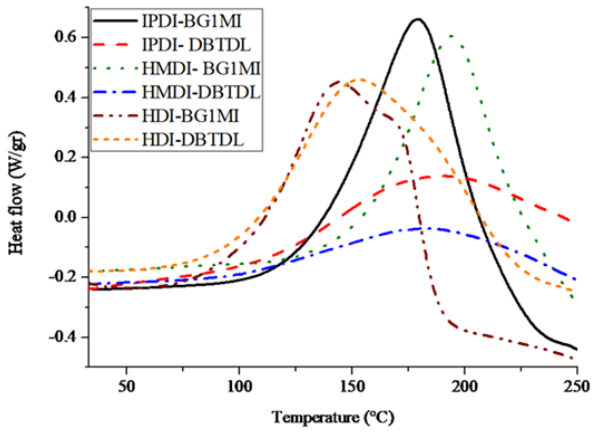

***Figure III-3**. DSC curves of formulations of PETMP-(IPDI/HMDI/HDI) and the catalysts in proportions of 0.5 phr.*

From Figure III-3, it can be seen that HDI, with a linear structure, is the most reactive monomer with both catalysts and it reacts slowly at temperatures about 75°C. On the other hand, HMDI reacts at higher temperatures than IPDI in both cases, but this effect is more noticeable in anionic conditions. The HDI cures rapidly with both catalysts, whereas IPDI and HMDI react faster when the base generator is used. The use of DBTDL needs higher temperature and longer reaction times to complete the process.

From this study, we can state that from the point of view of the kinetics and ease of preparation of these materials, BG1MI is the most advantageous catalyst and that 0.5 phr seems to be enough to reach a high crosslinking density with all the diisocyanates selected.

3.2. FTIR study of the curing evolution

The thiol-isocyanate reaction was followed by FT-IR spectroscopy to investigate the kinetics of the reaction and verify that complete formation of poly(thiourethane) networks was reached.

The FTIR spectra of the IPDI-0.5 phr of BG1MI formulation at different curing times were collected in Figure III-4. On the basis of the calorimetric curves, a temperature of 120°C was selected for the isothermal curing. The reduction in the isocyanate and thiol peaks, at 2270 cm^{-1} and 2570 cm^{-1}, respectively, was accompanied by the appearance of N-H st. (3350 cm^{-1}) and carbonyl stretching (1670 cm^{-1}) of the thiourethane groups, which are indicative of the network formation. The thiol band is very weak and has no kinetic significance. The carbonyl absorption peak of the thiourethane group is partially overlapped with the carbonyl ester absorption band of the PETMP and the deconvolution were done in order to extract quantitative information. As we can see in the spectrum registered after 60 min at 120 °C, some isocyanate absorption still remains, which indicates that this thermal treatment was not enough to reach the complete curing. The fully conversion of isocyanate was achieved after a post-curing treatment at 160 °C for 1 h. The limited conversion at 120 °C could be attributed to the vitrification of the material.

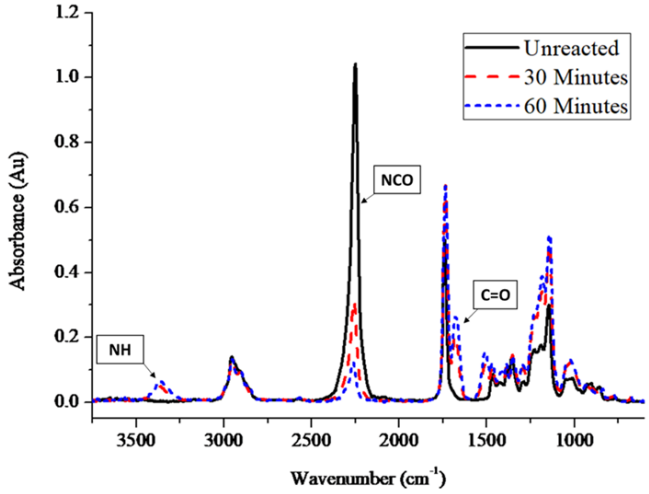

***Figure III-4**. FTIR spectra of the PETMP-IPDI and 0.5 phr of BG1MI at 120°C.*

The conversion of the isocyanate group at the temperature of 120 °C, for the formulation containing a stoichiometric amount of IPDI and PETMP with the different catalysts, was determined and represented in Figure III-5.

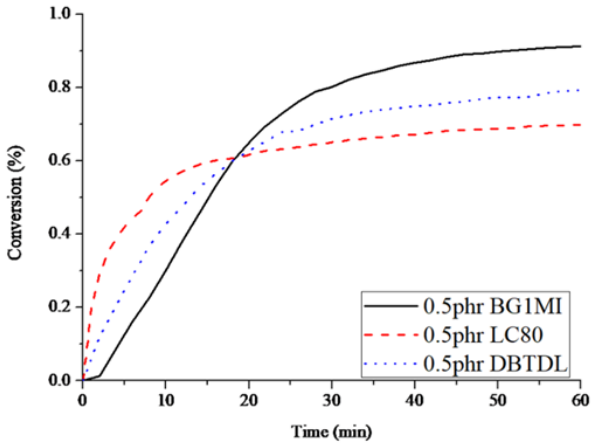

***Figure III-5**. Kinetic profile at 120°C of the conversion of NCO group in the formulation of IPDI and PETMP with 0.5 phr of the different catalysts obtained from FTIR analysis.*

After 1h at 120°C, the maximum conversion of the isocyanate group was obtained with the BG1MI catalyst, which reached a conversion higher than 90%. The reaction with the BG1MI latent catalyst does not start immediately, but after a short activation period; unlike the systems based on LC80 or DBTDL in which the reaction starts instantaneously at 120 °C. The quickest reaction occurs with LC80, but the conversion achieved is quite low. Complete conversion was achieved with all these catalysts when a post-curing at higher temperatures was performed.

From the studies of the curing process by DSC and FT-IR, the adequacy of BG1MI as the catalyst were proved. This catalyst allows a good control of the curing process while reaching the complete curing at moderated temperatures.

3.3 Thermal characterization of the poly(thiourethane) thermosets

According to the kinetic study, we selected only BG1MI and DBTDL as catalysts with a proportion of 0.5% to follow the investigation. Higher proportions of catalyst were not used, since 0.5% by wt. of catalyst is enough to complete the polymerization reaction, as demonstrated by FTIR studies.

Thus, we investigated the thermomechanical behaviour of all the materials prepared from formulations with the three diisocyanates selected and PETMP with 0.5 phr of DBTDL or BG1MI. Figure III-6 shows the tan δ (A) and storage modulus (B) curves obtained by DMTA. The main data extracted from these curves are collected in Table III-1.

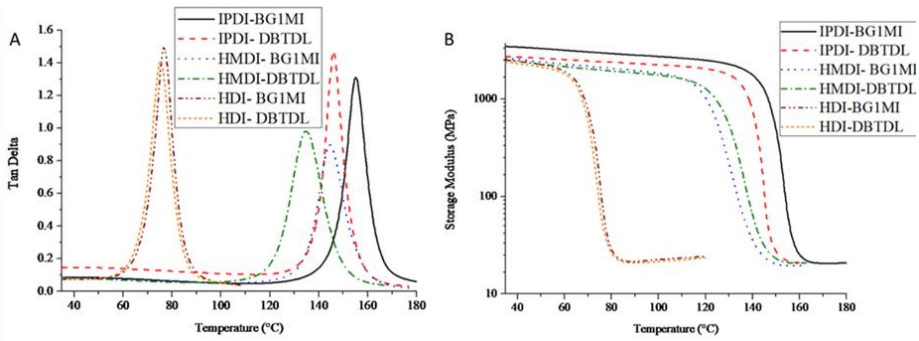

Figure III-6. *(A) tan δ and (B) storage modulus against temperature of the different materials prepared with PETMP-IPDI/HMDI/HDI-0.5phr of catalysts.*

The tan delta curves are very narrow indicating the formation of uniform network structures, thanks to the click reaction mechanism without any side-reaction. The materials obtained show values of FWHM (width of the curves at half height) in the range between 9 and 16 °C (see Table III-1), which are lower than those obtained by Shin *et al*. that reach values in the range from 15 to 28 °C [34]. These authors also prepared materials based on IPDI and PETMP by photoinitiation with a base generator, but a value of 16 °C of FWHM was obtained. This result can be justified by the fast curing performed in photochemical conditions [34].

Table III-1. *Thermal data obtained from the materials obtained from the different diisocyanates and PETMP with different catalysts at 0.5 phr.*

Sample	$T_{tan\delta}$[a] (°C)	FWHM[b] (°C)	Young's Modulus (GPa)	E'[c] (MPa)	$T_{2\%}$[d] (°C)	T_{max}[e] (°C)	Char Yield[f]
IPDI-0.5%BG1MI	153	11	2.8	23	284	305-347-437	3.0
IPDI-0.5%DBTDL	144	10	2.8	21	289	308-338-425	4.9
HMDI-0.5%BG1MI	140	16	2.2	19	287	316-348-453	2.9
HMDI-0.5%DBTDL	135	14	2.0	19	289	312-337-438	4.3
HDI-0.5%BG1MI	77	9	2.0	24	276	304-348-469	2.2
HDI-0.5%DBTDL	75	10	2.0	23	285	317-350-467	2.4

[a] Temperature of maximum of the tan δ at 1 Hz.
[b] FWHM stands by full width at half maximum.
[c] Relaxed modulus determined at the $T_{tan\ \delta}$ + 40°C (in the rubber state).
[d] Temperature of 2% of weight loss
[e] Temperatures of the maximum rate of the three steps of degradation
[f] Char residue at 600°C

The values of the temperature of the maximum of *tan* δ, reported in Table III-1, are dependent from both the monomer structure and the catalyst used. The flexible structure of HDI leads to lower *tan* δ temperatures in comparison to the materials containing rigid cycloaliphatic groups, without much difference on changing the catalyst. IPDI and HMDI derived materials show variations of *tan* δ peak on changing the catalyst, leading to higher temperature of *tan* δ values when the base generator was used. Although a post-curing at 170 °C for 2 hours or an increase in the DBTDL proportion were tested, the crosslinking density seems to be limited and this value did not increase. This fact can be related to the kinetic evolution of the curing process observed by DSC (Fig. III-3), in which DBTDL cures at higher temperature and the enthalpy released seems to be lower. IPDI derived materials present the highest $T_{\tan \delta}$ due to their higher compact and rigid network.

In Figure III-6B the evolution of storage modulus with the temperature is represented for all the samples. As we can see, the relaxation of the material takes place sharply with a significant change in the moduli in glass and rubber state. There are no big differences in the relaxed moduli (see Table III-1), but a certain correlation with the molecular weight between crosslinks can be appreciated. The highest molecular weight between crosslinks of HMDI materials leads to the lowest modulus. Although the difference is only slight, the use of DBTDL leads to a lower value, according to the lower crosslinking density achieved with this catalyst.

The highest value of Young's modulus, as expected, was reached with the material based on the IPDI which presents the most rigid network structure.

The thermal stability of the PTUs was analysed by TGA and the weight loss and the derivative curves are shown in Figure III-7. The data extracted from these experiments are collected in Table III-1.

Some authors already studied the degradation of poly(urethane)s [20] and poly(thiourethane-urethane)s [36] thermoplastics and a complex degradation mechanism, with two or three degradation steps, was reported. Depending on the aliphatic or aromatic character of the urethane structure the reversion of urethane to isocyanate and hydroxyl groups takes place between 120 to 250 °C, being the aliphatic ones the most stable. The first degradation step was attributed to this degradative process. The second step, at higher temperature, corresponds to a typical β-elimination process, if there are hydrogen atoms in γ-position. This process leads to the formation of a carbamic acid and an olefin. Carbamic acid, which is unstable, release carbon dioxide and the corresponding amine is formed. It has been reported that this process can lead to one or two degradation steps [37].

Reactive and Functional Polymers 134 (2019) 174–182

The derivative of TGA degradation curves (DTG) of the PTU thermosets prepared in the present work, Figure III-7, clearly presents three different degradation steps, with not many differences on changing the isocyanate and the catalyst.

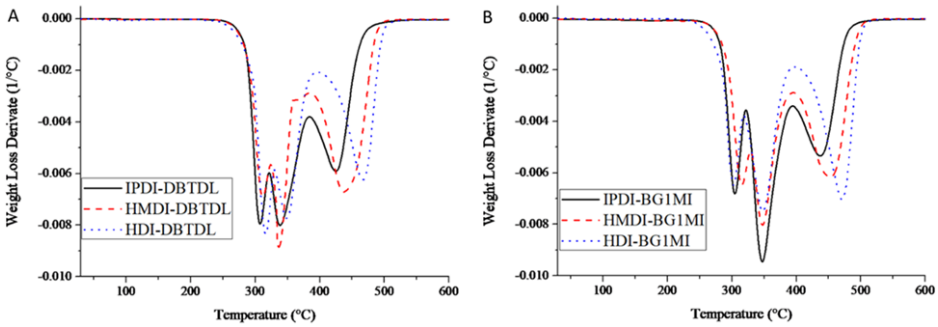

Figure III-7. *DTG curves of PETMP-(IPDI/HDMI/HDI) thermosets using 0.5 phr of BG1MI (A) and 0.5 phr of DBTDL as the catalysts.*

The first degradation step begins around 300 °C, which indicates that poly(thiourethane)s are more stable than their corresponding oxygen analogues, which decompose at about 250 °C [20]. In our case, two possible β-elimination processes can occur, because not only thiourethanes are present but also ester groups from the tetrathiol structure. Both β-elimination processes could overlap and contribute to the degradation maximum at about 350 °C. The degradation peak at the highest temperature must correspond to the fully degradation of the network. If we look to these temperatures of the maximum rate of degradation (Table III-1), we can see that the values for the last step are more dependent on the urethane structure. The char yields, Table III-1, are slightly higher for the materials prepared with DBTDL.

From these studies, we can state that these materials exhibit a quite good thermal stability, higher than the poly(urethane) analogues, with decomposition temperatures higher than 280 °C, except for the material obtained from HDI and the base generator that loss a 2% of weight at 276°C, attributable to its linear aliphatic structure.

3.4 Mechanical Characterization of the Materials

Microindentation hardness tests and tensile tests at break were performed for all the thermosets prepared. The data extracted from these tests are listed in Table III-2.

Table III-2. *Mechanical data determined from the materials obtained with the different diisocyanates and different catalysts.*

Sample	VH [a]	Tensile Modulus[b] (GPa)	σ_b [c] (MPa)	ε_b [d] (%)
IPDI-0.5%BG1MI	19.6 ± 0.7	2.1 ± 0.1	72.9 ± 2.6	5.8 ± 0.4
IPDI-0.5%DBTDL	19.2 ± 0.5	2.1 ± 0.1	76.1 ± 2.2	6.3 ± 0.8
HMDI-0.5%BG1MI	16.1 ± 0.7	1.7 ± 0.1	67.1 ± 1.7	6.4 ± 0.4
HMDI-0.5%DBTDL	15.9 ± 0.6	1.7 ± 0.1	64.1 ± 2.5	6.6 ± 0.8
HDI-0.5%BG1MI	13.2 ± 0.8	1.7 ± 0.1	47.3 ± 1.6	3.8 ± 0.2
HDI-0.5%DBTDL	12.4 ± 0.6	1.7 ± 0.1	44.6 ± 1.4	3.2 ± 0.1

[a] Vickers microindentation hardness.

[b] Tensile modulus at room temperature.

[c] Stress at break.

[d] Deformation at break.

Mechanical characteristics are fully dependent on the chemical structure of the network and crosslinking densities. The higher values of microindentation hardness were obtained for IPDI derived thermosets, due to its rigid structure. On increasing the flexibility of the selected isocyanate, a decrease in microindentation hardness was observed. The lowest values were obtained for HDI derived thermosets, with a long aliphatic chain between thiourethane moieties.

A similar influence on changing the monomer structure was expected in the tensile modulus, but the materials prepared from HMDI and HDI exhibited similar behaviour due to the glassy state at room temperature. However, the rigid and compact structure of IPDI leads to a notable higher modulus. These results are in accordance with those obtained from DMTA tests. The most relevant differences between these materials can be observed in the stress and strain at break values. The tensile strength is the highest when the rigid IPDI moiety was in the network structure and the lowest with the linear and aliphatic HDI. The strain at break, related to the ductility, is maximum for the poly(thiourethanes) based on HMDI, since materials based on HDI suffer an easier breakage at lower stress due to their significantly lower strength. The type of catalyst used seems not to influence in a significant manner the tensile characteristics of the thermosets as the values presented are similar.

4. Conclusions

The use of 1-methylimidazolium tetraphenylborate (BG1MI), as latent base catalyst, allowed a much better control of the thiol-iscoyanate reaction than the commonly used dibutyltin dilaurate (DBTDL). The reaction, using the BG1MI, begins at 120 °C and occurs rapidly. LC80, which is an encapsulated imidazole, did not show the expected latent behaviour in this curing process.

The conversion of isocyanates was higher than 90% with BG1MI, after 1 hour at 120 °C, whereas the use of DBTDL reached only a conversion of 75%. On increasing the temperature, the fully conversion was achieved with both catalysts.

Different poly(thiourethane) thermosets were prepared from three different isocyanates: isophorone diisocyanate (IPDI), 4,4'-methylene bis(cyclohexy isocyanate) (HMDI) and hexamethylene diisocyanate (HDI) and a tetrathiol, pentaerythritol tetrakis(3-mercaptopropionate) (PETMP) with DBTDL and BG1MI, as acid and basic catalysts.

All materials prepared showed very narrow *tan* δ curves, which stands for highly homogeneous networks. T_g values increase with increasing the rigidity of the isocyanate monomer, reaching a maximum value of 150 °C for IPDI derived materials. The use of the base generator as the catalyst leads to materials with higher T_g.

The initial degradation of these materials occurred at elevated temperatures than the related poly(urethanes). Their degradation curves allowed to detect three different degradation mechanisms. The first one, at the lowest temperature, corresponds to the reversion of thiourethanes to form isocyanate and thiol groups. On increasing the temperature, the β-elimination of the remaining thiourethanes and ester groups of the thiol structure occurs and then, at the highest temperature, the complete degradation of the network structure could be observed.

The mechanical behaviour of the prepared materials was correlated to the network structure, according to the rigid or flexible character of the selected diisocyanate monomer. IPDI derived materials are more strength, rigid and harder than those derived from HDI, which present the lowest mechanical performance. The materials obtained from the latent catalyst have similar mechanical characteristics to the ones obtained by using the commonly used DBTDL.

Acknowledgments

The authors would like to thank MINECO (Ministerio de Economia, Industria y Competitividad, MAT2017-82849-C2-1-R and 2-R) and Generalitat de Catalunya (2017-SGR-77) for their financial support.

References

[1] H.C. Kolb, M.G. Finn, K.B. Sharpless, Click chemistry: diverse chemical function from a few good reactions, *Angew. Chem*. **2001**, 40, 2004-2021.

[2] X. Ramis, X. Fernández-Francos, S. De La Flor, F. Ferrando, A. Serra, Click-Based Dual-Curing Thermosets, in Q. Guo, (Ed.), Thermosets: Structure, Properties and Applications, 2nd ed., Elsevier, Amsterdam, **2018**, Chap. 16.

[3] C.E. Hoyle, C.N. Bowman, Thiol–Ene click chemistry, *Angew. Chem.* **2010**, 49, 1540-1573.

[4] S. Chandrasekaran, Click Reactions in Organic Synthesis, Wiley-VCH, Weinheim, Germany, **2016**.

[5] A.B Lowe, Thiol-ene "click" reactions and recent applications in polymer and materials synthesis, *Polym. Chem.* **2009**, 1, 17-36.

[6] H. Li, B. Yu, H. Matushima, C.E. Hoyle, A.B. Lowe, The thiol–isocyanate click reaction: facile and quantitative access to ω-end-functional poly(N,N-diethylacrylamide) synthesized by RAFT radical polymerization, *Macromolecules* **2009**, 42, 6537-6542.

[7] E. Dyer, D.W. Osborne, The synthesis of polythiolcarbamates, *J. Polym. Sci.* **1960**, 47, 361-371.

[8] H.-W. Engels, H.-G. Pirkl, R. Albers, R. W. Albach, J. Krause, A. Hoffmann, H. Casselmann, J. Dormish, Polyurethanes: versatile materials and sustainable problem solvers for today's challenges*, Angew. Chem.* **2013** 52, 9422-9441.

[9] A.B. Lowe, C.N. Bowman, Thiol-X Chemistries in Polymer and Materials Science, RSC Polymer Chemistry Series 6, Croydon, UK, **2013**.

[10] K. Strzelec, N. Baczek, S. Ostrowska, K. Wasikowska, M.I. Szynkowska, J. Grams, Synthesis and characterization of novel polythiourethane hardeners for epoxy resins, *C. R. Chimie* **2012**, 15, 1065-1071.

[11] Q. Li, H. Zhou, A. Wicks, C.E. Hoyle, D.H. Magers, H.R. McAlexander, Comparison of small molecule and polymeric urethanes, thiourethanes, and dithiourethanes: hydrogen bonding and thermal, physical, and mechanical properties, *Macromolecules* **2009**, 42, 1824-1833.

[12] C. Lu, Z. Cui, Z. Li, B. Yang, J. Shen, High refractive index thin films of ZnS/polythiourethane nanocomposites, *J. Mater. Chem.* **2003**, 13, 526-530.

[13] C. Lu, C. Guan, Y. Liu, Y. Cheng, B. Yang, PbS/Polymer nanocomposite optical materials with high refractive index, *Chem. Mater*. **2005**, 17, 2448-2454.

[14] B. Jaffrennou, N. Droger, F. Mechin, J.-L. Halary, J.-P Pascault, Characterization, structural transitions and properties of a tightly crosslinked polythiourethane network for optical applications, *e-Polym.* **2005**, 82, 1618-7229.

[15] N.G. Ireni, R. Narayan, P. Basak, K.V.S.N. Raju, Poly(thiourethane-urethane-urea) as anticorrosion coatings with impressive optical properties, *Polymer* **2016**, 97, 370-379.

[16] J. Tan, C. Li, H. Li, H. Zhang, J. Gu, B. Zhang, H. Zhang, Q. Zhang, Water-borne thiol–isocyanate click chemistry in microfluidics: rapid and energy-efficient preparation of uniform particles, *Polym. Chem*. **2015**, 6, 4366-47373.

[17] C. Li, J. Tan, H. Li, D. Yin, J. Gu, B. Zhang, Q. Zhang, Thiol–isocyanate click reaction in a Pickering emulsion: a rapid and efficient route to encapsulation of healing agents, *Polym. Chem*. **2015**, 6, 7100-7111.

[18] J. Yan, S. Ariyasivam, D. Weerasinghe, J. He, B. Chisholm, Z. Chen, D. Webster, Thiourethane thermoset coatings from bio-based thiols. *Polym. Int*. **2012**, 61, 602-608.

[19] X. K. D. Hillewaere, R. F. A. Teixeira, L-T. T. Nguyen, J. A. Ramos, H. Rahier, F. E. Du Prez, Autonomous Self-Healing of Epoxy Thermosets with Thiol-Isocyanate Chemistry, *Adv. Funct. Mater*. **2014**, 24, 5575-5583.

[20] E. Delebecq, J.P. Pascault, B. Boutevin, F. Ganachaud, On the versatility of urethane/urea bonds: reversibility, blocked isocyanate, and non-isocyanate polyurethanes, *Chem. Rev.* **2012**, 113, 80-118.

[21] A.L. Silvia, J.C. Bordado, Recent developments in polyurethane catalysis: catalytic mechanism review. *Cat. Rev. - Sci. Eng.* **2004**, 46, 31-51.

[22] H. Sardon, A. Pascual, D. Mecerreyes, D. Taton, H. Cramail, J.L. Hendirck, Synthesis of polyurethanes using organocatalysis: a perspective, *Macromolecules* **2015**, 48, 315-3165.

[23] S. Kuypers, S.K. Paramanik, L. D'Olieslaeger, G. Reekmans, M. Peters, J. D'Haen, D. Vanderzande, T. Junkers, P. Adriaensens, A. Ethirajan, Interfacial thiol–isocyanate reactions for functional nanocarriers: a facile route towards tunable morphologies and hydrophilic payload encapsulation, *Chem. Commun.* **2015**, 51, 15858-15861.

[24] H. Salmi, X. Allonas, C. Ley, Polythiourethane networks catalyzed by photobase generators, *Prog. Org. Coatings* **2016**, 100, 81-85.

[25] J. Shin, H. Matsushima, M.C. Comer, C.N. Bowman, C.E. Hoyle, Thiol–Isocyanate–Ene ternary networks by sequential and simultaneous thiol click reactions, *Chem. Mater.* **2010**, 22, 2616-2625.

[26] J. Shin, H. Matsushima, J.W. Chan, C.E. Hoyle, Segmented polythiourethane elastomers through sequential thiol-ene and thiol-isocyanate reactions. *Macromolecules*, **2009**, 42, 3294-3301.

[27] S. Chatani, R. Sheridan, M. Podgorski, D.P. Nair, C.N. Bowman, Temporal control of thiol-click chemistry. *Chem. Mater.* **2013**, 25, 3897-3901.

[28] H. Matsushima, J. Shin, C.N. Bowman, C.E. Hoyle, Thiol-isocyanate-acrylate ternary networks by selective thiol-click chemistry, *J. Polym. Sci. Part A. Polym. Chem.* **2010**, 48, 3255-3264.

[29] A. Kultys, M. Rogulska, S. Pikus, The synthesis and characterization of new thermoplastic poly(thiourethane-urethane)s, *J. Polym. Sci. Part A. Polym. Chem.* **2008**, 46, 1770-1782.

[30] A.Basterretxea , Y. Haga, A. Sanchez-Sanchez, M. Isik, L. Irusta, M. Tanaka, K. Fukushima, H. Sardon, Biocompatibility and hemocompatibility evaluation of polyether urethanes synthesized using DBU organocatalyst. *Eur. Polym. J.* **2016**, 84, 750-758.

[31] Official Journal of the European Union 1.4.2010. Commission Regulation Nº 276/2010

[32] D. Guzmán, X. Ramis, X. Fernández-Francos, A. Serra, New catalysts for diglycidyl ether of bisphenol A curing based on thiol–epoxy click reaction, *Eur. Polym. J.* **2014**, 59, 377-386.

[33] O. Konuray, N. Areny, J.M. Morancho, X. Fernández-Francos, A. Serra, X. Ramis, Preparation and characterization of dual-curable off-stoichiometric amine-epoxy thermosets with latent reactivity. *Polymer* **2018**, 146, 42-52.

[34] J. Shin, J. Lee, H.M. Jeong, Properties of polythiouretanes prepared by thiol-isocyanate click reaction, *J. Appl. Polym. Sci.* **2018**, 135, 1-8.

[35] X. Sun, J.P. Gao, Z.Y. Wang, Bicyclic guanidinium tetraphenylborate: a photobase generator and a photocatalyst for living anionic ring-opening polymerization and cross-linking of polymeric materials containing ester and hydroxy groups, *J. Am. Chem. Soc.* **2008**, 130, 8130–8131.

[36] M. Rogulska, A. Kultys, E. Olszewska, New thermoplastics poly(thiourethane-urethane) elastomers based on hexane-1,6-diyl diisocyanate (HDI), *J. Therm. Anal. Calorim.* **2013**,114, 903-916.

[37] G. Trovati, E.A. Sanches, S.C. Neto, Y.P. Mascarenhas, G.O. Chierice, Characterization of polyurethane resins by FTIR, TGA, and XRD, *J. Appl. Polym. Sci.* **2010**, 115, 263-268.

Reactive and Functional Polymers 134 (2019) 174–182

Supporting Information

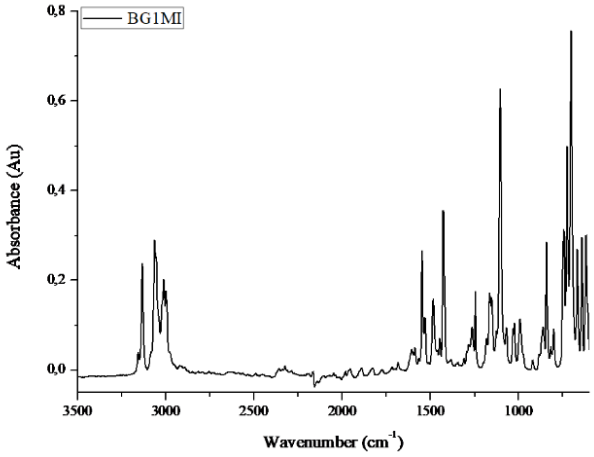

Figure III-S1. *FTIR spectra of BG1MI in the absorbance mode at room temperature.*

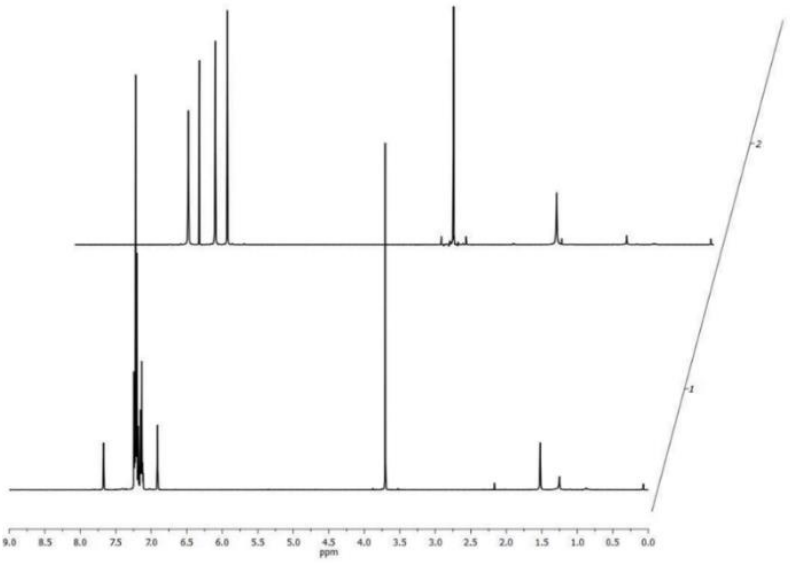

Figure III-S2. *1H-NMR spectra of 1-methyimidazole (on the top) and BG1MI (on the bottom) in $CDCl_3$ solution at 400 MHz.*

Chapter IV

Tailor-made thermosets obtained by sequential dual-curing combining isocyanate-thiol and epoxy-thiol *click* reactions

Polymer 174 (2019) 200–209

Tailor-made thermosets obtained by sequential dual-curing combining isocyanate-thiol and epoxy-thiol *click* reactions

Francesco Gamardella[1], Valentina Sabatini[1,2], Xavier Ramis[3], Àngels Serra[1]

[1] *Dept.of Analytical and Organic Chemistry, Universitat Rovira i Virgili, C/ Marcel·lí Domingo, 43007, Tarragona, Spain*

[2] *Chemistry Dpt., Università degli Studi di Milano, Via Golgi 19 20133 Milano, Italy*

[3] *Thermodynamics Laboratory, ETSEIB Universitat Politècnica de Catalunya, Av. Diagonal, 08028, Barcelona, Spain*

Abstract

In this work, a new family of thermosets based on thiol-isocyanate-epoxy networks was prepared via sequential dual-curing methodology where both reactions are activated by temperature. The sequential dual behaviour of the new system proposed is based on the faster reaction kinetic of the first curing stage, *i.e.* the isocyanate-thiol coupling, which proceeds at a relatively low temperature, compared to the second stage, *i.e.* the epoxy-thiol reaction, between the remaining thiol functionalities and the epoxy groups that takes place at a higher temperature. Furthermore, the effect of using different aliphatic isocyanates was investigated. Both reactions have a *click* character and the intermediate/final materials show a wide range of properties depending on the relative contribution of both curing stages, due to the selected ratio between the isocyanate and epoxy groups. The new thermosets obtained were characterized from the thermal and dynamic mechanical point of view, resulting excellent candidates as smart materials due to their narrow transitions, which favours fast and controlled changes in their macromolecular features.

Keywords:

thiol, isocyanate, epoxy, sequential dual-curing, thermosets.

1. Introduction

Thermosets have been known for over a hundred years and, nowadays these materials cover a broad range of applications in several high added-value sectors, *i.e.* aeronautical engineering, automotive industry, optoelectronics and coatings.[1-4] Furthermore, the success of these materials depends in part on the treatment techniques used to improve thermosets properties and, fortunately, the scientific research continues to thrive.

Nowadays, the dual-curing methodology represents an efficient way to enhance thermosets processing features. A dual-curing process is a combination of two different polymerization routes that can take place sequentially or simultaneously.[5] Sequential dual-curing systems are characterized by noteworthy improvements in terms of process design and control of the formed network.[6]

In this kind of synthetic methodology, materials can be partially cured before their processing, storage or assembly; on the other side, their final features can be attained whenever desired by means of thermal or UV-light sources to cure the resins completely. The different contributions of both curing reactions and the properties of the intermediate material can be easily controlled by changing the composition of the formulation, as well as cure technical parameters, *i.e.* the time and the reaction temperature.[7] Up to now, sequential curing systems are being used in several fields where tailored materials and flexible processes are mandatory, *e.g.* shape-memory materials, adhesive coatings, holography and lithography.[8-12]

The exploration of different processing routes does not represent the end of thermosets development cycle, but it marks the beginning of a new generation of materials that grows with each new monomer or with new proposed combinations of them. In this contest, despite poly(thiourethane)s (PTU) are widely used materials in optical applications thanks to their satisfactory mechanical, physical and optical features, PTU synthetic routes that lead to their formulation have not been widely studied as in the case of their oxygen analogs, poly(urethane)s (PU).[13-14]

Thiol-isocyanate coupling reactions to form thermosets have aroused recently some interest. For example Shin *et al.* reported a base catalysed thiol-isocyanate curing exploiting the use of different thiols in combination with isophorone diisocyanate (IPDI) and Gamardella *et al.* described the preparation and characterization of a new PTU thermoset family combining thiols with different kinds of aliphatic isocyanates by using latent catalysts that allows the control of the process.[15,16] However, only few works about PTU-based networks obtained via sequential dual-curing methodologies are reported until now in the scientific literature.

Sequential thiol-isocyanate and thiol-ene/acrylate reactions are the most common dual curing procedures studied.[17] Bowman et al. reported the preparation of thiol-isocyanate-ene networks based on two independent thiol-*click* reaction mechanisms: a thiol-alkene free radical photopolymerization and a base catalysed thiol-isocyanate anionic reaction.[18] Matsushima *et al.* described thiol-isocyanate-acrylate ternary networks formed by the combination of thiol-isocyanate coupling, thiol-acrylate Michael addition and acrylate homopolymerization.[19] These results suggest the high potentiality of this type of networks, obtained through dual-curing processes, being the key of its success the specialized engineering of manufacturing these materials.

Polymer 174 (2019) 200–209

Thus, taking all of this into account, in the present publication we report the preparation and characterization of a new family of thermosets based on thiol-isocyanate-epoxy networks where both reactions are activated by temperature. The sequential dual character of this curing system relies on the faster reaction kinetic of the isocyanate-thiol coupling that occurs at a relatively low temperature, compared to the epoxy-thiol reaction between the remaining thiol groups and the epoxy that takes place at a higher temperature.[8,16] The extent of the first curing step is controlled by the equivalent ratio between the isocyanate and thiol, r_{NCO}, which also controls the intermediate and final materials properties. It should also be noticed that both reactions have a *click* character implying that they are specific, without the formation of undesired by-products, and therefore they lead to homogeneous networks. In general, this type of thermosets is adequate to be applied as smart materials, since they have narrow transitions, which allows quick movements and a rapid change in their properties.

To this purpose, a reactive system containing a thiol crosslinker pentaerythritol tetrakis(3-mercaptopropionate), (S4), a diisocyanate monomer (isophorone diisocyanate (IPDI) or hexamethylene diisocyanate (HDI)) and an epoxy resin (diglycidyl ether of bisphenol A, DGEBA) was studied. 1-Methylimidazole (1MI) was used as the catalyst and its effect in terms of different loadings on curing process was investigated. Both diisocyanates were selected since they have different reactivity and their structure leads to materials with different characteristics.

The kinetics of both curing stages and the conversion achieved were studied by differential scanning calorimetry (DSC) and Fourier transform infrared spectroscopy (FTIR). Intermediate materials were characterized by calorimetry and fully cured samples by DSC, thermal dynamo mechanical (DMA) and thermogravimetric (TGA) analyses.

2. Experimental Methods

2.1. Materials

1-Methylimidazole (1MI), pentaerythritol tetrakis (3-mercaptopropionate) (S4, >95%, 122.17 g/eq), isophorone diisocyanate (IPDI, 98%, 111.14 g/eq) and hexamethylene diisocyanate (HDI, >99%, 84.10 g/eq) were supplied from Sigma Aldrich and used without further purification. Diglycidyl ether of bisphenol A (DGEBA, 170.21 g/eq) was supplied by Hexion Specialty Chemicals and dried in vacuum for 2 hours at 80°C before use.

2.2. Samples preparation

To investigate which is the best amount of catalyst to get duality, IPDI and HDI were alternatively mixed with S4 and DGEBA using a fixed ratio between the molar equivalents of isocyanate and thiol comonomers (r_{NCO}) of 0.5 eq_{NCO}/eq_t, and changing

the 1MI amount in the proportions 0.1, 0.05 or 0.025 phr (parts of catalyst for hundred parts of monomers mixture). Once selected the proportion of 0.025 phr of 1MI, samples were prepared varying the r_{NCO} as 0.2 and 0.8 eq_{NCO}/eq_t. The pure S4-isocyanate (r_{NCO}= 1) and S4-DGEBA (r_{NCO}= 0) formulations were also studied. The theoretical critical gelation ratio, r_c, was calculated using the Flory-Stockmayer equation (Eq. 1) in a similar manner as in a previous work, where f_{NCO} and f_t are the average functionalities of isocyanate (f_{NCO}=2) and S4 (f_t=4) comonomers.[20] Both families of thermosets studied are characterized by a r_c= 0.33.

$$r_c=\frac{1}{(f_{NCO}-1)\times(f_t-1)} \quad (1)$$

Formulations were prepared by adding the components into a 10 mL glass vial by the following order: i) 1MI; ii) S4; iii) DGEBA and iv) isocyanate. The whole mixture was manually stirred and immediately analysed. Table IV-1 shows the compositions of pure and dual formulations. Since S4 and DGEBA are present in all compositions, the dual samples were coded as "*x*_r_*y*", where *x* indicates the isocyanate used and *y* is the r_{NCO} chosen; in the case of pure formulations, *x* indicates if DGEBA or IPDI/HDI were selected. As an example, IPDI_r_0.5 is a formulation in which one half of S4 equivalents react with IPDI isocyanate equivalents and the other half react with DGEBA epoxy equivalents.

***Table IV-1**. Composition of the pure and dual formulations prepared.*

Sample	S4 (wt %)	DGEBA (wt %)	IPDI (wt %)	HDI (wt %)
DGEBA_r_0	41.8	58.2	-	-
IPDI_r_1	52.4	-	47.6	-
HDI_r_1	59.2	-	-	40.8
IPDI_r_0.2	43.5	48.5	7.9	-
IPDI_r_0.5	46.5	32.4	21.1	-
IPDI_r_0.8	49.8	13.9	36.3	-
HDI_r_0.2	44.4	49.5	-	6.1
HDI_r_0.5	49.0	34.1	-	16.9
HDI_r_0.8	54.7	15.2	-	30.1

Fully cured samples for dynamic mechanical (DMA) and thermogravimetric (TGA) analyses were prepared in an open mould, with dimensions of 1.5 × 5 × 15 mm^3, made by PTFE to avoid the presence of bubbles and to facilitate the samples release. The liquid formulations were poured into the mould and kept in an oven at 60°C for 60 min in the case of IPDI-based compositions and for 40 min for HDI formulations (stage 1); after which the samples were post-cured at 120°C for 120 min (stage 2) and then slowly cooled to room temperature inside the oven. The curing times reported

Polymer 174 (2019) 200–209

were optimized according to Fourier transform infrared spectroscopy (FTIR) and differential scanning calorimetry (DSC) analyses described in the following paragraphs. The samples were polished with sandpaper to obtain uniform final dimensions.

2.3. Characterization Techniques

DSC analyses were carried out on a Mettler DSC-821 instruments calibrated using indium (heat flow calibration) and zinc (temperature calibration) standards. Samples of approximately 8-10 mg were placed in aluminium pans with pierced lids and analysed in nitrogen atmosphere with a gas flow of 50 cm^3/min. Dynamic studies between 30 and 250°C with a heating rate of 10°C/min were performed to characterize the curing process and measure the final glass transition temperature (T_g). Dynamic curing tests were also performed with heating rates of 2, 5 and 20°C/min. The reaction enthalpy (Δh) was integrated from the calorimetric heat flow signal (dh/dt) using a straight baseline with the help of the STARe software. Due to the high reactivity of thiol-isocyanate reaction, the curing begins at room temperature during the preparation of the mixtures. In consequence, the relative conversions were used instead of absolute conversion.[21] The calorimetric relative conversion at a given temperature was determined as reported in Eq. 2.

$$x_{DSC} = \frac{\Delta h_T}{\Delta h_{tot}} \tag{2}$$

where Δh_T is the heat released up to T and Δh_{tot} the total reaction heat evolved in a dynamic run.

The T_gs of the intermediate materials were determined with the following procedure: i) isothermal curing at 60°C until the first reaction comes to the end (40 min for HDI and 60 min for IPDI mixtures); ii) dynamic heating from -50 to 100°C at 10°C/min. Furthermore, intermediate and final materials T_gs were estimated using the Fox copolymer rule given by Eq. 3 and 4 respectively.[22]

$$\frac{1}{Tg,1} = \frac{w_{NCO\text{-t}}}{T^{\infty}_{g(NCO\text{-t})}} + \frac{1\text{-}w_{NCO\text{-t}}}{T^{0}_{g(e\text{-t})}} \tag{3}$$

$$\frac{1}{Tg,2} = \frac{w_{NCO\text{-}t}}{T^{\infty}_{g(NCO\text{-t})}} + \frac{1\text{-}w_{NCO\text{-}t}}{T^{\infty}_{g(e\text{-t})}} \tag{4}$$

where $T_{g,1}$ and $T_{g,2}$ are the T_gs of intermediate material and final thermoset for any r_{NCO} considered. $w_{NCO\text{-t}}$ is the weight fraction of the isocyanate plus the part of thiol which participate in the first curing step; $T^{0}_{g(e\text{-t})}$ is the experimental T_g of the uncured epoxy-thiol system; $T^{\infty}_{g(NCO\text{-t})}$ and $T^{\infty}_{g(e\text{-t})}$ are the T_g of the cured isocyanate-thiol and epoxy-thiol systems, respectively.

To monitor the dual-curing process and to quantitatively determine the degree of cure, a FTIR spectrometer Bruker Vertex 70 with an attenuated total reflection

accessory with thermal control and a diamond crystal (Golden Gate Heated Single Reflection Diamond ATR Specac-Teknokroma) and equipped with a mid-band liquid nitrogen-cooled mercury-cadmium-telluride (MCT) detector was used. Real-time spectra were collected in absorbance mode with a resolution of 4 cm^{-1} in the wavelength range 4000 to 600 cm^{-1} averaging 20 scans for each spectrum. The first step of the dual-curing process was conducted at 60°C and the second one at 120°C. The characteristic absorbance peak of the isocyanate at 2280 cm^{-1} (vibration of -N=C=O groups) was used to monitor the conversion during thiol-isocyanate reaction.[23] The disappearance of the absorbance peak at 915 cm^{-1} was used to monitor the reaction of epoxy groups.[24] Absorbance of each scanned sample were normalized with that of the S4-ester group at 1730 cm^{-1}.[25] Isocyanate groups conversion (X_{NCO}) and epoxy groups conversion (X_e) were calculated by Eq. 5 and 6.

$$x_{NCO} = 1 - \frac{A_{2280}}{A_{2280,0}} \quad (5)$$

$$x_e = 1 - \frac{A_{915}}{A_{915,0}} \quad (6)$$

where A_{2280} and $A_{2280,0}$ are the normalized absorbances of the isocyanate peak at 2280 cm^{-1} at a given reaction time and at the beginning of the curing process, respectively and A_{915} and $A_{915,0}$ the normalized absorbances of the epoxy peak at 915 cm^{-1} at the same time than isocyanate peak.

The thermomechanical properties were evaluated using DMA Q800 (TA Instrument) equipped with a three-point bending clamp. Prismatic rectangular samples of 1.5 × 5 × 15 mm^3 were analysed from 30 to 150°C, at 1 Hz, 0.1% strain and with a heating rate of 3°C/min. The Young modulus were defined under flexural conditions at 30°C with a force ramp rate of 1N/min.

TGA analyses were carried out with a Mettler Toledo TGA2 thermo-balance. Cured samples, weighting around 10 mg, were degraded between 30 and 600°C at a heating rate of 10°C/min in N_2 atmosphere with a flow of 50 cm^3/min.

3. Theoretical Part

In non-isothermal kinetics of heterogeneous condensed phase reactions, it is usually accepted that the reaction rate is given by Eq. 7.[26,27]

$$\frac{d\alpha}{dt} = \beta \frac{d\alpha}{dT} = A\exp\left(-\frac{E}{RT}\right) f(\alpha) \quad (7)$$

where α is the degree of conversion, T temperature, t time, $f(\alpha)$ the differential conversion function, R the gas constant, β the linear constant heating rate $\beta = dT/dt$ and A and E the pre-exponential factor and the activation energy given by the Arrhenius equation.

Polymer 174 (2019) 200–209

By integrating Eq. 7, in non-isothermal conditions, the integral rate equation, so-called temperature integral, may be expressed as Eq. 8.

$$g(\alpha) = \int_0^{\alpha} \frac{d\alpha}{f(\alpha)} = \frac{A}{\beta} \int_0^{T} e^{-(E/RT)} dT \tag{8}$$

where $g(\alpha)$ is the integral conversion function.

By using the Coats-Redfern approximation to solve Eq. 8 and considering that $2RT/E$ is much lower than 1, the Kissinger-Akahira-Sunose (KAS) equation (Eq. 9) may be written[28-30]:

$$\ln\left(\frac{\beta}{T^2}\right) = \ln\left[\frac{AR}{g(\alpha)\,E}\right] - \frac{E}{RT} \tag{9}$$

For each conversion degree, the linear plot of $\ln(\beta/T^2)$ versus T^{-1} enables E and $\ln[AR/g(\alpha)E]$ to be determined from the slope and the intercept. Iso-conversional kinetic parameters were obtained in this work by using Eq. 9. If the reaction model, $g(\alpha)$, is known, the corresponding pre-exponential factor can be calculated for each conversion.

Rearranging Eq. 9, the Coats–Redfern equation can be written as Eq. 10.[31]

$$\ln\left(\frac{g(\alpha)}{T^2}\right) = \ln\left[\frac{AR}{\beta E}\right] - \frac{E}{RT} \tag{10}$$

For a given model and heating rate, the linear plot of the left-hand side of Eq. 10 versus T^{-1} allowed us to obtain the average activation energy and average pre-exponential factor from the slope and the intercept. In this study, we chose the kinetic model with an activation energy similar to that obtained iso-conversionally (Eq. 9) and with a good correlation coefficient in Eq. 10 (Coats-Redfern method).

The rate constant k and the reaction rate $d\alpha/dt$ were calculated for each conversion from non-isothermal E, and A data using the Arrhenius equation and Eq. 7 and the kinetic model, respectively.

Integrating Eq. 7 for isothermal experiments, we can obtain Eq.11:

$$\ln t = \ln\left[\frac{g(\alpha)}{A}\right] + \frac{E}{RT} \tag{11}$$

This equation relates, for each conversion, the temperature and the time of curing. The constant $\ln[g(\alpha)/A]$ is directly related to the value $\ln[AR/g(\alpha)E]$ by E/R, which can be deduced from the non-isothermal adjustment (Eq. 9), if isothermal and non-isothermal curing take place in the same conditions. In this work we used $\ln[AR/g(\alpha)E]$ and E/R obtained by dynamic experiments and Eq. 9 to estimate the time of curing for both curing stages by using Eq. 11.

4. Results and Discussion

4.1. Study of the dual curing by DSC and FTIR

Calorimetric kinetics and FTIR conversions of the sequential dual curing processes were studied using a fixed r_{NCO} equal to 0.5 eq_{NCO}/eq_t and varying the amount of catalyst, to improve the sequential character of the dual curing system. The use of different proportions of 1MI as the catalyst (0.1-0.05-0.025 phr) for the IPDI_r_0.5 (Figure IV-1a) and the HDI_r_0.5 (Figure IV-1b) systems was studied firstly through dynamic DSC studies.

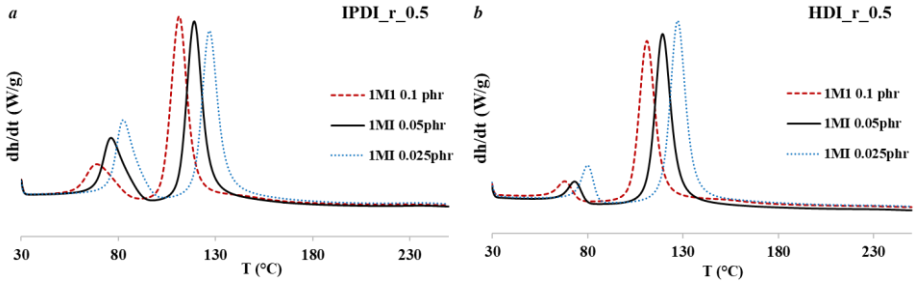

Figure IV-1. *DSC thermograms corresponding to the dynamic curing at 10°C/min with different 1MI amounts of a) IPDI_r_0.5 and b) HDI_r_0.5.*

It can be observed, that as the catalyst proportion increases, the exotherm related to the first stage shifts at lower temperatures, and the curve becomes flattened and is difficult to define and control the on-set and end-set temperatures of the isocyanate-thiol coupling. Due to the high reactivity at low temperatures of the thiol-isocyanate reaction in presence of a base, the process starts while we are adding the isocyanate to the corresponding formulation. It is worth to note that in all the samples there is a sequential succession of curing steps with a clear separation between both peaks, due to isocyanate-thiol and epoxy-thiol *click* reactions, respectively. Furthermore, the separation between both steps increases as the amount of 1MI decreases, allowing to obtain an excellent control over the global curing process. Comparing the curves for IPDI and HDI curing processes, we can state that the separation between both processes is more defined in HDI formulations.

Table IV-2 collects the most characteristic calorimetric data of the curing of the samples studied, in terms of heat reaction (Δh) and temperature of the maximum of exothermic peak (T_{peak}).

As we can see in the table, the heat released during the dynamic curing of the isocyanate-thiol reaction (Δh_{NCO}) is always lower in HDI formulations than in IPDI. In addition, this value decreases on increasing the amount of 1MI in the formulation. These observations indicate that HDI is more reactive than IPDI and that the mixtures begin to react during the preparation, leading to a loss of enthalpy.

Polymer 174 (2019) 200–209

On the other hand, when we compare the enthalpies released in the thiol-epoxy reaction for both type of formulations, the values obtained are comparable. As expected, the temperature of the maximum of the peaks corresponding to both processes (T_{peak}) increases on decreasing the proportion of 1MI in the formulation. Taking all of this into account, we have selected as optimal catalyst loading for thiol-isocyanate-epoxy networks 0.025 phr of 1MI.

***Table IV-2**. Calorimetric data of IPDI_r_0.5 and HDI_r_0.5 curing using 0.1-0.05-0.025 phr of 1MI.*

Sample	1MI (phr)	Δh_{NCO}[a] (J/g)	Δh_{NCO}[a] (kJ/eq)	Δh_e[b] (J/g)	Δh_e[b] (kJ/eq)	$T_{peak,NCO}$[c] (°C)	$T_{peak,e}$[d] (°C)
IPDI_r_0.5	0.1	60.2	31.7	247.7	130.2	69.1	112.8
	0.05	90.9	47.8	248.7	130.7	76.6	120.4
	0.025	103.7	54.5	252.3	132.6	82.7	127.5
HDI_r_0.5	0.1	24.6	12.3	252.3	125.8	68.4	112.3
	0.05	27.8	13.8	263.4	131.4	73.4	121.0
	0.025	40.1	19.6	272.5	135.9	80.3	128.8

[a] Enthalpy released in the thiol-isocyanate process by gr of mixture and by equivalent of isocyanate
[b] Enthalpy released in the thiol-epoxy process by gr of mixture and by equivalent of epoxide
[c] Temperature of the maximum of the peak of the thiol-isocyanate process
[d] Temperature of the maximum of the peak of the thiol-epoxy process

To obtain the kinetic parameters and the kinetic model, which best describes the reactive processes involved in our thiol-isocyanate-epoxy curing systems, dynamic DSC experiments were performed.

Figure IV-2 plots conversion against temperature, calculated according to Eq. 2, for isocyanate-thiol and epoxy-thiol reactions that occur at lower and higher curing temperatures, respectively, for IPDI_r_0.5 formulations at different heating rates (2, 5, 10 and 20°C/min). In Supporting Information, Figure IV-S1 reports the same study for HDI_r_0.5 formulations.

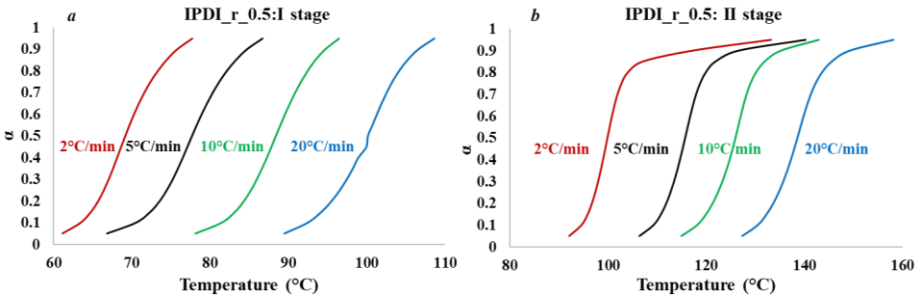

***Figure IV-2**. Degree of conversion versus temperature for IPDI_r_0.5. formulation with 0.025 phr of 1MI a) first and b) second stages.*

The kinetic parameters of non-isothermal curing for both curing stages obtained by DSC dynamic experiments are reported in Table IV-3 for IPDI_r_0.5 formulations. The results obtained for HDI_r_0.5 formulations are collected in Table IV-S1 (Supporting Information).

***Table IV-3**. Kinetic parameters of dynamic curing obtained by DSC of IPDI_r_0.5 formulation.*

Stage	α[a]	E[b] (kJ/mol)	$ln[AR/g(\alpha)E]$ ($K^{-1}\cdot s^{-1}$)	r[c]	$ln\ A$[d] (s^{-1})	k[e]	$d\alpha/dt$[f] (s^{-1})
first	0.1	72.49	15.11	0.990	23.43	1.07	0.64
	0.2	72.25	14.81	0.991	23.38	1.10	0.97
	0.3	71.66	14.49	0.992	23.21	1.12	1.18
	0.4	71.34	14.29	0.992	23.12	1.14	1.31
	0.5	71.47	14.25	0.993	23.19	1.16	1.36
	0.6	71.94	14.32	0.993	23.36	1.19	1.34
	0.7	72.83	14.52	0.993	23.66	1.21	1.23
	0.8	74.03	14.80	0.993	24.05	1.21	1.00
	0.9	75.39	15.07	0.993	24.46	1.18	0.61
second	0.1	70.13	11.31	0.997	19.78	0.06	0.04
	0.2	67.83	10.45	0.996	19.08	0.06	0.06
	0.3	66.35	9.91	0.996	18.64	0.06	0.08
	0.4	65.63	9.62	0.996	18.43	0.06	0.09
	0.5	65.49	9.52	0.996	18.40	0.07	0.10
	0.6	65.75	9.54	0.996	18.49	0.07	0.10
	0.7	66.13	9.58	0.997	18.61	0.07	0.09
	0.8	65.59	9.43	0.997	18.53	0.07	0.07
	0.9	63.69	8.49	0.999	17.64	0.06	0.04

[a] Conversion degree

[b] Activation energy

[c] Correlation coefficient

[d] Pre-exponential factor calculated using kinetic model A_3 and A_4 for the 1st and 2ndstage, respectively

[e] Rate constant calculated by Arrhenius equation

[f] Reaction rate calculated by Eq. 7.

From Table IV-3 it is possible to observe that the activation energy remains, during both curing stages, relatively constant. This result suggests that the reaction mechanism is the same in the whole range of curing, according to the *click* character of the reaction, and a single kinetic model is only needed to describe the curing. In many reaction processes the values of activation energy, due to the compensation effect between the activation energy and the pre-exponential factor, do not reflect exactly the reaction rate and it is better to discuss the rate constants calculated using Eq. 7 and the kinetic model.[32]

Polymer 174 (2019) 200–209

In accordance with the Coats-Redfern method described in the theoretical section, various kinetic models have been studied: diffusion (D_1, D_2, D_3, and D_4), Avrami-Erofeev (A_2, $A_{3/2}$, A_3, and A_4), power law, phase-boundary-controlled reaction (R_2 and R_3), autocatalytic ($n + m = 1$, 2 and 3), and order n ($n = 1$, 2 and 3).[33] We have found that all the systems studied follow at all heating rates an Avrami-Erofeev model A_3 (first curing stage) and A_4 (second curing stage). Although there is no reason for some of these models to have any physicochemical meaning in the curing processes, they can still be used to aid to the description of the calorimetric curve.

Table IV-3 also highlights the dual nature of the system studied since isocyanate-thiol coupling shows rate constants about fifteen times greater than epoxy-thiol reaction. HDI_r_0.5 shows the same behaviour, but in a more pronounced way (see Table IV-S1). Furthermore, it can be observed than the rate constant increases with the conversion, and after reaching a maximum, decreases in accordance with the autocatalytic nature of both curing stages. It is well known, that OH groups catalyzes the nucleophilic attack to the epoxides, due to the hydrogen bonding between hydroxylic protons, formed during the reaction, and the epoxides, facilitating the opening of the ring.[34] The attack of the thiol to the isocyanate can be also catalysed by the formation of hydrogen bonding, increasing the electrophilic character of the isocyanate group.

DSC dynamic studies provide information about the heat evolved in the overall reaction process but the evolution of the functional groups during curing and the structure of the network formed needs to be observed by FTIR spectroscopy. In this way, detailed data about the curing methodology can be obtained by determining the evolution of the absorption bands of the isocyanate and epoxide groups. This method allows the determination of the conversion progress at several reaction times for the different functional groups reacting during the curing process. As an example, Figure IV-S2 in Supporting Information shows some representative FTIR spectral regions collected during a) the first stage at 60°C and b) the second stage at 120°C of HDI_r_0.5 formulation. It can be observed the complete disappearance of the characteristic absorbance peaks of free isocyanate groups at 2280 cm^{-1} and epoxies at 915 cm^{-1}.

According to DSC results, we found in both formulations that the conversion was complete at the end of both curing stages, indicated by a fractional conversion of 0.5 and 1 at the end of stage 1 and stage 2, respectively.

Figure IV-3 shows the evolution of the bands of the reactive groups during the first and second stages of the curing for the HDI_r_0.5 mixture.

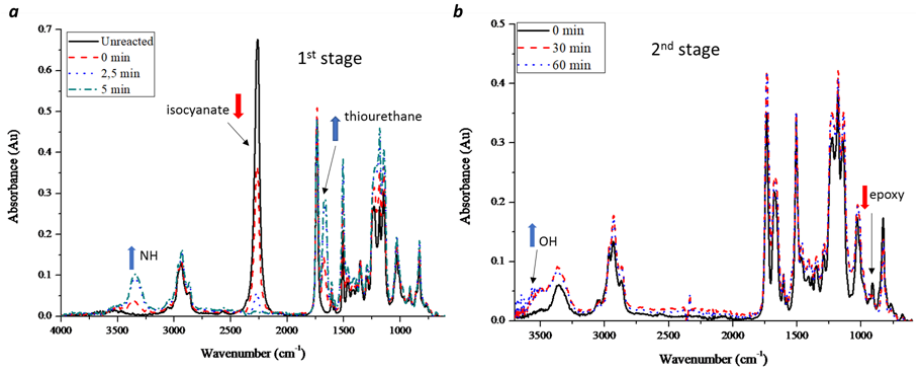

***Figure IV-3**. Evolution of the FTIR spectra during curing of HDI_r_0.5 mixture at a) 60°C, for 5 min during the 1st stage of curing and b) 120°C, for 60 minutes during 2nd stage of curing.*

As we can see, in the first curing stage (Figure IV-3) the isocyanate band completely disappears after 5 min of reaction at 60°C (red arrow), while thiourethane absorptions at 1670 and 3350 cm^{-1} are formed (blue arrows), indicating that the complete formation of thiourethane was achieved. The mixture with IPDI reacts more slowly as can be seen in Figure IV-S3 and a reaction time of 30 min is needed for the complete disappearance of the isocyanate band. In the second stage of the curing, hydroxyl absorptions appear during the process while the epoxy band at 915 cm^{-1} disappears. The second stage is finished in 60 min for both mixtures. Thiol absorptions at 2580 cm^{-1} can be detected but their evolution can be only followed from a qualitative point of view, due to its weak intensity. The peak at 1730 cm^{-1} attributed to the carbonyl absorption of ester groups of the S4 does not experiment any change during the curing process and has been used as internal reference for kinetic studies.

Several authors reported the formation of oxazolidone moieties in the curing of mixtures of isocyanate and epoxide.[35,36] This reaction can also lead to the formation of isocyanurate groups by cyclization of isocyanates at lower temperatures than oxazolidone moieties.[36] Therefore, the formation of isocyanurate rings could occur in the first stage of the curing of the dual process, in which the temperature is too low to allow the formation of oxazolidone moiety. In the FTIR spectra of the intermediate (Figure IV-3a) and final material (Figure IV-3b) no absorptions at 1715 cm^{-1}, typical of isocyanurate rings, nor absorptions at 1750-1740 cm^{-1}, indicative of oxazolidone formation, can be observed. This indicates that in the first stage of curing, in which isocyanate, thiol and epoxy groups coexist, the reaction of isocyanate and thiol is favoured, confirming its *click* character. In the second stage, the formation of oxazolidones cannot occur, since there is no unreacted isocyanate in the reactive mixture.

Figure IV-4 shows the FTIR conversion plot during isothermal curing at 60°C (isocyanate-thiol *click* reaction) and later at 120°C (epoxy-thiol *click* reaction) for

IPDI_r_0.5 and HDI_r_0.5 samples. The temperature of the first and second stages have been chosen according to DSC analyses and the isothermal reaction times, tentatively, estimated by using Eq. 11 and the isoconversional non-isothermal kinetic parameters previously determined (Tables IV-3 and S1).

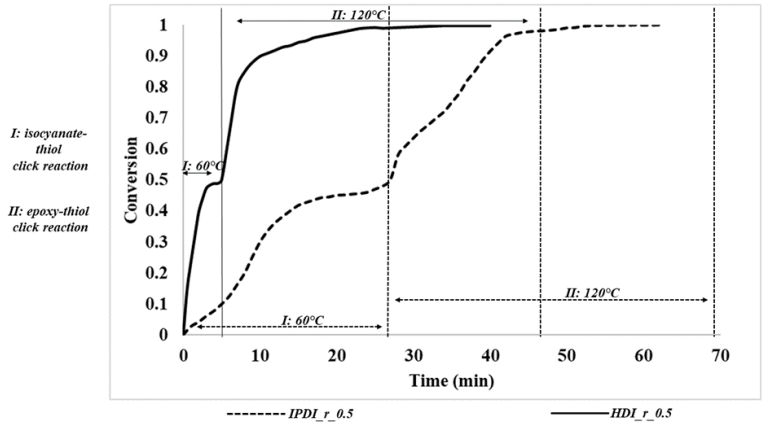

***Figure IV-4**. FTIR isocyanate and epoxy conversion during isothermal curing at 60°C (stage I) and at 120°C (stage II) for IPDI_r_0.5 and HDI_r_05 formulations.*

From the FTIR and DSC studies, it is evident that the first curing stage is faster for HDI formulations that for IPDI mixtures, as observed in a previous study, whereas the second stage is not affected by the isocyanate used in the formulation.[16]

Although the curing times for both curing stages can be easily calculated from the kinetic studies, the preparation of samples for DMTA in a metal mould in the oven requires longer times and an optimization of the curing schedule is always needed. Thus, by registering FTIR and DSC curves at different curing times, we optimized the curing schedule to achieve complete conversion of isocyanate and epoxy groups at the end of both stages. The optimized curing schedule is: i) stage 1 at 60°C for 1 hr in the case of IPDI and for 40 min with HDI; ii) stage 2 at 120°C for 2 hr for both systems studied. The curing times and temperatures reported here have been used for the preparation of thermosets with different compositions based on IPDI and HDI.

In order to know the influence of the composition of the formulation in the dual curing behaviour, we extended the calorimetric study to isocyanate contents 0.2 and 0.8. In Figure IV-5, the DSC curves for a) IPDI and b) HDI formulations showing the exotherms corresponding to each curing stage are represented.

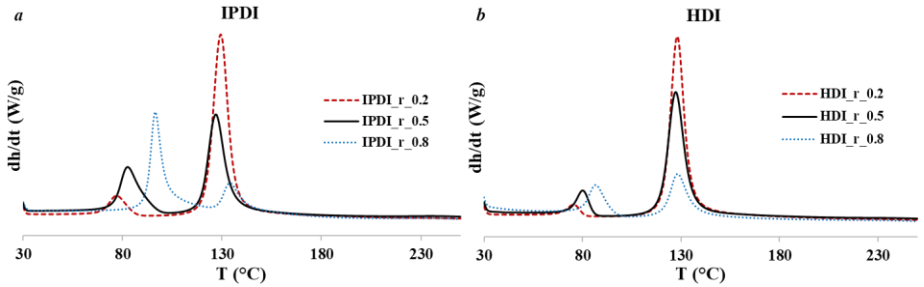

***Figure IV-5**. DSC thermograms corresponding to the dynamic curing at 10°C/min of different compositions of a) IPDI and b) HDI formulations.*

As we can see in the Figure IV-5, on increasing the isocyanate content (from r_{NCO} 0.2 to 0.8) the first curing stage shifts at higher temperatures whereas the second stage remains almost unchanged. This result suggests that an excess of thiol favours the nucleophilic thiol isocyanate reaction, but the network formed during first stage does not modify significantly the kinetics of the epoxy-thiol reaction. It should be noticed, that in all the formulations, in the second stage the epoxy-thiol proportions are stoichiometric. Although, all the formulations are characterized by a sequential succession of curing steps with a separation between both reaction peaks, in the case of IPDI_r_0.8 sample the separation between the curing stages is not clearly defined. This indicates that formulations with proportions of IPDI 0.8 or higher are not adequate for applications requiring sequentiality. It can be also stated that a better sequential dual-curing behaviour is obtained with epoxy-rich formulations.

The contribution of both isocyanate-thiol and epoxy-thiol reactions in terms of reaction heat for all the formulations prepared is reported in Table IV-4.

***Table IV-4**. Calorimetric data for both stages and theoretical and experimental $T_{g,1}$ and $T_{g,2}$.*

	1st stage		*2nd stage*		*1st stage*		*2nd stage*	
Sample	**Δh_{NCO} (J/g)**	**Δh_{NCO} (kJ/eq)**	**Δh_e (J/g)**	**Δh_e (kJ/eq)**	**$^{ther}T_{g,1}{}^{a}$ (°C)**	**$^{exp}T_{g,1}{}^{b}$ (°C)**	**$^{ther}T_{g,2}{}^{c}$ (°C)**	**$^{exp}T_{g,2}{}^{d}$ (°C)**
IPDI_r_0.2	40.4	56.7	376.4	131.9	-21.2	-18.8	60.4	54.6
IPDI_r_0.5	103.7	54.5	252.3	132.6	10.4	10.6	74.1	74.7
IPDI_r_0.8	159.2	49.4	56.7	70.8	57.8	57.8	91.3	92.9
HDI_r_0.2	17.3	23.7	356.2	122.5	-27.1	-36.4	52.2	52.6
HDI_r_0.5	40.1	19.6	272.5	135.9	-7.4	-3.3	51.4	52.9
HDI_r_0.8	63.4	17.8	108.0	120.7	21.5	28.3	50.5	48.7

[a] T_g value for the intermediate material calculated by the Fox Eq.

[b] Experimental T_g value for the intermediate material determined by DSC.

[c] T_g value for the final material calculated by the Fox Eq.

[d] Experimental T_g value for the intermediate material determined by DSC.

Polymer 174 (2019) 200–209

In a previous study in the latent catalysed curing of thiols and IPDI we determined an enthalpy by equivalent of 72 kJ/eq.[16] In the present study, the heat released by equivalent is lower. This is because this reaction begins at room temperature during the preparation of the reactive mixture and some heat get lost before DSC experiment. The higher reactivity of HDI leads to lower values of enthalpy released. It is reported that thiol-epoxy reactions release about 125 kJ per equivalent of epoxide.[37] As we can see in the Table IV-4, the thiol-epoxy reaction seems to be complete for all the formulations, with the exception of IPDI_r_0.8 in which a partial overlapping of both reactions occurs, which difficult the selection of the base-line. Thus, the measured heat released confirms the sequential dual character of these curing systems, except for IPDI_r_0.8 mixture.

4.2. Thermal and dynamo mechanical characterization

By using the Fox copolymer rule (Eq. 3 and 4) we are able to predict the T_gs of intermediate and final materials as function of the formulation composition, using the experimental T_g data of the uncured epoxy-thiol formulation, which is $T^0_{g(e\text{-}t)}$= -37.3°C and the T_gs of the pure thermosets: i) IPDI-thiol $T^{\infty}_{g(IPDI\text{-}t)}$= 105.4°C; ii) HDI-thiol, $T^{\infty}_{g(HDI\text{-}t)}$= 49.8°C and iii) epoxy-thiol, $T^{\infty}_{g(e\text{-}t)}$= 52.6°C.

Experimental T_g values have been determined by DSC in the intermediate and final curing stages. The values of experimental and calculated T_gs are collected in Table IV-4 for all the formulations studied. Figure IV-6 shows the dependence of the calculated and experimental T_gs in function of the different r_{NCO} compositions for a) IPDI and b) HDI mixtures. The theoretical critical gelation ratio, r_c, has been calculated by the Flory-Stockmayer theory (Eq. 1).

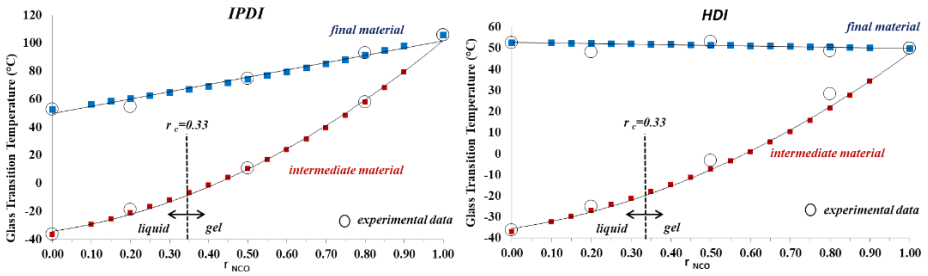

Figure IV- 6. *Plot of experimental (circles) and calculated (full squares) T_gs against r_{NCO} for a) IPDI and b) HDI dual curing formulations.*

As can be seen in Figure IV-6, a wide range of intermediate and final materials could be obtained using IPDI and HDI as isocyanates and different formulation compositions. Furthermore, there is a significant influence of the type of isocyanate on the intermediate and final T_gs, and the material properties, in particular in the final stage. Whereas IPDI fully cured thermosets show a great variation of the T_g with the composition (from 52.6 to 105.4 °C), all the HDI thermosets have similar values. This

is caused by the similar T_g values of the pure HDI-thiol and epoxy-thiol thermosets, 49.8 and 52.6°C, respectively. Calculated and experimental T_gs fully agree, especially for IPDI formulations, which indicates that the reactions implied occurred completely, without side-reactions, as expected from *click* processes.

Keeping in mind the value of r_c of 0.33 it is possible to obtain a gelled and therefore solid-like and shape-conformable intermediate materials, after the first stage, for compositions with $r_{NCO} > 0.33$ at compositions lower than this value, the material will be viscous with high adhesion properties.

The thermal stability of the thermosets was evaluated by thermogravimetry. Figure IV-7 shows the TGA curves for all formulations studied and the insets show the rate of weight loss against temperature (DTGA curves). The main data obtained for these experiments are collected in Table IV-5.

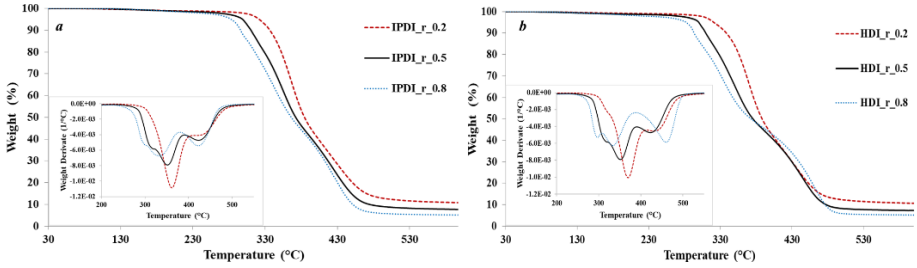

Figure IV-7*. TGA curves of a) IPDI and b) HDI thermosets with the different compositions selected. Insets show the rate of weight loss against temperature, DTGA.*

It can be observed that the degradation takes place in two principal steps, with a small shoulder at lower temperature of the first degradation step, which increases with the proportion of isocyanate in the formulation. The first stage, at the temperature range of 280-400°C, is characterized by the decomposition of thiourethane segments and it is reasonable to assume that the formation of the shoulder is significantly affected by the r_{NCO} chosen.[38] In a previous work of our group, based in poly(thiourethane) networks, a complex degradation mechanism with three different steps was observed.[16] Thus, on increasing the amount of these structures in the global network, the DTGA curves tend to become more complex with the clear appearance of a shoulder. The second degradation step, occurring at the temperature range 400-500°C, can be attributed to the degradation of hydroxy-thioether structures but also to the poly(thiourethane) structure.[8] This is evident if we compare the temperatures of the maximum rate of weight loss, higher in case of HDI thermosets, as seen in our previous study.[16] However, it should be pointed out that both degradation steps are strongly overlapped, and therefore it is not possible to attribute exclusively the first peak to the thiourethane structure and the second to the thiol-epoxy network. It must be considered that the thiol monomer randomly interconnects both types of networks, which are not independent each other. The overall thermal behaviour of

Polymer 174 (2019) 200–209

the samples prepared is then the result of the different stability of the chemical bonds formed during the first and the second stage.

***Table IV-5**. Thermogravimetric and thermomechanical data obtained for IPDI and HDI thermosets.*

Sample	$T_{2\%}$[a] (°C)	T_{max}[b] (°C)	Char Yield[c] (°C)	FWHM[d] (°C)	$T_{tan\ \delta}$[e] (°C)	E'[f] (MPa)	Young's Modulus[g] (GPa)
IPDI_r_0.2	287.6	362/446	9.9	9.5	80.1	19.1	2.1
IPDI_r_0.5	257.5	353/432	7.3	13	104.7	18.9	2.5
IPDI_r_0.8	227.6	333/423	4.8	13	129.4	18.8	3.2
HDI_r_0.2	299.7	369/442	10.7	10	62.6	13.0	1.5
HDI_r_0.5	268.3	349/445	7.4	9.5	66.0	13.5	1.7
HDI_r_0.8	217.3	333/460	5.2	11.5	69.5	14.2	1.9

[a] Temperature of 2% of weight loss

[b] Temperatures of the maximum rate of degradation of the two main steps

[c] Char residue at 600°C.

[d] Full width at half maximum of *tan δ* peak

[e] Temperature of the maximum of *tan δ* at 1 Hz

[f] Relaxed modulus determined at the $T_{tan\ \delta}$ + 40°C in the rubbery state

[g] Young modulus determined at 30°C under flexural conditions

From the values of the table, we can see that the higher the proportion of poly(thiourethane) fragments in the network the lower the thermal stability of the material. This is reflected in the initial degradation temperatures ($T_{2\%}$) and in the temperature of the maximum rate of degradation (T_{max}). IPDI thermosets presents a higher thermal stability than their HDI analogue. The presence of aromatic rings in the epoxy compound leads to a higher char yield in the thermosets with a higher proportion of DGEBA.

The thermomechanical behaviour of all the materials prepared was evaluated by DMTA analyses. Figure IV-8 presents the *tan δ* curves obtained for both types of materials. The main data extracted from DMTA tests are collected in Table IV-5. As we can see in Figure IV-8, the materials obtained are homogeneous with unimodal and narrow shapes despite the dual curing procedure applied in the preparation. The values of the width of the curve at half height (*FWHM*) are rather small, according to the *click* character of the curing reactions implied, without the formation of unexpected structures, and they are consistent with the ones reported by Gamardella *et al.* for pure thiol-isocyanate thermosets.[16] The high homogeneity of these materials and their narrow ranges of relaxation make these materials applicable to smart technologies and as shape memory materials, as for example in actuators, valves, robotics and optical applications, etc.[39-42]

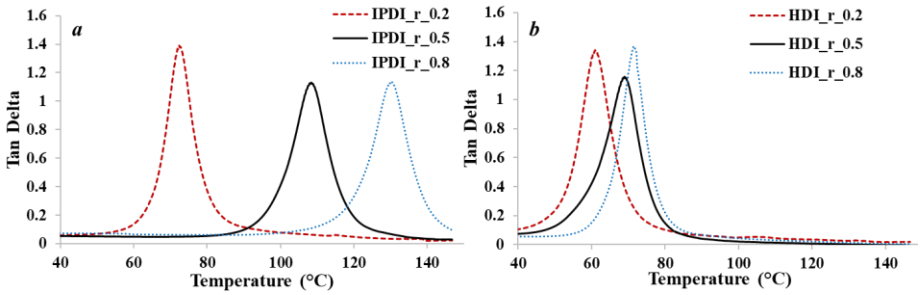

***Figure IV-8**. Tan δ and storage modulus against temperature of IPDI (a) and HDI (b) thermosets.*

The values of the temperature of the maximum of *tan δ* depend fundamentally on the structure of the isocyanate monomer, rigid and compact, in the case of IPDI, and flexible and linear for HDI. In the case of IPDI-based thermosets, the temperature of the maximum of *tan δ* increases as r_{NCO} increases, due to the high compactness and rigid structure of IPDI monomer and the possibility to enhance interactions between chains by hydrogen bonding. On the other side, with HDI samples, *tan δ* temperatures remain almost similar, in agreement with the trends observed by DSC measurements. The values obtained are a little lower than those obtained in pure poly(thiourethane) thermosets previously reported.[16] Furthermore, for all the samples studied the height of *tan δ* curve is comparable for all the thermosets.

There are no significant differences in the *E'* data for the IPDI samples prepared, but this value tends to decrease on increasing the amount of HDI in the material. Finally, the Young's modulus yields the highest values in the case of IPDI materials, due to their rigid network structure. Young moduli slightly increase on increasing the isocyanate content, due to the higher rigidity of poly(thiourethane) networks, which is enhanced by the presence of hydrogen bonding between chains.

4.3. Prospective applications

In this paragraph, we illustrate some possible applications of the prepared samples in the field of materials with shape memory behaviour. IPDI_r_0.5 and HDI_r_0.5 samples were chosen as representative samples. As shown in Figure IV-9, IPDI and HDI formulations, prepared as described in the experimental part, were poured into a Teflon mould and cured at 60°C for 40 min in the case of HDI samples and for 60 min in the case of IPDI materials (1st curing stage) to obtain intermediate prismatic shape materials (step *a*). Thanks to the deformability of these gelled intermediate materials, they were easily rolled onto stainless steel moulds having different geometries and covered with a Teflon layer (step *b*) obtaining bent-shaped surfaces. To obtain permanent shapes, the samples were heated up at 120°C for 120 min (2nd curing stage), cooled at room temperature and peeled off from the moulds (permanent shapes, step *c*).

Polymer 174 (2019) 200–209

The shape memory characterization consists of two steps: i) programming of temporary shape and ii) recovery of the original shape. The first step was performed between two stainless steel plates at 150°C (programming temperature) applying enough pressure to flatten the sample (step *d*). They were cooled down quickly to room temperature and the resulting material showed a prismatic flat shape. In the second step, once the temporary shape was programmed, the recovery of the original permanent bent shape was conducted by heating the samples at 120°C (step *e*). Since the results obtained seems to be highly promising, the complete study of the shape memory behaviour of the new materials prepared in this work will be carried out in future projects to explore their possible applications.

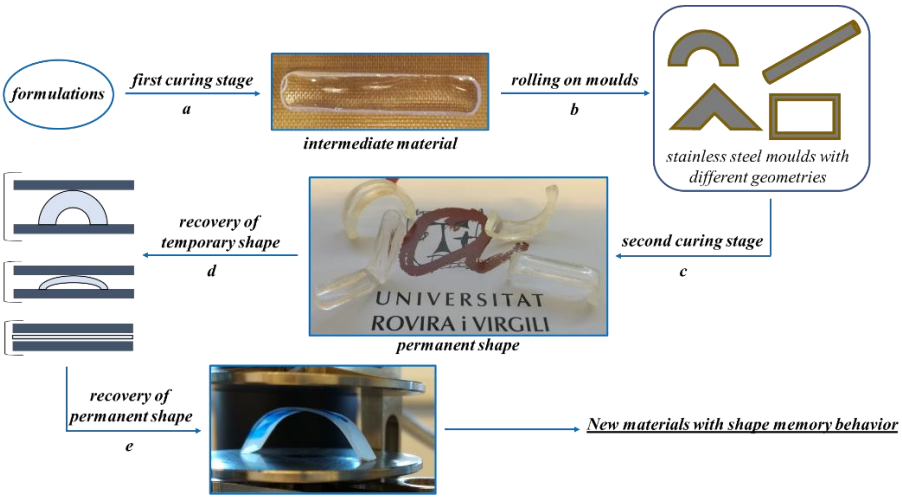

***Figure IV-9**. Representation of the bent-shaped sample processing, shape memory programming and recovery process.*

5. Conclusion

In this work, a new family of thermosets based on thiol-isocyanate-epoxy networks was developed by means of a dual curing process and exploiting the use of two different aliphatic isocyanates, isophorone diisocyanate and hexamethylene diisocyanate. The sequential dual character of this new curing system relies on the faster reaction kinetic of the isocyanate-thiol coupling that occurs at a relatively low temperature, compared to the epoxy-thiol reaction between the remaining thiol groups and the epoxy, taking place at higher temperature. The *click* character of both reactive processes prevents other side reactions to occur. The extent of the first curing step is controlled by the equivalent ratio between the isocyanate and thiol, which also tailors the intermediate and final materials properties. Therefore, it is possible to design intermediate materials, which can be gels or viscous liquids, depending on the proportion of isocyanate, and fully cured materials, which can be loosely or tightly crosslinked. The characteristics of the intermediate materials open the possibility to

be used as adhesives or to be conformed to create complex shapes that can be further crosslinked. Furthermore, the materials prepared show an interesting shape memory behaviour that will be further studied, and which opens the possibility to be applied in smart technologies.

Acknowledgments

The authors would like to thank MCIU (Ministerio de Ciencia, Innovación y Universidades) and FEDER (Fondo Europeo de Desarrollo Regional) (MAT2017-82849-C2-1-R and MAT2017-82849-C2-2-R) and to Generalitat de Catalunya (2017-SGR-77) for the financial support.

References

1. I. Hamerton, J. Kratz, In: Thermosets. Structure, Properties, and Applications Q. Guo, Ed., Elsevier, Amsterdam, NL, pp. 303-326, 2018.

2. J. Verrey, M.D. Wakeman, V. Michaud, J.-A.E. Månson, *Composites Part A* **2006**, 37, 9–22.

3. M. Giordano, A. Laudati, M. Russo, J. Nasser, G.V. Persiano, A. Cusano, *Thin Solid Films* **2004**, 450, 191–194.

4. X. Luo, P.T. Mather, *ACS Macro Lett.* **2013**, 2, 152–156.

5. D.P. Nair, N.B. Cramer, M.K. McBride, J.C. Gaipa, R. Shandas, C.N. Bowman, *Polymer* **2012**, 53, 2429–2434.

6. A. Belmonte, C. Russo, V. Ambrogi, X. Fernández-Francos, S. De la Flor, *Polymers* **2017**, 9, 113-132.

7. M. Sangermano, W. Carbonaro, G. Malucelli, A. Priola, *Macromol. Mater. Eng.* **2008**, 293, 515–520.

8. X. Fernández-Francos, A.O. Konuray, A. Belmonte, S. De La Flor, À. Serra, X. Ramis, *Polym. Chem.* **2016**, 7, 2280–2290.

9. P.T. Mather, X. Luo, I.A. Rousseau, *Annu. Rev. Mater. Res.* **2009**, 39, 445–471.

10. S.H. Cho, S.R. White, P.V. Braun, P. V., *Adv. Mater.* **2009**, 21, 645–649.

11. A.M. Prenen, J.C.A.H. Van der Werf, C.W.M Bastiaansen, D.J. Broer, *Adv. Mater.* **2009**, 21, 1751–1755.

12. Y. Huang, G.T. Paloczi, A. Yariv, C. Zhang, L.R. Dalton, *J. Phys. Chem. B* **2004**, 108, 8606–8613.

13. B. Jaffrennou, N. Droger, F. Méchin, J.L. Halary, J.P. Pascault, *e-Polymers* **2005**, 5, 1–19.

14. Z.S. Petrović, J. Ferguson, *Prog. Polym. Sci.* **1991**, 16, 695–836.

15. J. Shin, J. Lee, H.M. Jeong, *J. Appl. Polym. Sci.* **2018**, 135, 1–8.

16. F. Gamardella, X. Ramis, S. De la Flor, À. Serra, *React. Funct. Polym.* **2019**, 134, 174–182.

17. O.D. McNair, B.J. Sparks, A.P. Janisse, D.P. Brent, D.L. Patton, D.A. Savin, *Macromolecules* **2013**, 46, 5614–5621.

18. J. Shin, H. Matsushima, C.M. Comer, C.N. Bowman, C.E. Hoyle, *Chem. Mater.* **2010**, 22, 2616–2625.

19. H. Matsushima, J. Shin, C.N. Bowman, C. E. Hoyle, *J. Polym. Sci. Part A Polym. Chem.* **2010**, 48, 3255–3264.

20. A. Belmonte, X. Fernández-Francos, À. Serra, S. De La Flor, *Mater. Des.* **2017**, 113, 116–127.

21. S. Vyazovkin, N. Sbirrazzuoli, *Macromol.Rapid Commun.* **2000**, 21, 85–90.

22. T.G. Fox, *Bull. Am. Phys. Soc.* **1956**, 1, 123-132.

23. E. Papadopoulos, M. Ginic-Markovic, S. Clarke, *Macromol. Chem. Phys.* **2008**, 209, 2302–2311.

[24.] R. Thomas, C. Sinturel, J. Pionteck, H. Puliyalil, S. Thomas, *Ind. Eng. Chem. Res.* **2012**, 51, 12178-12191.

[25] S. Ye, N.B. Cramer, I.R. Smith, K.R. Voigt, C.N. Bowman, *Macromolecules* **2011**, 44, 9084-9090.

[26.] S. Vyazovkin, *Isoconversional Kinetics of Thermally Stimulated Processes*, Springer, New York, NY, USA, pp. 166-231, 2015.

[27.] S. Vyazovkin, N. Sbirrazzuoli, *Macromol. Chem. Phys.* **1999**, 200, 2294-2303.

[28.] A.W. Coats, J.P. Redfern, *Nature* **1964**, 201, 68-69.

[29.] H.E. Kissinger, *Anal. Chem.* **1957**, 29, 1702-1706.

[30.] R.L. Blaine, H.E. Kissinger, *Thermochim. Acta* **2012**, 540, 1-6.

[31.] S. Vyazovkin, D. Dollimore, *J. Chem. Inf. Model.* **1996**, 36, 42-45.

[32.] S. Vyazovkin, C.A. Wight, *Annu. Rev. Phys. Chem.* **1997**, 48, 125-149.

[33.] X. Ramis, J.M. Salla, J. Puiggalí, *J. Polym. Sci. Part A Polym. Chem.* **2005**, 43, 1166-1176.

[34.] B.A. Rozenberg, *Adv. Polym. Sci.* **1986**, 75, 113-165.

[35.] A. Bakry, R. Aversano, L. D'Ilario, V. Di Lisio, I. Francolini, A. Piozzi, A. Martinelli, *J. Appl. Polym. Sci.* **2016**, 133, 1-8.

[36.] M. Flores, X. Fernández-Francos, J.M. Morancho, À. Serra, X. Ramis, *J. Appl. Polym. Sci.* **2012**, 75, 2779-2789.

[37.] D. Guzmán, X. Ramis, X. Fernández-Francos, À. Serra, *RSC Advances* **2015**, 75, 101623-101633.

[38.] M. Rogulska, A. Kultys, E. Olszewska, *J. Therm. Anal. Calorim.* **2013**, 114, 903–916.

[39.] T. Hisaaki, H. Hisashi, Y. Etsuko, H. Shunichi, *Smart Mater. Struct.* **1996**, 5, 483-491

[40.] B. Yang, W.M. Huang, C. Li, C.M. Lee, L. Li, *Smart Mater. Struct.* **2004**, 13, 191–195.

[41.] Y. Yang, Y. Chen, Y. Li, M.Z.Q. Chen, Y. Wei, *Soft Rob.* **2017**, 4, 147–162.

[42.] B.S. Lee, B.C. Chun, Y.C. Chung, K.I. Sul, J.W. Cho, *Macromolecules* **2001**, 34, 6431–6437.

Polymer 174 (2019) 200–209

Supporting Information

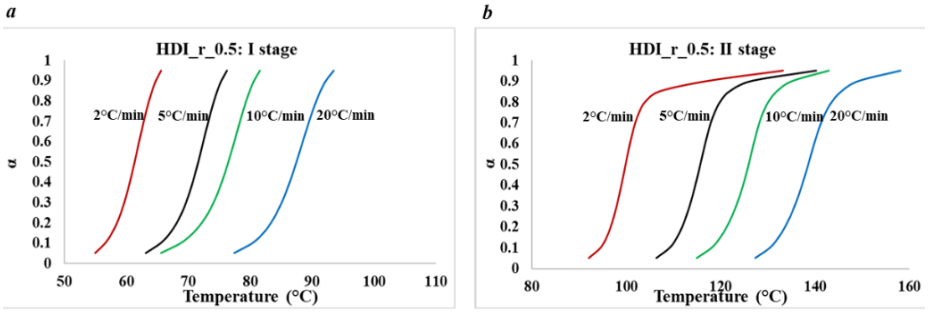

Figure IV-S1. *HDI_r_0.5. degree of conversion versus temperature of a) first and b) second stages.*

Table IV-S1. *Kinetic parameters of dynamic curing obtained by DSC of HDI_r_0.5 formulation.*

Stage	α[a]	E[b] (kJ/mol)	$ln[AR/g(\alpha)E]$ ($K^{-1}\cdot s^{-1}$)	R[c]	$ln\ A$[d] (s^{-1})	k[e]	$d\alpha/dt$[f] (s^{-1})
first	0.1	89.70	21.89	0.978	30.43	4.55	2.74
	0.2	87.25	20.77	0.986	29.53	4.08	3.60
	0.3	86.05	20.21	0.989	29.11	3.94	4.16
	0.4	85.25	19.82	0.990	28.83	3.88	4.46
	0.5	84.62	19.51	0.991	28.63	3.85	4.53
	0.6	84.04	19.24	0.992	28.43	3.83	4.34
	0.7	83.55	18.99	0.992	28.27	3.82	3.89
	0.8	82.99	18.71	0.992	28.08	3.79	3.13
	0.9	82.18	18.33	0.991	27.81	3.73	1.95
second	0.1	70.13	11.31	0.998	21.50	0.10	0.07
	0.2	67.83	10.45	0.999	21.04	0.10	0.11
	0.3	66.35	9.91	0.999	21.70	0.11	0.14
	0.4	65.63	9.62	0.999	20.47	0.11	0.16
	0.5	65.49	9.52	0.999	20.34	0.11	0.16
	0.6	65.75	9.54	0.999	20.28	0.11	0.16
	0.7	66.13	9.58	0.999	20.23	0.11	0.15
	0.8	65.59	9.43	0.999	20.36	0.10	0.12
	0.9	63.69	8.49	0.988	26.49	0.05	0.04

[a] Conversion degree

[b] Activation energy

[c] Correlation coefficient

[d] Pre-exponential factor calculated using kinetic model A_3 and A_4 for the 1st and 2ndstage, respectively

[e] Rate constant calculated by Arrhenius equation

[f] Reaction rate calculated by Eq. 7.

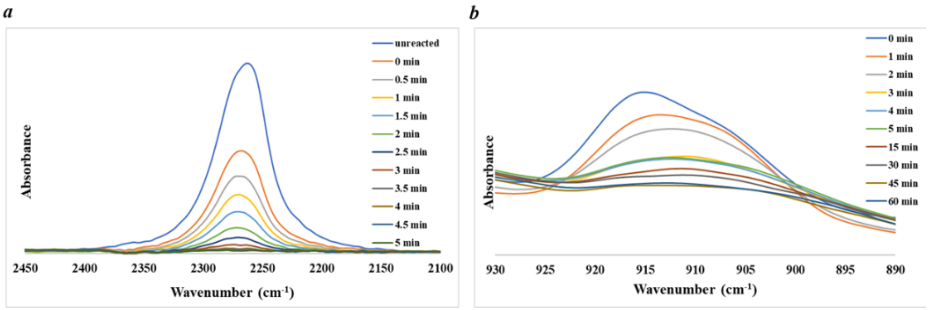

Figure IV-S2. *FTIR spectral zones of HDI_r_0.5 mixture at a) 60°C, for 5 minutes during isocyanate-thiol reaction (isocyanate absorption) and b) 120°C, for 60 minutes during epoxy-thiol click reaction (epoxy absorption).*

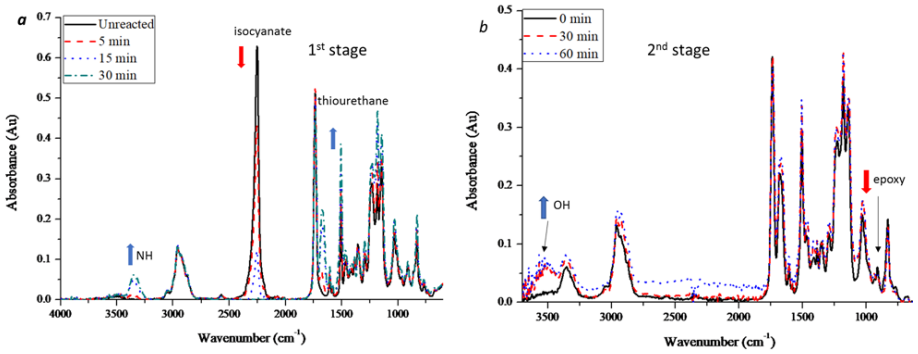

Figure IV-S3*. Evolution of the FTIR spectra during curing of IPDI_r_0.5 mixture at a) 60°C, for 30 min during the 1st stage of curing and b) 120°C, for 60 minutes during 2nd stage of curing.*

Chapter V

Actuator behavior of tailored poly(thiourethane) shape-memory thermosets

Actuator behavior of tailored poly(thiourethane) shape-memory thermosets

Francesco Gamardella[1], Xavier Ramis[2], Àngels Serra[1], Silvia De la Flor[3]

[1] Dept.of Analytical and Organic Chemistry, Universitat Rovira i Virgili, C/ Marcel·lí Domingo, 43007, Tarragona, Spain

[2] Thermodynamics Laboratory, ETSEIB Universitat Politècnica de Catalunya, Av. Diagonal, 08028, Barcelona, Spain

[3] Department of Mechanical Engineering, Universitat Rovira i Virgili, Av. Països Catalans, 26, 43007 Tarragona, Spain

Abstract

In this work, a new family of poly(thiourethane) shape memory thermosetting actuators was developed and characterized. These materials can be easily prepared from mixtures of two different aliphatic diisocyanates and a trithiol in the presence of a latent catalyst, allowing an easy manipulation of the formulation. Rheological studies of the curing process confirm the latent character of the formulations. The glass transition temperatures and the mechanical properties can be modified by varying the proportion of diisocyanates (hexamethylene diisocyanate, HDI, and isophorone diisocyanate, IPDI) with stoichiometric amounts of trimethylolpropane tris(3-mercaptopropionate). The shape-memory behavior was deeply investigated under three different conditions: unconstrained, partially constrained and fully constrained. The tests were performed in single cantilever bending mode to simulate conditions more closely like to real complex mechanics of thermomechanical actuators under flexural performances. The complex recovery process in single cantilever bending mode was compared with that obtained using tensile mode. The results evidenced that the amount of recovery force in fully constrained conditions, or energy released during the recovery process in partially constrained, can be modulated by simple changing the proportion of both diisocyanates. A simple model based on Timoshenko beam theory was used for the prediction of the amount of work released. The reported results are an important guideline to design shape-memory materials based on poly(thiourethane) networks, establishing criteria for the choice of the material depending on the expected application.

Keywords:

poly(thiourethane), shape-memory, thermosets, latency, actuator, single cantilever.

1. Introduction

Shape-memory polymers (SMPs) are a promising class of smart materials that are capable to adopt a temporary shape, recovering their original shape upon the application of an external stimulus [1,2]. This effect usually consists in a thermomechanical process, during which the material is heated up to a temperature close to or higher than a structural transition temperature of the network (T_{trans}) and it is deformed to this temporary shape by applying an external stress. The T_{trans} of a SMP usually coincides with the polymer's glass transition temperature (T_g) or melting temperature (T_m). T_{trans} is an important parameter in SMP design, and it can be modified by changing the network structure of the polymer. This temporary shape can be fixed by cooling down the polymer below its T_{trans}. Thus, the work carried out on the sample to change the macromolecular conformation is accompanied by a change in entropy, leaving the material in a high-energy state. After that, the original shape can be recovered by subsequently heating above T_{trans}, and the strain energy stored during the process can be released [3-5].

Consequently, SMPs are capable of displacing loads during the recovery process, releasing their accumulated energy, behaving like a smart actuator [6-8]. These outstanding properties have attracted a great interest in the last decades, and their use in a wide range of applications such as biomedicine [9,10], aerospace [11], textile engineering [12] and many others [13] have been studied.

Among SMPs, thermoset-based SMPs are increasingly studied for their easy processing, durability, and superior thermal and mechanical performance in comparison to common shape-memory elastomers or thermoplastic-based SMPs [14,15]. In particular, high-performance shape memory thermosets (HPSMTs) are particularly interesting for industrial applications, since they can perform mechanical work against external loads [16,17]. Our research group has contributed significantly to this field studying and characterizing several HPSMTs based on epoxy resins [18-21].

Polyurethanes (PUs) are one of the most widely studied class of shape memory polymers, thanks to their structural versatility, easy processing, low cost and high number of monomers available on the market [22,23]. Poly(thiourethane)s (PTUs) are related to their oxygen counterparts, showing comparative properties due to the presence of similar hydrogen bonding, but they did not receive the same interests from the scientific community. The formation of PTUs by nucleophilic addition of thiol to an isocyanate in presence of a base catalyst, leads to a very fast and efficient click reaction with high conversion and without the presence of unexpected groups [24]. Moreover, high refractive index and excellent mechanical properties make poly(thiourethane)s interesting candidates for many advanced applications as optical devices, lenses, advanced coatings and medical technology [25-28]. Despite these

excellent features, the possibility of using PTUs as shape memory polymers is relatively unexplored. Only few articles on comprehensive studies of the shape memory of PTUs have been published in the last decades [29-31], and their use as thermomechanical actuators is still unexplored. Our research group have already tested qualitatively the potentiality of these materials as shape memory polymers, preparing thermosets with different advanced characteristics. We prepared a family of thiol-isocyanate-epoxy materials obtained via sequential dual-curing methodology [32] and PTU covalent adaptable networks that present shape-memory characteristics combined with the possibility to modify their permanent shape [33].

Bowman and co-workers developed SMPs using the thiol-isocyanate reaction in conjunction with methacrylate homopolymerization [29] and thiol-Michael addition to form networks via two-stage polymerization [30]. Nguyen *et al.* synthetized urethane-thiourethane networks with shape memory properties and self-healing ability via Diels-Alder chemistry [31]. Despite these excellent papers on the subject, all these systems involved complex chemistry and multiple preparation steps, limiting their possible large-scale applications at industrial level. Herein, we report a new type of shape memory poly(thiourethane) networks, obtained from commercially available monomers making their preparation feasible on industrial scale.

We have synthetized a family of novel thermosets based on thiol-isocyanate “click” chemistry, in presence of a Lewis base, evaluating their performance as thermomechanical actuators. A thermal latent base (1-methylimidazolium tetraphenylborate) which release 1MI at temperatures higher than 100 °C, previously developed by our group, has been selected as the catalyst [34,35]. The use of such latent base represents an interesting opportunity to reach a temporal control of the reaction, offering the possibility to prepare the PTU thermosets in a controlled way; since the use of bases such as amines leads to a too quick thiol-isocyanate reaction, as already demonstrated in our previous paper [34]. To study the change of the material properties according to the structural characteristics of the network, PTU thermosets were prepared by varying the proportion of the flexible hexamethylene diisocyanate (HDI) and the more rigid isophorone diisocyanate (IPDI) with stoichiometric amounts of trimethylolpropane tris(3-mercaptopropionate) (S3). First, the effect of changing the diisocyanate monomer ratio on the curing schedule of the latent system was evaluated by rheological measurements. After that, a detailed thermal and mechanical characterization was performed using thermogravimetric analysis (TGA) and dynamic mechanical analysis (DMA) to have a better understanding of the relationship between network structure and thermomechanical properties. Then, to evaluate their ability to generate work during the recovery process and, in consequence, evaluate their performance as SM actuators, the shape-memory behavior of the PTU thermosets was investigated under three different conditions:

unconstrained, partially-constrained and fully constrained. Since shape-memory actuators are commonly used as smart mechanisms for autonomous control in industrial applications, and the real operational conditions usually involve flexural instead of tension or compression actuation designs. The testing mode chosen for this study was the single cantilever mode, thus simulating an open-valve mechanism. The reported results will provide an important guideline to design shape-memory materials based on poly(thiourethane) networks, establishing criteria for choice of the material structure depending on the expected application.

2. Experimental Methods

2.1. Materials

Trimethylolpropane tris(3-mercaptopropionate) (S3), hexamethylene diisocyanate (HDI), isophorone diisocyanate (IPDI), 1-methylimidazole (1MI) and sodium tetraphenylborate ($NaBPh_4$) from Sigma-Aldrich (Saint Louis, MO, USA) were used as received. The base generator, 1-methylimidazolium tetraphenylborate (BG1MI) was synthesized according to a reported methodology [35, 36]. 10 mmol of 1MI were solubilized in 2.6 mL of H_2O slightly acidified with 1 mL of conc., 36% HCl solution. 11 mmol of $NaBPh_4$ were solubilized in water and stirred until complete homogenization. The two aqueous solutions were mixed, and a white salt was formed as a precipitate. The salt was filtered, washed thoroughly with distilled water and MeOH, then recrystallized from a 4:1 mixture of MeOH and $CHCl_3$, filtered and dried. The purity of the synthesized compound was assessed via differential scanning calorimetry (DSC) thermal scan and its melting point was found to be similar to the reported by other equivalent salts in the literature [37-38].

The chemical structures of the reactants used in the preparation of the materials are shown in Scheme V-1.

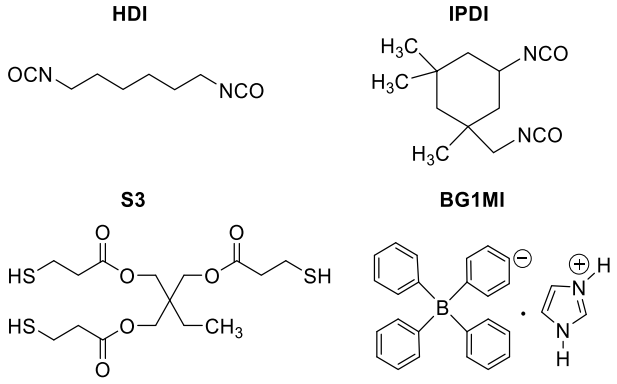

Scheme V-1. *Schematic representation of the chemical substances used.*

2.2. Sample preparation

The composition of the formulations with different proportions of (HDI /IPDI) with stoichiometric amount of S3 are detailed in Table V-1. 0.1 % wt of latent catalyst BG1MI was added to the corresponding amount of S3. The catalyst was dissolved in S3 at 80 °C until a homogeneous mixture was obtained. The mixture was poured onto aluminium moulds and cured 2 h at 100 °C and 1 h at 125 °C with a post-curing of 2 h at 150 °C.

***Table V-1**. Composition of the formulations prepared by changing the HDI/IPDI proportion in molar and weight percentages. The thiol (S3) is added in stoichiometric proportions and the latent base in 0.1 phr in reference to the thiol amount.*

Sample	Mole ratio (HDI/IPDI) (%)	Weight ratio (S3/HDI/IPDI) (%)
HDI	100:0	61:39:0
80HDI_20IPDI	80:20	60:30:10
60HDI_40IPDI	60:40	58:22:20
40HDI_60IPDI	40:60	57:14:29
20HDI_80IPDI	20:80	56:7:37
IPDI	0:100	54:0:46

2.3. Characterization techniques

2.3.1. Rheological characterization

The evolution of the curing process was monitored through rheometric measurements using a TA Instruments AR G2 (New Castle, USA) rheometer equipped with electrical heated plates (EHP) in a parallel plate geometry (25-mm diameter disposable aluminium plates). To confirm the latent character of the formulations and determine the effect of the different proportions of both isocyanates on the curing, dynamo-mechanical experiments were performed at 100 °C to determine the time needed for the different formulations to reach the gel point. The rheometer oven was pre-heated at 100 °C and, once the temperature was equilibrated, the formulation was quickly placed between the parallel plates and the distance between the plates was settled at 1 mm. Complex viscosity (η) and viscoelastic properties were recorded as function of time at three different frequencies: 1, 3 and 10 Hz. The experiments were conducted in the range of linear viscoelasticity obtained from constant shear elastic modulus (G') in a strain sweep experiment at 1 Hz. Gel points were determined as the point where the viscosity diverges towards infinite.

2.3.2. Thermal characterization

The thermal stability of the samples was evaluated by thermogravimetric analysis (TGA), using a Mettler Toledo TGA2 thermobalance. Pieces of cured samples of 10-15 mg were degraded between 30 and 600 °C at 10 °C/min under inert atmosphere (N_2 at 50 mL/min).

2.3.3. Thermo-mechanical characterization

A DMA Q800 (TA Instruments New Castle, USA) equipped with a 3-point-bending clamp (with a span of 15 mm) was used for the analysis of the thermo-mechanical properties of the materials. The experiments were performed at a heating rate of 3 °C/min, from 30 to 160 °C, at 1 Hz and 0.1% of strain. Prismatic rectangular samples were thoroughly polished until uniform dimensions of about 30×5×1.5 mm^3 were obtained. The glass transition temperature T_g was determined by the peak of the tan δ curve. The full width at half maximum (FWHM) was also determined as this parameter helps to quantify the homogeneity of the network structure. The values of storage modulus, *E',* below and above glass transition were evaluated. The $T_g^{E'}$ was calculated as the peak of the loss modulus. A peak in the deformability is obtained at this temperature coinciding with the onset of the mechanical relaxation and this temperature, as explained later, is relevant in shape memory characterization.

2.3.4. Mechanical characterization

The flexural modulus (*E*) of the materials was determined at $T_g^{E'}$ in three-point bending mode on rectangular samples (30 x 5 x 1.5 mm^3) using the DMA Q800. A force ramp with a constant rate of 1 N/min was imposed ensuring that only the viscoelastic behaviour of the material was evaluated. Three samples of each material were analysed and the results were averaged.

2.3.5. Shape memory characterization

To characterize the shape-memory behaviour of the PTU thermosets as bending-type thermo-mechanical actuators, the DMA Q800 single cantilever clamp was selected. DMA Q800 has the advantage in terms of accuracy of the applied load and displacement measurements in comparison with standard testing machines, when specimens with small cross sections are tested. Single cantilever mode consists of anchoring the sample on one end by the stationary clamp and attaching to a moveable clamp on the other. Through this moveable clamp, the apparatus applies a controlled force while the displacement is simultaneously recorded. It is important to emphasize that the span (L=17.5 mm) between these two anchoring points may vary, since the moveable clamp can present a minor lateral movement and so, it should be measured prior to each test. Moreover, the clamping ends introduce shear deformation in the sample that should be taken into account when computing the relation between force and displacement. The basic characteristics of this mode as well as the equivalent

mechanical model (cantilever beam with end force) are represented in Fig. V-1(a-b). In Figure V-1(c-d) some pictures of the real disposition of the sample (undeformed and deformed) in the clamp are also presented.

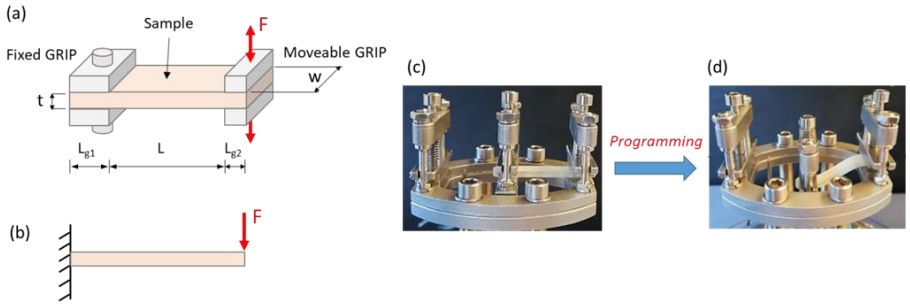

Figure V-1. *Single cantilever DMA operational mode (a) schematic representation and basic parameters; (b) mechanical model. Arrangement of the sample with its original (c) and programmed (d) shape.*

In this bending mode, the relation between the force (*F*) applied and the displacement measured in the moveable clamp (*d*) can be modelled as a first approximation using Timoshenko beam theory and correcting it by including a factor for 3D clamping effects. Consider a static linear elastic beam clamped at one end and with a point force applied at the other end where the cross-section remains parallel to the force (this last condition represents the movable clamp where the force is measured). Although in Figure 1(d) it can be appreciated that this is not a typical cantilever beam (where one of the ends is free), as a first approximation it can be referred as such. Using Timoshenko beam theory, the vertical displacement can be determined using the zero-angle boundary conditions at both ends and a zero-displacement in the clamped end. The resulting maximum displacement (*d*) takes the value:

$$d = \frac{F \cdot L^3}{12 \cdot E \cdot I \cdot \alpha_c}\left(1 + \frac{2}{\kappa}(1+\upsilon)\left(\frac{t}{L}\right)^2\right) \quad (1)$$

$$\alpha_c = 0.7616 - 0.02713 \cdot \sqrt{\frac{L}{t}} + 0.1083 \cdot \ln\left(\frac{L}{t}\right) \quad (2)$$

Where *d* is the maximum vertical displacement of the beam (in the tip), *F* is the force applied an *L* is the free length between the clamped end and where the force is applied (*i.e.* the distance between the clamps themselves, not the distance between the midpoints of the clamps). *E* is the flexural modulus of the linear elastic material; υ is its Poisson's ratio; *t* is the thickness of the cross-sectional area; $I = w \cdot t^3/12$ is the second moment of area of the rectangular cross-section and κ is the Timoshenko's shear coefficient (5/6 for a rectangular cross-section). The clamping correcting factor introduced by DMAQ800 to consider the deformation of the sample within the clamped region is α_c and is given by the manufacturer.

Prismatic rectangular samples of 5 mm in width (*w*) and 1.5 mm in thickness (*t*) have been tested in three different conditions: unconstrained, partially-constrained and fully-constrained. In all cases, there is a programming of the sample prior to the recovery process. Depending on the experiment performed in the recovery process, different DMA Q800 customized operation methods were used. The sample mounting and the recovery analysis are depicted in Figure V-2.

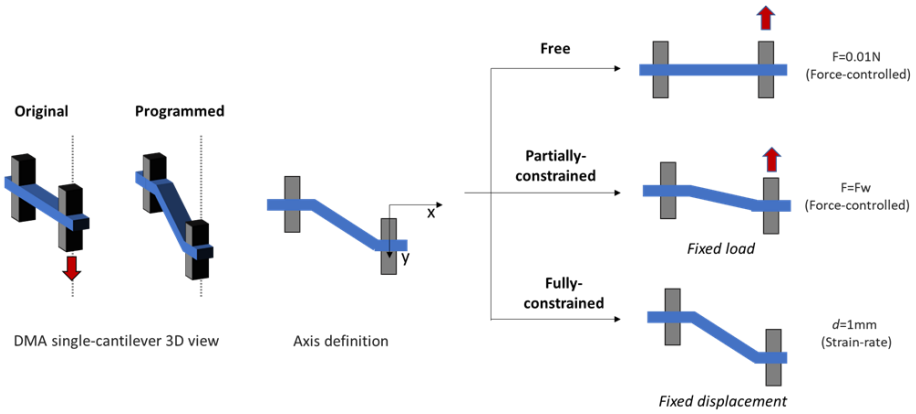

Figure V-2. *Illustration of the DMA testing depending on the experiment conditions.*

The temporary shape was fixed using a force-controlled mode, following the thermomechanical procedure called programming, this procedure consists of different steps. First, the specimen was heated up to the programming temperature (T_{prog}) and deformed until reaching an imposed displacement d_{max}. The T_{prog} chosen was $T_g^{E'}$, as it is demonstrated that it is the best programming condition to store the maximum amount of entropic energy [8,17]. When d_{max} was reached, the sample was rapidly cooled down to room temperature (well below its T_g) to fix the temporary shape. After that, depending on the shape memory test, the experiments were carried out under different conditions.

For comparison purposes, the same d_{max} must be imposed at $T_g^{E'}$ to all the samples and this value must be compatible with the physical limits of the DMA. Thus, d_{max} was chosen to be equal to 14 mm. The theoretical force F, able to produce this d_{max}, was also calculated using Equation (1) with the flexural modulus measured at $T_g^{E'}$ and compared to the experimental force needed for this displacement in order to validate the assumed Timoshenko beam theory.

For the unconstrained procedure, after the programing step, the DMA was set in force-controlled mode, the applied force was released and only a minimal force of 0.01 N was imposed to register the recovery process. The sample was heated at 3 °C/min to a temperature above T_g while recording the displacement of the movable clamp $d_y(T)$, thus measuring the shape-memory recovery process (SR) determined by the following equation:

$$SR(T) = \frac{d_{max} - d_y(T)}{d_{max}} \quad (3)$$

where d_{max} is the programmed displacement and $d_y(T)$ is the displacement reached by the movable clamp during the recovering process. The recovery process ended with a displacement $d_y(T_{end})$ which represents the amount of deformation that the sample is not able to recover. These curves were normalized for comparison purposes (0 means no recovery and 1 means completely recovered).

To analyse the effect of the different formulations on the shape-recovery process the shape-recovery curves $SR(T)$ were differentiated with respect to the temperature by using equation (4) thus obtaining the instantaneous shape-recovery speed $SR_{speed}(T)$ as a measure of the shape-recovery sharpness. Using the $SR_{speed}(T)$ curve, the temperature corresponding to the maximum recovery speed was determined as the peak of the curve (T_{peak}).

$$SR_{speed}(T) = \frac{dSR(T)}{dT} \quad (4)$$

The shape-recovery rate (V_r), a measure of the average shape-recovery speed, was evaluated from $SR(T_1)$ = 0.15 to $SR(T_2)$ = 0.85, that is in the range between 15% and 85% of the shape recovery process (*i.e*. avoiding the early and final stages) using equation (5):

$$V_r(\%/\text{min}) = \frac{SR_{15\%-85\%}}{\Delta t_{SR_{15\%-85\%}}} \quad (5)$$

Finally, the recovery-ratio was calculated by equation (6):

$$R_r = \left(1 - \frac{d_y(T_{end})}{d_{max}}\right) \cdot 100 \quad (6)$$

Fully-constrained experiments were performed to calculate the maximum recovery force that the PTUs were able to generate. To do that, the experiments were carried out in strain-rate mode imposing a minimum constant displacement (1.0 μm) while heating the sample at 3 °C/min. The force generated by the sample, $F_y(T)$, was measured during the recovery process, until reaching a maximum value F_{max}.

To evaluate the mechanical work generated, partially-constrained experiments were performed in force-controlled mode applying a constant force (F_w) equal to the 50% of the force generated for each sample during the fully-constrained experiments (F_{max}). Then, the sample was heated up to the recovery temperature while the displacement of the movable clamp was measured. The relative work (W_{rel}) developed by the sample was calculated using equation (7). In this expression, for comparison purposes, the final displacement reached, $d_y(T_{end})$ has been normalized with respect to the maximum displacement, d_{max} imposed during programming.

$$W_{\text{rel}} = F_w \cdot \frac{d_{max} - d_y(T_{\text{end}})}{d_{max}} \quad (7)$$

In equation (7) F_w is the constant force applied on the sample, d_{max} is the deflection after the programming process and d_y (T_{end}) is the displacement reached by the movable clamp at the end of the recovery process.

The theoretical relative work that the sample could perform can be deduced assuming that all the force produced by the sample during the shape-recovery process is equal to the force given to program the sample in the temporary-shape (F_{prog}). F_{prog} can be deduced, as explained before, from equation (1) using Timoshenko beam theory assuming d_{max}=14 mm (the maximum deflection imposed in programing) and with the flexural modulus measured at $T_g^{E'}$. Once F_{prog} is determined, the theoretical displacement that the sample could reach in the recovery process, $d_{y\text{-}theor}$ (T_{end}) can be determined again by equation (1) but considering that the force applied by the DMA, F_w, acts in opposite direction during the recovery experiment. Thus, in equation (1), F is calculated as $F = F_{prog}\text{-}F_w$. Finally, the theoretical relative work can be calculated as:

$$W_{\text{rel-theor}} = F_w \cdot \frac{d_{max} - d_{y-theor}(T_{\text{end}})}{d_{max}} \quad (8)$$

For a better comprehension of the stress-strain behaviour in single cantilever bending, the shape-memory behaviour under unconstrained conditions was also analysed using a tension-film clamp (the simplest stress-state possible in mechanics) and compared with the behaviour in bending mode. The experiments were conducted in controlled-force mode on rectangular specimens with dimensions of 20×5×0.5 mm^3. Under this tensile mode, the sample was heated up to the programming temperature and loaded at 1 N/min until a programming stress (σ_{prog}) equal to 75 % of the stress at break reached (σ_{prog}=0.75·σ_{break}). The permanent shape was recovered by heating the programmed sample at 3 °C/min to a temperature above T_g. The recovery process ended with a deformation value of ε_p, which represents the amount of deformation that the sample was not able to recover. The shape-memory recovery (SR) was determined using equation (9).

$$\text{SR}(T) = \frac{\varepsilon_{max} - \varepsilon_p}{\varepsilon_{max}} . 100 \quad (9)$$

Where ε_{max} is the deformation corresponding at the 75% of the strain at break and ε_p is the value of the deformation at the end of the recovery process.

3. Results and Discussion

Two different isocyanates were selected as starting monomers, hexamethylene diisocyanate (HDI) with a linear and flexible structure and isophorone diisocyanate (IPDI) more rigid due to the presence of a cyclohexane ring in the structure. Both were crosslinked with a trifunctional thiol (S3) in the presence of a base to obtain PTUs with different mechanical and thermal properties. Fixing the thiol at the stoichiometric proportion and the amount of catalyst in the formulation and varying only the proportion of both aliphatic diisocyanates, it can be analysed the influence of the compositional ratio on the dynamic mechanical and thermal properties of poly(thiourethane) networks.

3.1. Rheological study

As a first step of the material characterization, the rate of the network formation was analysed by means of a rheological study. During the curing process, the physical state of the formulation changes from a liquid to a sol/gel rubber and then to a glassy or solid and the rate at which this occurs depends on several factors such as: monomer structure, catalyst type, amount of catalyst, curing temperature, etc.; all of them affecting the processing conditions [39]. The gel point represents the endpoint for a formulation to flow in a mould or to be applied in an industrial process. After the gel point, it is difficult or impossible the manipulation of the mixture and therefore the time at which it occurs has a great technological relevance. With this rheological study, we aim to demonstrate the latent character of the formulation and evaluate the effect of changing the diisocyanate monomer ratio on the gel time of the system. The isothermal curing processes of the different formulations prepared were investigated in the rheometer, to obtain the polymerization time dependence on the diisocyanate proportion, determining the time gel at 100 °C. The changes in complex viscosity (η) as a function of time at 100 °C for all the formulations are shown in Figure V-3.

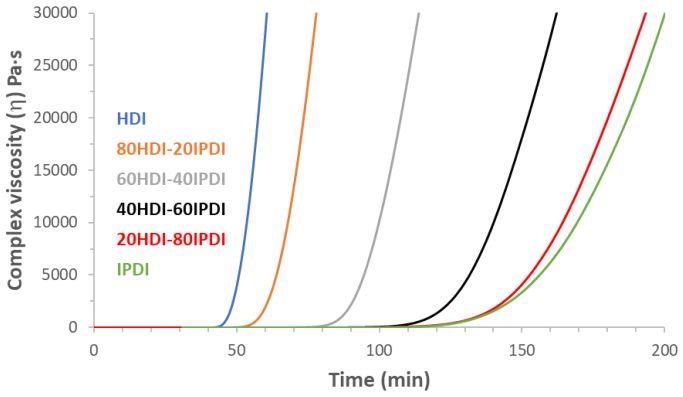

Figure V-3. *Time sweep experiment for the different formulations prepared at 100°C.*

As we can see in Figure V-3, at the beginning of the curing stage the viscosity remains constant for several time, and then, at a certain point a rapid increase in viscosity is observed, demonstrating the latent character of the formulations. The critical gel time was determined as the time in which the viscosity diverges towards infinity without reaching a steady state [40]. The gel times obtained are given in Table V-2.

Table V-2. *Rheological, thermal (TGA) and thermomechanical (DMA) data obtained for the PTU samples.*

	Rheometer	TGA	DMA					
Sample	**Gel Time [1] (min)**	**$T_{2\%}$[2] (°C)**	**$T_g^{E'}$[3] (°C)**	**$T_{g\text{-}tan\delta}$[4] (°C)**	**E'_g[5] (GPa)**	**E'_r[6] (MPa)**	**FWHM[7] (°C)**	**E'_g / E'_r**
HDI	48	276	44	57	2.3	10	8.5	164
80HDI-20IPDI	58	273	55	65	2.3	12	10	176
60HDI-40IPDI	83	269	75	85	2.8	12	11	200
40HDI-60IPDI	120	269	84	97	2.9	13	13	223
20HDI-80IPDI	133	269	97	108	3.0	14	13	214
IPDI	137	267	114	125	3.2	13	11	246

[1] Gel point determined at the time when the viscosity diverges toward infinity.
[2] Temperature of 2% of weight loss determined by TGA in N_2 at 10 °C/min
[3] Temperature of the peak of the loss modulus.
[4] Temperature of maximum of the tan δ.
[5] Glassy modulus determined at 25°C
[6] Relaxed modulus determined at the $T_{tan\,\delta}$ + 30°C (in the rubber state).
[7] Full width at half maximum of tan δ.

The gelation time depends on the stoichiometry of the formulation since the reactivity of both diisocyanates is different. The more flexible structure of HDI, with respect to IPDI, presents greater mobility which can affect the rate of the curing reaction. In the HDI both isocyanate groups are linked to a methylene carbon, but in IPDI one of the isocyanates is linked to a methine carbon in the cyclohexane ring, which can experiment steric hindrance to the attack to the thiol groups, reducing in this way its reactivity. According to these factors, the time to reach the gelation increases with the proportion of IPDI in the reactive mixture.

3.2 Thermal degradation study

A thermal degradation study was performed to ensure that all the samples are fully stable in the temperature range used in the shape memory process. The thermal stability of the PTUs was analysed by TGA and the derivative curves of the TGA degradation are shown in Fig. V-4, where the overlapped curves are shifted for a better understanding. The initial degradation temperature ($T_{2\%}$) extracted from these experiments are collected in Table V-2. All of them present a high thermal stability, with a $T_{2\%}$ around 270 °C for all samples, with a slight decrease on increasing IPDI

content in the samples. Figure V-4 shows that there are barely differences in the degradation evolution for all the materials evaluated.

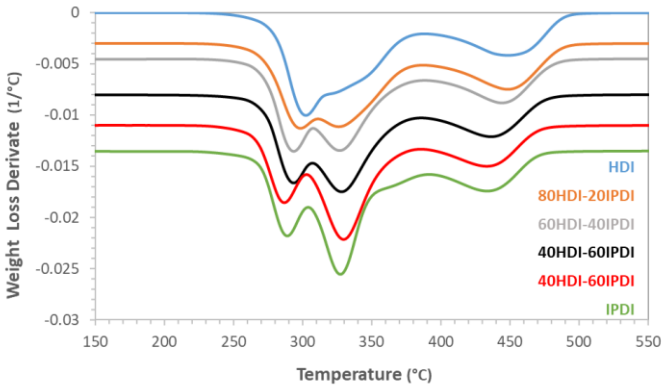

***Figure V-4**. DTG curves of the poly(thiourethane)s prepared (the curves are shifted for a better understanding).*

As we can see in Fig. V-4, the degradation mechanism is quite complex, presenting three different stages. The first degradation step is attributed to the carbonyl sulphide elimination, as already demonstrated by Rogulska *et al* [41] and by our group, with a maximum placed around 300 °C [35]. This first peak is shifted to higher temperature when increasing the amount of HDI. The second step is associated with the decomposition of the ester bond of the thiol structural units. First and second peaks of degradation are more overlapped on increasing the proportion of HDI in the formulation. The third degradation peak corresponds to the fully degradation of the network. From the degradation study, we can state that all these materials are fully stable up to temperatures around 250 °C and, consequently, in the entire working temperature range in the shape memory behaviour.

3.3 Thermomechanical analysis

To determine the effect of changing the proportion of both aliphatic diisocyanates on the network homogeneity and on the glass transition temperature, dynamic thermomechanical analyses of PTUs were performed. The resultant plots are shown in Figure V-5 and the main data extracted from thermomechanical tests are summarized in Table V-2.

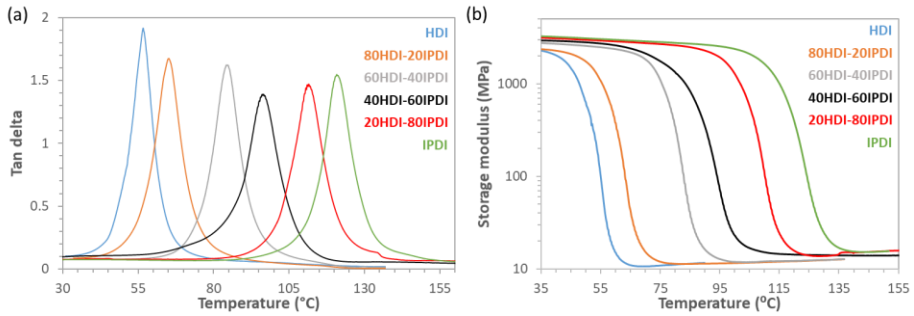

***Figure V-5**. (a) Evolution of tan δ and (b) storage modulus with temperature of the different poly(thiourethane) samples.*

As shown in Table V-2, the glass transition temperatures and the storage moduli at glassy state can be tailored by varying the proportion of both isocyanates in the samples. As the content of IPDI increases, due to its high rigidity, higher values of T_g and E'_g are obtained. By mixing both diisocyanates, we obtained a wide range of glass transition temperatures between 57 °C and 125 °C, referred to the tan delta peak. The storage modulus at 30 °C significantly increases as the IPDI content increases, from 2.3 to 3.2 GPa, moving from the more flexible structure to the rigid one.

All these thermomechanical changes were obtained without affecting the homogeneity of the sample as shown by the very narrow *tan δ* curves in Figure V-5. The slight decrease of the height of *tan δ* curve for samples prepared with higher content of IPDI is indicative of a more densely crosslinked network with more restricted mobility. The high homogeneity of the samples is derived from the click character of the thiol-isocyanate reaction catalysed by a base, and it is demonstrated by the low values of the width of the curve at half height (FWHM) in the range between 8.5 °C and 13 °C. To achieve good fixation and fast recovery, a high homogeneity of the material is crucial for shape-memory applications, because the narrower the transition, the faster the recovery process.

In terms of shape-memory properties, the E'_g/E'_r ratio is higher than 100 in all cases. This means two orders of magnitude, which is high enough to expect good shape-memory properties in terms of shape-fixation and shape-recovery. This parameter increases as the proportion of IPDI increases. In all the materials the value of the rubbery modulus E'_r is similar regardless of the structural differences, therefore the E'_g/E'_r ratio is mainly governed by E'_g.

In light of these considerations, we can state that the main thermomechanical properties such as T_g, $T_g^{E'}$ or storage moduli E'_g of the PTUs can be easily tuned by changing the structure and composition of the isocyanate monomer. These changes were achieved by maintaining the uniformity of the network associated with thiol-isocyanate polymeric materials. Therefore, we can obtain different materials with a

wide range of thermomechanical properties that meet the requirements in terms of E'_g/E'_r, and that can present exciting characteristics for shape-memory applications.

3.4 Shape-memory results

3.4.1 Unconstrained recovery

The shape-memory properties, as explained in the experimental part, were analysed in three different conditions. First of all, the unconstrained recovery experiments were carried out to evaluate the shape-memory effect of the different PTUs prepared. This shape memory characterization consists of two steps: programming of temporary shape and recovery of the original shape without any constraints. The maximum displacement, d_{max}, imposed in programming was set to 14 mm and, consequently, for comparison purposes, the dimensions (thickness and width) in all the samples were the same. The theoretical force *F* generated during programming was computed with equation (1), with the bending stiffness measured at $T_g^{E'}$ for each sample, and this force was compared to the experimental one. In Figure V-6 this comparison, together with the bending stiffness at $T_g^{E'}$ is presented. As it can be observed in Figure V-6(a), in all the samples, the predicted forces are higher than the experimental ones. This is because the theoretical model predicts a linear behaviour, in which *F* and d_{max} are proportional while, but the stress-strain behaviour at $T_g^{E'}$ is viscoelastic and only linear and proportional during the initial part. Nevertheless, the assumption of the Timoshenko beam model can be used as an upper boundary limit for a simple initial prediction. It is worth noting that for the 20HDI-80IPDI and IPDI, due to the high rigidity of the samples, the predicted forces were higher than the limits of the DMA (18 N). To avoid this problem, in these two samples, the thickness was reduced to 1.3 mm instead of 1.5 mm. That is the reason why the forces in 40HDI-60IPDI, 20HDI-80IPDI and IPDI are very similar. To avoid these small differences in dimensions, the stress corresponding to this force was calculated using bending stress-strain relations and represented in Figure V-6(b). This relation can be only used for comparison purposes because, as it will be demonstrated later, the stress-state along the sample is much more complex.

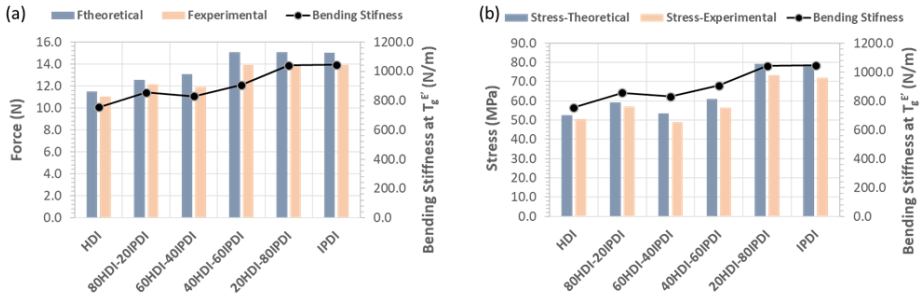

Figure V-6. *Theoretical and experimental forces (a) and stresses (b) in the programming process. Bending stiffness obtained for each sample is also indicated.*

The free-recovery processes for all the samples are shown in Figure V-7, in which the shape-recovery (*SR*) and the recovery speed (SR_{speed}) are plotted as function of the temperature. The main parameters obtained from these tests are presented in Table V-3. It is important to notice that all the samples were able to recover the original shape, with shape-recovery ratios, R_r, close to 100%. The value of R_r slightly decreases as the IPDI content increases, obtaining the lowest R_r with the material completely based on IPDI. This is probably due to a stress hardening process taking place during the loading process that generates permanent deformation in the network structure after programming the temporary shape [15].

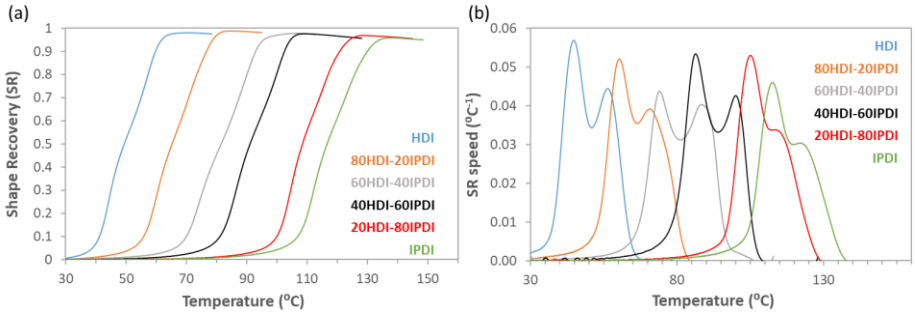

Figure V-7. *(a) Shape-memory unconstrained recovery experiment, shape-recovery (SR) against temperature. (b) Derivative of the shape-recovery with respect to temperature (SR_{speed}) as function of temperature.*

Table V-3. *Parameters obtained from the shape-memory tests (unconstrained, fully-constrained and partially-constrained experiments) of the different materials: Recovery-rate (R_r), shape-recovery speed (V_r), peak temperature of the derivate of the shape recovery (T_{peak}), shape-recovery force (F_{max}), relative work (W_{rel}).*

	Unconstrained				Fully-constrained		Partially-constrained
Sample	R_r (%)	V_r (%/min)	$T_{I\text{-}peak}$ (°C)	$T_{II\text{-}peak}$ (°C)	F_{max} (N)	T_{peak} (°C)	W_{rel} mN/(mm/mm)
HDI	98.0	13.5	44.8	57.0	7.4	42.8	501.5
80HDI-20IPDI	98.0	12.4	60.3	70.8	8.5	58.6	542.7
60HDI-40IPDI	97.5	11.1	74.0	88.2	9.3	72.4	560.5
40HDI-60IPDI	97.6	12.3	86.3	99.9	9.1	84.8	585.9
20HDI-80IPDI	96.8	11.9	105.0	111.2	7.6	102.0	503.1
IPDI	95.9	11.8	112.6	122.0	8.5	111.8	660.9

The shape-recovery speed curves (SR_{speed}) presented in Figure V-7(b) show that the materials prepared with high content of HDI are slightly faster than the materials based on IPDI. The values of recovery rate (V_r), presented in Table V-3, increase from 11.8 %/min for IPDI to 13.5 %/min in HDI sample. As expected, the increase of the content of IPDI in the formulation produces a decrease in V_r due to the lower mobility of the network structure and the slightly higher heterogeneity also highlighted by the FWHM parameter.

The curves of the derivative of the shape-recovery shown in Figure V-7(b) present a different shape respect to the one usually observed when testing in tensile mode. These curves present two peaks ($T_{I\text{-}peak}$ and $T_{II\text{-}peak}$ in Table V-3) reflecting the temperatures where the recovery process is maximum. These temperatures are strictly related to the glass transition temperature of the material and are located close to the values of $T_g^{E'}$ and $T_{g\text{-}tan\,\delta}$ (see Table V-2). The fact that these curves present two maximum peaks instead only one like in tensile mode, is probably related to the complex stress state suffered by the samples in single cantilever bending mode. This is also evident in Figure V-7(a) where the curves present a slight shoulder in the middle of the recovery process. During the programming process in this stress-state mode, unlike in tension mode, the stress distribution is not uniform along the beam, being the maximum programming bending stress located near the fixed and moveable clamp while the minimum stress is located in the centre of the beam. To evidence this stress concentration effect, the mechanical behaviour of the sample 60HDI-40IPDI programmed at $T_g^{E'}$ was modelled using the classical beam theory in Finite Element Analysis using Ansys® Academic Research Mechanical, Release 2019R2. It is important

to mention that the moveable clamp measures L_{g2} = 6.35 mm, while the fixed clamp measures L_{g1} = 7.625 mm and the load applied in the deformation process is distributed along L_{g1}, as observed in Figure V-1(a). Therefore, these lengths should be taken into account when modelling the imposed displacement in the moveable clamp and the fixed support in the Finite Element Modelling simulation. The programmed sample (directional displacement of 14 mm) is shown in Figure V-8(a). In Figure V-8(b) the resultant stress state due to the programming (Von Mises stress) is shown, where the maximum stress locations are pointed out. Note that the stress obtained by the simulation is slightly higher than the theoretical one, as plotted in Figure V-6(b), because of the differences in the way the displacement is applied, the constrains and second-order effects.

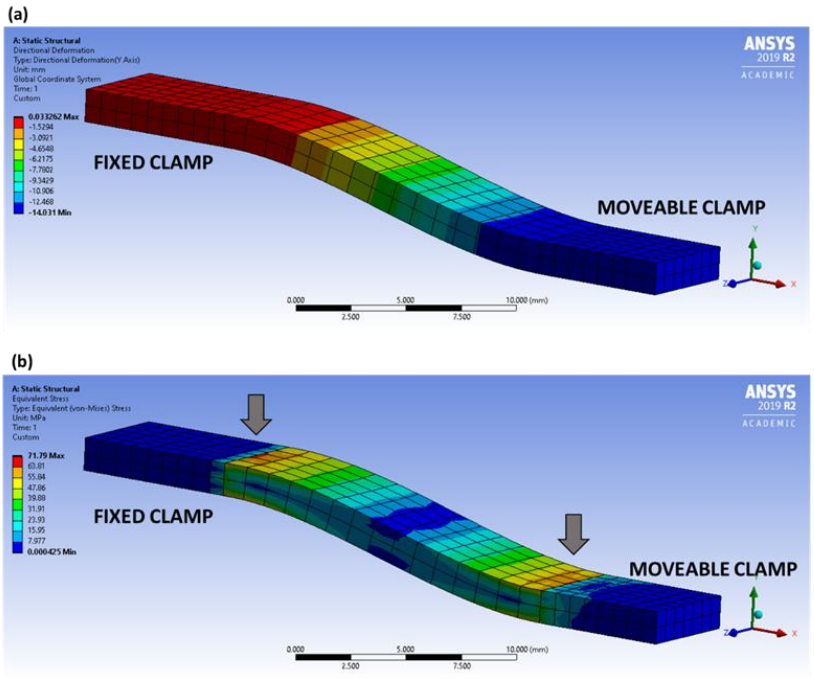

Figure V-8. *Finite Element Modelling of the programmed sample 60HDI-40IPDI (d_{max}=14 mm) in single cantilever mode using classical beam theory. (a) Deformed beam after programming and (b) Von Mises stress distribution where the points of maximum stress are indicated with arrows.*

To demonstrate that the shape of the SR curves (Figure V-7) in the free recovery process is related to the complex stress-state to which the sample is subjected in single cantilever mode and not to the network structure of the material; the shape memory effect was also evaluated in tension mode, using film-tension clamp, and compared with the results previously obtained.

For this comparison, we selected the material with 60% of HDI and 40% of IPDI to have at the same time the presence of both isocyanates. The comparison of the two recovery processes can be observed in Figure V-9.

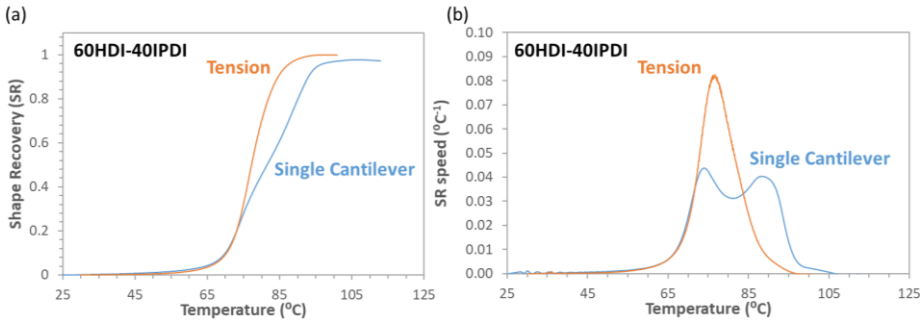

Figure V-9. Shape-memory unconstrained recovery experiment with tensile and single cantilever clamp for the material prepared with S3-60HDI-40IPDI: (a) Shape Recovery *vs.* temperature and (b) (SR_{speed}) *vs.* temperature.

As can be seen in Figure V-9, the recovery process in tensile mode is uniform with a progressive evolution, clearly visible in the derivative of the shape recovery, that presents only one peak at 77 °C. This SR process is faster in tensile (V_r = 19.1%/min) compared to single cantilever-bending mode (V_r = 11.1%/min), due to the simplicity in the stress and strain state along the sample in the first mode. Nevertheless, the mechanics of a complex SMP actuator look like a cantilever mode rather than a tensile mode (for example, in functional mechanisms like flexural jointed mechanisms and other robotic systems, especially in the micro-domain). These results put in evidence that the use of the single cantilever clamp affects the shape recovery process, producing two different recovery phenomena as evidenced from the derivative of SR, even if in both cases the materials were able to recover their original shape.

3.4.2 Fully-constrained recovery tests

To determine the maximum forces generated by the SMPs under a completely impeded scenario, fully-constrained experiments were carried out. The curves of the force generated, and the force rate calculated against temperature, *dF/dT*, are presented in Figure V-10. The parameters obtained are summarized in Table V-3.

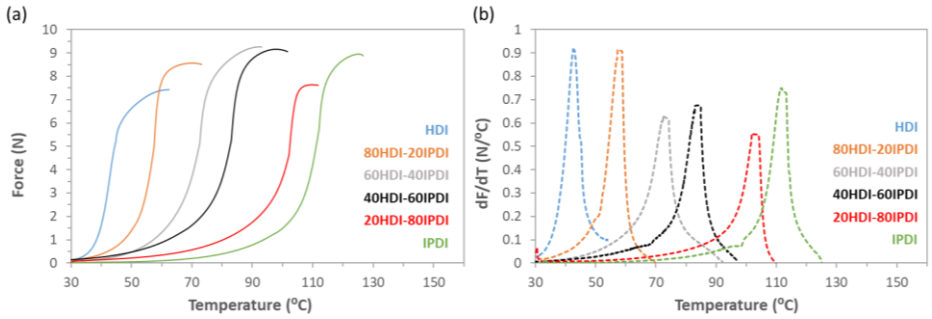

Figure V-10. *(a) Force generated with increasing temperature in fully-constrained recovery experiments; (b) derivative of the force generated with respect to the temperature (dF/dT), as function of temperature.*

The force generated is strictly related to the network structure, more densely crosslinked networks usually produce higher driving forces being the crosslinking density the most important factor in the generation of the recovery force. Since the crosslinking density is related to the value of the modulus in rubbery state, materials with a higher value of relaxed modulus, usually, are able to generate higher recovery forces [18], if no hardening effects are present. In our case, as the relaxed moduli (Table V-2) are very similar for all the PTUs prepared, the forces generated are expected to be similar for all the materials. As it can be observed in Figure V-10(a), during the recovery process the forces progressively increase with temperature until reaching a maximum value. These maximum forces produced are relatively high and similar for all the materials, reaching values between 7.4 N and 9.3 N. For materials with lower content of IPDI, as E'_r is slightly lower, the forces generated are also slightly lower (7.4 N and 8.5 N). As the IPDI content increases, F_{max} increases (around a maximum of 9.3 N for sample 40HDI-60IPDI). For samples with the highest content of IPDI, although with a similar E'_r to 40HDI-60IPDI, F_{max} is limited, probably due to a strain hardening process that may cause small irreversible plastic deformation in the network structure.

In a similar way to the SR_{speed}, the force rate, dF_y/dT in (N/°C), is plotted in Figure V-10(b). Paying attention to the peak of these curves, it is clear that the T_{peak} is strictly related to the glass transition temperature of the materials, since the maximum rate of force generated is located close to the $T_g^{E'}$, according to the unconstrained experiments.

The force applied for programming the samples were also compared with the force generated in fully constrained conditions. In Figure V-11, these values for each sample in terms of force (Figure V-11(a)) and stress (Figure V-11(b)) are presented. The stress generated by the PTUs were calculated using bending stress-strain relations with the purpose of eliminating the influence of sample dimensions. In terms of efficiency, all the samples except those with higher proportion of IPDI "lost" around 25-30% of the

stress. Samples 20HDI-80IPDI and IPDI lost around 53% probably due to the hardening process and plastic deformation that took place during the loading process as already mentioned. The values of stress must be considered only for comparison purposes (to obtain values independent of dimensions) because, as it has been already said, the stress-state is much more complex.

These results are considerable higher than the ones reported by Belmonte *et al.* [21] using thiol-epoxy shape-memory actuators under 3-point bending conditions. Although the values of E_r' in [21] are considerable higher than PTUs values of E_r', the force generated by the PTUs are higher than the values reported by Belmonte *et al.* which were not greater than 3 N (or 6 MPa in terms of stress to obtain values independent of dimensions).

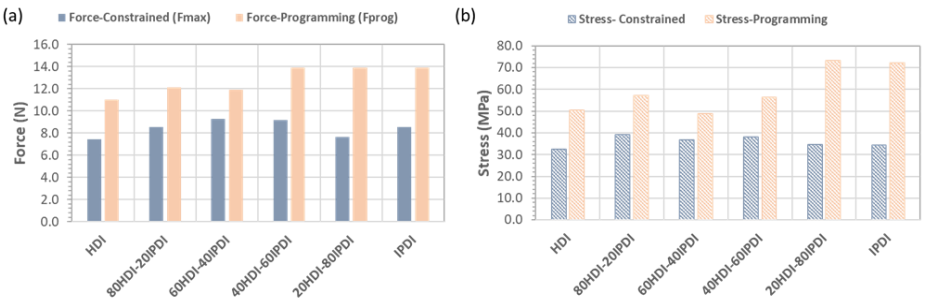

Figure V-11. *(a) Maximum force generated in fully-constrained recovery experiments (F_{max}) compared to the maximum force needed in programming (F_{prog}); (b) for comparison purposes these forces have been made independent from dimensional parameters thus calculating the corresponding stresses.*

3.4.3 Partially-constrained recovery tests

Partially-constrained experiments were performed to fully characterize the PTU thermosets as actuators, because the primary use of a polymer actuator is to recover its shape by working against a force, thus developing work.

In this test, a constant force, F_w, was imposed at the moveable clamp and the work generated during the recovery-process was calculated using equation (8). To avoid the break of the sample, the force applied was calculated as the 50% of the maximum force generated during the fully-constrained experiments (*i.e.* $F_w = 0.5*F_{max}$). It is important to notice that all the samples were able to produce positive work in the shape recovering process, even if the force applied on the samples was greater than 3.5 N. The values obtained from the partially-constrained experiments are presented in Figure V-12(a). For a better comparison, the stress corresponding to F_w and the strains corresponding to the displacements can be simply computed with bending stress-strain relations. Thus, the work developed during the constrained recovery can be calculated per unit volume (kJ/m^3) as:

$$W_{\mathrm{rel}}(kJ/m^3) = \sigma_w \cdot (\varepsilon_{dmax} - \varepsilon_{dy(Tend)}) \quad (10)$$

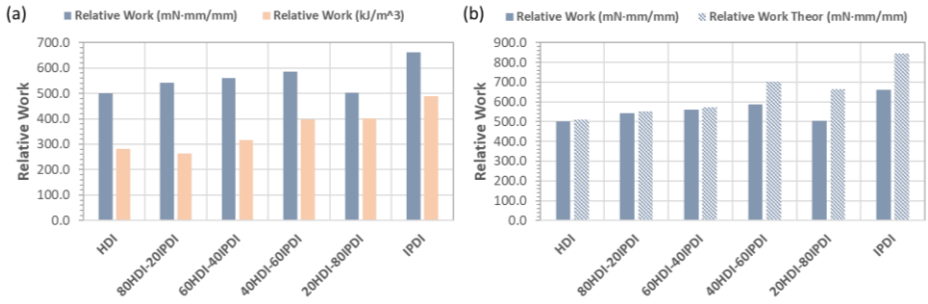

Figure V-12. *(a) Experimental relative work output for all the PTUs prepared; (b) comparison between experimental and theoretical relative work generated.*

The amount of work generated presents comparable values for all the materials prepared. Among them, the material with 100% IPDI was able to generate the best result in terms of work, reaching a maximum value of around 660 mN*m/m (around 490 kJ/m^3) due to its higher rigidity. The thermomechanical parameter that governs the work developed is E'_g/E'_r. Although in the IPDI sample, the applied F_w is comparatively lower with respect to other PTU samples (due to its relative lower F_{max}) the work generated is the highest due to the highest E'_g/E'_r ratio. The values obtained with the poly(thiourethane) thermosets are considerably higher than the values reported by Belmonte *et al.* [21] with dual cured thiol-epoxy polymers, who obtained a maximum value of 314 mN*mm/mm in 3-point bending conditions.

As explained in the experimental part, the maximum theoretical work, that the materials are able to generate, can be estimated assuming that the sample produces a force during the recovery process equal to F_{prog}; i.e. there are no energy losses during programming and therefore, all programmed force is released later during the recovery-process. In Figure V-12(b) the comparison between the experimental and theoretical work is presented. It can be observed that the Timoshenko beam theory predicts an upper maximum limit that fits quite well with the work developed by the samples, given the best adjustment for samples with lower proportion of IPDI. As it was explained in free-recovery experiments, the predicted F_{prog} is higher than the experimental ones because the model assumes a linear and proportional behaviour, without any strain hardening effect that probably takes place in samples with higher proportion of IPDI and that reduces the recovery process.

These results indicate that all the poly(thiourethane) thermosets synthetized exhibit good performance during the partially-constrained experiments in single cantilever mode. In this way, the possibility of obtaining actuators with different activation temperatures by varying the T_g has been demonstrated by only changing the

diisocyanate structure, so that they better match with potential future applications without influencing their ability to perform a work.

4. Conclusions

In this work, we developed a new family of shape-memory actuators based on poly(thiourethane) networks using two different aliphatic isocyanates, isophorone diisocyanate (IPDI) and hexamethylene diisocyanate (HDI) and a trifunctional thiol (S3) acting as the crosslinker. The curing of thiol-isocyanate formulations was influenced by the proportion and structure of the diisocyanate monomers. The use of 1-methylimidazolium tetraphenylborate (BG1MI), as a latent base catalyst, allowed a control of the reaction using both aliphatic diisocyanates. The materials showed high homogeneity within a broad range of glass transition temperatures between 50 and 120 °C. The T_g values increased on increasing the content of the rigid IPDI monomer.

The SMP behaviour of the poly(thiourethane)s were fully characterized as potential actuators in single cantilever bending mode to reproduce real mechanics of complex SMP actuators as in functional mechanisms. Three different scenarios were tested: unconstrained, partially constrained and fully constrained. Free-recovery experiments showed an efficient recovery process for all the materials prepared. Fully-constrained recovery experiments indicated a notable capacity of these materials to generate force, with a maximum value obtained higher than 9 N, thanks to the combination of the two different diisocyanate monomers selected. Partially-constrained recovery experiments demonstrated the ability of these materials to produce high levels of work output, despite the complex stress and strain state caused by the single cantilever clamp. Using classical Timoshenko beam theory, the maximum potentiality of these materials can be efficiently predicted as a first approximation both in programming, unconstrained and partially constrained conditions.

In conclusion, we have demonstrated the ability of this new series of poly(thiourethanes)to be used as smart materials and the possibility to combine different diisocyanate monomers to tune the thermomechanical properties without affecting the homogeneity of the sample and preserving the shape-memory ability.

Acknowledgments

The authors would like to thank MINECO (Ministerio de Economia, Industria y Competitividad, MAT2017-82849-C2-1-R and 2-R) and Generalitat de Catalunya (2017-SGR-77) for their financial support.

References

1. Hager, M.D.; Bode, S.; Weber, C.; Schubert, U.S. Shape memory polymers: Past, present and future developments. *Prog. Polym. Sci.* **2015**, 49-50, 3-33.
2. Zhao, Q.; Qi. J.; Xie, T. Recent progress in shape memory polymer: New behavior, enabling materials, and mechanistic understanding. *Prog. Polym. Sci.* **2015**, 79, 49-50.
3. Hu, J.; Zhu, Y.; Huang, H.; Lu, J. Recent advances in shape–memory polymers: Structure, mechanism, functionality, modelling and applications. *Prog. Polym. Sci.* **2012**, 37, 1720-1763.
4. Souri, M.; Lu, Y.C.; Erol, A.; Pulla, S.S.; Karaca, H.E. Characterization of unconstraint and constraint shape recoveries of an epoxy based shape memory polymer. *Polym. Test.* **2015**, 41, 231-238.
5. Lendlein, A.; Gould O.E. C. Reprogrammable recovery and actuation behaviour of shape- memory polymers. *Nat. Rev. Mater.* **2019**, 4, 116-133.
6. Berg, G. J.; McBride, M. K.; Wang, C.; Bowman, C. N. New directions in the chemistry of shape memory polymers. *Polymer* **2014**, 55, 5849-5872.
7. Anthamatten, M.; Roddecha, S.; Li, J. Energy storage capacity of shape-memory polymers. *Macromolecules* **2013**, 46, 4230-4234.
8. Belmonte, A.; Guzmán, D.; Fernández-Francos, X.; De la Flor, S. Effect of the network structure and programming temperature on the shape-memory response of thiol-epoxy “click” systems. *Polymers* **2015**, 7, 2146-2164.
9. Small, W.; Singhal, P.; Wilson, T. S.; Maitland, D. J. Biomedical applications of thermally activated shape memory polymers. *J. Mater. Chem.* **2010**, 20, 3356-3366.
10. Hardy, J. G.; Palma, M.; Wind, S. J.; Biggs, M. J. Responsive biomaterials: Advances in materials based on shape-memory polymers. *Adv. Mater.* **2016**, 28, 5717-5724.
11. Liu, Y.; Du, H.; Liu, L.; Leng, J. Shape memory polymers and their composites in aerospace applications: a review. *Smart Mater. Struct.* **2014**, 23, 023001.
12. Hu, J.; Chen, S. A review of actively moving polymers in textile applications. *J. Mater. Chem.* **2010**, 20, 3346-3355.
13. Pilate, F.; Toncheva, A.; Dubois, P.; Raquez, J.-M. Shape-memory polymers for multiple applications in the materials world. *Eur. Polym. J.* **2016**, 80, 268-294.
14. Xie, F.; Huang, L.; Leng, J.; Liu, Y. Thermoset shape memory polymers and their composites. *J. Intel. Mat. Syst. Str.* **2016**, 27, 2433-2455.
15. Belmonte, A.; Fernández-Francos, X.; De la Flor, S. New understanding of the shape-memory response in thiol-epoxy click systems: towards controlling the recovery process. *J. Mater. Sci.* **2017**, 52, 1625-1638.
16. Small, W.; Singhal, P.; Wilson, T. S.; Maitland, D. J. High performance shape memory epoxy/carbon nanotube nanocomposites. *ACS Appl. Mater. Inter.* **2016**, 8, 311-320.
17. Russo, C.; Fernández Francos, X; De la Flor, S. Shape-memory actuators based on dual-curing thiol-acrylate-epoxy thermosets. *Express Polym. Lett.* **2020**, 15, 58-71.
18. Belmonte, A.; Fernández-Francos, X.; De la Flor, S. Thermomechanical characterization of thiol-epoxy shape memory thermosets for mechanical actuators design. *AIP Conf. Proc.* **2018**, 030012, 1-12.

19. Santiago, D.; Fabregat-Sanjuan, A.; Ferrando, F.; De la Flor, S. Recovery stress and work output in hyperbranched poly(ethyleneimine)-modified shape-memory epoxy polymers. *J. Polym. Sci. Part B: Polym. Phys.* **2016**, 54, 1002-1013.
20. Belmonte, A.; Lama, G. C.; Gentile, G.; Cerruti, P.; Ambrogi, V.; Fernández-Francos, X.; De la Flor, S. Thermally-triggered free-standing shape-memory actuators. *Eur. Polym. J.* **2017**, 97, 241-252.
21. Belmonte, A.; Russo, C.; Ambrogi, V.; Fernández-Francos, X.; De la Flor, S. Epoxy-based shape-memory actuators obtained via dual-curing of off-stoichiometric "thiol-epoxy" mixtures. *Polymers* **2017**, 9, 113-132.
22. Mather, P. T.; Luo, X.; Rousseau, I. A. Shape memory polymer research. *Annu. Rev. Mater. Res.* **2009**, 39, 445-471.
23. Kausar, A. Review on technological significance of photoactive, electroactive, pH-sensitive, water-active, and thermoresponsive polyurethane materials. *Polym. Plast. Technn. Eng.* **2017**, 56, 606-616.
24. Delebecq, E.; Pascault, J. P.; Boutevin, B.; Ganachaud, F. On the versatility of urethane/urea bonds: reversibility, blocked isocyanate, and non-isocyanate polyurethane. *Chem. Rev.* **2013**, 113, 80-118.
25. Ireni, N.G.; Narayan, R.; Basak, P.; Raju, K.V.S.N. Poly(thiourethane-urethane-urea) as anticorrosion coatings with impressive optical properties. *Polymer* **2016**, 97, 370-379.
26. Li, C.; Tan, J.; Li, H.; Yin, D.; Gu, J.; Zhang, B.; Zhang, Q. Thiol–isocyanate click reaction in a Pickering emulsion: a rapid and efficient route to encapsulation of healing agents. *Polym. Chem.* **2015**, 6, 7100-7111.
27. Yan, J.; Ariyasivam, S.; Weerasinghe, D.; He, J.; Chisholm, B.; Chen, Z.; Webster, D. Thiourethane thermoset coatings from bio-based thiols. *Polym. Int.* **2012**, 61, 602-608.
28. Jia, Y.; Shi, B.; Jin, J.; Li, J. High refractive index polythiourethane networks with high mechanical property via thiol-isocyanate click reaction. *Polymer* **2019**, 180, 121746.
29. Podgórski, M.; Nair, D. P.; Chatani, S.; Berg, G.; Bowman, C. N. Programmable mechanically assisted geometric deformations of glassy two-stage reactive polymeric materials. *ACS Appl. Mater. Inter.* **2014**, 6, 6111-6119.
30. Podgórski, M.; Wanga, C.; Bowman, C. N. Multiple shape memory polymers based on laminates formed from thiol-click chemistry-based polymerizations. *Soft Matter.* **2015**, 11, 6852-6858.
31. Nguyen, L. T.; Truong, T. T.; Nguyen, H. T.; Le, L.; Nguyen, V. Q.; Van Le, T.; Luu, A. T. Healable shape memory (thio)urethane thermosets. *Polym. Chem.* **2015**, 6, 3143-3154.
32. Gamardella, F.; Sabatini, V.; Ramis, X.; Serra, A. Tailor-made thermosets obtained by sequential dual-curing combining isocyanate-thiol and epoxy-thiol click reactions. *Polymer* **2019**, 174, 200-209.
33. Gamardella, F.; Guerrero, F.; De la Flor, S.; Ramis, X.; Serra, A. A new class of vitrimers based on aliphatic poly(thiourethane) networks with shape memory and permanent shape reconfiguration, *Eur. Polym. J.* **2019**, 122, 109361.

34. Gamardella, F.; Ramis. X.; De la Flor, S.; Serra, A. Preparation of poly(thiourethane) thermosets by controlled thiol-isocyanate click reaction using a latent organocatalyst. *React. Funct. Polym.* **2019**, 134, 174-182.
35. Gamardella, F.; Muñoz, S.; De la Flor, S.; Ramis, X.; Serra, A. Recyclable Organocatalyzed Poly(Thiourethane) Covalent Adaptable Networks. *Polymers* **2020**, 12, 2913.
36. Konuray, O.; Areny, N.; Morancho, J.M.; Fernández-Francos, X.; Serra, A.; Ramis, X. Preparation and characterization of dual-curable off-stoichiometric amine-epoxy thermosets with latent reactivity, *Polymer* **2018**, 146, 42-52.
37. Konuray, O.; Liendo, F.; Fernández-Francos, X.; Serra, A; Sangermano, M.; Ramis, X. Sequential curing of thiol-acetoacetate-acrylate thermosets by latent Michael addition reactions. *Polymer* **2017**, 113, 193-199.
38. Sun, X.; Gao, J.P.; Wang Z.Y. Bicyclic guanidinium tetraphenylborate: a photobase generator and a photocatalyst for living anionic ring-opening polymerization and cross-linking of polymeric materials containing ester and hydroxy groups. *J. Am. Chem. Soc.* **2008**, 130, 8130-8131.
39. Shonaike, G. O.; Advani, S. G. Advanced Polymeric Materials: Structure Property Relationships. CRC Press, Boca Raton, FL, USA **2003**.
40. Winter, H. H.; Chambon, F. Analysis of linear viscoelasticity of a crosslinking polymer at the gel point. J. Rheol. **1986**, 30, 367-382.
41. Rogulska, M.; Kultys, A.; Olszewska, E. New thermoplastics poly(thiourethane-urethane) elastomers based on hexane-1,6-diyl diisocyanate (HDI). *J. Therm. Anal. Calorim*. **2013**, 114, 903-916.

Chapter VI

A new class of vitrimers based on aliphatic poly(thiourethane) networks with shape memory and permanent shape reconfiguration

European Polymer Journal 122 (2020) 109361

A new class of vitrimers based on aliphatic poly(thiourethane) networks with shape memory and permanent shape reconfiguration

Francesco Gamardella[1], Federico Guerrero,[1] Silvia De la Flor,[2] Xavier Ramis[3] and Angels Serra[1]

[1] *Dept.of Analytical and Organic Chemistry, Universitat Rovira i Virgili, C/ Marcel·lí Domingo, 43007, Tarragona, Spain*

[2] *Department of Mechanical Engineering, Universitat Rovira i Virgili, Av. Països Catalans, 26, 43007 Tarragona, Spain*

[3] *Thermodynamics Laboratory, ETSEIB Universitat Politècnica de Catalunya, Av. Diagonal, 08028, Barcelona, Spain*

Abstract

Vitrimers are a new promising class of polymeric materials, which are attracting increasing attention thanks to their thermosetting characteristics with their capability of being reprocessed and recyclable, which make them more environmentally friendly in reference to the conventional thermosets. In the present study, we report a new class of vitrimeric materials consisting in poly(thiourethane) networks. These materials can be easily prepared from readily available isocyanate and thiol monomers in the presence of dibutyltin dilaurate (DBTDL) as the catalyst. The reaction has a *click* nature and therefore leads to highly homogeneous networks. The materials studied behave as conventional thermosets until the topological rearrangement started. Freezing topological temperatures (T_v) between 95 and 132 °C were determined depending on the amount of catalyst in the material. The vitrimers prepared showed good shape memory and welding abilities and a high optical transparency and therefore they have a great potentiality in advanced engineering applications. The occurrence of the trans-thiocarbamoylation reaction, responsible of the rearrangement, has been confirmed by using model compounds. The materials remained unaltered after reprocessing, which was proved by means of FTIR and thermomechanical studies.

Keywords:

vitrimers; poly(thiourethane); thermosets; shape-memory; click reaction.

Chapter VI

1. Introduction

Thermosetting polymers are very useful in a broad range of industrial applications, due to their chemical, thermal and environmental resistance and excellent mechanical performance. However, the existence of covalent bonds in the three dimensions of the network prevents reshaping, reprocessing, or recycling and makes difficult their reparation. To avoid these drawbacks a new family of materials, called vitrimers, has been developed. These new materials combine the excellent performance of thermosets with some of the processability advantages of thermoplastics [1, 2, 3].

Vitrimers consist in three-dimensional polymeric structures with dynamic covalent bonds within an organic network, which can lead to topological changes without affecting the average crosslinking degree. This fact allows reshaping, self-welding, reprocessing and not less important, the elimination of internal stresses, which appear during their curing or service-life [4].

This type of materials shows a characteristic transition temperature, T_v, also called topology freezing transition temperature, that corresponds to a reversible transition from viscoelastic solid to a viscoelastic liquid. This temperature depends on the kinetics of the reversible reaction, responsible of the topological changes in the network structure [5].

In advanced technologies, there is a great demand for smart materials, especially for shape memory thermosets. They are quite advantageous in comparison to thermoplastics, since they have higher thermal stability, fixation ability and shape-recovery rate and can perform higher levels of mechanical work [6, 7].

The introduction of a new class of vitrimers with good shape memory behaviour can overcome the limitations of the traditional thermosets in the formation of sophisticated and geometrically complex forms, thanks to the combination of elasticity (shape memory) and plasticity (vitrimers). In addition, these materials, after recycling, can also exhibit comparable mechanical performance [8, 9, 10].

In recent years, different reversible exchange reactions have been explored for the preparation of vitrimers [4]. Among them, transesterification [1, 5], transamination [11], disulfide exchange [12, 13], transalkylation [14], siloxane equilibrium [15], dioxaborolane metathesis [16], amine-urea exchange [17] and transcarbamoylation [18, 19] can be mentioned. These exchange reactions are the responsible of the reformation of the network structure. These chemical processes are triggered by external stimuli, usually by heating, and the exchange rate can be enhanced by the addition of catalysts [4].

Polyurethanes have a broad application because of their versatility. They are durable and tough, and they have been applied in the field of elastomers, coatings, rigid foams and adhesives [20]. The vitrimeric characteristics of polyurethane thermosets has

been already reported [21, 22]. Dynamic exchange reactions have already been demonstrated in a variety of poly(hydroxyurethane) materials [23]. In addition, their shape memory behaviour has also been reported.

Poly(thiourethane)s, also called poly(thiocarbamate)s, are related to the above-mentioned materials, but they present several advantages. Since they are obtained by *click-type* reactions from isocyanates and thiols, the network structure is highly homogeneous and consequently relaxation processes occur in a narrow temperature range [24]. Thiol-isocyanate reaction does not present by-reactions such as occurs in the polyurethane synthesis, which leads to the formation of allophanate units in the network structure. In addition to that, poly(thiourethane) thermosets have quite valuable properties such as biocompatibility, flexibility and excellent optical transparence [25].

Herein, we report a new type of vitrimers with shape memory performance based on poly(thiourethane) networks. Because the vitrimeric behaviour in poly(urethanes) was attributed to a transcarbamoylation reaction, it was hypothesized that trans-thiocarbamoylation could also lead to a rapid exchange allowing reshaping, self-welding and stress dissipation, even in a more efficient way, due to the presence of sulphur, which has an enhanced reactivity in front of its oxygen analogues.

The materials prepared can be easily obtained from commercially available precursors. In the present case, hexamethylene diisocyanate (HDI) and trimethylolpropane tris(3-mercaptopropionate) (S3) in stoichiometric proportions were selected as starting monomers and a Lewis acid (dibutyltin dilaurate, DBTDL) was used as a catalyst. Although this type of materials can be obtained from different monomers, the study was carried out with only one type of material as a proof of concept.

It should be noticed that in the literature, there are no references to the trans-thiocarbamoylation process in absence of thiol in excess, nor in the field of materials science, nor in the field of pure organic chemistry. Moreover, the trans-carbamoylation previously proposed by Yan *et al.*, as the responsible of the reversible structural change in those vitrimers, was not structurally demonstrated by these authors [21].

2.Experimental part

2.1 Materials

Trimethylolpropane tris(3-mercaptopropionate) (S3), hexamethylene diisocyanate (HDI), n-butanethiol, 2-methyl-1-propanethiol, n-butyl isocyanate, tert-butyl isocyanate and dibutyltin dilaurate (DBTDL) from Sigma-Aldrich were used as received.

2.2 Preparation of the formulations

HDI and S3 were mixed in stoichiometric proportions, 2 mol of S3 per 3 mol of HDI. The selected amount of DBTDL was first dissolved in the isocyanate and the corresponding amount of thiol was then added. Different formulations were prepared with 1, 2 and 4 phr of DBTDL (parts of catalysts per hundred parts of thiol). The mixtures were manually stirred until homogeneity at room temperature and freshly used.

2.3 Synthesis of the model compounds

S-Butyl butylcarbamothioate (L-L) was prepared by reacting stoichiometric proportions of n-butanethiol and n-butyl isocyanate with a 5 wt% of DBTDL at 90 °C in a 10 mL flask under argon atmosphere for 96 h. The final product was purified by eliminating unreacted volatile products at vacuum in the rotary evaporator. ^{1}H NMR ($CDCl_3$, δ in ppm) (see Figure VI-S1): 5.25 (1H), 3.28 (2H), 2.90 (2H), 1.59 (2H), 1.50 (2H), 1.39 (2H), 1.35 (2H), 0.93 (3H) and 0.90 (3H).

S-isobutyl tert-butylcarbamothioate (I-T) was prepared as described before for L-L, starting from stoichiometric proportions of 2-methyl-1-propanethiol and tert-butyl isocyanate. ^{1}H NMR ($CDCl_3$, δ in ppm) (see Figure VI-S2): 5.15 (1H), 2.75 (2H), 1.80 (1H), 1.33 (9H) and 0.95 (6H).

2.4 Trans-thiocarbamoylation assessment

An equimolar mixture of S-butyl butylcarbamothioate (L-L) and S-isobutyl tert-butylcarbamothioate (I-T) with 5 wt.% of DBTDL was heated under argon atmosphere at 120 °C for 24 h. The mixtures before and after heating were analyzed by gas chromatography equipped with a mass detector (see Figure VI-1). The mass spectra registered for each compound can be visualized in Figures VI-S3, VI-S4, VI-S5 and VI-S6 in SI.

2.5 Sample preparation

For DMTA analysis, films were prepared by pouring the formulations on pre-silanized glasses and using Teflon spacers to ensure a homogeneous thickness of 0.5 mm. The formulations were cured at 60°C, 80°C, 100°C and 150°C for two hours at each temperature. The films were die-cut to obtain a rectangular specimen of 20 x 5 x 0.5 mm^3 dimensions.

2.6 Characterization techniques

^{1}H NMR spectra were registered in a Varian Gemini 400 spectrometer. $CDCl_3$ was used as the solvent. For internal calibration the solvent signal corresponding to $CDCl_3$ at 7.26 ppm. Separation and detection of the mixture components were performed in a HP6890 gas chromatograph and 5973 Mass selective detector (Agilent Technologies. Waldbronn, Germany), using a HP-5MS capillary column (30 m × 0.25 mm × 0.25 m) provided by Agilent.

FTIR spectra were registered with a Bruker Vertex 70 equipped with a Golden Gate heated single reflection diamond ATR in the absorbance mode at a resolution of 4 cm^{-1} in the wavelength range of 400 to 4000 cm^{-1}. The typical absorption bands of the poly(thiourethane) vitrimer obtained with a 4% of DBTDL were followed during heating in the ATR in the temperature range from 155 to 200 °C keeping the temperature of the ATR for 10 min at each temperature tested. The material before and after being reprocessed at 180 °C for 40 min was analyzed at room temperature.

The viscoelastic and thermo-mechanical properties were evaluated by using a DMA Q800 analyzer from TA Instruments (New Castle, DE, USA).

2.7 Stress relaxation tests

Tensile stress relaxation tests were conducted using a film tension clamp on samples with the same dimensions as previously defined. The sample was firstly equilibrated at 160 °C and left isothermally at this temperature for 3 min, then a constant strain of 1.5 % (to ensure the material is within the linear range) was applied on the sample and the consequent stress level was measured as function of time. Then the strain was removed, and the process was repeated every 5 °C until the final test temperature, 190 °C, is reached.

The relaxation stress $\sigma(t)$ was normalized by the initial stress σ_0 and the relaxation times (τ) were determined as the time necessary to relax $0.37 \cdot \sigma_0$. With the relaxation times obtained at each temperature, the activation energy values E_a were calculated for each vitrimer, using an Arrhenius-type equation:

$$\ln(\tau) = \frac{E_a}{RT} - lnA \quad (1)$$

where, τ is the time needed to attain a given stress relaxation value (37 %), A is a pre-exponential factor and R is the gas constant. From the Arrhenius relation, the temperature of topology freezing (T_v) was obtained as the temperature at which the material reaches a viscosity of 10^{12} Pa·s. For our system the value of T_v could also be extrapolated from the Arrhenius fitting to a relaxation time of around 10^5 s. This time is deduced from the Maxwell's relation ($\eta = E' * \tau *$) and assuming E' (obtained from the DMTA experiments) being relatively invariant in the rubbery state.

To compare the time to reach the complete relaxation of the stress (i.e. a normalized stress less than 10^{-2}) of poly(thiourethane)s vitrimers obtained with different contents of DBTDL, a single stress relaxation test was performed at the temperature of 180°C with the same constant strain of 1.5%.

2.8 Creep experiments

Creep and recovery properties were studied by the same DMA Q800 apparatus equipped with a film tension clamp.

All the samples were stretched under a stress of 0.1 MPa at 180 °C for 30 min, then the stress was immediately released, and the sample was left to recover for 30 min. For comparative purposes between the rubbery and the vitrimeric state, a sample with a 4% of DBTDL content was also tested, under the same creep conditions, at 70°C (slightly above T_g).

For the determination of the viscosity at each temperature needed for the representation of the Fragility Angell Plot, a series of creep experiments were carried out on films at temperatures between 70 and 180 °C, increasing 10 °C in each scan. To perform the tests, the selected temperature was equilibrated for 3 min and then a stress level of 0.1 MPa was applied for 30 min. The viscosity η (Pa·s) was then obtained from the slope of the graph strain-temperature and represented in front of T_v/T thus obtaining the Angell Fragility Plot.

2.9 Tan δ determination

To study the influence of the trans-thiocarbamoylation process on the thermo-mechanical properties, the evolution of tan δ and storage modulus with temperature was investigated after performing several stress relaxation experiments. A sample was tested in tension in the DMA Q800 analyzer, at a heating rate of 3°C/min from 30 to 125°C with a frequency of 1 Hz and 0.1 % of strain. Then the sample was left to completely relax at 180 °C with a strain level of 1.5 % for 25 minutes. After the sample was relaxed, another thermomechanical tests, with the same conditions as the initials, was performed. This process was repeated 2 times.

2.10 Dilatometry tests

Dilatometry was performed with the tension film geometry in the DMA Q800 analyzer on the samples with the same dimensions as described before. The length of the sample was continuously measured while increasing the temperature at a heating rate of 1 °C/min from 25 to 250 °C. A slight stress of 0.01 MPa was applied during the experiment to avoid buckling.

3. Results and discussion

To prove that trans-thiocarbamoylation can occur on heating thiocarbamates in the presence of a Lewis acid such as DBTDL, we synthesized and characterized two different model compounds (L-L and I-T) and then, they were heated for 24 h at 120 °C under inert atmosphere. Scheme VI-1 depicts the structure of the model compounds and the structure of the rearranged compounds expected.

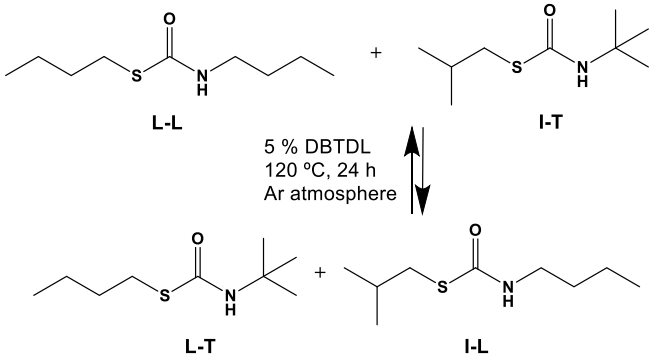

Scheme VI-1. *Model compounds synthesized and structure of the compounds formed by trans-thiocarbamoylation rearrangement.*

The mixture before and after heating was investigated by gas chromatography coupled to a mass spectrometer detector and the chromatograms are represented in Figure VI-1. As we can see in the figure, the two peaks of the mixture before reaction were transformed into four peaks after the reaction. By mass spectrometry the structure of the two new compounds appearing as two new peaks was characterized and they correspond to the products designed as L-T and I-L in Figure VI-1. The characterization of the model compounds and the mass spectra obtained of these eluted products are given in the supporting information (Figures VI-S1- S6).

As we can see in the chromatogram, after reaction no traces of initial thiol or isocyanate were observed, which indicates that the trans-thiocarbamoylation reaction occurs through a concerted mechanism and not by dissociation of thiourethanes to form thiol and isocyanate and further coupling.

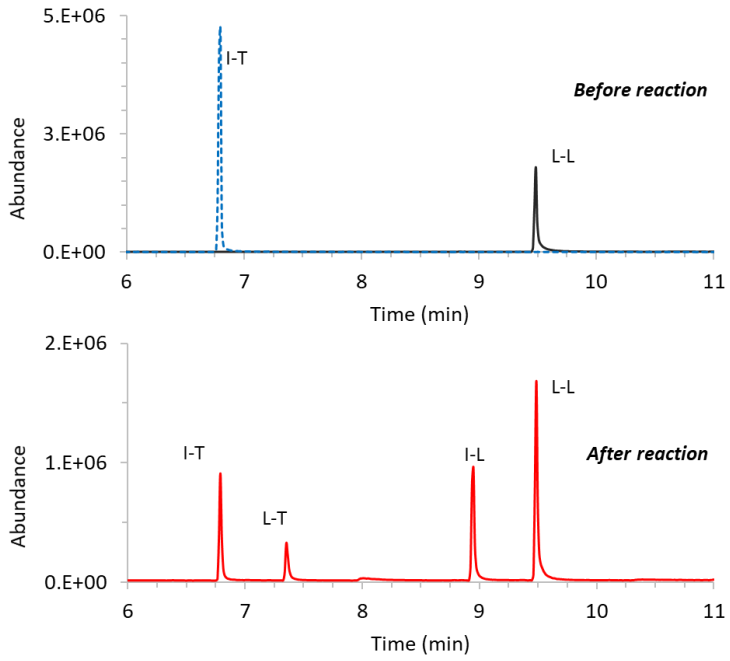

***Figure VI-1**. Trans-thiocarbamoylation reaction scheme and gas-chromatograms of the mixture before and after reaction.*

Once confirmed the viability of the interchange process the characterization of the crosslinked materials was performed. The preparation of the material from HDI and S3 with different proportions of DBTDL (1, 2 and 4 phr) is described in the experimental part. Three different proportions of catalyst were used in the formulation to investigate if in these materials, the increase in the amount of catalyst also increases the rate of interchange reaction, enhancing the reshaping velocity as it was reported for other vitrimeric materials [4].

From the DMTA analysis the values of the temperature at peak of tan δ for the materials prepared with different proportions of DBTDL were determined and they are collected in Table VI-1. As we can see, both the $tan\delta$ evolution (and the corresponding peak of tanδ) and the storage modulus are not influenced by the amount of catalyst (see Figure VI-S7 and VI-S8 in SI) which indicates that the materials have similar thermomechanical behavior, i.e. the evolution of the $tan\delta$ and the storage modulus present the same shape and almost the same values throughout all the temperature range.

Table VI-1. *Temperature at peak of tanδ and topology freezing temperature, activation energy and time for complete stress relaxation at 180 °C. Adjusting parameters for the Arrhenius eq. were also included.*

Sample	$T_{tan\delta}$ (°C)	T_v (°C)	$\tau_{180°C}$ (min)	E_a (kJ/mol)	lnA (s)	r^2
1% DBTDL	57	132	126	102	18.9	0.99
2% DBTDL	57	109	79	73	11.6	0.99
4% DBTDL	57	96	20	72	12.0	0.98

The time and temperature dependent relaxation modulus of the dynamic network was investigated in order to determine the vitrimeric nature of the materials. With this purpose, the stress relaxation behaviour of the samples prepared containing different proportions of DBTDL was studied by DMTA to evaluate the trans-thiocarbamoylation reaction rate and the results are shown in Figure VI-2.

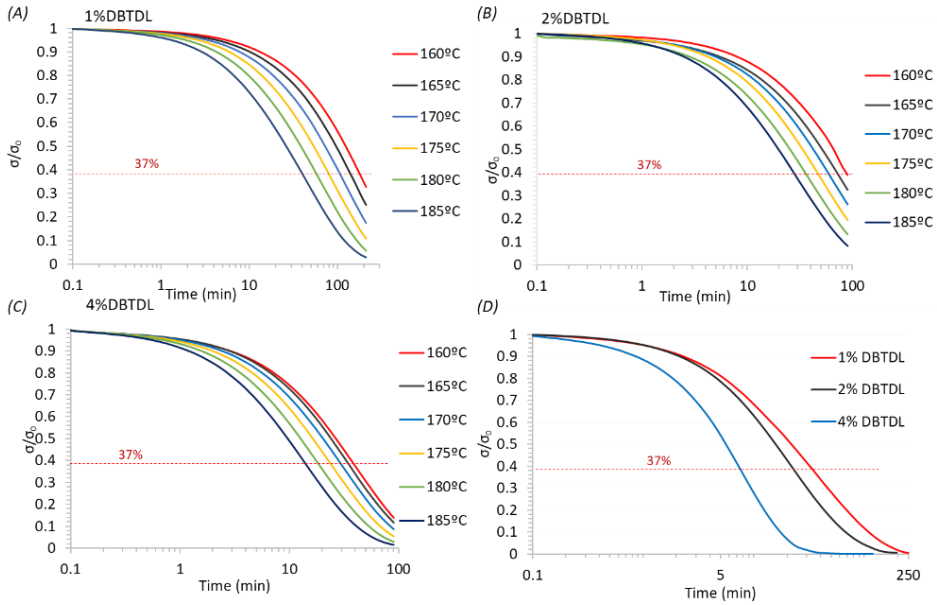

Figure VI-2. *Normalized stress relaxation plot as a function of time at various temperatures from (160 to 185 °C) during 90 min for the samples with 1 % (A), 2% (B) and 4 % of catalyst (C). Normalized stress relaxation behaviour at 180 °C, for the samples with different DBTDL amounts (D). The reference σ/σ_0=0.37 is highlighted.*

As observed in the figure VI-2, the amount of catalyst in the sample has a big influence in the stress-relaxation behavior. This fact agrees with the results obtained by Zheng *et al.* [18] in poly(urethane) vitrimers and confirms that DBTDL acts as catalyst in both the formation of poly(thiourethane)s and in the trans-thiocarbamoylation process. The greater the catalyst amount the faster is the relaxation process. The times needed

to achieve the complete stress relaxation at 180 °C ($\tau_{180°C}$) are collected in Table VI-1. As we can see, the time needed to reach a complete relaxation state (zero stress) that enables the permanent reshaping of the material is drastically reduced by more than 80% (from 126 to 20 min) on increasing the amount of DBTDL from 1 to 4 phr.

At higher temperatures the viscosity of the vitrimers is controlled by chemical exchange reactions, leading to a temperature-viscosity relation that follows the Arrhenius law like in inorganic silica materials. In contrast, in dissociative covalent adaptable networks, the drop-in viscosity usually is more abrupt with temperature if compared to the associative CANs [2]. According to that, the logarithm of the relaxation times, for a relaxation value of 63% (σ/σ_0=0.37), was plotted as a function of the inverse of temperature, fitting an Arrhenius-like behavior. The activation energy (E_a) of the rearrangement process, using an Arrhenius-type equation, was determined (see Figure VI-3 and Table VI-1).

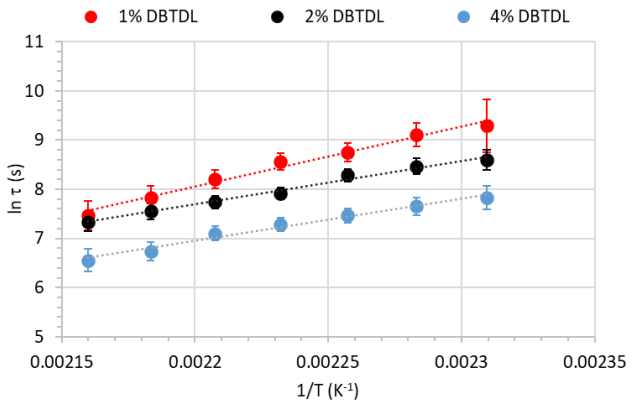

***Figure VI-3**. Arrhenius plot of relaxation times against temperature for the materials with different proportions of catalyst, measured from stress relaxation experiments.*

As we can see in Figure VI-3, the rate of the relaxation process increases with the temperature and fits perfectly with an Arrhenius-like relaxation time dependence.

From the Arrhenius plot, we can also determine the topology freezing transition temperature, T_v, that is defined, as explained before, as the temperature at which the material reaches a viscosity of 10^{12} Pa·s [1]. In Table VI-1 the calculated E_a values are reported, the values are reduced from 132 to 96 °C on increasing the catalyst content. It is noteworthy that, although the correlations are very strong and the models are significant in all cases for a 95% confident level, limited errors in activation energy give great errors in the relaxation time and, consequently, in the T_v.

It is important to highlight that the values reported in Table VI-1 for E_a are significantly lower than those reported for poly(urethane) transcarbamoylation processes, which are 130.5 and 183.7 kJ/mol [21]. The E_a is higher with 1 phr of DBTDL but similar when

the amount of catalyst was 2 or 4 phr (72-73 kJ/mol), unlike the results reported by Leibler *et al.* [5], in which the E_a in polyester vitrimers remained constant with the amount of catalyst. As the activation energy allows us to predict the relaxation stress rate within a temperature range [26,27]. These values indicate that the sensitivity of the exchange reaction to a temperature change would be similar with proportions of catalyst of 4 and 2 phr (similar E_a), but the relaxation time would be lower for a given temperature with 4 phr.

The effect of the temperature on the creep behavior was studied in order to confirm that the materials flow at temperatures higher than T_v. Figure VI-4A shows the creep plot at 70 and 180 °C for the material containing 4 phr of DBTDL.

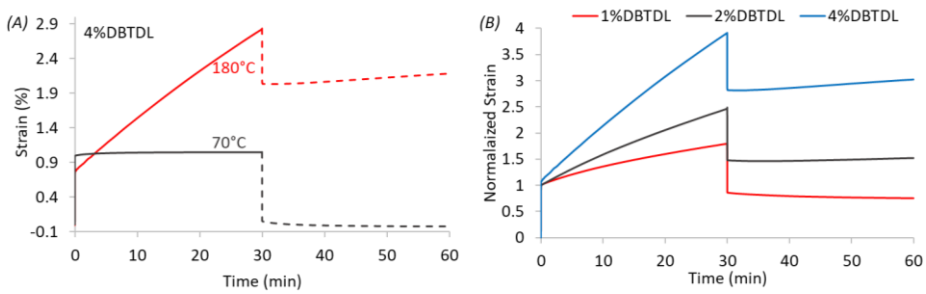

Figure VI-4. *Creep and recovery curves at 70 and 180 °C for the sample with 4 % of DBTDL (A) and with different proportions of DBTDL at 180 °C (B).*

As we can see, at the lowest temperature (70°C) the material does not present plastic deformation when the stress is released, behaving like a thermoset above its T_g (rubber-like behavior) whereas at a temperature higher than T_v the material elongates as a viscoelastic liquid and in the recovery process a permanent deformation remains, due to the topology rearrangement produced by the trans-thiocarbamoylation process. In Figure VI-4B the effect of the amount of catalyst in the creep behavior is shown. On increasing the DBTDL proportion both the elongation and the plastic deformation increase, and after the instantaneous stress release the strain cannot be recovered, which confirms the vitrimeric characteristics of these materials. From these tests we can state that poly(thiourethane) networks can be deformed, reshaped and reprocessed at temperatures higher than their T_v.

The Angell fragility plot is represented in Figure VI-5, where it is shown how the materials prepared behave like thermosetting vitrimers.

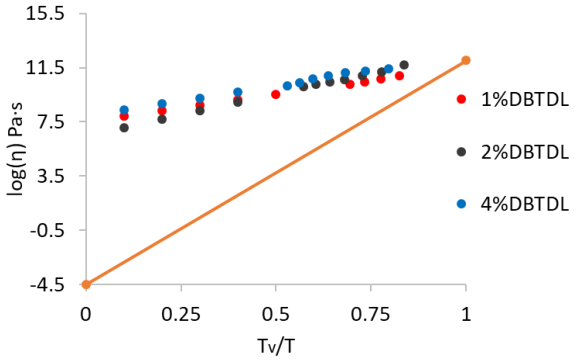

***Figure VI-5**. Angell fragility plot of the logarithm of the viscosity as a function of the inverse temperature, scaled to T_v, for the different materials. For comparative purposes, the relation for silica is included as a reference of an ideal strong liquid [28, 29].*

At temperature above T_v, the exchange reactions are active, and the relaxation time and the viscosity follow the Arrhenius law, as occurs in "strong glass formers" like inorganic silica materials (taken as ideal strong liquids) [28, 29]. This is in contrast with the behaviour of thermoplastic materials and dissociative covalent adaptable networks, which are "fragile liquids". At higher temperature, as stated before, the viscosity of such materials suffers a very sharp decrease [2].

The vitrimeric behaviour of these materials was studied by tensile dilatometry experiments (Figure VI-6) where a slight stress of 0.01MPa was applied to prevent buckling. At low temperatures, the glass transition, T_g, is evidenced by a first change in the slope of the strain, produced by the change of thermal expansion coefficient, CTE. After that, CTE remains constant, such as in a typical thermosetting polymer, until at a certain point in which the exchange reactions are so evident, leading to a significant increase in CTE; more evident with a higher proportion of catalyst.

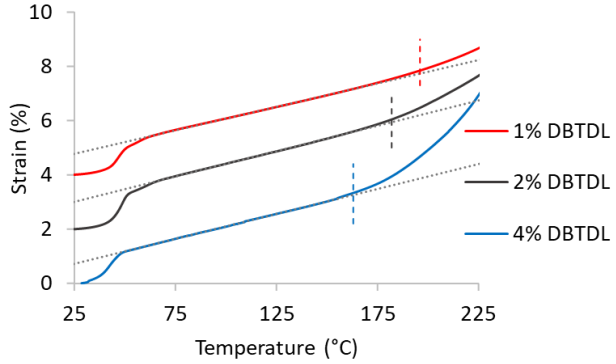

***Figure VI-6**. Dilatometry experiments with heating rate of 1 °C/min for the materials with 1, 2 and 4% of DBTDL (the curves are shifted only for a better understanding).*

The interchange mechanism in poly(thiourethane) vitrimers was structurally studied by FTIR spectroscopy at different temperatures, to check if there was any change in the carbonyl region the absorptions of the ester group in the thiol structure at 1730 cm^{-1} and thiourethane group at 1670 cm^{-1} was monitored. In Figure VI-7, we can see how these bands remain practically unaltered during the heating process, considering the thermosensitivity of the bands. Moreover, any typical absorption of isocyanate groups at 2270 cm^{-1} appeared during the heating process. It should be noted that in case of thiourethane dissociation, isocyanate band would appear and thiourethane band would be decreased. In this way, FTIR-ATR studies structurally confirm that thiourethane groups are not broken in the 155-200°C temperature range and that the rearrangement of this group is associative with a concerted mechanism.

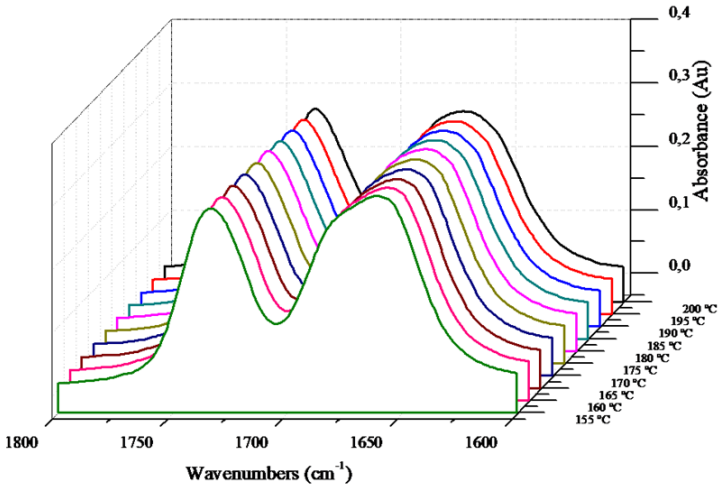

***Figure VI-7**. FTIR carbonylic absorptions of the ester (1730 cm^{-1}) and thiourethane groups (1670 cm^{-1}) of a cured sample with 4% of DBTDL registered after heating for 10 min at each temperature from 155 to 200 °C.*

The thermal stability of these materials in the reprocessing range was studied by thermogravimetry. The TGA curves are shown in SI Figure VI-S9. By this study we could see that the materials with different proportions of DBTDL began to lose weight (1% and 2%) at temperatures around 260 and 270 °C, respectively, much higher than the interchange temperature.

Besides the vitrimeric behaviour, the materials prepared also possess shape memory effect (SME). Figure VI-8 shows a visual qualitative assessment of the shape memory and vitrimeric behaviour. The rectangular initial sample (I) was programmed at 80°C to a folded temporary shape, followed by a rapid cooling to room temperature. When heating at T> 80°C, the initial shape was recovered as a consequence of its elasticity-based shape memory effect. By annealing for 40 min at 180 °C ($T>T_v$), the initial sample can be permanently bended to a new shape (II) as a result of the plasticity of the

vitrimer. This new permanent shape can be programmed into another temporary shape that can be recovered on heating at *T*> 80°C. The figure shows a third plastic reshape (III) with the same annealing treatment, which further shows a third temporary shape after the corresponding programming cycle. These cycles can be repeated many times, according to the good thermal stability of these materials at this range of temperature and their elastic/plastic characteristics. It should be noted the high transparency of the samples prepared that is not lost after reshaping.

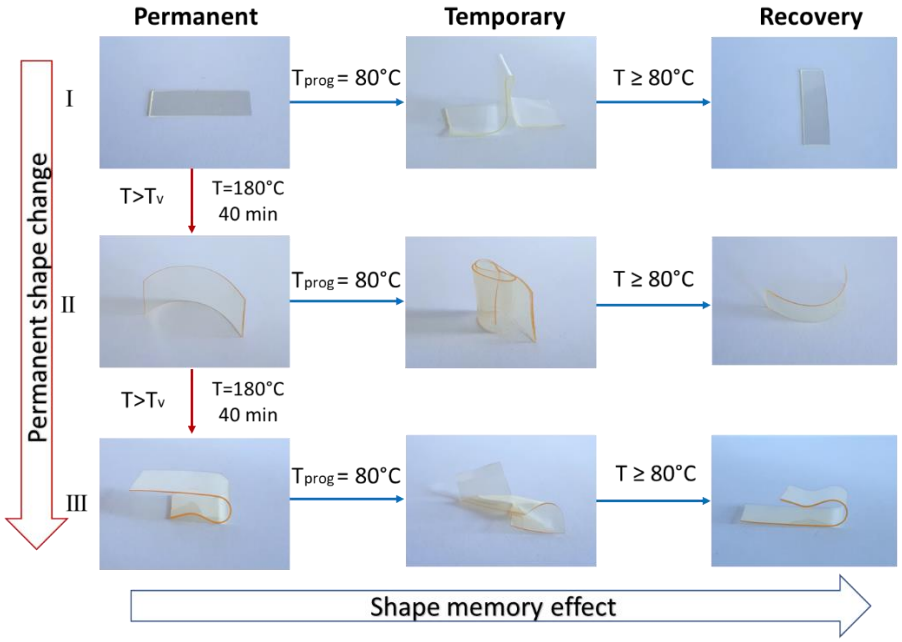

***Figure VI-8**. Qualitative demonstration of shape memory behaviour and permanent/plastic shape change for the poly(thiourethane) vitrimer with a 4% of DBTDL.*

Once reprocessed, the sample was investigated by FTIR (Figure VI-S10), confirming that no variation in the structure of the network had occurred. The material was also subjected to two thermal reprocessing cycles (relaxation process at 180°C, 25 min), verifying that the peak of *tan* δ remained stable without any variation, as can be seen in Figure VI-9.

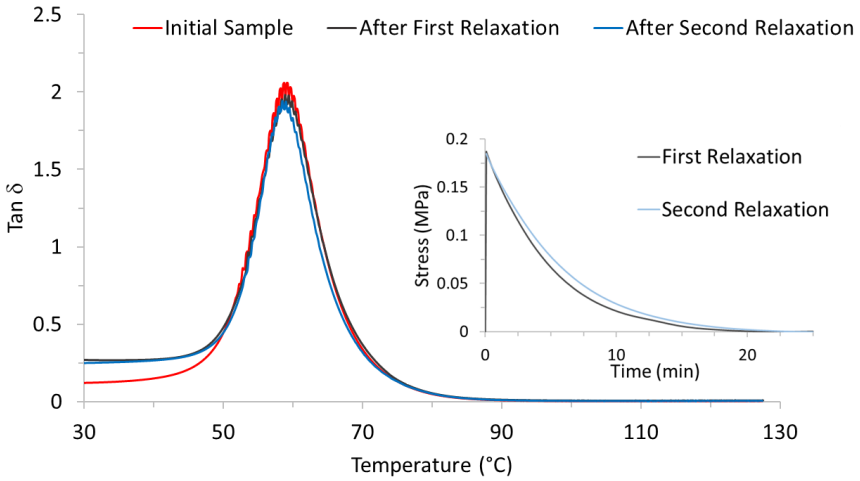

***Figure VI-9**. Tan δ against temperature of the poly(thiourethane) with a 4% of DBTDL sample before and after two relaxation processes. Inset: stress relaxation process in front of time.*

From these experiments we can state that the materials can be reprocessed at high temperatures under a mechanical action. In addition to their vitrimeric characteristics and the shape memory capabilities, they also possess a high welding ability, as it is visually shown in Figure VI-10.

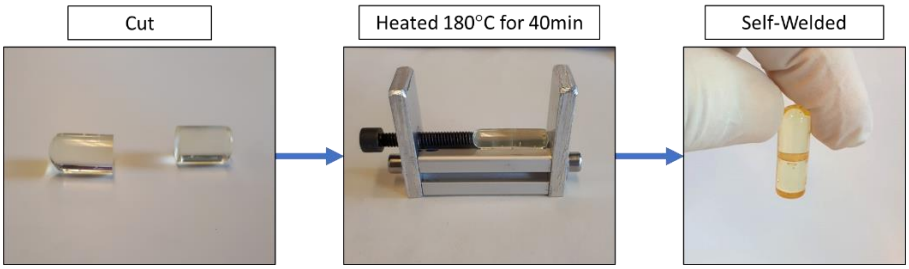

***Figure VI-10**. Visual demonstration of the self-welding ability of the poly(thiourethane) vitrimer heating under pressure for 40 min.*

4. Conclusions

In the present study, we have demonstrated that aliphatic poly(thiourethane)s networks are a new class of vitrimers with shape memory and self-welding characteristics. These materials can be prepared from commercially available monomers, by an easy procedure, using DBTDL as the catalyst. The synthetic reaction has *click* characteristics, which assures a great homogeneity of the network structure.

The trans-thiocarbamoylation reaction was proposed as the responsible of the reshaping ability of these vitrimers. The exchange mechanism was chemically assessed by the use of model compounds and gas chromatography coupled to mass

spectrometry. The non-diassociative character of the trans-thiocarbamoylation process has been confirmed in the materials by FTIR spectroscopy.

The materials prepared with different amounts of DBTDL present lower freezing topological temperature on increasing the amount of catalyst. The activation energy is different for 1 phr of DBTDL but similar with 2 or 4 phr, indicating that the dependence of the trans-thiocarbamoylation reaction rate on the temperature change is similar with these proportions of catalyst, but with different relaxation times for a given temperature. As emphasized by the Angell fragility plot the materials prepared resulted strong glass formers.

By performing thermomechanical analyses before and after several reprocessing test, it was proved that the materials kept their thermomechanical characteristics. Also, the FTIR spectra remained unaltered after heating and reprocessing.

The vitrimers developed show shape memory characteristics, self-welding ability and high transparency, which combined with the possibility of topological rearrangements, confer these materials promising possibilities for smart technological applications.

Acknowledgements

The authors would like to thank MCIU (Ministerio de Ciencia, Innovación y Universidades) and FEDER (Fondo Europeo de Desarrollo Regional) (MAT2017-82849-C2-1-R and MAT2017-82849-C2-2-R) and Generalitat de Catalunya (2017-SGR-77) for the financial support.

References

1. Montarnal, D.; Capelot, M.; Tournilhac, F.; Leibler, L. Silica-Like Malleable Materials from Permanent Organic Networks. *Science* **2011**, 334, 965-968.

2. Denissen, W.; Winne, J.M.; Du Prez, F.E. Vitrimers: permanent organic networks with glass-like fluidity. *Chem. Sci.* **2016**, 7, 30-38.

3. Kloxin, J.C.; Bowman, C.N. Covalent adaptable networks: smart, reconfigurable and responsive network systems. *Chem. Soc. Rev.* **2013**, 42, 7161-7173.

4. Zhang, Z.P.; Rong, M.Z.; Zhang, M.Q. Polymer Engineering based on reversible covalent chemistry: A promising innovative pathway towards new materials and new functionalities. *Prog. Polym. Sci.* **2018**, 80, 39-93.

5. Capelot, M.; Unterlass, M.M.; Tournilhac, F.; Leibler, L. Catalytic control of the vitrimer glass transition. *ACS Macro Lett.* **2012**, 1, 789-792.

6. Zhao, Q.; Qi. J.; Xie, T. Recent progress in shape memory polymer: New behavior, enabling materials, and mechanistic understanding. *Prog. Polym. Sci.* **2015**, 79, 49-50.

7. Santiago, D.; Fabregat-Sanjuan, A.; Ferrando, F.; De la Flor, S. Recovery stress and work output in hyperbranched poly(ethyleneimine)-modified shape-memory epoxy polymers. *J. Polym. Sci. B.* **2016**, 54, 1002.

8. Zhao, Q.; Zou, W.; Luo, Y.; Xie, T. Shape memory polymer network with thermally distinct elasticity and plasticity. *Sci Adv.* **2016**, 2, e1501297.

9. Zou, W.; Dong, J.; Luo, Y.; Zhao, Q.; Xie, T. Dynamic Covalent Polymer Networks: from Old Chemistry to Modern Day Innovations. *Adv. Mater.* **2017**, 29, 160610.

10. Wang, Y.; Pan, Y.; Zheng, Z.; Ding, X. Reprocessable and Multiple Shape Memory Thermosets with Reconfigurability. *Macromol. Rapid Commun.* **2019**, 1900001.

11. Denissen, W.; Rivero, G.; Nicolaÿ, R.; Leibler, L.; Winne, J.M.; Du Prez, F.E. Vinylogous Urethane Vitrimers. *Adv. Funct. Mater.* **2015**, 25, 2451-2457.

12. Canadell, J.; Goosens, H.; Klumperman, B. Self-Helaing Materials Based on Disulfide Links. *Macromolecules* **2011**, 44, 2536-2541.

13. Azcune, I.; Odriozola, I. Aromatic disulfide crosslinks in polymer systems: Self-healing, reprocessability, recyclability and more. *Eur. Polym. J.* **2016**, 84, 147-160.

14. Hendriks, B.; Waelkens, J.; Winne, J.M.; Du Prez, F.E. Poly(thioether) Vitrimers via Transalkylation of Trialkylsulfonium Salts. *ACS Macro Lett.* **2017**, 6, 930-934.

15. Wu, X.; Yang, X.; Yu, R.; Zhao X-J.; Zhang, Y.; Huang, W. A facile access to stiff epoxy vitrimers with excellent mechanical properties via siloxane equilibration. *J. Mater. Chem. A*, **2018**, 6, 10184-10188.

16. Röttger, M.; Domenech, T.; van der Weegen, R.; Breuillac, A.; Nicolaÿ, R.; Leibler, L. High-performance vitrimers from commodity thermoplastics through dioxaborolane metathesis. *Science* **2017**, 356, 62-65.

17. Erice, A.; Ruiz de Luzuiraga, A.; Matxain, J.M.; Ruipérez, F.; Asua, J.M.; Grande, H.J.; Rekondo, A. Reprocessable and recyclable crosslinked poly(urea-urethane)s based on dynamic amine/urea exchange. *Polymer* **2018**, 145, 127-136.

18. Zheng, N.; Fang, Z.; Zou, W.; Zhao, Q.; Xie, T. Thermoset Shape-Memory Polyurethane with Intrinsic Plasticity Enabled by Transcarbamoylation. *Angew. Chem. Int.* **2016**, 55, 11421-11425.

19. Fortman, D. J.; Brutman, J. P.; Cramer, C. J.; Hillmyer, M. A.; Dichtel, W. R. Mechanically Activated, Catalyst-Free Polyhydroxyurethane Vitrimers. *J. Am. Chem. Soc.* **2015**, 137, 14019-14022.

20. Akindoyo, J. O.; Beg, M. D. H.; Ghazali, S.; Islam, M. R.; Jeyaratnama, N.; Yuvaraj, A. R. Polyurethane types, synthesis and applications–a review. *RSC Adv.* **2016**, 6, 114453-114482.

21. Yan, P.; Zhao, W.; Fu, X.; Kong, W.; Zhou, C.; Lei, J. Multifunctional polyurethane-vitrimers completely based on transcarbamoylation of carbamates: thermally-induced dual-shape memory effect and self-welding. *RSC Adv.* **2017**, 7, 26858-26866.

22. Zheng, N.; Hou, J.; Xu, Y.; Fang, Z.; Zou, W.; Zhao, Q.; Xie, T. Catalyst-Free Thermoset Polyurethane with Permanent Shape Reconfigurability and Highly Tunable Triple-Shape Memory Performance. *ACS Macro Lett.* **2017**, 6, 326-330.

23. Delebecq, E.; Pascault, J.P.; Boutevin, B.; Ganachaud F. On the Versatility of Urethane/Urea Bonds: Reversibility, Blocked Isocyanate, and Non-isocyanate Polyurethane. *Chem. Rev.* **2012**, 113, 80-118.

24. Gamardella, F.; Ramis. X.; De la Flor, S.; Serra, A. Preparation of poly(thiourethane) thermosets by controlled thiol-isocyanate click reaction using a latent organocatalyst. *React. Funct. Polym.* **2019**, 134, 174-182.

25. Jaffrennou, B.; Droger, N.; Mechin, F.; Halary, J. L.; Pascault, J.P. Characterization, structural transitions and properties of a tightly crosslinked polythiourethane network for optical applications. *e-Polym.* **2005**, 82, 1618-7229.

26. Altuna, F.I.; Hoppe, C.E.; Williams, R.J.J. Shape memory epoxy vitrimers based on DGEBA crosslinked with dicarboxylic acids and their blends with citric acid. *RSC Adv.* **2016**, 6, 88647-88655.

27. Altuna, F.I.; Hoppe, C.E.; Williams, R.J.J. Epoxy vitrimers with a covalently bonded tertiary amine as catalyst of the transesterification reactions. *Eur. Polym. J.* **2019**, 113, 297-304.

28. Kelton; K.F. Kinetic and structural fragility-a correlation between structures and dynamics in metallic liquids and glasses. *J. Phys. Condens. Matter* **2017**, 29, 023002.

29. Angell, C.A. Formation of Glasses from Liquids and Biopolymers. *Science* **1995**, 267, 1924-1935.

European Polymer Journal 122 (2020) 109361

Supporting Information

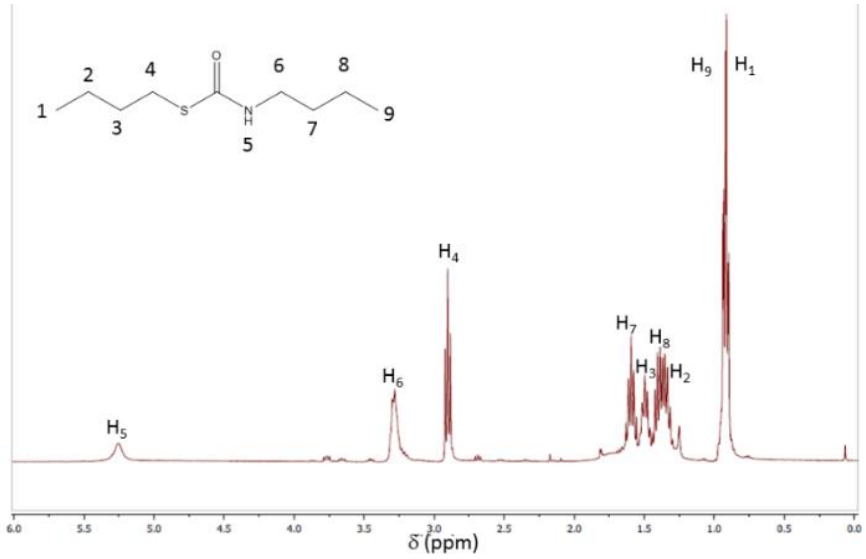

Figure VI-S1. *^{1}H NMR spectra of S-butyl butylcarbamothioate (L-L) in $CDCl_3$.*

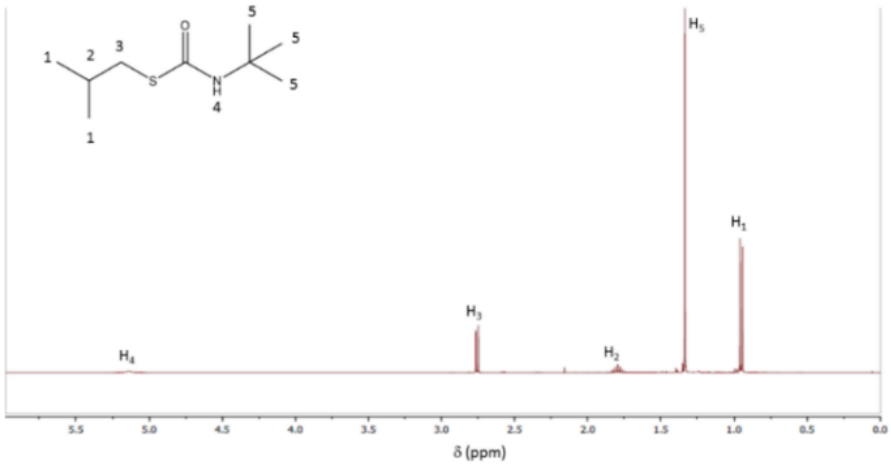

Figure VI-S2. *^{1}H NMR spectra of S-isobutyl tert-butylcarbamothioate (I-T) in $CDCl_3$.*

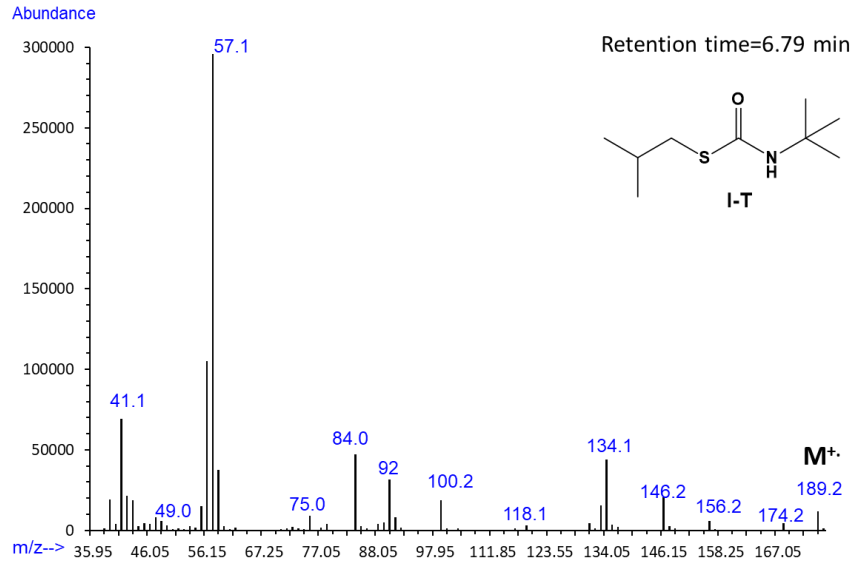

Figure VI-S3. *Mass spectra of the eluted product that corresponds to the S-isobutyl tert-butylcarbamothioate.*

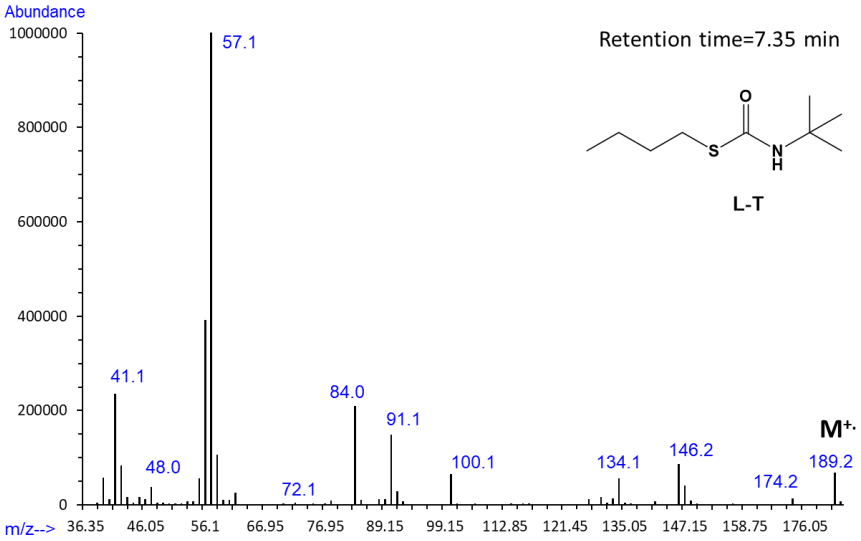

Figure VI-S4. *Mass spectra of the eluted product that corresponds to the S-butyl tert-butylcarbamothioate.*

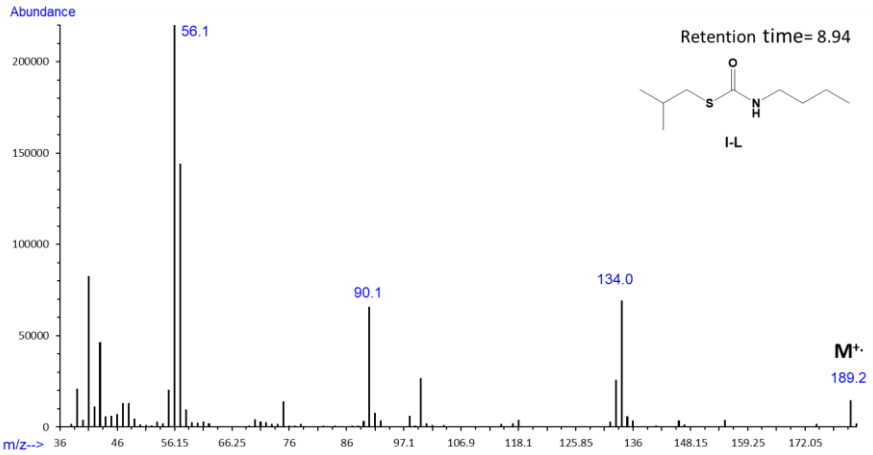

Figure VI-S5. *Mass spectra of the eluted product that corresponds to the S-isobutyl butylcarbamothioate.*

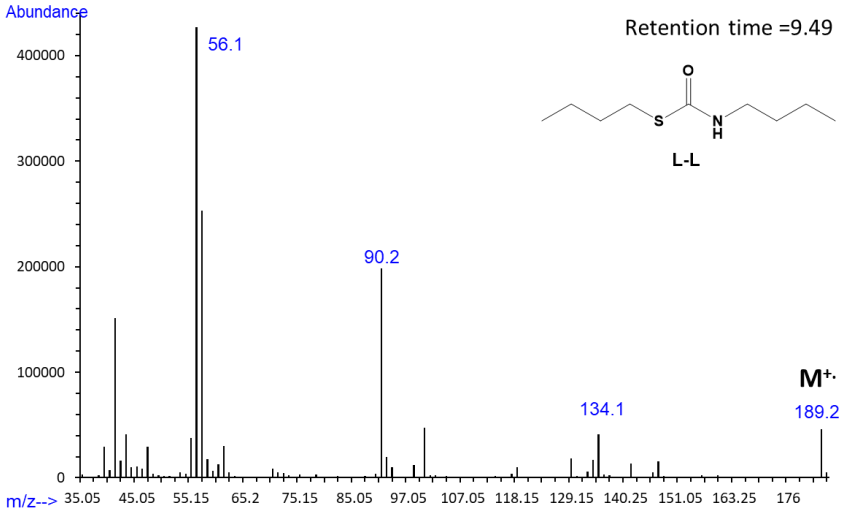

Figure VI-S6. *Mass spectra of the eluted product that corresponds to the S-butyl butylcarbamothioate.*

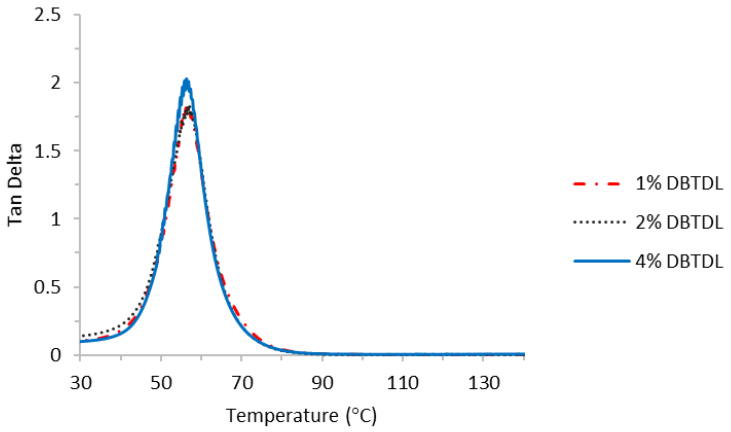

Figure VI-S7. *Tan δ against temperature of the materials prepared with different proportions of DBTDL.*

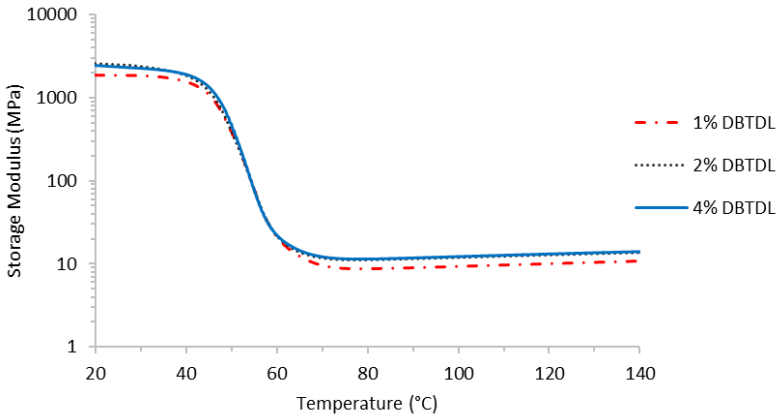

Figure VI-S8. *Storage Modulus against temperature of the materials prepared with different proportions of DBTDL.*

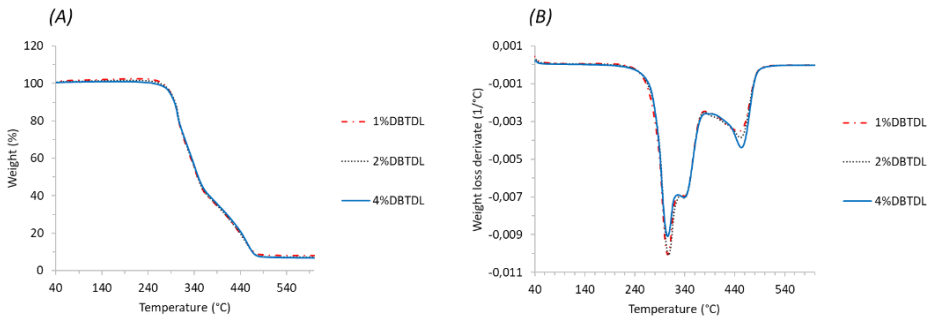

Figure VI-S9. *TGA curves of the samples prepared with different proportions of DBTDL (A). The rate of weight loss against temperature, DTGA (B).*

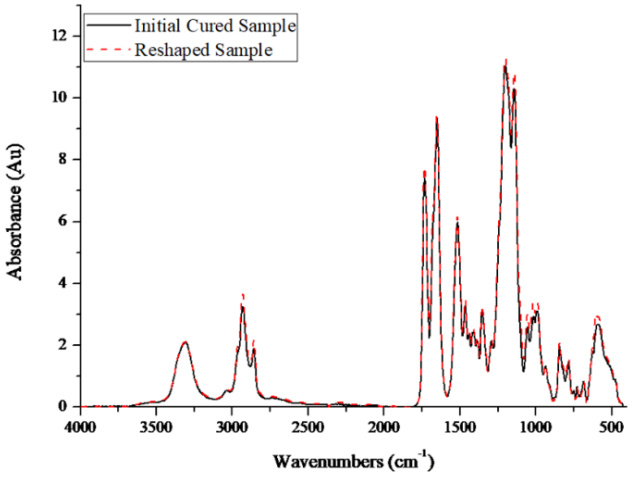

Figure VI-S10. *FTIR of poly(thiourethane) with a 4% of DBTDL before and after reshaping at 180 °C for 40 min registered at room temperature.*

Chapter VII

Recyclable poly(thiourethane) vitrimers with high T_g. Influence of the isocyanate structure

Reactive and Functional Polymers 151 (2020) 104574

Recyclable poly(thiourethane) vitrimers with high T_g. Influence of the isocyanate structure

Francesco Gamardella[1], Silvia De la Flor,[2] Xavier Ramis[3] and Angels Serra[1]

[1] *Dept.of Analytical and Organic Chemistry, Universitat Rovira i Virgili, C/ Marcel·lí Domingo, 43007, Tarragona, Spain*

[2] *Department of Mechanical Engineering, Universitat Rovira i Virgili, Av. Països Catalans, 26, 43007 Tarragona, Spain*

[3] *Thermodynamics Laboratory, ETSEIB Universitat Politècnica de Catalunya, Av. Diagonal, 08028, Barcelona, Spain*

Abstract

Networked poly(thiourethane) materials, with T_gs around 130 °C, were synthetized in stoichiometric proportions starting from two aliphatic isocyanates (isophorone diisocyanate, IPDI and 4,4'-methylene bis(cyclohexyl isocyanate), HMDI) and an aromatic diisocyanate (toluene-2,4-diisocyanate, TDI) with the same trithiol as comonomer (trimethylol propane tris(3-mercaptopropionate), S3) in presence of dibutyltin dilaurate (DBTDL) as the catalyst. The higher reactivity of TDI allowed the preparation of this material in absence of catalyst.

The evolution of the curing process was followed by FTIR. Thermomechanical studies were performed to determine their viscoelastic properties and their vitrimeric behaviour. The materials were able to reach a complete relaxation stress state thanks to the exchange process of the thiourethane moiety. Among them, TDI derived material experimented the fastest relaxation. The materials were also characterized by thermogravimetry and tensile tests.

The recycled materials, obtained by grinding the original thermosets and hot-pressing the powder, were fully characterized by mechanical, thermomechanical and FTIR studies; which allowed to confirm their recyclability without appreciable changes in the network structure. The presence of DBTDL in the materials was proved to be necessary to reach a good recyclability.

Keywords:

vitrimers; poly(thiourethane); thermosets; recyclability; covalent adapatable networks.

1. Introduction

Traditionally, polymers are classified in two main types: thermoplastic and thermosets depending on their thermal behaviour. Thermoplastics depending on their structure are subdivided into semicrystalline and amorphous polymers. The firsts have a relatively sharp melting point after which they can flow. The others become soft after their glass transition and more fluid as additional heat is applied. These characteristics allow them to be easily processed and recycled, but they are relatively weak, and they can suffer degradation by heat, solvents and environmental attack. On the other hand, thermosetting polymers, thanks to their permanent covalent bonds in the network structure, show outstanding mechanical and thermal properties, allowing them to be widely used in industrial applications where high mechanical performances and dimensional stability are required. However, their permanent three-dimensional structure hinders reshaping, reprocessing, or recycling once they are cured, resulting in a serious environmental issue. For these reasons, they are considered among the most difficult materials to be recycled.[1,2]

With the aim to combine the advantages of both type of polymers, thermoplastics and thermosets, in the last decades many researchers have focused their attention on the field of dynamic polymers. They were designed by incorporating reversible covalent bonds into the polymeric network to obtain the so called CANs (covalent adaptable networks).[3-5] With this approach, a “third” class of polymers, called vitrimers, was discovered in 2011 by Leibler and co-workers, who reported the malleability of both epoxy-carboxylic acid and epoxy-anhydride networks.[6] These materials can lead to topological rearrangement via transesterification, keeping constant their crosslinking density.[7]

To develop new CANs, different reversible exchange reactions have been explored, such as: transesterification,[6,8] transamination,[9,10] disulfide exchange,[11,12] transalkylation,[13] siloxane equilibrium,[14] dioxaborolane metathesis,[15] amine-urea exchange,[16] and transcarbamoylation.[17,18]

If we focus our attention on the family of vitrimers based on poly(urethane) structures, it should be mentioned that Tobolsky and co-workers in 1956[19] observed that poly(urethane)s could experiment chemical stress relaxation at high temperature. However, this article had not attracted much attention and the explanation of this behaviour was not completely clarified. Recently, carbamate exchange has been recognized as the responsible of the vitrimeric behaviour of poly(urethane) thermosets, and it constitutes one of the most used mechanism in the preparation of dynamic networks.[20-24] Poly(urethane)s, thanks to their structural versatility, have a broad range of applications in different industrial fields as elastomers, coatings, rigid foams and adhesives.[25]

Poly(thiourethane)s (PTUs) are related to their oxygen counterparts, showing comparative properties due to the presence of similar hydrogen bonding, but they possess several advantages. The formation of PTUs from isocyanates and thiols is described as a *click-type* reaction; therefore, it is not accompanied by side-reactions contrary to what occurs in the poly(urethane) synthesis.[26,27] Moreover, poly(thiourethane) thermosets show a high refractive index thanks to the presence of sulphur into the backbone of the polymeric structure, making them good candidates for optical applications.[28,29]

Recently, our research group[30] demonstrated that PTUs derived from 1,6-hexamethylene diisocyanate (HDI) and trimethylolpropane tris(3-mercaptopropionate) (S3) can behave as vitrimers when stoichiometric ratios of thiol-isocyanate were reacted in the presence of a Lewis acid catalyst, such as dibutyltin dilaurate (DBTDL). The reversible thiocarbamate exchange was demonstrated by means of equilibrating model compounds. Moreover, the influence of the proportion of catalyst in the vitrimeric characteristics of poly(thiourethane) thermosets was also demonstrated. Similarly, Torkelson and co-workers[31] reported that thiourethane linkages, based on an aromatic diisocyanate monomer, follow associative and dissociative reversible pathways, depending on whether an excess or a stoichiometric amount of thiol has been added to the formulation. In both cases, they use the simultaneous presence of two different catalysts, triphenylphosphine and 1,8-diazabyciclo [5.4.0] undec-7-ene (DBU) and the crosslinked materials have an elastomeric nature. By using model compounds and by means of TGA coupled with gas-chromatography and mass spectrometry they proved the dissociative character of exchange mechanism, but these aromatic poly(thiourethane) materials did not lead to significant changes when the material was reprocessed.

Although both articles focused on the reprocessable character of poly(thiourethane) networks, the relaxation rates were very different, about 8 min to reach a value of σ/σ_0 = 1/e at 180 °C in the case of our previous studies, and less than 10 s at 150 °C in the Torkelson's work. These differences could be related to the aromatic character of the isocyanate selected as the monomer, the lower crosslinking density they reached, due to the presence of the long poly(propylene oxide) structures in the isocyanate monomer, which leads to T_gs around -25 °C, and the differences in the catalysts and their proportions.

Despite the previous work reported on this topic, the nature of the stress relaxation and reprocessing of this class of materials remains quite unexplored. Herein, we investigate the potentiality of this class of dynamic polymers based on poly(thiourethane) networks, to obtain vitrimers with high glass transition temperatures (T_g) and a fast exchange mechanism. This remains one of the most challenging goals in this field, since almost all the vitrimers reported in the literature

show T_gs lower than 100 °C, which limits their applicability in some industrial fields, where high thermal and mechanical performance at elevated temperature is required. In the literature, we found only few reports on reprocessable thermosets with high T_g: a self-healable epoxy-anhydride thermoset based on renewable vanillin and guaiacol starting compounds with a T_g of 187 °C,[32] but with broad relaxation processes, a lignin-based vitrimer for recoverable adhesive with T_g in the range from 95 to 133 °C,[33] and a vitrimer based on silyl ether exchange reported by Guan *et al*. with a T_g of 125 °C.[34]

It should be taken into account, that the viscoelastic properties of vitrimers at high temperatures are firstly controlled by the velocity of the dynamic exchange mechanism responsible of the vitrimeric behaviour, which can be accelerated by increasing the amount of catalyst,[8,28] or by the presence of unreacted groups in non-stoichiometric systems. Secondly, the macroscopic flow can be influenced by the network architecture. The introduction of flexible structures seems to increase the rate of the exchange mechanism, leading in some cases to elastomeric characteristics.[35]

Encouraged by the results of our previous work, we selected three different diisocyanates with a rigid structure to prepare PTUs with high T_g and to explore the influence of the macromolecular architecture on their viscoelastic properties at high temperatures. Two of the diisocyanates selected are aliphatic: isophorone diisocyanate (IPDI) and 4,4'-methylene bis(cyclohexyl isocyanate) (HMDI) while toluene 2,4-diisocyanate (TDI) was selected as an aromatic one. We chose trimethylolpropane tris(3-mercaptopropionate) (S3) as trifunctional thiol. The structure of these compounds is represented in Scheme VII-1. Thiol and isocyanate groups were reacted in stoichiometric proportions and a Lewis acid (dibutyltin dilaurate, DBTDL) was used as the catalyst. Taking advantage of the high reactivity of aromatic isocyanates, we prepared a PTU, derived from TDI, in absence of catalyst to study its possible vitrimeric behaviour.

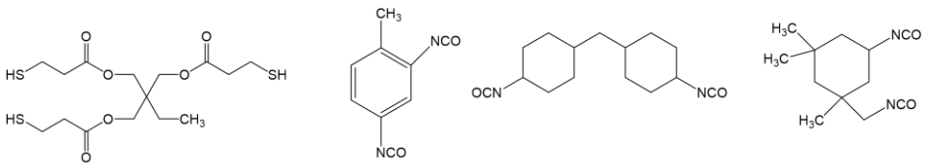

S3 **TDI** **HMDI** **IPDI**

Scheme VII-1. *Structure of the starting compounds*

2. Experimental part

2.1 Materials

Trimethylolpropane tris(3-mercaptopropionate) (S3), toluene 2,4-diisocyanate (TDI) and dibutyltin dilaurate (DBTDL) from Sigma-Aldrich were used as received. Isophorone diisocyanate (IPDI) and 4,4'-methylene bis(cyclohexyl isocyanate) (HMDI) from Acros Organics were used without previous purification.

2.2. Preparation of the formulations

The different diisocyanates and S3 were mixed in stoichiometric proportions: 2 mol of S3 per 3 mol of the selected diisocyanate. The catalyst, DBTDL, was first dissolved in the isocyanate and the corresponding amount of thiol was then added. The formulations with aliphatic diisocyanates were prepared with 4 phr of DBTDL (parts of catalysts per hundred parts of thiol), while the formulations with TDI were prepared with 2 phr of DBTDL or without, due to the higher reactivity of the aromatic diisocyanate towards thiol. The mixtures were manually stirred until homogeneity at room temperature, and freshly used.

Table VII-1. *Formulations used to prepare poly(thiourethane) thermosets.*

Sample	Formulation	Diisocyanate (g)	Thiol (g)	DBTDL (g)
IPDI	S3_IPDI_4%DBTDL	1.67	2.00	0.08
HMDI	S3_HMDI_4%DBTDL	1.97	2.00	0.08
TDI	S3_TDI_2%DBTDL	1.31	2.00	0.04
TDI_nc	S3_TDI_0%DBTDL	1.31	2.00	-

For a better understanding, the formulations detailed in Table VII-1 have been designed with an acronym that represents the isocyanate chosen in the preparation of the material. TDI_nc accounts for the material prepared from TDI without any catalyst.

2.3. Sample preparation

For DMTA analysis, films were prepared by pouring the formulations on pre-silanized glasses and using Teflon spacers to ensure a homogeneous thickness of 0.5 mm. The formulations were cured at 80 °C, 100 °C, 125 °C for 1h at each temperature and 160 °C for 2 h. In the case of free catalyst formulation, a post curing at 175 °C for 2h was required. The films were die-cut to obtain a rectangular specimen of 20 x 5 x 0.5 mm^3 dimensions.

2.4. FTIR analysis

To monitor the evolution of isocyanate/thiol groups during the isothermal curing at 130 °C and to quantitatively determine the rate of curing, a FTIR spectrometer Bruker Vertex 70 with an attenuated total reflection accessory with thermal control and a diamond crystal (Golden Gate Heated Single Reflection Diamond ATR Specac-Teknokroma) and equipped with a mid-band liquid nitrogen-cooled mercury-cadmium-telluride (MCT) detector was used. Real-time spectra were collected in absorbance mode with a resolution of 4 cm^{-1} in the wavelength range 4000 to 600 cm^{-1} averaging 10 scans for each spectrum. The spectra were corrected for the wavelength dependence of the absorbance in ATR devices. The characteristic absorbance peak of the isocyanate at 2280 cm^{-1} (vibration of -N=C=O groups) was used to monitor the conversion of the isocyanate group during thiol-isocyanate reaction. Absorbance of each scanned sample were normalized with that of the S3-ester group at 1720 cm^{-1}. Isocyanate group conversion (X_{NCO}) were calculated by Eq. 1.

$$x_{NCO} = 1 - \frac{A_{2280}}{A_{2280,0}} \quad (1)$$

where A_{2280} and $A_{2280,0}$ are the normalized absorbances of the isocyanate peak at 2280 cm^{-1} at a given reaction time and at the beginning of the curing process.[36]

2.5. Dissolution experiments

Dissolution experiments of cross-linked polymers were performed by the following procedure. Pieces of poly(thiourethane) samples of 0.2-0.3 g, which were weighed before the experiment, were placed into a vial. The vial was filled with 1,2-dichlorobenzene, closed and heated at 150 °C for 24 h and then the vial was cooled down to room temperature. The polymer sample was washed by dichloromethane and the sample was then dried under reduced pressure at 80 °C overnight. After cooling down to room temperature, the sample was weighed, and the gel fraction was calculated.

2.6. Thermal degradation studies

The thermal stability of the cured samples was studied by thermogravimetric analysis (TGA), using a Mettler TGA/SDTA 851e thermobalance. All experiments were performed under inert atmosphere (N_2 at 100 mL/min). Pieces of cured samples of 10-15 mg were degraded between 30 and 600 °C at a heating rate of 10 °C/min.

2.7. Stress relaxation tests

Tensile stress relaxation tests were conducted in a DMA Q800 analyser using a film tension clamp on samples with the same dimensions as previously defined. The sample was firstly equilibrated at 160 °C and left isothermally at this temperature for 3 min, then a constant strain of 1.5 % (to ensure the material is within the linear range) was applied on the sample and the consequent stress level was measured as function

of time. Then the strain was removed, and the process was repeated every 5 °C until the final test temperature, 190 °C, is reached. The relaxation stress $\sigma(t)$ was normalized by the initial stress σ_0 and the relaxation times (τ) were determined as the time necessary to relax $0.37 \cdot \sigma_0$ i.e. ($\sigma = 1/e \cdot \sigma_0$). With the relaxation times obtained at each temperature, the activation energy values E_a were calculated for each vitrimer, using an Arrhenius-type equation:

$$\ln(\tau) = \frac{E_a}{RT} - lnA \quad (2)$$

where, τ is the time needed to attain a given stress relaxation value ($0.37\sigma_0$), A is a pre-exponential factor and R is the gas constant. From the Arrhenius relation, the temperature of topology freezing (T_v) was obtained as the temperature at which the material reaches a viscosity of 10^{12} Pa·s. Using Maxwell's relation and E' determined from DMTA (assuming E' being relatively invariant in the rubbery state), τ^* was determined to be around 10^5 s in our systems. The Arrhenius relationship was then extrapolated to the corresponding value of τ^* to determine T_v in each sample.

To compare the time to reach the complete relaxation of the stress (i.e. a normalized stress less than 10^{-2}) of the poly(thiourethane) vitrimers obtained with different diisocyanates, a single stress relaxation test was performed at the temperature of 180 °C with the same constant strain of 1.5 %.

2.8. Creep experiments

Creep and recovery properties were studied in tension by the same DMA Q800 apparatus equipped with the film tension clamp. All the samples were stretched under a stress of 0.1 MPa at 180 °C for 30 min, then the stress was immediately released, and the sample was left to recover for 30 min.

For the determination of the viscosity at each temperature needed for the representation of the Angell fragility plot, a series of creep experiments were carried out on films at temperatures between 130 and 180 °C, increasing 10 °C in each scan. To perform the tests, the selected temperature was equilibrated for 3 min and then a stress level of 0.1 MPa was applied for 30 min. The viscosity η (Pa·s) was obtained from the creep plots, considering the linear part of variation of the strain and fitting it with a linear regression. The strain rate $\dot{\varepsilon}$ was determined from the slope of the linear fit. The viscosity η was calculated using the following expression:

$$\eta = \frac{\sigma}{\dot{\varepsilon}} \quad (3)$$

and represented in front of T_g/T thus obtaining the Angell fragility plot.

2.9. Dilatometry tests

Dilatometry experiments in tension were performed with the film tension clamp in the DMA Q800 analyzer on the different PTU samples with the same dimensions as

described before. The length of the sample was continuously measured while increasing the temperature at a heating rate of 1 °C/min from 25 to 250 °C. A slight stress of 0.01 MPa was applied during the experiment to avoid buckling.

2.10. Recycling

Original and recycled samples were tested until break in tensile mode at room temperature using an electromechanical universal testing machine (Shimadzu AGS-X) with a 1000 N load cell at 5 mm/min and using Type V samples according to ASTM D638-14 standard. Three samples of each material were analyzed and the results were averaged.

The recycled samples were obtained by grinding the crosslinked polymers, and hot pressing into an aluminium mould at 165 °C for 2.5 h with 8 MPa. In order to analyse the average size of the powder obtained, a micrograph was taken with an optical microscope. The image taken was processed and analysed obtaining the average value and the maximum size of the particles. The new film obtained were die-cut in Type V samples and were tested under the same conditions.

3. Results and discussion

3.1 Study of the curing process

Although the preparation of poly(thiourethane) thermosets can be accomplished with the help of basic and acid catalyst, their vitrimeric characteristics are enhanced by the presence of a Lewis acid. In our previous papers,[26,30] we determined how small amounts of DBTDL (0.5-1 phr) were enough to reach fully crosslinked poly(thiourethane) networks. However, the amount of catalyst had a great influence in the rate of the relaxation process when studying their vitrimeric behaviour. Thus, 4 phr of DBTDL were added in the preparation of the vitrimer obtained from HDI and S3 to shorten the relaxation time. According to that, we selected this proportion of DBTDL for preparing the samples with the aliphatic isocyanates selected, but the high reactivity of the aromatic diisocyanate forced us to reduce the amount of catalyst to 2 phr. Since this compound was highly reactive, we also prepared samples with S3, without any catalyst, reaching a fully cured material.

The evolution of the thiol-isocyanate reaction during the curing process was followed by FT-IR spectroscopy to investigate the kinetics of the reaction and how the different isocyanate monomers could influence the rate and curing schedule. In the spectrum, the reduction of the isocyanate peak, at 2280 cm^{-1}, was accompanied by the appearance of N-H st. (3350 cm^{-1}) and carbonyl st. (1670 cm^{-1}) of the thiourethane groups, which are indicative of the poly(thiourethane) formation. The carbonyl absorption of the thiourethane groups is partially overlapped with the carbonyl ester absorption of the thiol, taken as the reference band, and the deconvolution was done in order to extract quantitative information.

The isothermal curing temperature in the FTIR/ATR experiments for kinetics evaluation was set at 130 °C and the evolution of the curing process was followed by the diminution of the isocyanate band. Figure VII-1 shows the conversion curves against time for all the formulation studied. As we can see in Figure VII-1, all the reactions proceed quickly during the first minutes and then they slow down. However, it is evident that the aromatic isocyanate, TDI, leads to the fastest reaction, even without catalyst. Among the aliphatic diisocyanates, the reactivity of IPDI is higher than HMDI. Since a plateau is reached at long reaction times, higher temperatures must be used in order to reach full cure. Therefore, to cure the samples for mechanical and thermal characterization we performed a post-curing at 160 °C for 2 h and proved the full conversion by FTIR (see Fig VII-S1, in supporting information).

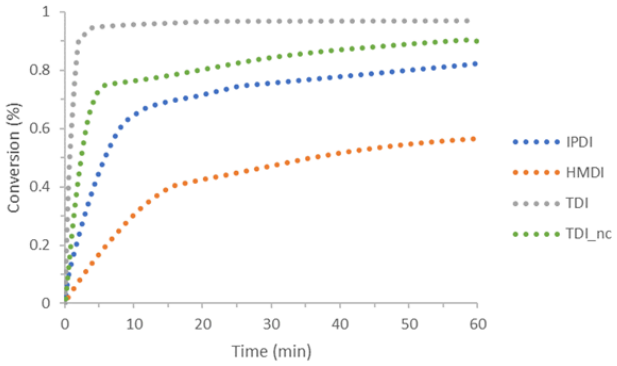

Figure VII-1. *Kinetic profile at 130 °C of the conversion of NCO group in the different poly(thiourethane) formulations obtained from FTIR analysis.*

3.2. Characterization of the thermosets

To prove the thermosetting character of the poly(thiourethane)s prepared, we determined the gel content of all the samples in 1,2-dichlorobenzene for 24 h at 150 °C, the calculated values are collected in Table VII-2. Once, the solvent was completely removed the gel content was higher than 95% in all the materials tested, verifying their thermosetting nature.

The thermal stability of the PTUs was analysed by TGA and the weight loss and the derivative curves are shown in Figure VII-2. The data extracted from these experiments are collected in Table VII-2.

As we can see in Figure VII-2A, there are not many differences among all the materials evaluated, neither in the stability nor in the degradation processes. The degradation mechanism is quite complex, with three different stages although partially overlapped. The reversion of the urethane to isocyanate in poly(urethane)s (PUs) between 120-250 °C is described in the literature.[37,38] Thus, we can deduce that in PTUs this reversion could also occur. However, in Figure VII-2B the first degradation

process leading to weight loss begins at 220 °C, with a maximum degradation rate above 300 °C. This indicates a higher thermal stability of PTUs in front of PUs. The peaks at higher temperatures can be attributed to the β-elimination processes of the esters present in the network structure.

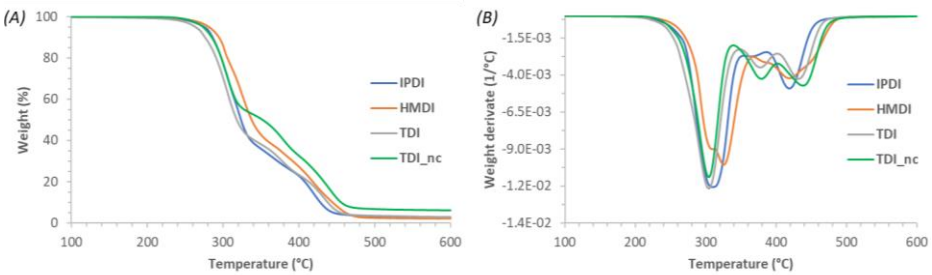

Figure VII-2. *(A) TGA curves and (B) DTG curves of the different poly(thiourethane)s prepared.*

In Table VII-2, we can see that the temperature for the 2% of weight loss is around 260 °C for the PTUs based on aliphatic monomers. When the isocyanate is TDI, this temperature is slightly lower ($T_{2\%}$=243 °C), indicating that the aromatic PTUs are less stable at high temperatures than the aliphatic ones. However, the material prepared from TDI without any catalyst begins to degrade at higher temperature, indicating that the first degradation process is catalysed by DBTDL. The thermoset that shows the highest stability is the one obtained from HMDI isocyanate. The lower temperature of initial degradation in aromatic poly(thiourethane)s in comparison with the aliphatic ones could be related to a partial dissociative character of the aromatic, as it has been previously reported.[21,30,31]

Table VII-2. *Gel content, thermal stability and thermomechanical data of the thermosets prepared.*

Sample	Gel content (%)	$T_{(2\%)}$[a] (°C)	T_{max}[b] (°C)	$T_{tan\ \delta}$[c] (°C)	FWHM[d] (°C)	E'[e] (MPa)
IPDI	97	255	310/379/419	129	12.6	11.5
HMDI	95	262	325/367/419	124	13.6	10.7
TDI	99	243	304/378/431	128	13.0	13.9
TDI_nc	98	258	304/379/438	126	14.4	11.0

[a] Temperature of the 2% of weight loss

[b] Temperature of the maximum rate of the three-step degradation

[c] Temperature of the maximum of the tan δ peak.

[d] Full width at half maximum of the tan δ peak.

[e] Relaxed modulus determined at the temperature of the maximum of tan δ peak + 30 °C

In order to investigate the thermomechanical behaviour of all the materials prepared from the three diisocyanates selected, a DMTA analysis was conducted. Fig. VII-3A and 3B show the evolution of *tan δ* and storage modulus with temperature. The main data extracted from these curves are collected in Table VII-2.

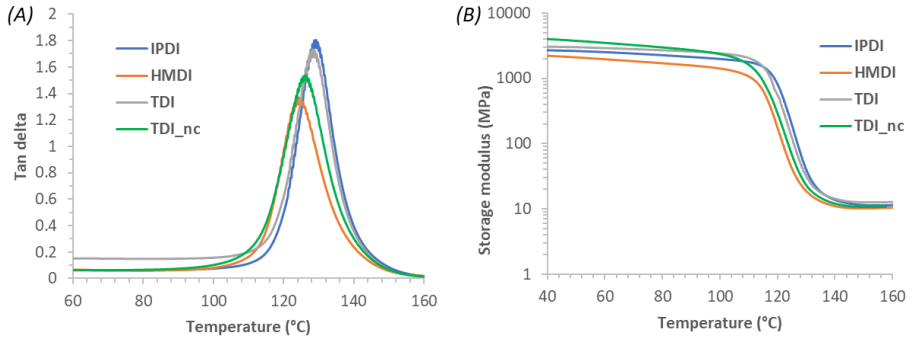

Figure VII-3. *(A) Tan δ and (B) storage modulus evolution with temperature for the different materials prepared.*

All the curves of the materials prepared show a *tan δ* peak higher than 120 °C, without many differences among them. The *tan δ* curves are quite narrow indicating the formation of uniform network structures (see Table VII-2) with a FWHM around 13 °C, thanks to the click reaction mechanism. The relaxation of the materials takes place sharply with a significant change in the moduli from the glass to the rubbery state. There are no significant differences in the relaxed moduli, but the thermoset prepared from TDI in the presence of catalyst leads to the highest value meaning that the use of DBTDL as the catalyst in TDI formulations seems to increase slightly the degree of crosslinking achieved.

3.3. Vitrimeric characterization

The viscoelastic properties at elevated temperatures were determined by stress relaxation experiments in DMTA to investigate the influence of the structure of the isocyanate in the different PTUs prepared.[30] At the selected temperatures, a constant strain of 1.5 % was applied on the samples and the stress was followed as function of time and the characteristic relaxation times ($\tau_{1/e}$) were determined as the point when a relaxation value of 1/e (σ/σ_0=0.37) was reached.

The stress relaxation curves of the different PTUs are presented in Figure VII-4, we can see that all the materials can completely relax the stress at high temperature, showing the expected vitrimeric characteristics.

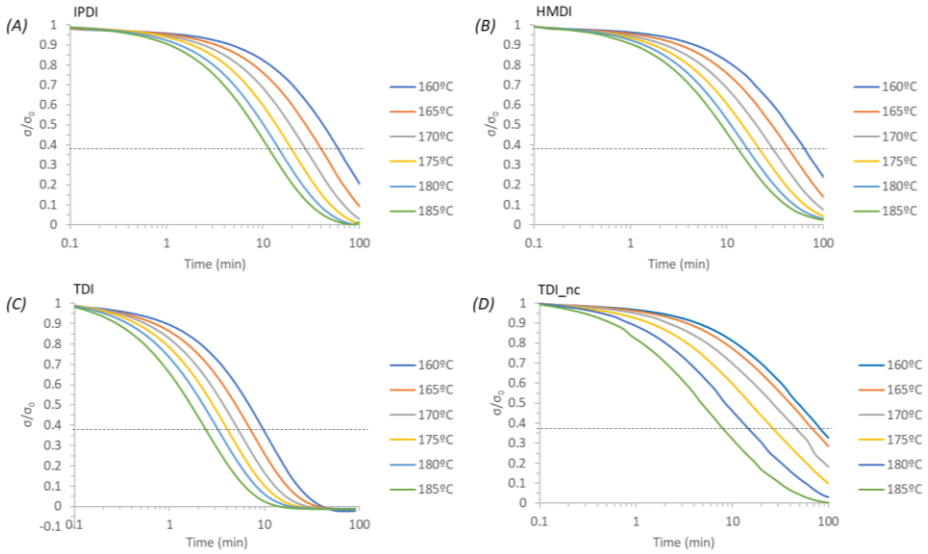

Figure VII-4. *Normalized stress relaxation plots as a function of time at various temperatures from (160 to 185 °C) during 100 min for the different poly(thiourethane) samples. The value of* $\sigma/\sigma_0 = 0.37$ *is highlighted.*

For comparative purposes, the stress relaxation curves at 180 °C of the different PTUs are presented in Figure VII-5A and the characteristic relaxation times ($\tau_{1/e,180°C}$) are collected in Table VII-3.

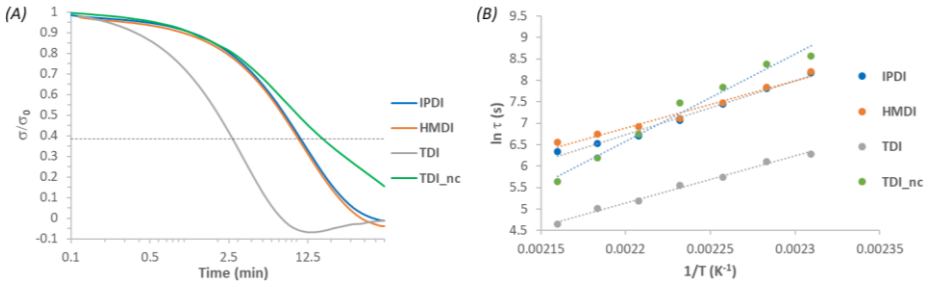

Figure VII-5. *Normalized stress relaxation behaviour at 180 °C (A). Arrhenius plot of relaxation times against the inverse of temperature measured by stress-relaxation experiments for the PTUs prepared (B).*

As we can see in Figure VII-5A, the relaxation process of the aromatic poly(thiourethane) prepared with DBTDL as the catalyst is the fastest one, reaching the 63 % of stress relaxation in only 2.9 min. On the other hand, the TDI sample without DBTDL needs 18.4 min to reach the same relaxation level under the same conditions. This means that although DBTDL is not required to reach a complete curing it affects considerably the rate of rearrangement of the groups responsible of the network relaxation. In a previous paper[30] we demonstrated that trans-thiocarbamoylation can occur in this type of materials, allowing the network to relax

and opening the possibility of reshaping. In that work, it was put in evidence that the amount of catalyst affects considerably the relaxation rate. In Figure VII-5A no differences in the relaxation rate, between aliphatic PTUs, are observed.

As shown in Figure VII-4, there is a clear dependence of the relaxation time on the temperature for all the PTUs prepared, fitting perfectly with an Arrhenius-like relaxation behaviour (see Figure VII-5B). By the Arrhenius equation, the activation energy (E_a) of the exchange mechanism and the topology freezing transition temperature, T_v (the temperature at which the material reaches a viscosity of 10^{12} Pa·s, i.e. $\tau \approx 10^5$ s) were determined and the values are collected in Table VII-3. It should be noted, in Figure VII-5B, the different behaviour of the TDI material without catalyst in reference to the others. This material relaxes faster than the aliphatic PTUs at high temperature, but slower at low temperature. Again, this could be related to the differences in the exchange mechanism in the sample without catalyst that can experiment variations in the associative/dissociative competitive mechanisms at different temperatures. Nevertheless, the fastest material in the relaxation process is the aromatic PTU in all the temperature range, although it has a lower proportion of DBTDL than aliphatic PTUs.

Table VII-3. *Time to reach a value of σ/σ_0=0.37 at 180 °C, topology freezing temperature, kinetic and adjusting parameters for the Arrhenius equation.*

	Relaxation experiment				*Creep experiment*	
Sample	$\tau_{1/e,180°C}$ **(min)**	T_v **(°C)**	E_a **(kJ/mol)**	r^2	E_a **(kJ/mol)**	r^2
IPDI	11.1	117±5	107±5	0.99	130±7	1.00
HMDI	10.7	110±8	92±6	0.98	130±4	0.99
TDI	2.9	88±4	91±3	0.99	115±5	0.99
TDI_nc	18.4	137±7	186±14	0.98	144±9	0.99

The aliphatic structures rend values of E_a in the range of 92 to 107 kJ/mol, slightly higher than those determined for hexamethylene diisocyanate derived materials (which was 72 kJ/mol).[30] The role of the catalyst in the rearrangement process is evidenced by the value of the activation energy, reducing it from 186 to 91 kJ/mol in TDI derived materials. The former activation energy is in agreement with the value of 183.7 kJ/mol reported by Xie *et al.*[39] who prepared a catalyst-free polyurethane thermoset based on an aromatic diisocyanate (4,4'-methylene bis(phenyl isocyanate)).

It should be mentioned that the materials obtained in this work (except that prepared without catalyst) present a hypothetical T_v lower than T_g (from DMTA characterization) although at temperatures below T_g no segmental movement occurs

to allow the exchange reaction. By heating above the T_g of the materials, the segmental movement starts gradually while the exchange reactions are already fast, and the exchange reaction becomes the dominating factor for the stress relaxation.[9,34,40] For this reason, the materials prepared, especially the aromatic poly(thiourethane) with catalyst, have a very fast relaxation process.

To further analyze the viscoelastic properties of the PTUs and to confirm that the PTUs behave like a viscoelastic liquid at elevated temperatures, the effect of the temperature on the creep behaviour was studied. Figure VII-6 shows the creep behaviour for all the samples at 130 °C (temperature around $T_{tan\,\delta}$) and at 180 °C (temperature around $T_{tan\,\delta}$ + 50 °C to assure a high mobility).

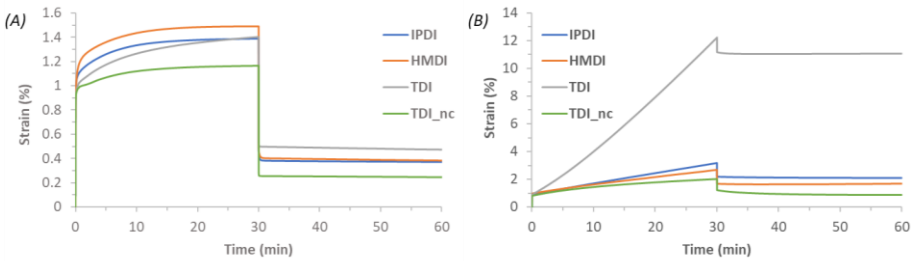

Figure VII-6. *Creep recovery curves at 130 °C (A) and 180 °C (B) for all the PTUs prepared.*

Thermosets generally exhibit good resistance to creep thanks to their permanent network structure, presenting a constant deformation in time when a constant external stress is applied, and no plastic deformation appears when the stress is released. Contrarily, our materials, when tested at 130 °C with a constant stress, increase the deformation progressively, presenting a slight plastic deformation when the stress returns to zero. This increase in deformation with time (deformation rate) is higher at higher temperature (180 °C) confirming that the PTU vitrimers behave like a viscoelastic liquid. At this temperature, the materials recover only their initial elastic response and a permanent deformation remains due to the topological rearrangement of the network structure. The material prepared from TDI in the presence of DBTDL shows a very high deformation rate at 180 °C and, consequently, a very high plastic deformation, confirming the outstanding vitrimeric characteristics of this material.

From the creep experiments, the viscosities at different temperatures can be deduced for each sample and represented in the Angell fragility plot. In this plot (Figure VII-7) the variation of the viscosity with the inverse of temperature, scaled to T_g, is presented for all the materials. At temperatures higher that their T_g, all of them behave as “strong glass formers” like inorganic silica materials. The exchange reactions follow an Arrhenius law, in contrast to the behaviour of thermoplastic materials, which are “fragile liquids”. From these plots it is possible to obtain the activation energy for all

the materials tested (results are presented in Table VII-3). As it can be seen, the activation energies are slightly different from those obtained from relaxation tests but follow the same trend: the lowest E_a is obtained for TDI materials in the presence of catalyst and the highest is in absence of DBTDL. The aliphatic PTUs show the same E_a, as expected.

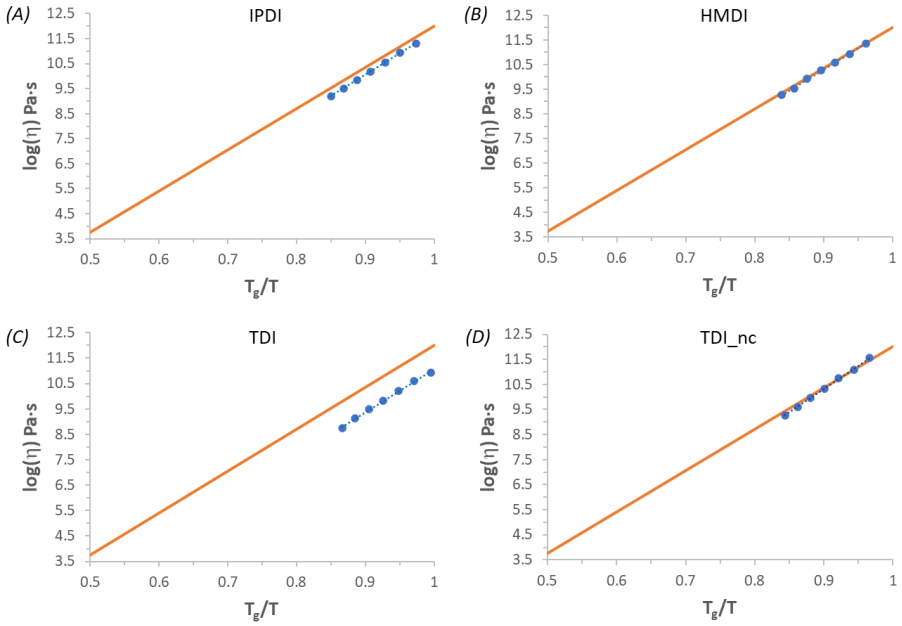

Figure VII-7. *Angell fragility plot representing the logarithm of the viscosity as a function of the inverse temperature, scaled to T_g (assuming T_g as $T_{tan\,\delta}$), for the different materials. The relation for silica is included as a reference of an ideal strong liquid.*

Network relaxation was also analysed by dilatometry experiments and the behaviour for all the samples is collected in Figure VII-8. Classical thermosets exhibit a lower thermal expansion coefficient (CTE) in reference to the non-crosslinked polymers and above their T_g the CTE remains constant for a permanently crosslinked network, In Figure VII-8 two changes in the slope of CTE can be appreciated, a first one at $T=T_g$, after which the slope remains constant, as observed in thermosetting polymers. The second change occurs when the exchange reactions start, leading to a significant increase in CTE, typical of the vitrimeric behaviour.

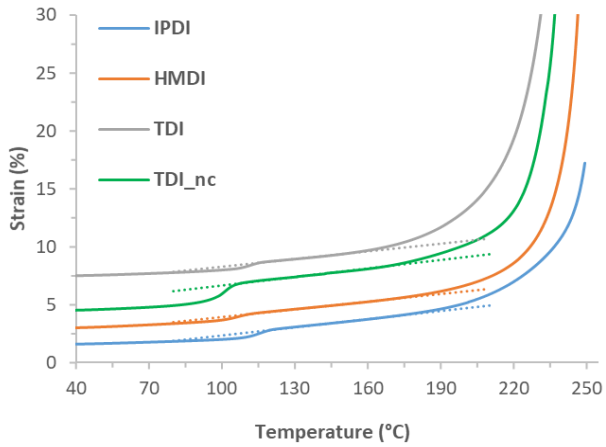

Figure VII-8. *Dilatometry experiments performed with a heating rate of 1 °C/min for the different materials (the curves are shifted only for a better understanding).*

3.4. Recyclability

To investigate the recyclability of the crosslinked PTUs prepared, the materials were grinded into small particles and the powder obtained was hot pressed at 165 °C for 2.5 h to obtain the recycled films. In order to determine the average size of the powder obtained, a micrograph was taken with an optical microscope and the particle size measured. The average size measured was 1.2 mm with a standard deviation of 0.6 mm and the maximum size was 2.4 mm.

As we can see in Figure VII-9, the original materials show good transparency and an excellent uniformity, properties that are quite well preserved with only a slight colour change after recycling.

To fully characterize the original and the recycled samples, they were subjected to uniaxial tensile test until break, DMTA and FTIR analysis. Dog-bone-shaped samples (Figure VII-S2) of all the original and recycled poly(thiourethane)s were tested with a universal tensile machine. The stress-strain behaviour of the virgin materials was registered and compared with the recycled ones.

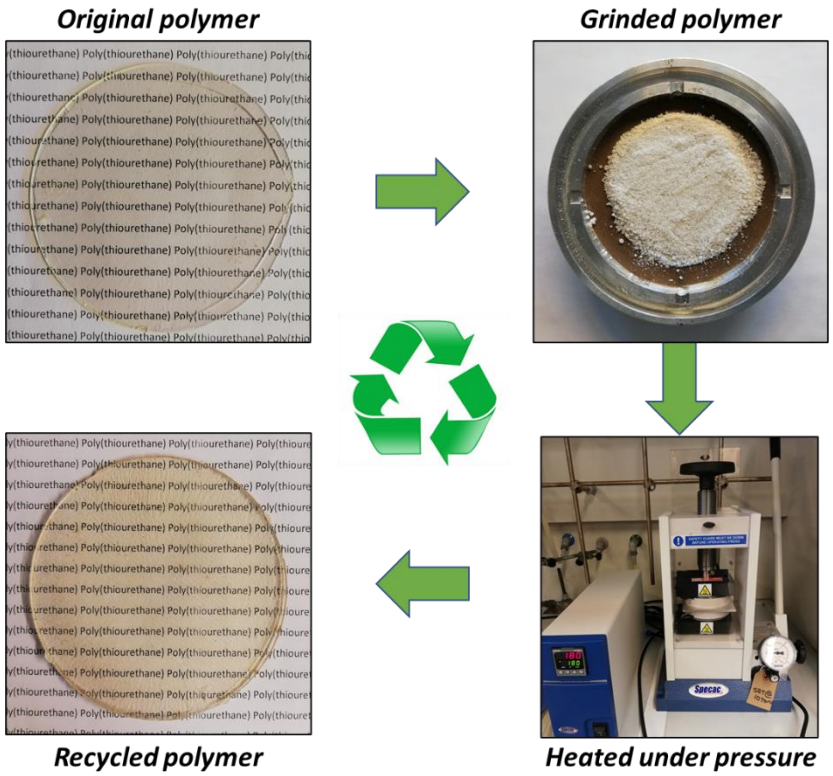

Figure VII-9. *Photographs of the original, grinded and recycled sample, together with the hot press device used in the reprocessing.*

Results from the tensile tests show that all the original materials are relatively rigid at room temperature and do not experiment high deformations before breaking due to their crosslinked character. The rigid structure of the isocyanates selected is reflected in the notable high moduli reached in all the samples, being the lowest value for the HDMI vitrimers thanks to its more flexible structure. With respect to the stress and strain at break values, the materials behave similarly, being again the HDMI the one that presents higher ductility. The TDI-nc is the one with lower strength, probably due to its network heterogeneity and slightly lower crosslinking density.

It can be appreciated in Table VII-4 that all materials behave mechanically quite well after the recycling process. The rigidities of the recycled samples remain similar while their strength is around 70% of the original value for the aromatic PTU with catalyst and 60% for the aliphatic ones. It is important to remark the extremely harsh conditions of the recycling process. The mechanical grinding can affect the integrity of all the bonds forming the network structure and not only those in thiourethane groups. The fact that the materials are not elastomers but thermosets with a high T_g and rigidity, also complicates the achievement of high quality samples.

Table VII-4. *Tensile data of the original and recycled PTUs and DMTA data of the reprocessed materials. For comparison purposes, the DMTA data of original materials in Table VII-2 have also been included. The mean value of three different samples tested is shown. Coefficients of variations are less than 7 % for stress and strain results and less than 5 % for the tensile moduli.*

Original						
Sample	E^a **(GPa)**	$\sigma_{max}{}^b$ **(MPa)**	$\varepsilon_{max}{}^c$ **(%)**	$T_{tan\delta}{}^d$ **(°C)**	**FWHM^e (°C)**	E'^f **(MPa)**
IPDI	5.1	154.8	4.4	129	12.6	11.5
HMDI	3.1	140.7	5.9	124	13.6	10.7
TDI	5.2	155.4	3.3	128	13.0	13.9
TDI_nc	4.8	126.5	3.2	126	14.4	11.0
Recycled						
Sample	E^a **(GPa)**	$\sigma_{max}{}^b$ **(MPa)**	$\varepsilon_{max}{}^c$ **(%)**	$T_{tan\delta}{}^d$ **(°C)**	**FWHM^e (°C)**	E'^f **(MPa)**
IPDI	3.4	92.1	4.5	127	13.6	10.7
HMDI	2.9	83.0	4.0	124	14.0	10.5
TDI	5.5	106.0	2.1	127	13.0	13.6
TDI_nc	3.8	82.8	2.5	120	23.4	10.8

a. Tensile modulus at room temperature.

b. Stress at break

c. Strain at break.

d. Temperature of the maximum of the *tan δ* peak.

e. Full width at half maximum of the *tan δ* peak.

f. Relaxed modulus determined at the temperature of the maximum of *tan δ* peak + 30 °C

To compare the thermomechanical behaviour of the original and recycled samples, *tan δ* curves extracted from DMTA analysis are presented in Figure VII-10 and the most typical data are collected in Table VII-4. In Figure VII-10, it can be appreciated that the thermomechanical behaviour of the aliphatic materials is almost similar in the original and the recycled samples, remaining the shape of *tan δ* curves unaltered with only a slight shift to lower temperatures within experimental error.

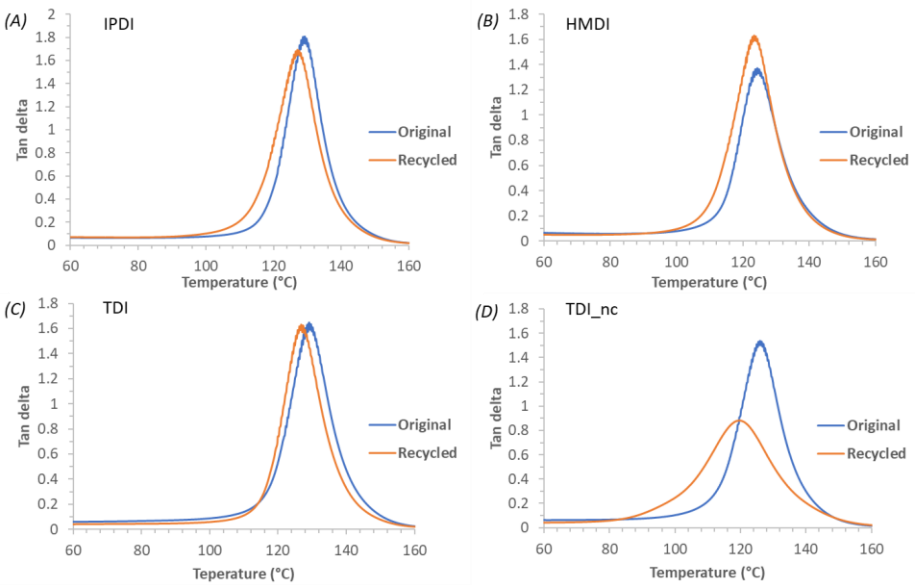

Figure VII-10. *Dependence of tan δ versus temperature of the different materials prepared before and after recycling.*

The recycled materials derived from the aromatic TDI show a different behaviour depending on the presence or absence of catalyst. In TDI sample prepared with DBTDL the maximum of the *tan δ* peak remains practically unaltered, but the material TDI-nc shows a much broader peak and is shifted at lower temperatures, which indicates a loss of the homogeneity during recycling and changes in the network structure. From this result, it is again evident the important role of DBTDL as the catalyst in the vitrimeric behaviour. To ensure that the slight changes in the *tan δ* behaviour found in the materials are only due to the harsh conditions of the recycling process and not to a change in the crosslinking density, the storage moduli were determined and they are compared in Figure VII-S3. In this figure, it can be observed that the glassy and rubbery moduli remain unaltered after recycling in all the samples, although some slight changes in the transition process can be observed. These differences can be due to the harsh recycling conditions previously mentioned, that has obviously slightly altered the network structure, but not the crosslinking density. To prove that the variations are only due to the recycling process, we have subjected an original TDI sample with catalyst to a series of two relaxation cycles and verifying that the peak of *tan δ* and the storage modulus remained constant, as can be seen in Figure VII-S4. The DMTA analyses confirm that the material is fully reshapable.

To reveal the underlying mechanisms of network rearrangement and to know if changes in the chemical structure of the materials after recycling have occurred, the FTIR spectra of the original and recycled materials were recorded and compared (see Figure VII-S5). The FTIR spectra of the PTUs prepared in the presence of DBTDL remain

almost identical after the recycling process, showing any significant chemical degradation, which proves the recyclability of this class of materials in the presence of catalyst. On the other hand, in absence of catalyst, only the intensity of the peaks of the FTIR spectrum of the recycled TDI-nc is changed.

4. Conclusions

In this work we developed different reprocessable and recyclable poly(thiourethane) thermosets starting from commercially available aromatic and aliphatic diisocyanate monomers and a trithiol in the presence of DBTDL as the catalyst. The resulting materials show high homogeneity and transparency with glass transition temperatures around 130 °C. The reactivity of aromatic diisocyanates allowed the preparation of aromatic PTUs without catalyst, the materials obtained were not fully recyclable.

The materials prepared can undergo topological rearrangement by exchange reactions allowing a complete stress relaxation and reorganization of the network, faster in the materials prepared from the aromatic isocyanate.

The catalyst plays an important role in the rearrangement process, evidenced by the shift in the value of activation energy of the exchange reaction, reducing it from 186 to 91 kJ/mol in TDI derived materials.

By performing mechanical, thermomechanical and FTIR analyses before and after the recycling process, it was proved that the materials in the presence of catalyst kept their crosslinked network structure and their mechanical performance.

These characteristics confer these materials promising possibilities for practical and smart technological applications in different fields, thanks to their high glass transition temperature, transparency and good mechanical performance combined with the ability of being recyclable under harsh conditions.

Acknowledgements

The authors would like to thank MCIU (Ministerio de Ciencia, Innovación y Universidades) and FEDER (Fondo Europeo de Desarrollo Regional) (MAT2017-82849-C2-1-R and MAT2017-82849-C2-2-R) and Generalitat de Catalunya (2017-SGR-77) for the financial support.

References

[1] W. Post, A. Susa, R. Blaauw, K. Molenveld, R. J. I. Knoop, A Review on the potential and limitations of recyclable thermosets for structural applications, *Polym. Rev.* **2019**, 60, 1-30.

[2] L. Imbernon, S. Norvez, From landfilling to vitrimer chemistry in rubber life cycle*, Eur. Polym. J.* **2016**, 82, 347-376.

[3] M. K. McBride, B. T. Worrell, T. Brown, L. M. Cox, N. Sowan, C. Wang, M. Podgorski, A. M. Martinez, C. N. Bowman, Enabling applications of covalent adaptable networks, *Annu. Rev. Chem. Biomol. Eng.* **2019**, 10, 175-198.

[4] J. M. Winne, L. Leibler, F. E. Du Prez, Dynamic covalent chemistry in polymer networks: a mechanistic perspective, *Polym. Chem.* **2019**, 10, 6091-6108.

[5] J.C. Kloxin, C.N. Bowman, Covalent adaptable networks: smart, reconfigurable and responsive network systems, *Chem. Soc. Rev.* **2013**, 42, 7161-7173.

[6] D. Montarnal, M. Capelot, F. Tournilhac, L. Leibler, Silica-like malleable materials from permanent organic networks, *Science* **2011**, 334, 965-968.

[7] W. Denissen, J. M. Winne, F. E. Du Prez, Vitrimers: permanent organic networks with glass-like fluidity, *Chem. Sci.* **2016**, 7, 30-38.

[8] M. Capelot, M. M. Unterlass, F. Tournilhac, L. Leibler, Catalytic control of the vitrimer glass transition, *ACS Macro Lett.* **2012**, 1, 789-792.

[9] W. Denissen, G. Rivero, R. Nicolaÿ, L. Leibler, J. M. Winne, F. E. Du Prez, Vinylogous urethane vitrimers, *Adv. Funct. Mater.* **2015**, 25, 2451-2457.

[10] C. Taplan, M. Guerre, J. M. Winne, F. E. Du Prez, Fast processing of highly crosslinked, low-viscosity vitrimers, *Mater. Horiz.* **2020**, 7, 104-110.

[11] J. Canadell, H. Goosens, B. Klumperman, Self-helaing materials based on disulfide links, *Macromolecules* **2011**, 44, 2536-2541.

[12] I. Azcune, I. Odriozola, Aromatic disulfide crosslinks in polymer systems: Self-healing, reprocessability, recyclability and more, *Eur. Polym. J.* **2016**, 84, 147-160.

[13] B. Hendriks, J. Waelkens, J. M. Winne, F. E. Du Prez, Poly(thioether) vitrimers via transalkylation of trialkylsulfonium salts, *ACS Macro Lett.* **2017**, 6, 930-934.

[14] X. Wu, X. Yang, R. Yu, X-J. Zhao, Y. Zhang, W. Huang, A facile access to stiff epoxy vitrimers with excellent mechanical properties via siloxane equilibration, *J. Mater. Chem. A* **2018**, 6, 10184-10188.

[15] M. Röttger, T. Domenech, R. Van der Weegen, A. Breuillac, R. Nicolaÿ, L. Leibler, High-performance vitrimers from commodity thermoplastics through dioxaborolane metathesis, *Science* **2017**, 356, 62-65.

[16] A. Erice, A. Ruiz de Luzuiraga, J. M. Matxain, F. Ruipérez, J. M. Asua, H. J. Grande, A. Rekondo, Reprocessable and recyclable crosslinked poly(urea-urethane)s based on dynamic amine/urea exchange, *Polymer* **2018**, 145, 127-136.

[17] N. Zheng, Z. Fang, W. Zou, Q. Zhao, T. Xie, Thermoset shape-memory polyurethane with intrinsic plasticity enabled by transcarbamoylation, *Angew. Chem. Int.* **2016**, 38, 11421-11425.

[18] D. J. Fortman, J. P. Brutman, C. J. Cramer, M. A. Hillmyer, W. R. Dichtel, Mechanically activated, catalyst-free polyhydroxyurethane vitrimers, *J. Am. Chem. Soc.* **2015**, 137, 14019-14022.

[19] J. A. Offenbach, A. V. Tobolsky, Chemical relaxation of stress in polyurethane elastomers, *Colloid Sci.* **1956**, 11, 39-47.

[20] X. Chen, L. Li, T. Wei, D. C. Venerus, J. M. Torkelson, Reprocessable polyhydroxyurethane network composites: effect of filler surface functionality on crosslink density recovery and stress relaxation, *ACS Appl. Mater. Interf.* **2019**, 11, 2398-2407.

[21] X. Chen, L. Li, K. Jin, J. M. Torkelson, Reprocessable polyhydroxyurethane networks exhibiting full property recovery and concurrent associative and dissociative dynamic chemistry via transcarbamoylation and reversible cyclic carbonate aminolysis, *Polym. Chem.* **2017**, 8, 6349-6355.

[22] N. Zheng, J. Hou, Y. Xu, Z. Fang, W. Zou, Q. Zhao, T. Xie, Catalyst-free thermoset polyurethane with permanent shape reconfigurability and highly tunable triple-shape memory performance, *ACS Macro Lett.* **2017,** 6, 326-330.

[23] P. Yan, W. Zhao, X. Fu, W. Kong, C. Zhou, J. Lei, Multifunctional polyurethane-vitrimers completely based on transcarbamoylation of carbamates: thermally-induced dual-shape memory effect and self-welding, *RSC Adv.* **2017**, 7, 26858-26866.

[24] D. J. Fortman, D. T. Sheppard, W. R. Dichtel, Reprocessing cross-linked polyurethanes by catalyzing carbamate exchange, *Macromolecules* **2019**, 52, 6330-6335.

[25] J. O. Akindoyo, M. D. H. Beg, S. Ghazali, M. R. Islam, N. Jeyaratnama, A. R. Yuvaraj, Polyurethane types, synthesis and applications-a review, *RSC Adv.* **2016**, 6, 114453-114482.

[26] F. Gamardella, X. Ramis. S. De la Flor, A. Serra, Preparation of poly(thiourethane) thermosets by controlled thiol-isocyanate click reaction using a latent organocatalyst, *React. Funct. Polym.* **2019**, 134, 174-182.

[27] H. Li, B. Yu, H. Matushima, C. E. Hoyle, A. B. Lowe, The thiol-isocyanate click reaction: facile and quantitative access to ω-end-functional poly(N,N-diethylacrylamide) synthesized by RAFT radical polymerization, *Macromolecules* **2009**, 42, 6537-6542.

[28] B. Jaffrennou, N. Droger, F. Mechin, J. L. Halary, J. P. Pascault, Characterization structural transitions and properties of a tightly crosslinked polythiourethane network for optical applications*, e-Polym.* **2005**, 82, 1618-7229.

[29] L. Liu, Z. Zheng, X. Wang, Preparation and properties of polythiourethane/ZnS nanocomposites with high refractive index, *J. Appl. Polym. Sci.* **2010**, 117, 1978-1983.

[30] F. Gamardella, F. Guerrero, S. De la Flor, X. Ramis, A. Serra, A new class of vitrimers based on aliphatic poly(thiourethane) networks with shape memory and permanent shape reconfiguration, *Eur. Polym. J.* **2019**, 122, 109361.

[31] L. Li, X. Chen, J. M. Torkelson, Reprocessable polymer networks via thiourethane dynamic chemistry: recovery of cross-link density after recycling and proof of principle solvolysis leading to monomer recovery, *Macromolecules* **2019**, 52, 8207-8216.

[32] T. Liu, C. Hao, S. Zhang, X. Yang, L. Wang, J. Han, Y. Li, J. Xin, J. Zhang, A self-healable high glass transition temperature bioepoxy material based on vitrimer chemistry, *Macromolecules* **2018**, 51, 5577-5585.

[33] S. Gao, Y. Liu, S. Feng, Z. Lu, Reprocessable and degradable thermoset with high Tg cross-linked via Si-O-Ph bonds, *J. Mater. Chem. A* **2019**, 7, 17498-17504.

[34] Y. Nishimura, J. Chung, H. Muradyan, Z. Guan, Silyl ether as a robust and thermally stable dynamic covalent motif for malleable polymer design, *J. Am. Chem. Soc.* **2017**, 42, 14881-14884.

[35] M. Guerre, C. Taplan, R. Nicolaÿ, J. M. Winne, F. E. Du Prez, Fluorinated, vitrimer elastomers with a dual temperature response, *J. Am. Chem. Soc.* **2018**, 140, 13272-13284.

[36] F. Gamardella, V. Sabatini, X. Ramis, A. Serra, Taylor-made thermosets obtained by sequential dual-curing combining isocyanate-thiol and epoxy-thiol click reactions, *Polymer* **2019**, 174, 200-209.

[37] E. Delebecq, J. P. Pascault, B. Boutevin, F. Ganachaud, On the versatilty of urethane/urea bonds: reversibility, blocked isocyanate, and non-isocyanate polyurethanes, *Chem. Rev.* **2012**, 113, 80-118.

[38] G. Trovati, E. A. Sanches, S. C. Neto, Y. P. Mascarenhas, G. O. Chierice, Characterization of polyurethane resins by FTIR, TGA, and XRD, *J. Appl. Polym. Sci.* **2010**, 115, 263-268.

[39] N. Zheng, J. Hou, Y. Xu, Z. Fang, W. Zou, Q. Zhao, T. Xie, Catalyst-free thermoset polyurethane with permanent shape reconfigurability and highly tunable triple-shape memory performance, *ACS Macro Lett.* **2017**, 6, 326-330.

[40] Z. Ma, Y. Wang, J. Zhu, J. Yu, Z. Hu, Bio-based epoxy vitrimers: reprocessibility, controllable shape memory and degradability, *J. Polym. Sci., Part A: Polym. Chem.* **2017**, 55, 1790-1799.

Supporting Information

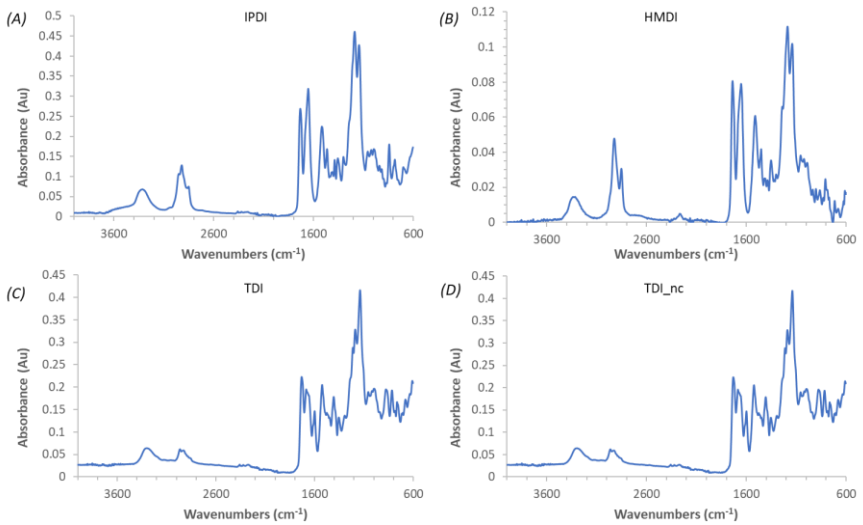

Figure VII-S1. *FTIR of cured poly(thiourethane)s registered at room temperature.*

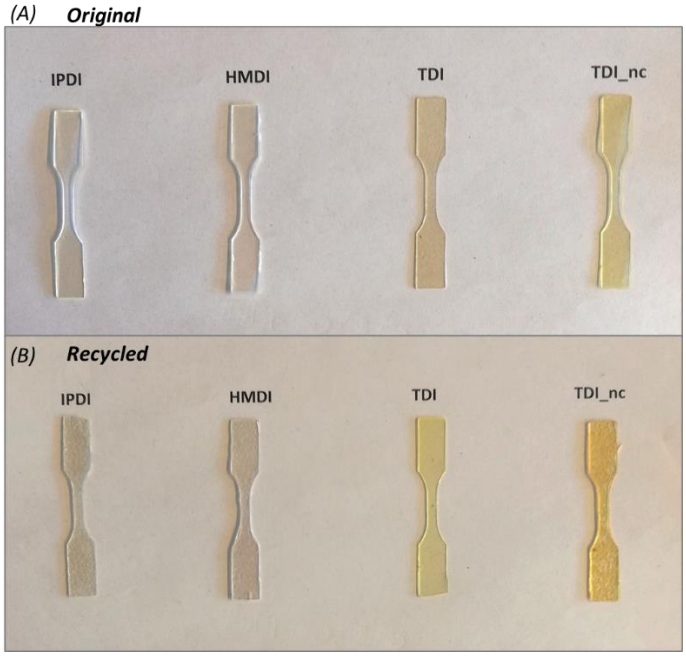

Figure VII-S2. *(A) Original and (B) recycled dog-bone PTU samples.*

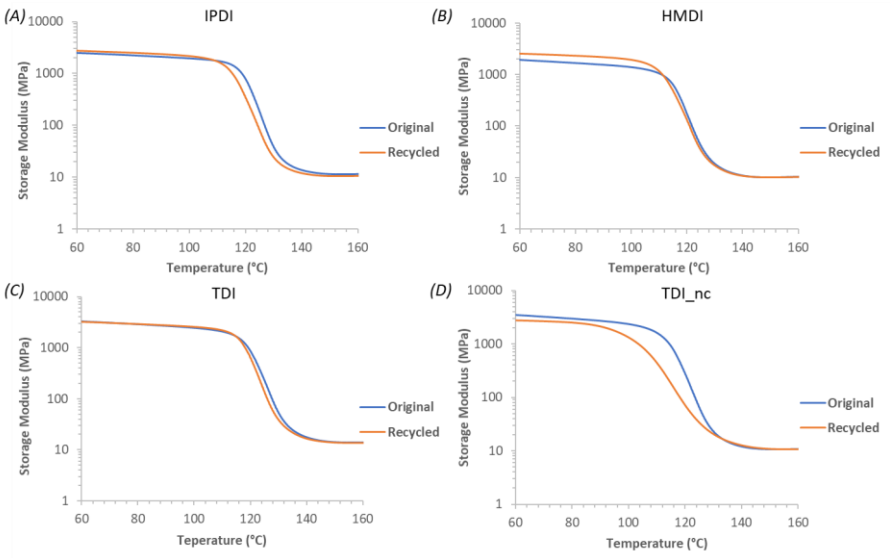

Figure VII-S3. *Storage modulus evolution with temperature of poly(thiourethane)s before and after recycling.*

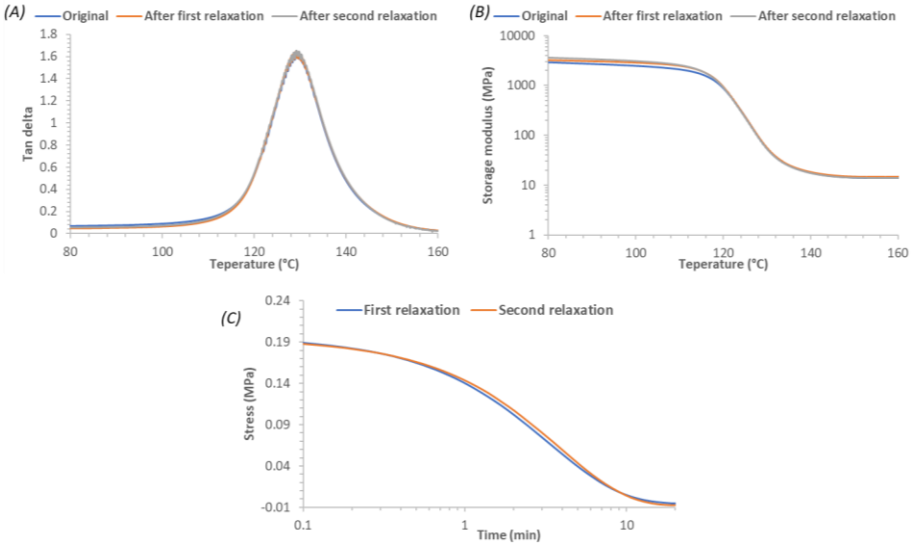

Figure VII-S4. *(A) Evolution of tan δ and (B) storage modulus against temperature of the TDI based PTU with a 2% of DBTDL sample before and after two relaxation processes at 180 °C. (C) Evolution of the two-stress relaxation process in front of time.*

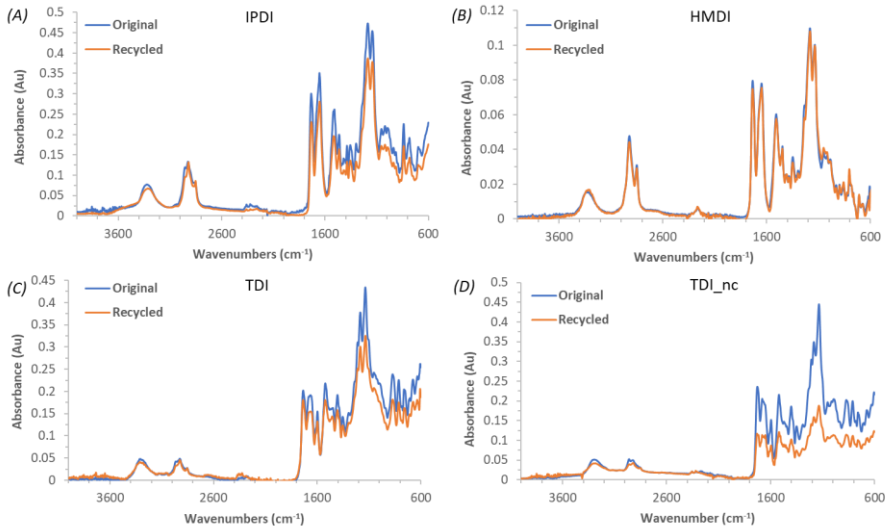

Figure VII-S5. *FTIR of poly(thiourethane)s before and after recycling registered at room temperature.*

Chapter VIII

Recyclable Organocatalyzed Poly(Thiourethane) Covalent Adaptable Networks

Polymers 2020, 12, 2913

Recyclable Organocatalyzed Poly(Thiourethane) Covalent Adaptable Networks

Francesco Gamardella[1], Sara Muñoz,[2] Silvia De la Flor[2], Xavier Ramis[3], Àngels Serra[1]

[1] Department of Analytical and Organic Chemistry, Universitat Rovira i Virgili, C/ Marcel·lí Domingo, 43007, Tarragona, Spain

[2] Department of Mechanical Engineering, Universitat Rovira i Virgili, Av. Països Catalans, 26, 43007 Tarragona, Spain

[3] Thermodynamics Laboratory, ETSEIB Universitat Politècnica de Catalunya, Av. Diagonal, 08028, Barcelona, Spain

Abstract

New tetraphenylborate salts, derived from highly basic and nucleophilic amines: 1,5-diazabicyclo[4.3.0]non-5-ene (DBN), 1,8-diazabicyclo(5.4.0)undec-7-ene (DBU) and triazabicyclodecene (TBD), were applied to the preparation of networked poly(thiourethane)s (PTUs). The PTUs showed a vitrimer-like behavior, with higher stress relaxation rates than PTUs prepared by using dibutyl thin dilaurate (DBTDL) as the catalyst. The use of these salts, which release the amines when heated, instead of the pure amines, allows the formulation to be easily manipulated to prepare any type of samples. The materials prepared from stoichiometric mixtures of hexamethylene diisocyanate (HDI), trithiol (S3) and with a 10% of molar excess of isocyanate or thiol were characterized by FTIR, thermomechanical analysis, thermogravimetry, stress relaxation tests and tensile tests, thus obtaining a complete thermal and mechanical characterization of the materials.

The recycled materials, obtained by grinding the original PTUs and hot-pressing the small pieces in the optimized time and temperature conditions, were fully characterized by mechanical, thermomechanical and FTIR studies. This allowed to confirm their recyclability without appreciable changes in the network structure and performance. From several observations, the dissociative interchange trans-thiocarbamoylation mechanism was evidenced as the main responsible of the topological rearrangements at high temperature, however resulting in a vitrimeric-like behavior.

Keywords:

vitrimers; poly(thiourethane); thermosets; recyclability; covalent adaptable networks; organocatalyst.

Chapter VIII

1. Introduction

Thermosetting polymers, thanks to their permanent covalent bonds in the network structure, show outstanding mechanical and thermal properties. However, their permanent three-dimensional structure hindered this material to be melted or dissolved in any solvents, making impossible reprocessing and recycling them. In view of the increasing amount of plastic generated, the recycling of this type of polymers is extremely important to prevent that they end up in landfills and contaminate the environment. The development of covalent adaptable networks (CANs), covalently cross-linked polymers with the ability to be reshaped, to flow and to self-repair, represents a promising approach to improve the lifetime and recyclability of the thermosetting polymers [1-4].

Recently, networked poly(thiourethane)s (PTUs) have been reported as a new class of CANs thanks to the presence of thiourethane groups that can undergo exchange reactions at moderate temperatures [5-8]. PTUs are formed by the very efficient coupling reaction between thiols and isocyanate, which in the presence of a base catalyst can be considered a *click* type reaction. The reaction is very fast without the formation of by-products and can be performed in air atmosphere without the use of solvents. The resulting network structure presents high homogeneity and transparency with a high refractive index thanks to the presence of sulphur into the network structure [9,10]. The above mentioned characteristics, together with their good mechanical properties and easy preparation make them interesting for many advanced applications and therefore worth to be further investigated, representing an interesting alternative to the more common poly(urethane)s.

Poly(urethane)s (PUs) have already been reported to experiment network reconfiguration by trans-carbamoylation [11,12]. Poly(thiourethane)s are the sulphur analogues of poly(urethane)s, and thus, they can behave in a similar manner by a trans-thiocarbamoylation process. Moreover, since thiols are more acidic than alcohols and sulphide anions are more nucleophilic than alkoxides and better leaving groups, some positive kinetic effects in the bond interchange of poly(thiourethane)s could be foreseen. In two previous papers from our research group [6,7], we proved the existence of a reversible thiocarbamate exchange reaction in PTUs and the possibility to recycle them. In both studies, a tin-catalyst was used and the influence of the amount of the catalyst on the relaxation rate was demonstrated. When comparing the relaxation behaviour of poly(thiourethane) and poly(urethane) networks it can be observed that the activation energy, E_a, is significantly lower for the former (between 70-100 kJ/mol) [6,7] than for the latter (around 140 kJ/mol) [13], which confirms the kinetic effect produced by the substitution of oxygen by sulphur.

In an excellent paper from Hillmeyer's group, a mechanistic study of the exchange mechanism in poly(urethane) networks in the presence of a Lewis acid, tin (II) octoate,

has been reported [14]. The urethane reversion to isocyanate and alcohol was demonstrated to be the main responsible of the exchange mechanism. For these materials, a dissociative mechanism was proposed, in absence of free hydroxyl groups in the network, although the relaxation studies showed a vitrimer-like behaviour without any sudden decrease in viscosity, fitting an Arrhenius model. Similarly, in our studies, a vitrimeric behaviour was observed in the case of poly(thiourethane) networks prepared with a tin-catalyst [6,7].

The preparation of PTU networks has been classically performed by the use of dibutyltin dilaurate (DBTDL) as the catalyst, since the use of bases such as amines leads to a too quick reaction [15,16]. However, the use of amines is quite convenient, because it is described that it leads to a click-reaction that produces a more homogeneous network without the formation of unexpected moieties [17,18]. To avoid these limitations, in a previous paper [19], we investigated the advantages of using a thermally triggered base generator (1-methylimidazolium tetraphenylborate, BGMI), an organocatalyst, which liberates the corresponding amine at a defined temperature, allowing a good temporary control of the thiol-isocyanate reaction. Organocatalysts are more environmentally favourable than tin-catalyst from a toxicity and pollution point of view, being considered greener than metallic catalysts [20,21].

As the use of catalysts plays a key role also in the rate of dynamic covalent-bonds exchange, their appropriate selection could affect the mechanism and the kinetics of the exchange process, tuning the desired reconfiguration properties [22,23]. As already studied by our research group, PTUs relax faster at higher catalyst concentration of DBTDL [6].

Regarding to the trans-thiocarbamoylation process, Torkelson *et al.* [5] described that thiourethane linkages can be rearranged through associative and dissociative reversible pathways, depending on the proportion of thiol in the formulation. These poly(thiourethane) elastomers were prepared from aromatic diisocyanates, in the presence of a strong base 1,8-diazabicyclo(5.4.0)undec-7-ene (DBU) (0.0005 %) and a 3 % of triphenylphosphine (PPh_3). DBU was used to form the network and PPh_3 contributed significantly to the efficient reprocessing of the elastomer.

Very recently, Bowman *et al*. [8] reported the recyclability of poly(thiourethane) elastomers using three different type of catalysts: nucleophilic, basic, and dual-role. The dual-role catalyst, 1,5-diazabicyclo[4.3.0]non-5-ene (DBN), leads to the most effective synergetic associative and dissociative thiourethane bond exchange mechanism. The dual associative-dissociative mechanism catalyzed by base-nucleophiles has been proposed by Bowman *et al.* [24] as depicted in Scheme VIII-1.

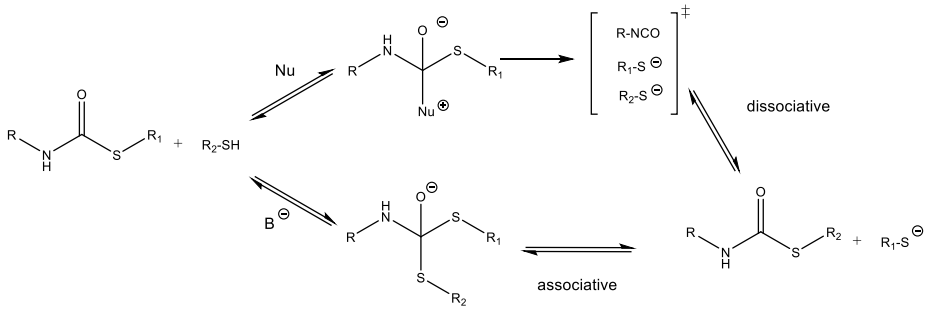

Scheme VIII-1. *Associative-dissociative trans-thiocarbamoylation exchange mechanisms catalyzed by bases and nucleophiles, proposed by Bowman et al. [24].*

In light of these considerations, the use of thermally generated base catalysts represents an interesting opportunity to reach a temporal control of the curing reaction offering, at the same time, the possibility to increase the amount of catalyst which could help to improve the rate of the exchange process. The use of such catalysts does not require any solvents as it was reported by Torkelson [5] and Bowman [18].

In the present work we explore and report the ability to undergo stress-relaxation of poly(thiourethane) networks prepared by using different tetraphenylborate salts of the following amines: 1-methylimidazole (1MI), 4-(dimethylamino)pyridine (DMAP), 1,8-diazabicyclo- (5.4.0)undec-7-ene (DBU), 1,5-diazabicyclo[4.3.0]non-5-ene (DBN) and triazabicyclodecene (TBD). Moreover, we investigate the relaxation behaviour of these materials and their thermal behaviour by thermogravimetry, to reach a good understanding of safe recycling conditions.

As in our previous study [6], 1,6-hexamethylene diisocyanate (HDI) and trimethylolpropane tris(3-mercaptopropionate) (S3) have been selected as the monomers in both stoichiometric proportions and in excess of one of them. The virgin and recycled materials have been characterized by thermomechanical and mechanical tests, which proved, together with FTIR analysis, that the recycling process can be performed if the experimental conditions are properly selected.

2. Experimental part

2.1 Materials

Trimethylolpropane tris(3-mercaptopropionate) (S3), hexamethylene diisocyanate (HDI), dibutyltin dilaurate (DBTDL), 1-methylimidazole (1MI) (pK_a = 7.1, N = 11.9) [25], triazabicyclodecene (TBD) (pK_a = 14.4, N = 16.16) [25] and sodium tetraphenylborate ($NaBPh_4$) from Sigma-Aldrich were used as received. 4-(Dimethylamino)pyridine (DMAP) (pK_a = 9.7, N = 14.95) [26], 1,5-diazabicycle[4.3.0]non-5-ene (DBN) (pK_a = 13.7, N = 15.50) [8] and 1,8-diazabicyclo(5.4.0)undec-7-ene (DBU) (pK_a = 13.5, N = 15.29)

[26] were supplied by Acros Organics. Methanol (MeOH) and chloroform ($CHCl_3$) were supplied by VWR and were used as received.

2.2 Preparation of organocatalysts (BG)

Base generators (BG)s from different amines were synthesized by us according to a reported methodology [27]. Firstly, 10 mmol of the selected amine were solubilized in 2.6 mL of water slightly acidified with 1 mL of conc., 36% HCl solution. 11 mmol of $NaBPh_4$ were solubilized in water and stirred until complete homogenization. The two aqueous solutions were mixed, and a white salt was formed as a precipitate. The salt was filtered, washed thoroughly with distilled water and MeOH, then recrystallized from a 4:1 mixture of MeOH and $CHCl_3$, filtered and dried under mild temperature and vacuum. The purity of the synthesized compound was assessed via differential scanning calorimetry (DSC) thermal scan and its melting point was found to be similar to what is reported by other equivalent salts in literature [28-30]. The different base generators prepared where named as BGXXX, where XXX indicates the base used.

2.3. Preparation of the formulations

To prepare the different formulations, the amount of base generator (BG) was conveniently selected to release 0.05% mol of the selected base. The BG of the selected base was first added to the thiol and the system was kept under stirring at 110 °C for 45 min until complete solubilization. The mixture was cooled down at room temperature and then the required amount of diisocyanate was added, manually stirred, and immediately poured in a mould or sent to analysis.

As an example, the formulations were composed by 1.90 g (11.29 mmol) of HDI, 3 g (7.53 mmol) of S3 and 0.77 mg (0.0094 mmol) of 1MI or 3.99 mg (0.0094 mmol) of BG1MI.

For the recycling and degradation studies, the thermosetting PTUs were also prepared with different stoichiometric ratios and 0.1% mole of BGDBU was added as the catalyst. Typical amounts used are reported in the table below.

Table VIII-1. *Formulations used to prepare poly(thiourethane) thermosets.*

Formulation	**Diisocyanate (g)**	**Thiol (g)**	**BGDBU 0.1% (mg)**
10 % exc HDI	2.09	3.00	9.30
Stochiometric	1.90	3.00	9.30
10 % exc S3	1.90	3.30	9.30

2.4. Sample preparation

For DMTA analysis, films were prepared by pouring the formulations on pre-silanized glasses and using Teflon spacers to ensure a homogeneous thickness of 0.5 mm. The formulations were cured at 60 °C, 100 °C, 130 °C for 1h at each temperature. The films were die-cut to obtain a rectangular specimen of 20 x 5 x 0.5 mm^3 dimensions.

2.5. Stress relaxation tests

Tensile stress relaxation tests were conducted in a TA Instruments DMA Q800 analyser using a film tension clamp on samples with the same dimensions as previously defined. To compare the rate of relaxation of the poly(thiourethane) vitrimers obtained using different catalysts, a single stress relaxation test was performed at 180 °C for 1 h at a constant strain of 1.5 %.

To obtain the activation energy (E_a) for each material, the sample was firstly equilibrated at 130 °C for 5 min, and a constant strain of 1.5 % was applied, measuring the consequent stress level as function of time. After releasing the strain, the process was repeated increasing 10 °C until the final test temperature, 170 °C, was reached. The relaxation stress $\sigma(t)$ was normalized by the initial stress σ_0 and the relaxation times (τ) were determined as the time necessary to relax $0.37 \cdot \sigma_0$ i.e. ($\sigma = 1/e \cdot \sigma_0$). With the relaxation times obtained at each temperature, the activation energy values E_a were calculated using an Arrhenius-type equation:

$$ln(\tau) = \frac{E_a}{RT} - lnA \quad (1)$$

where, τ is the time needed to attain a given stress relaxation value ($0.37\sigma_0$), A is a pre-exponential factor and R is the gas constant. From the Arrhenius relation, the temperature of topology freezing (T_v) was obtained as the temperature at which the material reaches a viscosity of 10^{12} Pa·s. Using Maxwell's relation and E' determined from DMTA (assuming E' being relatively invariant in the rubbery state), τ^* was determined to be around 10^5 s in our systems. The Arrhenius relationship was then extrapolated to the corresponding value of τ^* to determine T_v for each sample. To evaluate the thermo-mechanical properties of the different materials prepared, the evolution of tan d and storage modulus with the temperature was investigated. A sample was tested in tension in the DMA Q800 analyzer, at a heating rate of 3 °C/min from 0 to 120 °C with a frequency of 1 Hz and 0.1% of strain.

2.6. Thermal degradation studies

The thermal stability of the cured samples was studied by thermogravimetric analysis (TGA), using a Mettler TGA/SDTA 851e thermobalance. All experiments were performed under inert atmosphere (N_2 at 100 mL/min). Pieces of cured samples of 10-15 mg were degraded between 30 and 600 °C at various heating rates of 1, 2, 5 and 10 °C/min.

2.7. FTIR analysis

Fourier-transform infrared (FTIR) spectra were registered with a Bruker Vertex 70 in absorbance mode at a resolution of 4 cm^{-1} in the wavelength range of 400–4000 cm^{-1}. The instrument is equipped with attenuated total reflection (ATR) accessory (Golden GateTM, Specac Ltd.) which is temperature controlled (heated single-reflection diamond ATR crystal).

The evolution of the FTIR spectra of the poly(thiourethane) materials were followed isothermally at 180 °C in the ATR. The materials before and after being degraded in dynamic TGA until 260 °C and 340 °C were analysed at room temperature. The spectra of original and recycled PTUs were also recorded at room temperature.

2.8. Gas Chromatography-Mass Spectrometry (GC-MS) analyses

The stoichiometric PTU was degraded by heating 2 g of the material at 200 °C for 1 h in a sealed vial. The detection of the derived volatile products was performed in a HP6890 gas chromatograph and 5973 Mass selective detector (Agilent Technologies. Waldbronn, Germany), using a HP-5MS capillary column (30m×0.25mm×0.25 m) provided by Agilent.

2.9. Recycling

The recycled samples were obtained by cutting the crosslinked polymers and hot pressing at 15 MPa into an aluminium mould at 130 °C for 3 h. Recycled samples were die-cut in Type V from the new film obtained and were tested in tensile under the same conditions.

Original and recycled samples were tested until break in tensile mode at room temperature using an electromechanical universal testing machine (Shimadzu AGS-X) with a 1000 N load cell at 5 mm/min and using Type V samples according to ASTM D638-14 standard. Three samples of each material were tested, and the average results presented.

2.10. Dissolution experiments

Dissolution experiments of cross-linked polymers were performed by the following procedure. Pieces of poly(thiourethane) samples of 0.1-0.2 g, which were weighed before the experiment, were placed into a vial. The vial was filled with 1,2-dichlorobenzene (DCB) or dimethyl sulfoxide (DMSO) closed and heated at 150 °C for 24 h and then the vial was cooled down to room temperature. The polymer sample (if it still exists) was washed by dichloromethane and dried under reduced pressure at 80 °C overnight. After cooling down to room temperature, the sample was weighed, and the gel fraction was calculated.

2.11. Kinetic analysis

From the dynamic experiments carried out using a thermobalance the mass loss of the sample is recorded. The degree of conversion is defined as:

$$\alpha = \frac{m_0 - m}{m_0 - m_\infty} \quad (2)$$

where m is the mass corresponding to a temperature T, m_0 is the initial mass and m_∞ is the mass of the substance at the end of the experiment.

In non-isothermal kinetics of heterogeneous condensed phase reactions, it is usually accepted that the reaction rate is given by Eq. 3 [31,32].

$$\frac{d\alpha}{dt} = \beta \frac{d\alpha}{dT} = A\exp\left(-\frac{E}{RT}\right) f(\alpha) \quad (3)$$

where α is the degree of conversion, T temperature, t time, $f(\alpha)$ the differential conversion function, R the gas constant, β the linear constant heating rate $\beta = dT/dt$ and A and E the pre-exponential factor and the activation energy given by the Arrhenius equation.

By integrating Eq. 3, in non-isothermal conditions, the integral rate equation, so-called temperature integral, may be expressed as Eq. 4.

$$g(\alpha) = \int_0^\alpha \frac{d\alpha}{f(\alpha)} = \frac{A}{\beta}\int_0^T e^{-(E/RT)} dT \quad (5)$$

where $g(\alpha)$ is the integral conversion function.

By using the Coats-Redfern approximation to solve Eq. 4 and considering that $2RT/E$ is much lower than 1, the Kissinger-Akahira-Sunose (KAS) equation (Eq. 5) may be written as [33-35]:

$$\ln\left(\frac{\beta}{T^2}\right) = \ln\left[\frac{AR}{g(\alpha)\,E}\right] - \frac{E}{RT} \quad (5)$$

For each conversion degree, the linear plot of $\ln(\beta/T^2)$ versus T^{-1} enables E and $\ln[AR/g(\alpha)E]$ to be determined from the slope and the intercept. Isoconversional kinetic parameters were obtained in this work by using Eq. 5.

Integrating Eq. 3 for isothermal experiments, we can obtain Eq. 6:

$$\ln t = \ln\left[\frac{g(\alpha)}{A}\right] + \frac{E}{RT} \quad (6)$$

This equation relates, for each conversion, the temperature and the time of degradation. The constant $\ln[g(\alpha)/A]$ is directly related to the value $\ln[AR/g(\alpha)E]$ by

E/R, which can be deduced from the non-isothermal adjustment (Eq. 5), if isothermal and non-isothermal curing take place under the same conditions.

In this work, we have used ln [*AR*/*g*(*α*)*E*] and *E/R* obtained by dynamic experiments and Eq. 5 and Eq. 6 to estimate the temperature at which the material can be recycled without significant thermal degradation.

3. Results and Discussion

3.1. Study of the effect of the catalyst on the relaxation behaviour

The viscoelastic properties of poly(thiourethane) thermosets prepared from stoichiometric amounts of HDI and S3, in the presence of a base catalyst (1MI) and without using any solvent were firstly investigated. In the presence of a base, the thiol-isocyanate reaction is very fast, and the system is difficult to process due to the low pK_a of thiol species and their easy deprotonation in presence of the base. Especially in presence of a base with a high value of pK_a, the reaction reaches the 100 % of conversion in few seconds, even when greatly reducing the amount of catalyst. The mechanism of thiol-isocyanate reaction in presence of a base is proposed in Scheme VIII-2.

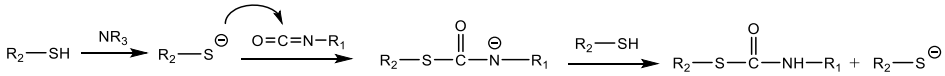

***Scheme VIII-2**. Proposed mechanisms of poly(thiouretane) formation in the presence of a basic catalyst.*

Based on the expertise of our research group on temporal and kinetic control of the curing processes, we chose as the catalyst a base generator that releases the base after the application of an external stimulus, as shown in Scheme VIII-3.

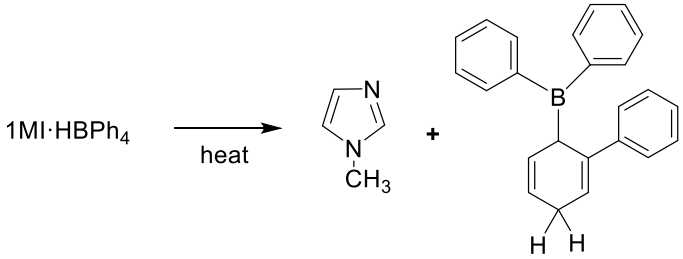

***Scheme VIII-3.** Thermal activation of the base generator BG1MI.*

The use of such latent bases could also allow us to increase the amount of catalyst in the formulation, which hypothetically could lead to an acceleration of the exchange mechanism.

The effect of using the BG on the thermal and rheological properties of the material was evaluated and compared with a similar system prepared using the corresponding base catalyst. We selected as the base one with lower pK_a and N values and we

prepared two samples of poly(thiourethane) from HDI and S3, one with 0.05 % mole of 1MI and another with the same mole proportion of BG1MI.

The thermal behaviour of the materials prepared with the same mol proportion of 1MI and BG1MI was compared by means of TGA and DMTA tests. The plots are shown in Figures VIII-S1 and S2 in the supporting information. The use of BG1MI instead of 1MI does not affect the thermal stability of the material and the TGA curves appear almost overlapped, with a 2% of weight loss at 269 °C for the material obtained with 1MI and at 271 °C for the other one. The peak of tan δ obtained by DMTA remains practically unchanged for both materials with a shift in the temperature peak of only 2 °C, higher in case of the material prepared with 1MI. These results put in evidence that the use of the base generator derivative facilitates the manipulation of the initial formulation without any impact on the thermal characteristics of the material.

The stress relaxation curves obtained by DMTA of both PTUs are presented in Figure VIII-1.

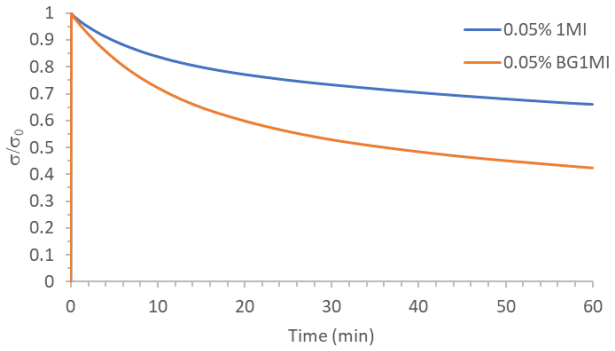

Figure VIII-1. *Normalized stress relaxation behaviour at 180 °C of the samples prepared with the same mol amount of 1MI and BG1MI.*

In the figure, we can see how the materials relax the stress at 180 °C, showing a quite slow relaxation process in both cases. However, it is evident that the use of BG1MI affects positively the relaxation rate if compared with 1MI. This effect is probably due to the presence of tetraphenylboronic acid released during the activation of the 1-methylimidazolium tetraphenylborate which act as additional catalyst. From this result, we can deduce that 1MI at this concentration is not an efficient catalyst to enhance the carbamate exchange process. Therefore, the effect on the stress relaxation process of base generators prepared from DMAP, DBN, DBU and TBD, with higher values of pK_a and N, had to be tested.

The relaxation rates of PTUs prepared with the different base generators were investigated at elevated temperatures (Figure VIII-2) and the resulting relaxation behaviour was compared with a PTU prepared by using DBTDL as the catalyst [6]. In

all the BG samples, 0.05 % mol of each tetraphenylborate salt has been used as the catalyst.

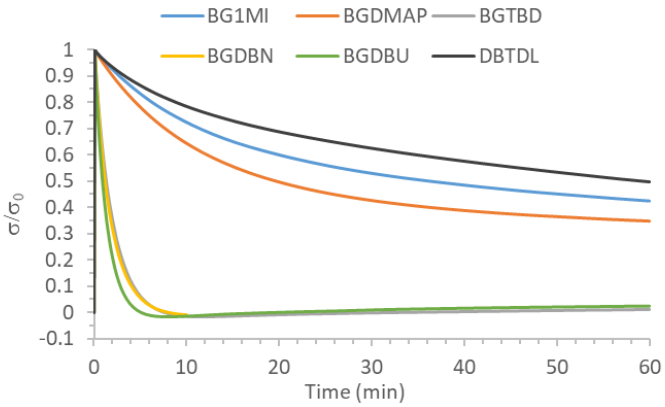

Figure VIII-2. *Normalized stress relaxation plot at 180 °C of different poly(thiourethane) samples prepared with 0.05 % mol of the different catalysts.*

The relaxation times ($\tau_{0.37}$), determined at the point when the stress decreased to *1/e* (37 %) of its initial value, are collected in Table VIII-2. We can see in the figure how the mol proportion used in the case of DBTDL is not enough to obtain a fast relaxation process in the analysed time scale; higher amount of acid catalyst is needed to effectively catalyse the exchange reaction [5,6]. From the relaxation curves it is clear how the base generators of strong bases and high nucleophilicity (DBN, DBU and TBD) accelerate the exchange mechanism, reaching $t_{0.37}$ in less than 2 min, in accordance with the conclusion reached by Bowman *et al*. [8] by using DBN as the catalyst. However, there is not a clear dependence of the relaxation time with the pK_a or N for the strong bases used, probably also due to the fact that the values of pK_a and N of each base are not too different from each other. Among all the BG screened, we selected BGDBU as the catalyst to continue with further investigation, according to the fastest relaxation achieved with this system.

Table VIII-2. *Characteristic relaxation time to reach a value of σ/σ_0 = 0.37 at 180°C in a stress relaxation experiments for PTU samples with a 0.05% in mol of the different catalysts used.*

Sample	$\tau_{0.37}$ (min)[1]
BG1MI	Not reached in 1 h
BGDMAP	45
BGTBD	1.7
BGDBN	1.7
BGDBU	1.3
DBTDL	Not reached in 1 h

[1] Time to reach a value of σ/σ_0 = 0.37 at 180 °C

To see the effect of the proportion of BGDBU on the relaxation rate, we prepared a sample doubling the amount of the catalyst (0.1 % mol) in the formulation, proving that the rate of the exchange process increased significantly, as it can be seen in Figure VIII-3. The $\tau_{0.37}$ at 180 °C is reached after only 30 seconds confirming the positive influence of the catalyst concentration on the relaxation rate. A parallel behaviour was already observed for the DBTDL catalyst in our previous paper, but with slower relaxation rates [6].

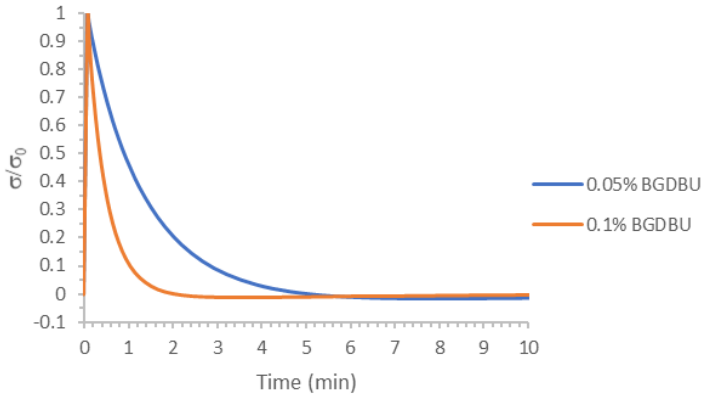

***Figure VIII-3**. Normalized stress relaxation plot at 180 °C of PTUs prepared with different mol proportions of BGDBU.*

According to these results, we selected as the optimal catalyst molar proportion 0.1 % to follow the study. Higher proportions of catalyst were not used since the BG becomes difficult to dissolve in the thiol during the preparation of the formulation.

3.2. Study of the effect of the stoichiometry of the formulation

The second main objective of this work consisted in the evaluation of the influence of the isocyanate/thiol ratio on the exchange mechanism and the relaxation behaviour. The materials tested in the following sections were prepared to build evidence of the associative and/or dissociative trans-thiocarbamoylation exchange mechanism and their effect on the viscoelastic behaviour. It was reported by Torkelson [5] and Bowman [8] that an associative exchange reaction occurs in the presence of an excess of thiol, while a dissociative exchange mechanism occurs when no excess of thiols is available. Both mechanisms can occur at the same time when stoichiometric thiol-isocyanate balance is maintained in the presence of a dual-role basic and nucleophilic catalyst. To be representative of the discussed cases, in addition to the thiol/isocyanate stoichiometric material we prepared other two PTUs: 1) one with an excess of 10 % in mol of HDI, with the assumption that this amount does not leave unreacted thiols in the thermosets and 2) another with an excess of 10 % in mol of thiol to facilitate the associative pathway. A series of stress relaxation experiments

were conducted on these three different systems calculating their activation energy as it is represented in Figure VIII-4.

As shown in Figure VIII-4, a fast stress relaxation was observed for all the systems at all temperatures analysed. The relaxation times are very similar for the three PTUs prepared and the characteristic time of relaxation decreased from approximately 30 min to 1 min as the temperature increased from 130 to 170 °C. The highest relaxation rate was obtained for the system with an excess of isocyanate.

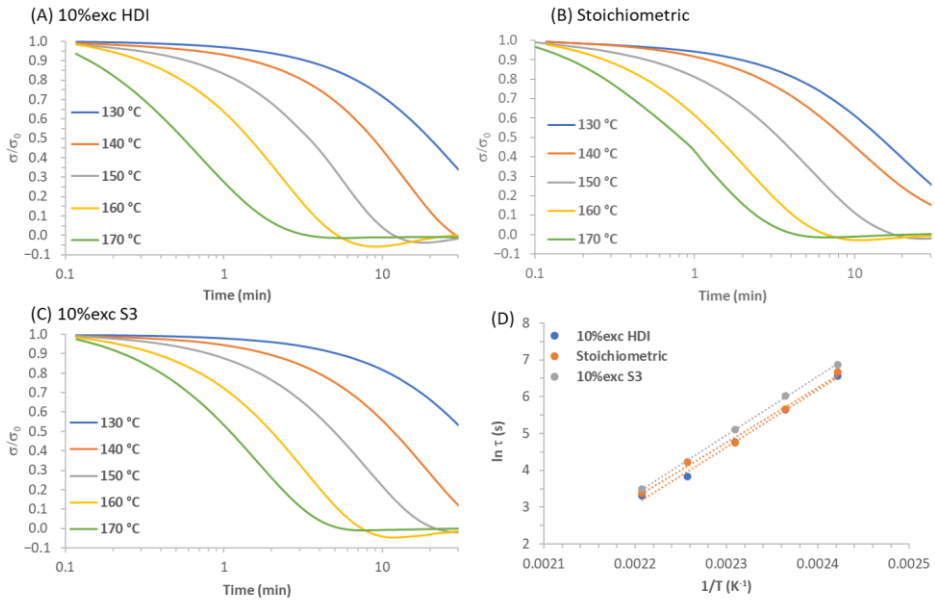

Figure VIII-4. *(A-C) Normalized stress relaxation plots as a function of time at various temperatures from 130 to 170 °C during 30 min. (D) Arrhenius plot for the different poly(thiourethane) samples with 0.1% of BGDBU.*

The logarithm of the relaxation times was plotted as a function of the inverse of temperature for all the materials prepared, fitting perfectly with an Arrhenius-like behaviour. The activation energies and the topology freezing temperatures were calculated by the Arrhenius equation using the slope of the straight line. The values obtained are collected in Table VIII-3. As it can be appreciated, the activation energies are similar for the three PTUs studied, around 120-130 kJ/mol. Moreover, from the stress relaxation experiments, no significant differences in the behaviour are appreciable that can lead us to consider a clear change in the trans-thiocarbamoylation pathways by changing the stoichiometry of the formulation in the selected range. It can be observed that the materials prepared with an excess of thiol, which should enhance the associative exchange rate, are the slowest materials in the relaxation process. This behaviour seems to suggest that dissociative mechanism is predominant with the catalyst used.

Table VIII-3. *Activation energy, topology freezing temperature and time for reach a value of $\sigma/\sigma_0 = 0.37$ from the stress relaxation experiments at different temperatures.*

Sample	E_a (kJ/mol)	T_v (°C)	$t_{0.37-130°C}$ (min)	$t_{0.37-140°C}$ (min)	$t_{0.37-150°C}$ (min)	$t_{0.37-160°C}$ (min)	$t_{0.37-170°C}$ (min)
10 % exc HDI	132	94	27.8	11.7	4.7	1.9	0.8
Stoichiometric	117	87	21.5	13.0	4.8	1.9	1.1
10 % exc S3	127	96	45.2	16.0	6.9	2.7	1.5

3.3. Study of the thermal stability of the PTUs prepared

The thermal stability of the PTUs prepared by using BGDBU as the catalyst was evaluated by TGA and compared with the material prepared from DBTDL, since it is important to prove that at the reshaping temperature the material does not loss any volatile product. Moreover, the study of the thermal degradation mechanism could help to disclose about the adoption of a dissociative interchange mechanism. The TGA and the derivative of the loss weight curve (DTG) curves are shown in Figure VIII-5.

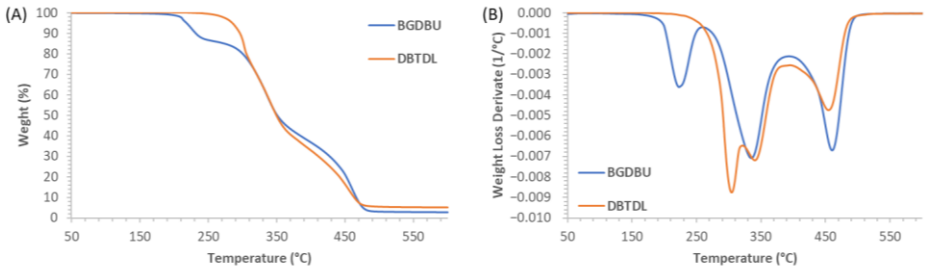

Figure VIII-5*. (A) TGA curves and (B) DTG curves of the poly(thiourethane)s prepared with 0.1% of BGDBU and 1% of DBTDL.*

As we can see from Figure VIII-5, the thermal stability of the material based on BGDBU decreases if compared with the PTU prepared with the acidic catalyst, DBTDL.

DTG plot shows three clear degradation steps for both materials. The maximum of the first degradation peak appears at 305 °C for DBTDL sample whereas in the case of BGDBU samples it is shifted to lower temperature (around 220 °C) and becomes well separated from the second one. Since the first degradation step was attributed, in several studies on PU [36], to the reversion of urethanes to isocyanate and alcohols, it can be easy to make the assumption that an analogous degradation to isocyanate and thiols could occur in PTU networks [37]. It should be noticed, that in a previous study we could not see great differences between the materials prepared with DBTDL and those prepared using BG1MI as the catalyst [19]. This means, that DBU has a main role in the thermal degradation of the PTUs prepared with BGDBU, which could be attributed to its higher nucleophilic character, facilitating a dissociative mechanism.

Analysing the TGA curves of the PTUs prepared with different thiol-isocyanate stoichiometric ratio (see Figure VIII-6) and in presence of BGDBU, it can be observed that the 2 % of loss in weight (given in Table VIII-4) occurs at temperatures around 210 °C for all the samples, without significant differences among them. DTG curves are very similar for all the materials and show the three decomposition processes. The first degradation step, at around 220 °C, relates to a 15 % of mass loss, the second peak, at 340 °C, is related to a mass loss of an additional 45 % and the third step is associated with a complete degradation of the network. No differences in the thermal degradation are appreciable on changing the stoichiometry of one of the monomers used in the preparation of the material and this could be related to the similar behaviour observed in the relaxation experiments of the three samples.

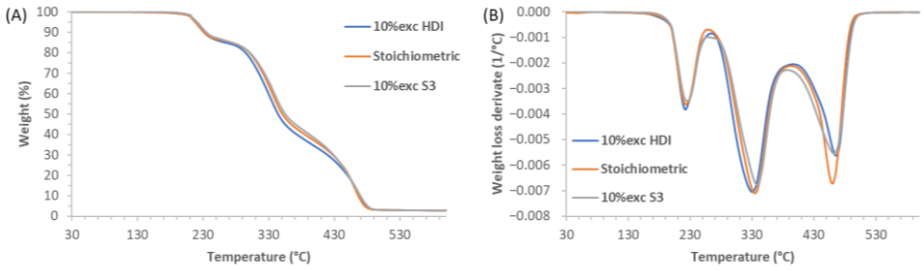

Figure VIII-6. *TGA curves (A) and DTG curves (B) of the poly(thiourethane)s prepared from different stoichiometric formulations with 0.1 % of BGDBU.*

The good separation between the three different processes has driven us to perform a kinetic analysis of the degradation process. Thus, we carried out an isoconversional analysis of the three degradation steps to calculate the activation energy and the kinetic parameters which best describe the degradation processes of PTUs. To this aim, a series of TGA dynamic experiments were performed at different heating rates as shown in Figure VIII-S3 for the stoichiometric PTU. As expected, as the heating rate increases, the TGA and DTG curves shift to higher temperatures.

Table VIII-4. *Temperature of initial degradation and activation energies of the degradation steps of the PTUs prepared with 0.1 % of BGDBU.*

Sample	$T_{2\%}$ (°C)	E_{α} I peak (kJ/mol)	E_{α} II peak (kJ/mol)	E_{α} III peak (kJ/mol)
10 % exc HDI	209	127	170	257
Stoichiometric	209	130	158	275
10 % exc S3	212	139	149	259

From the dynamic isoconversional kinetic study, we calculated the activation energy for the three different materials, using the Eq. (5) applied to the degradation process

in N_2 atmosphere. Since isoconversional activation energies are relatively constant during each degradation step, their average values are reported in Table VIII-4.

The kinetic of each degradation step was studied, considering in Eq. (2) as final mass (m_∞) the mass of the remaining material at the end of this stage. The E_α during the first degradation step, calculated as described in the Section 3, remains relatively constant implying that a single degradation mechanism occurs in the considered range of temperatures. The E_α calculated is around 130 kJ/mol. This value of E_α is comparable for all the different PTUs analysed, and its minimum value is observed for the material prepared with an excess of isocyanate.

For a better understanding of the processes that occur during the decomposition of the PTU, FTIR analyses were performed on the partially degraded material after step 1 and step 2 of degradation. The material was heated up in the TGA until finishing each degradation step, and then the partially degraded samples were analysed by FTIR-ATR at room temperature. In Figure VIII-S4, the FTIR of the initial and the degraded material until 260 °C are presented. From the spectra it is possible to observe how the characteristic carbonyl band of thiourethane at 1670 cm^{-1} is almost completely disappeared during the first degradation step demonstrating the decomposition of the thiourethane group. However, any absorption of isocyanate at 2250 cm^{-1} could be detected, such as reported by Rogulska *et al.* [37], who observed a small peak, attributable to isocyanate formation during degradation, although in that case DBTDL was used as the catalyst. To analyse the second degradative process, the material was heated up in the TGA until 340 °C and the FTIR spectra was collected (presented in Figure VIII-S5). Analysing the spectra, we can state that the second degradation step is associated with the decomposition of the ester bond of the thiol structural units, as evidenced by the drastic decrease of the peak at 1710 cm^{-1}.

Additionally, the volatiles produced during the first decomposition step were studied by gas chromatography coupled to a mass spectrometer detector (GC-MS), following the procedure described in the section 2.8. Figure VIII-S6 illustrates the chromatographic profile of volatile compounds obtained by GC-MS, where two main peaks were detected and identified by mass spectroscopy (Figures VIII-S7 and S8). The peak at 2.28 min is due to the formation of benzene in the degradation and it can be associated to the aromatic ring of the tetraphenylboronic acid. The peak at 1.21 min is due to the formation of carbonyl sulphide, which indicates that at high temperatures the thiourethane moiety is decomposed mainly through a CSO elimination, which is the responsible of the initial weight loss. This is in accordance with the results of the degradation study previously reported by Rogulska *et al.* [37], where the elimination of CSO and formation of an amine was found to be the main responsible for the degradation of poly(thiourethane) polymers. It must be pointed out, that CSO can only be formed directly from the thiourethane moieties and not

after scission of this group. No free diisocyanate was detected by GC-MS, which may indicate that the reversion of thiourethane linkages to isocyanate and thiol is very fast and reversible, and no loss of diisocyanates or thiols was detected. This observation fits with the results of our previous studies [6] in which, during the interchange mechanism of a model compound, no free thiols or isocyanate were detected. Thus, associative and dissociative trans-thiocarbamoylation mechanisms behave similarly in terms of average crosslinking density during the topological changes, and therefore any sudden decrease of the viscosity during reshaping processes is produced.

Although no significant differences in weight loss were determined by TGA on changing the stoichiometry of the material, FTIR-ATR was used to analyse structural effects of a change in stoichiometric when heating the samples at 180 °C during 4 h. We have selected this temperature to detect the occurrence of a possible dissociation process of poly(thiourethane) in isocyanate and thiol groups, which could be evidenced by the appearance of an isocyanate absorption peak. For comparison purposes, we also analysed a PTU sample obtained with DBTDL. The spectra registered during the thermal treatment are shown in Figure VIII-7.

It is possible to see in Figure VIII-7 that the starting spectra of the samples prepared with BGDBU or DBTDL are identical, and only in the initial spectra of the PTU with an excess of isocyanate can be appreciated the typical absorption peak at 2270 cm^{-1}, corresponding to the unreacted isocyanate. During the heat treatment at 180 °C for 4 h it is possible to observe the degradation processes and that the intensity of the different peaks was reduced. However, isocyanate absorption was not detected in any case. The typical carbonyl band of thiourethane at 1670 cm^{-1} was almost drastically reduced after the heating process due to the degradation of these moieties. Instead, in presence of 1 % of DBTDL in stoichiometric formulation no appreciable evidence of degradative process is detected, confirming that thiourethane groups are not decomposed as already shown in our previous work [6]. From this thermal study, we can conclude that the use of base generators derived from high nucleophilic bases, like DBU, is quite convenient for a fast reshaping and relaxation stress purposes, but too high temperatures or too long processing times should be avoided, since both can lead to a decomposition of the materials, that worsen the mechanical performance.

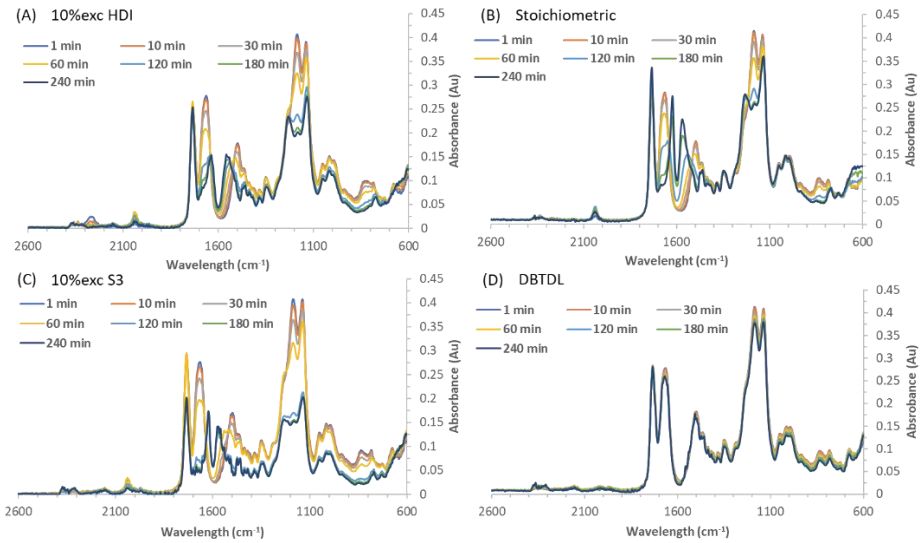

Figure VIII-7. *FTIR of the different poly(thiourethane) samples with 0.1% of BGDBU and 1% of DBTDL registered during 4 h at 180°C.*

3.4. Study of the recycling process

To investigate the recyclability of the three different crosslinked PTUs prepared, the materials were cut into small pieces and hot pressed at 15 MPa in an aluminium mould. The temperature of the recycling process has been selected according to the isothermal degradation times estimated by using Eq. 5 and the isoconversional non-isothermal kinetic parameters previously determined. Thus, 130 °C was chosen as the temperature that combines a fast relaxation process together with a high thermal stability, since by the data obtained at 130 °C a weight loss of 1 % is estimated to be above 9 h.

Figure VIII-8 shows the pictures taken from the original, grinded, and reprocessed samples prepared as described in the experimental part. As we can see, the original and the recycled materials show both good transparency. It can be also appreciated the excellent uniformity of the recycled sample.

Figure VIII-8. *Photographs of the original, grinded, and recycled sample prepared from stoichiometric PTU with a 0.1 % of BGDBU.*

To evaluate the recyclability of the PTUs prepared, the original and the recycled samples were subjected to uniaxial tensile test, DMTA and FTIR analysis. Dog-bone-shaped samples of the original and recycled PTUs were tested at room temperature until break and their stress-strain behavior analyzed, obtaining the tensile modulus and the yield stress and strain. These mechanical parameters as well as thermomechanical data obtained are collected in Table VIII-5.

Table VIII-5. *Mechanical and thermomechanical results of the original and recycled PTUs materials tested. The average value of the results for three different samples tested is presented. Coefficients of variations are less than 7 % for stress and strain results and less than 5 % for the tensile moduli.*

Original						
Sample	E [1] **(GPa)**	σ_{max} [2] **(MPa)**	ε_{max} [3] **(%)**	$T_{tan\delta}$ [4] **(°C)**	**FWHM** [5] **(°C)**	E' [6] **(MPa)**
10 % exc HDI	1.7	30.4	3.0	56.3	9.6	11.4
Stoichiometric	2.5	45.1	2.5	57.4	9.9	12.7
10 % exc S3	1.8	31.4	2.7	49.0	10.8	9.6
Recycled						
Sample	E [1] **(GPa)**	σ_{max} [2] **(MPa)**	ε_{max} [3] **(%)**	$T_{tan\delta}$ [4] **(°C)**	**FWHM** [5] **(°C)**	E' [6] **(MPa)**
10 % exc HDI	1.6	28.9	3.1	56.3	10.7	11.3
Stoichiometric	2.1	43.3	2.8	57.5	9.2	13.0
10 % exc S3	1.8	32.2	2.5	49.2	10.9	9.2

[1] Tensile modulus at room temperature.

[2] Yield Stress.

[3] Yield Strain.

[4] Temperature of the maximum of the *tan* δ peak.

[5] Full width at half maximum of the *tan* δ peak.

[6] Relaxed modulus determined at the temperature of the maximum of *tan* δ peak + 30 °C.

From the tensile tests, it can be observed that the mechanical properties of the PTUs after the first recycling process are very similar to those of the original samples for all the systems studied. The stoichiometric material, as expected, is the most rigid at room temperature, showing the highest values of tensile modulus and yield stress, in the original and recycled samples. Moreover, the recycled sample of the stoichiometric material presents excellent mechanical performance in comparison with the original one, *i.e.* a tensile modulus around 85 % of the original modulus and a yield stress of almost 96 %. The materials prepared out of stoichiometry also showed a very similar mechanical behaviour with a tensile modulus of 1.7 and 1.8 GPa for the material prepared with an excess of isocyanate and thiol, respectively. The mechanical properties of the recycled samples in these two materials are perfectly recovered with values that fall within the range of the experimental error.

To compare the thermomechanical behaviour of the original and recycled samples, the variation of the storage modulus and the *tan d* curves with the temperature extracted from DMTA analysis are presented in Figure VIII-9 and the most representative data are collected in Table VIII-5. In the figure, it can be appreciated that the thermomechanical behaviour of the original and recycled materials is very similar, remaining both, shape and position of *tan δ* curves, unaltered. From these results, we can asset that these thermosets can be recycled without significant difference in the thermomechanical properties, showing the promising use of BGDBU as efficient catalyst to the trans-thiocarbamoylation exchange of poly(thiourethane)s.

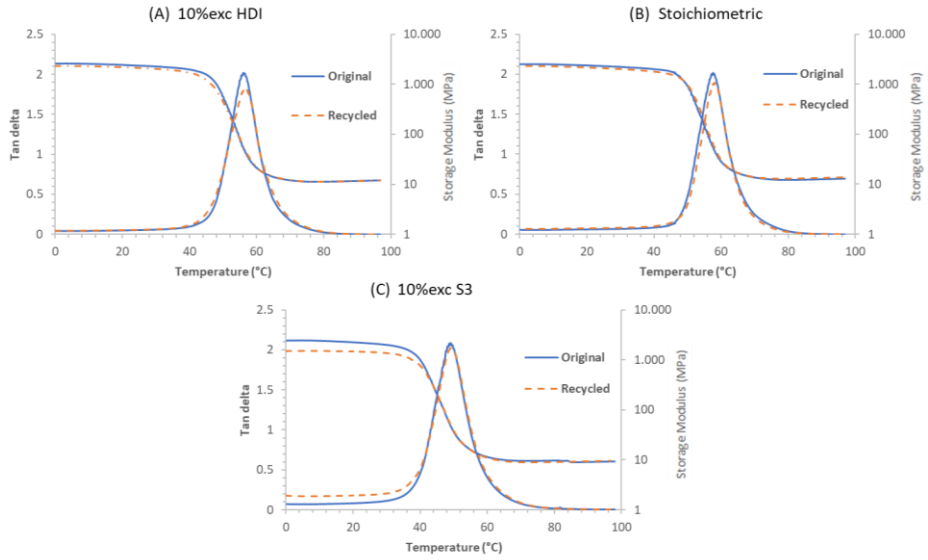

Figure VIII-9. *Dependence of tan δ and storage modulus versus temperature of the different materials prepared before and after recycling.*

To confirm that no changes in the chemical structure of the materials have occurred after the recycling process, the FTIR spectra of the original and recycled materials were recorded and overlapped (see Figure VIII-10). The FTIR spectra of the PTUs prepared remain almost identical after the recycling process. The only appreciable changes are detected in the material prepared with an excess of isocyanate where it is possible to see how the absorption band of the isocyanate cannot be detected in the recycled material. Thus, we can confirm the recyclability of this class of thermosets even in different stoichiometric ratios in the presence of a strong basic and nucleophilic catalyst, as reported by Bowman [8] for DBN catalyst in elastomeric PTUs.

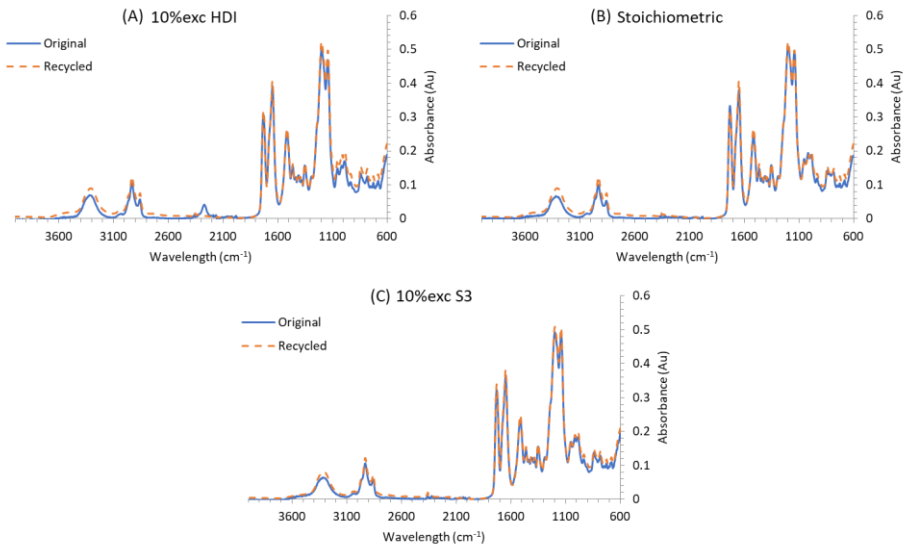

Figure VIII-10. *FTIR of poly(thiourethane)s before and after recycling registered at room temperature.*

3.5. Dissolution experiments

Typical thermosets do not solubilize in any type of solvent. However, covalent adaptable networks can be solubilized by a suitable solvent when their chemical exchange process proceeds through a dissociative mechanism. The possibility to undergo complete dissolution of these reprocessable thermosets could constitute an alternative chemical recycling route to the mechanical recycling previously studied.

Hillmeyer *et al*. [14] recently reported that poly(urethane) thermosets can be dissolved in dimethyl sulfoxide (DMSO), thus demonstrating the dissociative nature of the urethane exchange pathway, although the same sample was not soluble in a chlorinated aromatic solvent. This was attributed to the fact that the sample had increased swellability in DMSO, because of the higher polarity. In our study, we tried to dissolve the PTU polymer in DMSO and dichlorobenzene (DCB). After leaving the PTUs for 24 h at 150 °C in both solvents, we noticed that the sample in DCB swollen but not dissolve and once the solvent was completely removed the soluble fraction was only 4 %. However, the sample immersed in DMSO was almost completely dissolved after 24 h, as we can observe in Figure VIII-S9. The dissolution of the sample in DMSO confirms that the dissociative exchange mechanism plays a role in the reconfiguration of the network. In fact, when a good solvent such as DMSO is used, the broken chains remain in solution without reverting to cross-linked PTU networks, which would be insoluble.

4. Conclusions

In this work, the catalytic effectiveness of tetraphenylborate derivatives of DBN, DBU and TBD in the trans-thiocarbamoylation process in poly(thiourethane) thermosets was put in evidence. The relaxation rate of the PTUs prepared with the above-mentioned catalysts was faster than the one prepared with DBTDL. The great catalytic effect is due not only to the high basicity and nucleophilicity of the amines, but also to the presence of the tetraphenylboric acid, which is formed when the amine has been thermally released.

Moreover, the use of the tetraphenylborate salts of these amines is advantageous in comparison to the use of the free amines concerning the manipulation of the formulation: it helps to delay the pot-life of the mixture, and gives the possibility to increase the amount of catalyst in the formulation without using any solvent, increasing thus the exchange rate of the covalent bond.

The poly(thiourethane)s networks show, in the presence of these new catalysts, a vitrimer-like behaviour with the possibility to be reshaped and recycled. The materials obtained degrade at temperatures lower than those obtained with DBTDL as the catalyst. Therefore, the recycling parameters, temperature and time were properly selected by a thermal degradation study, demonstrating that under adequate recycling conditions the materials kept its good thermal and mechanical performance and its chemical structure. Materials with a 10 % of molar stoichiometric imbalance, in isocyanate or thiol groups, do not show appreciable differences in relaxation rate and recycling capability.

Moreover, it was demonstrated that the thermal degradation leads to an initial loss of carbonyl sulfide without dissociation of thiourethane moieties to isocyanate and thiol groups. This observation, together with the proved solubility of the material in DMSO and the unaffected relaxation rate in the presence of an excess of thiol, confirms that the exchange mechanism is mainly dissociative, but with a very fast equilibrium process that leads to a vitrimer-like behavior.

Acknowledgements: The authors would like to thank MCIU (Ministerio de Ciencia, Innovación y Universidades) and FEDER (Fondo Europeo de Desarrollo Regional) (MAT2017-82849-C2-1-R and MAT2017-82849-C2-2-R), Generalitat de Catalunya (2017-SGR-77) and Universitat Rovira i Virgili (2019PFR-URV-81 for the financial support.

References

[1] Scheutz, G.M.; Lessard, J.J.; Sims, M.B.; Sumerlin, B.S. Adaptable Crosslinks in Polymeric Materials: Resolving the Intersection of Thermoplastics and Thermosets. *J. Am. Chem. Soc.* **2019**, 141, 16181-16196.

[2] Podgórski, M.; Fairbanks, B.D.; Kirkpatrick, B.E.; McBride, M.; Martinez, A.; Dobson, A.; Bongiardina, N.J.; Bowman, C.N. Toward Stimuli-Responsive Dynamic Thermosets through Continuous Development and Improvements in Covalent Adaptable Networks (CANs). *Adv. Mater.* **2020**, 32, 1906876.

[3] Guerre, M.; Taplan, C.; Winne, J. M.; Du Prez, F. E. Vitrimers: directing chemical reactivity to control material properties. *Chem. Sci.* **2020**, 11, 4855-4870.

[4] Elling, B.R.; Dichtel, W.R. Reprocessable Cross-Linked Polymer Networks: Are Associative Exchange Mechanisms Desirable? *ACS Cent. Sci*. **2020**, 6, 1488-1496.

[5] Li, L.; Chen, X.; Torkelson, J.M. Reprocessable polymer networks via thiourethane dynamic chemistry: recovery of cross-link density after recycling and proof of principle solvolysis leading to monomer recovery. *Macromolecules* **2019**, 52, 8207-8216.

[6] Gamardella, F.; Guerrero, F.; De la Flor, S.; Ramis, X.; Serra, A. A new class of vitrimers based on aliphatic poly(thiourethane) networks with shape memory and permanent shape reconfiguration. *Eur. Polym. J.* **2020**, 122, 109361.

[7] Gamardella, F.; De la Flor, S.; Ramis, X.; Serra, A. Recyclable poly(thiourethane) vitrimers with high Tg. Influence of the isocyanate structure. *React. Funct. Polym.* **2020**, 151, 104574.

[8] Wen, Z.; Han, X.; Fairbanks, B.D.; Yang, K.; Bowman C.N. Development of thiourethanes as robust, reprocessable networks. *Polymer* **2020**, 202, 122715.

[9] Ireni, N.G.; Narayan, R.; Basak, P.; Raju, K.V.S.N. Poly(thiourethane-urethane-urea) as anticorrosion coatings with impressive optical properties. *Polymer* **2016**, 97, 370-379.

[10] Jaffrennou, B.; Droger, N.; Mechin, F.; Halary, J. L.; Pascault, J.P. Characterization structural transitions and properties of a tightly crosslinked polythiourethane network for optical applications. *e-Polym.* **2005**, 82, 1618-7229.

[11] Zheng, N.; Fang, Z.; Zou, W.; Zhao, Q.; Xie, T. Thermoset shape-memory polyurethane with intrinsic plasticity enabled by transcarbamoylation. *Angew. Chem.* **2016**, 128, 11593-11597.

[12] Chen, X.; Li, L.; Jin, K.; Torkelson, J. M. Reprocessable polyhydroxyurethane networks exhibiting full property recovery and concurrent associative and dissociative dynamic chemistry via transcarbamoylation and reversible cyclic carbonate aminolysis. *Polym. Chem.* **2017**, 8, 6349-6355.

[13] Fortman, D.J.; Sheppard, D.T.; Dichtel, W.R. Reprocessing cross-linked polyurethanes by catalyzing carbamate exchange. *Macromolecules* **2019**, 52, 6330-6335.

[14] Brutman, J.P.; Fortman, D.J.; De Hoe, G.X.; Dichtel, W.R.; Hillmyer, M.A. Mechanistic study of stress relaxation in urethane-containing polymer networks. *J. Phys. Chem. B.* **2019**, 123, 1432-1441.

[15] Kultys, A.; Rogulska, M.; Pikus, S. The synthesis and characterization of new thermoplastic poly (thiourethane–urethane)s. *J. Polym. Sci., Part A: Polym. Chem.* **2008**, 46, 1770-1782.

[16] Lu, C.; Guan, C.; Liu, Y.; Cheng, Y.; Yang, B. PbS/Polymer nanocomposite optical materials with high refractive index. *Chem. Mater*. **2005**, 17, 2448-2454.

[17] Chandrasekaran, S. *Click Reactions in Organic Synthesis*, Wiley-VCH: Weinheim, Germany, 2016.

[18] Shin, J.; Matsushima, H.; Comer, C. M.; Bowman, C. N.; Hoyle, C. E. Thiol-isocyanate-ene ternary networks by sequential and simultaneous thiol click reactions. *Chem. Mater.* **2010**, 22, 2616-2625.

[19] Gamardella, F.; Ramis. X.; De la Flor, S.; Serra, A. Preparation of poly(thiourethane) thermosets by controlled thiol-isocyanate click reaction using a latent organocatalyst. *React. Funct. Polym*. **2019**, 134, 174-182.

[20] Oliveira, V.D.G.; Cardoso, M.F.D.C.; Forezi, L.D.S.M. Organocatalysis: A Brief Overview on Its Evolution and Applications. *Catalysts* **2018**, 8, 605.

[21] Sardon, H.; Pascual, A.; Mecerreyes, D.; Taton, D.; Cramail, H.; Hedrick, J.L. Synthesis of polyurethanes using organocatalysis: a perspective. *Macromolecules* **2015**, 48, 3153-3165.

[22] Van Zee, N.J.; Nicolaÿ, R. Vitrimers: Permanently crosslinked polymers with dynamic network topology. *Prog. in Polym. Sci.* **2020**, 104, 101233.

[23] Denissen, W.; Droesbeke, M.; Nicolaÿ, R.; Leibler, L.; Winne, J. M.; Du Prez, F.E. Chemical control of the viscoelastic properties of vinylogous urethane vitrimers. *Nat. Comm.* **2017**, 8, 1-7.

[24] Huang, S.; Podgórski, M.; Han, X.; Bowman, C. N. Chemical recycling of poly(thiourethane) thermosets enabled by dynamic thiourethane bonds. *Polym. Chem.* **2020**, 11, 6879.

[25] Maji, B.; Stephenson, D.S.; Mayr. H. Guanidines: Highly Nucleophilic Organocatalysts. *Chem. Cat. Chem.* **2012**, 4, 993-999.

[26] Baidya, M.; Mayr, H. Nucleophilicities and carbon basicities of DBU and DBN. *Chem. Commun.* **2008**, 15, 1792-1794.

[27] Rodima, T.; Kaljurand, I.; Pihl, A.; Mäemets, V.; Leito, I.; Koppel I. A. Acid-base equilibria in nonpolar media. 2.1 Self-consistent basicity scale in THF solution ranging from 2-methoxypyridine to EtP1(pyrr) phosphazene. *J. Org. Chem.* **2002**, 67, 1873-1881.

[28] Konuray, O.; Fernández-Francos, X.; Ramis, X. Latent curing of epoxy-thiol thermosets. *Polymer* **2017**, 116, 191-203.

[29] Konuray, O.; Liendo, F.; Fernández-Francos, X.; Serra, À; Sangermano, M.; Ramis, X. Sequential curing of thiol-acetoacetate-acrylate thermosets by latent Michael addition reactions. *Polymer* **2017**, 113, 193-199.

[30] Sun, X.; Gao, J.P.; Wang Z.Y. Bicyclic guanidinium tetraphenylborate: a photobase Generator and A Photocatalyst for living anionic ring-opening polymerization and cross-linking of polymeric materials containing ester and hydroxy groups. *J. Am. Chem. Soc*. **2008**, 130, 8130-8131.

[31] S. Vyazovkin, *Isoconversional Kinetics of Thermally Stimulated Processes*, Springer: Birmingham, Alabama, 2015, 166-231.

[32] Vyazovkin, S.; Sbirrazzuoli, N. Kinetic methods to study isothermal and nonisothermal epoxy-anhydride cure. *Macromol. Chem. Phys.* **1999**, 200, 2294-2303.

[33] Coats, A.W.; Redfern J.P. Kinetic parameters from thermogravimetric data. *Nature* **1964**, 201, 68-69.

[34] Blaine, R.L.; Kissinger, H.E. Homer Kissinger and the Kissinger equation. *Thermochim. Acta* **2012**, 540, 1-6.

[35] Ramis, X.; Cadenato, A.; Salla, J.M.; Morancho, J.M.; Vallés, A.; Contat, L.; Ribes, A. Thermal degradation of polypropylene/starch-based materials with enhanced biodegradability. *Polym. Degrad. Stab.* **2004**, 86, 483-491.

[36] Delebecq, E.; Pascault, J.P.; Boutevin, B.; Ganachaud, F. On the versatility of urethane/ urea bonds: reversibility, blocked isocyanate, and non-isocyanate polyurethanes. *Chem. Rev.* **2012**, 113, 80-118.

[37] Rogulska, M.; Kultys, A.; Olszewska, E. New thermoplastics poly(thiourethane-urethane) elastomers based on hexane-1,6-diyl diisocyanate (HDI). *J. Therm. Anal. Calorim.* **2013**, 114, 903-916.

Supporting Information

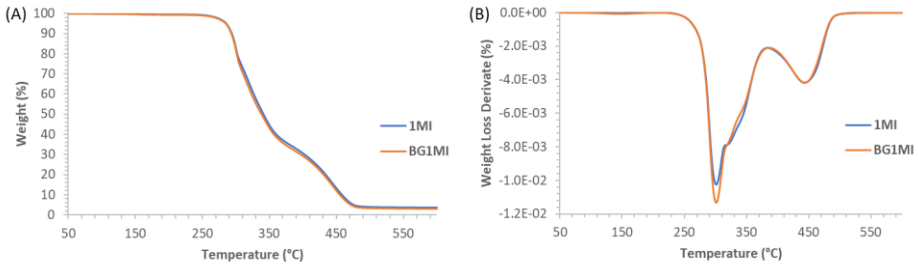

Figure VIII-S1. *TGA curves of the samples prepared with the same mol proportion of 1MI and BG1MI (A). Curves of the rate of weight loss against temperature, DTG (B).*

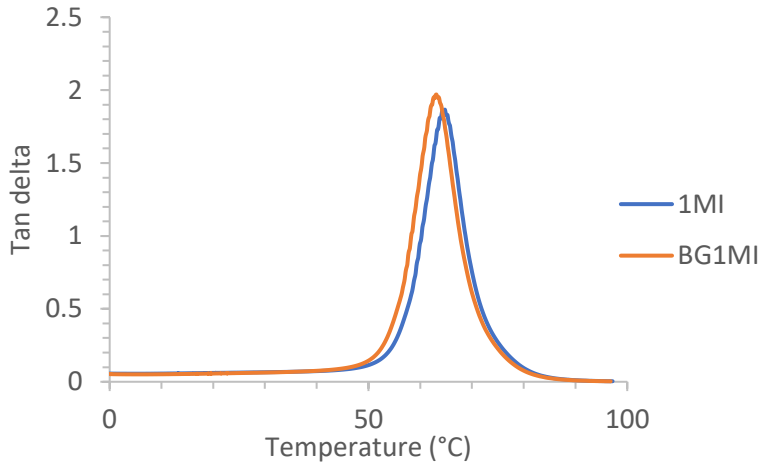

Figure VIII-S2. *Evolution of tan δ against temperature of the PTU samples prepared with the same mol proportion of 1MI and BG1MI*

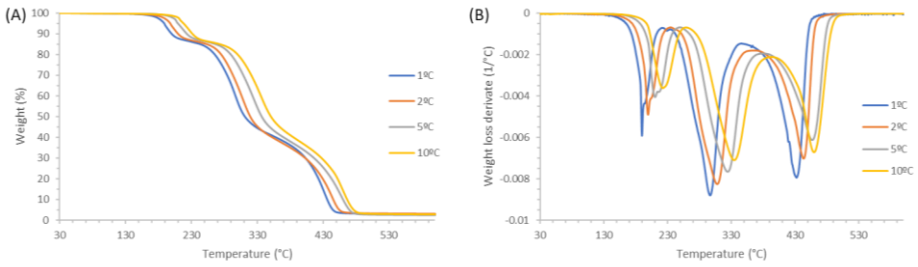

Figure VIII-S3*. (A) TGA and (B) DTG curves of the poly(thiourethane)s prepared in stoichiometric ratio with 0.1% of BGDBU as the catalyst at different heating rates.*

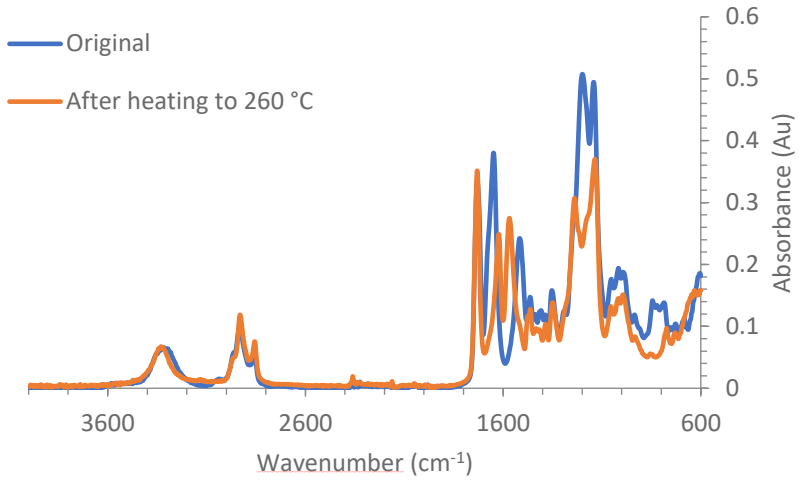

Figure VIII-S4. *FTIR of stoichiometric poly(thiourethane), registered at room temperature, before and after heating up the material until 260 °C in the TGA at 10 °C/min.*

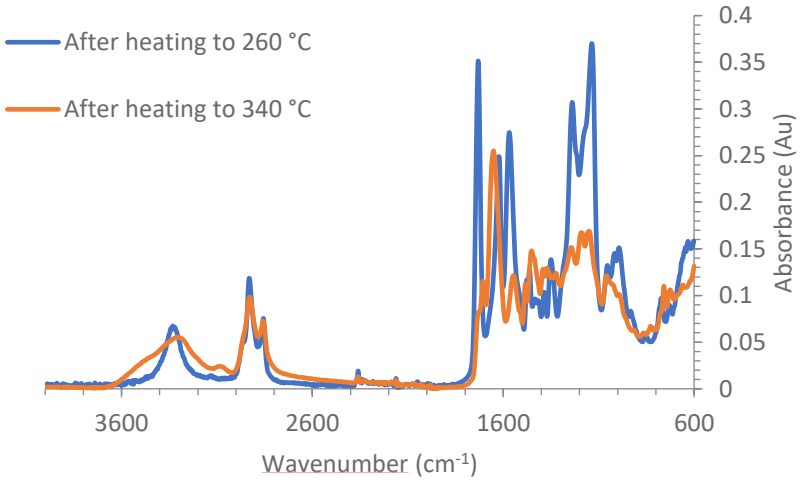

Figure VIII-S5. *FTIR of stoichiometric poly(thiourethane), registered at room temperature, after heating up the material until 340 °C in the TGA at 10 °C/min.*

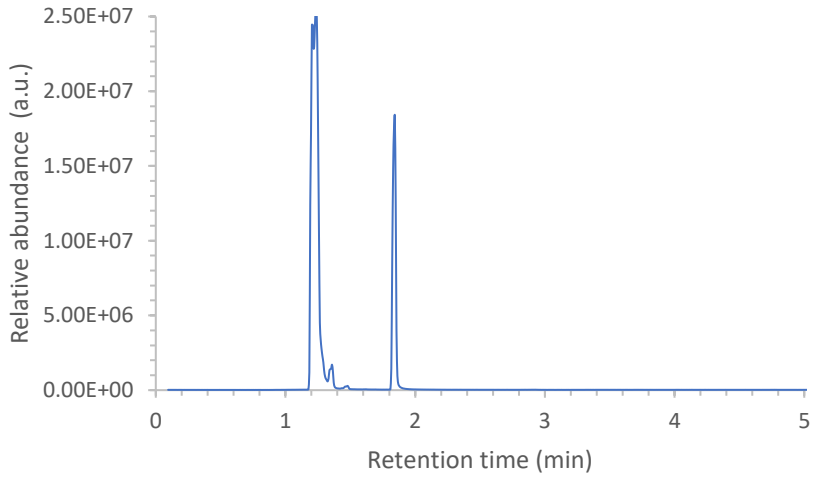

Figure VIII-S6. *Gas-chromatograms of the sample after heating a stoichiometric PTU sample for 1h at 200 °C.*

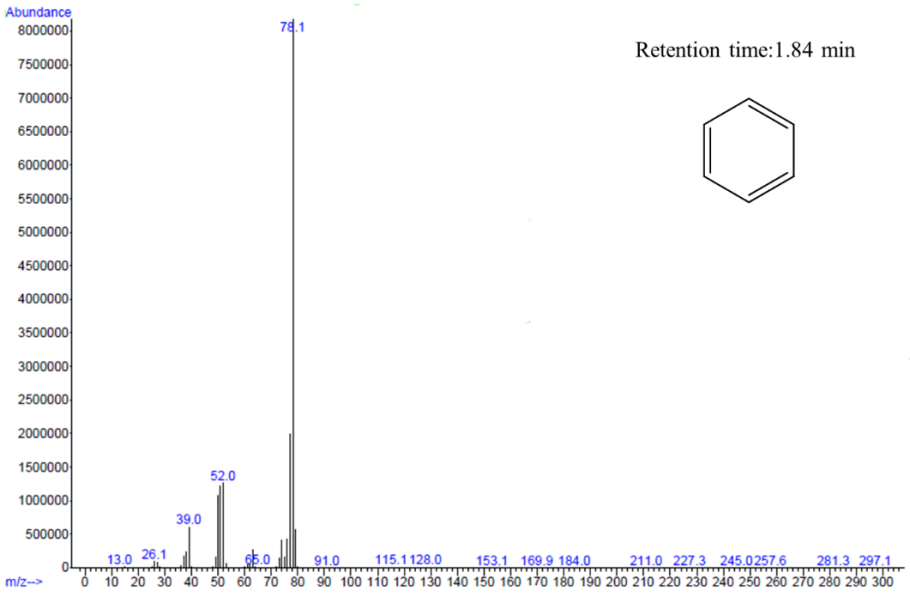

Figure VIII-S7. *Mass spectra of the eluted product at 1.84 min, identified as benzene, that corresponds to the decomposition of the sodium tetraphenylborate moiety.*

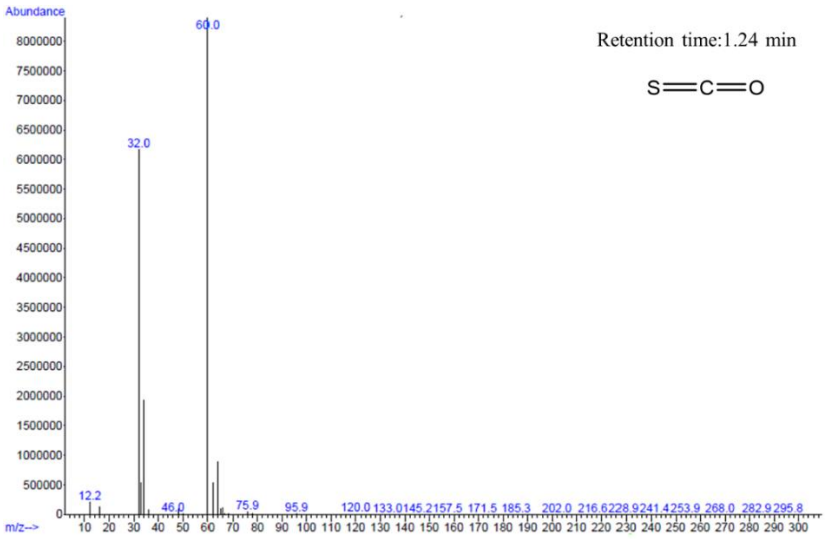

Figure VIII-S8. *Mass spectra of the eluted product at 1.24 min that corresponds to the carbonyl sulphide.*

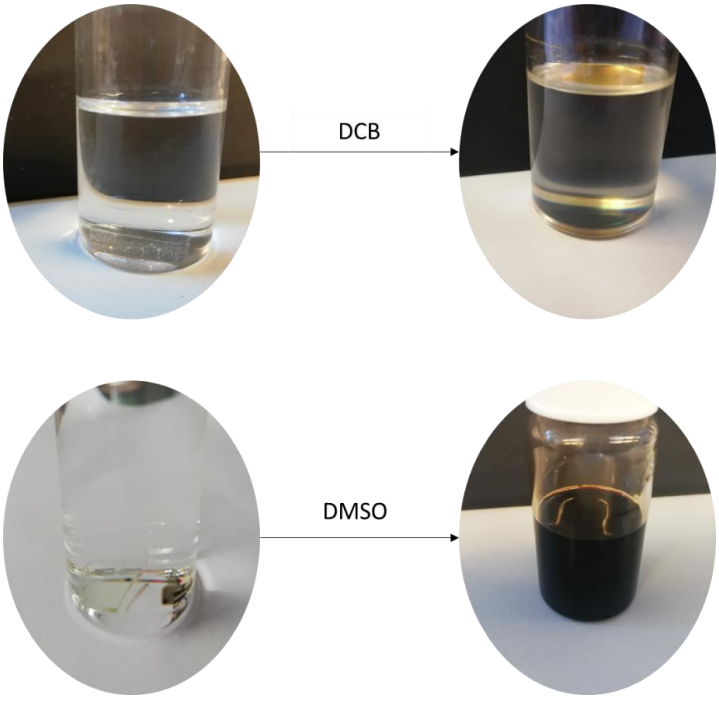

Figure VIII-S9. *Dissolution experiment at 150 °C in dimethyl sulfoxide (DMSO) and dichlorobenzene (DCB). The sample is at the bottom of the vial in DMSO but floats in DCB, due to the different density of the solvent.*

Chapter IX

General Conclusions

Conclusions

The main conclusions of this work are extracted from the five different sections according to the specific objectives reported in the aim of the thesis.

I) Poly(thiourethane) thermosets were prepared using tetrathiol with different aliphatic diisocyanates in acid and basic conditions. The use of 1-methylimidazolium tetraphenylborate (BG1MI), as a thermal latent base catalyst, allowed a better control of the reaction than the commonly used dibutyltin dilaurate (DBTDL). The thermo-mechanical properties of the thermosets obtained using the different catalysts are comparable.

II) Sequential dual-curing processing using “thiol-isocyanate” and “thiol-epoxy” click reactions was successfully achieved by appropriately adjusting the curing conditions. The faster isocyanate-thiol coupling reaction occurs at lower temperature leading to stable intermediate materials, while the epoxy-thiol reaction takes place when the temperature is increased above 80 °C. The physical properties of the intermediate and fully cured materials can be tuned adjusting the isocyanate/epoxy proportion. Moreover, the materials prepared showed an interesting shape memory behaviour, as they present a narrow transition temperature, emphasizing the *click* character of both reactive processes.

III) A new family of shape-memory polymers based on thiol-isocyanate networks using two different aliphatic isocyanates were successfully synthesized. The ability of this class of materials to act as polymer actuators was demonstrated. The thermomechanical properties can be tuned by changing diisocyanate structures, without affecting the homogeneity of the sample and preserving the shape-memory ability. With the reported results an important guideline to design shape-memory materials based on poly(thiourethane) networks depending on the expected application has been provided.

IV) We demonstrated that the thiourethane dynamic chemistry can be used to produce reprocessable materials. Firstly, by means of model compounds the reversible nature of thiourethane linkages was demonstrated. Then, PTU thermosets were synthesized by the reaction of hexamethylene diisocyanate (HDI) and trimethylolpropane tris(3-mercaptopropionate) (S3) in presence of DBTDL. The viscoelastic properties of these materials, determined via stress relaxation experiments, showed a linear evolution of the viscosity with temperature, indicating an associative character. The relaxation rate increased as the catalyst amount was increased. The thermomechanical characteristics and the FTIR spectra remained unaltered, after performing a series of relaxation experiments.

V) Reprocessable and recyclable poly(thiourethane) thermosets with high glass transition temperatures were obtained by changing the structure of the diisocyanates

to more rigid aliphatic and aromatic monomers. Among them, the aromatic diisocyanate derived material experimented the fastest relaxation process. The complete recyclability of the PTU materials was proved by means of DMA, FTIR and mechanical tests. From these experiments, the key role of DBTDL in the rearrangement process and in the recyclability was put in evidence.

VI) The PTUs prepared using latent base generators showed a faster exchange mechanism in reference to the materials prepared with DBTDL, reaching a complete relaxation in less than 2 min at 180 °C. PTU materials with a 10 % of excess of thiol groups did not show appreciable differences in relaxation rate and recycling capability.

We proved that thiourethane networks can be completely dissolved in dimethyl sulfoxide and that the thermal degradation of PTUs leads to an initial loss of carbonyl sulfide without appreciable dissociation of thiourethane moieties to isocyanate and thiol groups.

VII) In light of these considerations, we can state that the exchange mechanism in presence of organocatalysts is mainly dissociative, as PTUs can be dissolved in an appropriate solvent and the excess of thiols did not change the relaxation behavior. The exchange mechanism presents a very fast equilibrium process that leads to a vitrimer-like behaviour. Therefore, we have demonstrated that PTUs can be conveniently synthesized, optimizing the catalyst selection, to be considered as sustainable alternative to current thermosets.

UNIVERSITAT
ROVIRA i VIRGILI